



# University of HUDDERSFIELD

## University of Huddersfield Repository

Bullock, Samantha Jane

Metallo-supramolecular chemistry of polydentate ligands and the solid state studies of diphenylcarbazide and dithizone

### Original Citation

Bullock, Samantha Jane (2014) Metallo-supramolecular chemistry of polydentate ligands and the solid state studies of diphenylcarbazide and dithizone. Doctoral thesis, University of Huddersfield.

This version is available at <http://eprints.hud.ac.uk/id/eprint/24695/>

The University Repository is a digital collection of the research output of the University, available on Open Access. Copyright and Moral Rights for the items on this site are retained by the individual author and/or other copyright owners. Users may access full items free of charge; copies of full text items generally can be reproduced, displayed or performed and given to third parties in any format or medium for personal research or study, educational or not-for-profit purposes without prior permission or charge, provided:

- The authors, title and full bibliographic details is credited in any copy;
- A hyperlink and/or URL is included for the original metadata page; and
- The content is not changed in any way.

For more information, including our policy and submission procedure, please contact the Repository Team at: [E.mailbox@hud.ac.uk](mailto:E.mailbox@hud.ac.uk).

<http://eprints.hud.ac.uk/>

**METALLOSUPRAMOLECULAR CHEMISTRY OF  
POLYDENTATE LIGANDS AND THE SOLID STATE  
STUDIES OF DIPHENYLCARBAZIDE AND DITHIZONE**

**SAMANTHA BULLOCK**

A thesis submitted to the University of Huddersfield in partial fulfilment of the requirements  
for the degree of Doctor of Philosophy

The University of Huddersfield

September 2014

## **Copyright statement**

The author of this thesis (including any appendices and/or schedules to this thesis) owns any copyright in it (the "Copyright") and s/he has given The University of Huddersfield the right to use such copyright for any administrative, promotional, educational and/or teaching purposes.

Copies of this thesis, either in full or in extracts, may be made only in accordance with the regulations of the University Library. Details of these regulations may be obtained from the Librarian. This page must form part of any such copies made.

The ownership of any patents, designs, trademarks and any and all other intellectual property rights except for the Copyright (the "Intellectual Property Rights") and any reproductions of copyright works, for example graphs and tables ("Reproductions"), which may be described in this thesis, may not be owned by the author and may be owned by third parties. Such Intellectual Property Rights and Reproductions cannot and must not be made available for use without the prior written permission of the owner(s) of the relevant Intellectual Property Rights and/or Reproductions

## Contents

|  |      |
|--|------|
| List of Abbreviations.....                                   | viii |
| Acknowledgements.....  | x    |
| Abstract.....  | xi   |
| 1. Introduction.....   | 1    |
| 1.0 Supramolecular chemistry.....                            | 1    |
| 1.1 Origin of supramolecular chemistry.....                  | 1    |
| 1.2 Supramolecular interactions.....                         | 2    |
| 1.2.1 Ion-ion interactions.....                              | 3    |
| 1.2.2 Ion-dipole interactions.....                           | 4    |
| 1.2.3 Dipole-dipole interactions.....                        | 4    |
| 1.2.4 Hydrogen bonding.....                                  | 5    |
| 1.2.5 $\pi$ - $\pi$ stacking interactions.....               | 5    |
| 1.3 Host guest chemistry.....                                | 6    |
| 1.3.1 Crown Ethers.....                                      | 7    |
| 1.4 Self-assembly.....                                       | 11   |
| 1.5 Metallosupramolecular chemistry.....                     | 13   |
| 1.5.1 Racks.....   | 14   |
| 1.5.2 Ladders.....   | 15   |
| 1.5.3 Grids.....   | 16   |
| 1.5.4 Cages.....   | 18   |
| 1.6 <i>Helicates</i> .....                                   | 21   |
| 1.6.1 Helicate Nomenclature.....                             | 22   |
| 1.6.2 Homonuclear Helicates.....                             | 22   |
| 1.6.3 Heteroleptic Helicates.....                            | 25   |
| 1.6.4 Unsaturated Helicates.....                             | 26   |
| 1.6.5 Directional Helicates.....                             | 27   |
| 1.6.6 Heteronuclear Helicates.....                           | 29   |
| 1.6.7 Enantioselective and Diastereoselective Helicates..... | 31   |
| 1.6.8 Meso Helicates.....                                    | 34   |
| 1.7 Circular Helicates.....                                  | 36   |
| 1.8 Ligand Recognition.....                                  | 51   |
| 1.8.1 Ligand Programming.....                                | 54   |
| 1.8.2 Allosteric Interactions.....                           | 58   |

|   |     |
|---|-----|
| 1.8.3 Ditopic Ligands .....   | 59  |
| 2. Self-assembly of helicates and circular helicates using N-oxide containing ligands.....                | 62  |
| 2.1 Ligand synthesis.....   | 65  |
| 2.1.1 Synthesis of 1-N-oxide-2,2'-bipyridine-6'-thioamide (6) .....                                       | 65  |
| 2.1.2 Synthesis of Ligands $L^1$ - $L^3$ .....  | 66  |
| 2.1.3 Synthesis of $L^4$ .....  | 67  |
| 2.2 Coordination Chemistry .....  | 68  |
| 2.2.1 Complexes of $L^1$ with copper (II) .....   | 68  |
| 2.2.2 Coordination chemistry of $L^2$ with nickel (II).....   | 71  |
| 2.2.3 Coordination chemistry of $L^3$ with copper (II) .....  | 74  |
| 2.2.4 Coordination chemistry of $L^4$ with cobalt (II) .....  | 77  |
| 2.3 Discussion .....  | 82  |
| 3. Polydentate ligands containing a central phenol unit and their self-assembly with metal ions .....     | 86  |
| 3.1 Ligand synthesis.....   | 88  |
| 3.1.1 Synthesis of Ligands $L^5$ and $L^6$ .....  | 88  |
| 3.1.2 Synthesis of Ligands $L^7$ .....  | 89  |
| 3.2 Coordination Chemistry .....  | 90  |
| 3.2.1 Complexes of $L^5$ and zinc (II) .....  | 90  |
| 3.2.2 Complexes of $L^6$ and silver (I) .....   | 93  |
| 3.2.3 Complexes of $L^6$ and cadmium(II) .....  | 96  |
| 3.2.4 Complexes of $L^7$ and cobalt(II) .....   | 102 |
| 3.2.3 Complexes of $L^7$ and zinc(II) .....   | 106 |
| 3.3 Discussion .....  | 112 |
| 4. Formation of a head-to-tail tetranuclear circular helicate .....                                       | 121 |
| 4.1 Ligand synthesis.....   | 123 |
| 4.1.1 Freidel-Craft acylation of pyrene .....   | 123 |
| 4.1.2 Synthesis of 1,3-di( $\alpha$ -bromoacetyl)pyrene (3).....  | 123 |
| 4.1.3 Synthesis of $L^8$ .....  | 124 |
| 4.2 Coordination Chemistry .....  | 125 |
| 4.2.1 Complexes of $L^8$ and copper (II).....   | 125 |
| 4.3 Solution Studies.....   | 129 |
| 4.3.1 Solution state characterisation of HT-[Cu <sub>4</sub> ( $L^8$ ) <sub>4</sub> ] <sup>8+</sup> ..... | 129 |
| 4.4 Discussion .....  | 130 |

|  |     |
|--|-----|
| 5. Solid state studies of the coordination chemistry of diphenylcarbazide and dithizone.     | 133 |
| 5.1 Introduction.....  | 133 |
| 5.1.1 Diphenylcarbazide.....   | 133 |
| 5.1.2 Dithizone .....  | 142 |
| 5.1.3 Aim.....   | 154 |
| 5.2 Coordination chemistry of DPC.....   | 156 |
| 5.2.1 Complexes of DPC and cadmium (II) .....  | 156 |
| 5.2.2 Complexes of DPC and copper (II).....  | 158 |
| 5.2.3 Complexes of DPC with chromium (III) and vanadium (III) .....                          | 162 |
| 5.3 Coordination chemistry of DPTC .....   | 165 |
| 5.3.1 Complexes of DPTC and mercury (II).....  | 165 |
| 5.3.2 Complexes of DPTC with mercury (II) and silver (I).....                                | 166 |
| 5.3.3 Complexes of DPTC with copper (II) perchlorate.....                                    | 170 |
| 5.3.4 Complexes of DPTC with copper (II) tetrafluoroborate .....                             | 176 |
| 5.3.5 Complexes of DPTC with copper (II) acetate.....  | 180 |
| 5.4 Discussion .....   | 182 |
| 6. Conclusion .....  | 190 |
| 7. Experimental .....  | 193 |
| 7.1 Preparation of L <sup>1</sup> , L <sup>2</sup> , L <sup>3</sup> and L <sup>4</sup> ..... | 193 |
| 7.1.1 Synthesis of bipyridine 1-N-oxide (2).....   | 193 |
| 7.1.2 Synthesis of 6-carbonitrile-2,2'-bipyridine (3).....                                   | 194 |
| 7.1.3 Synthesis of 6'-cyano-2,2'-bipyridine-1-oxide (4).....                                 | 195 |
| 7.1.4 Synthesis of 2,2'-bipyridine-bis-1,1'-oxide (6) .....                                  | 196 |
| 7.1.5 Synthesis of 6'-cyano-2,2'-bipyridine-1-oxide (4).....                                 | 197 |
| 7.1.6 Synthesis of 1-N-oxide-2,2'-bipyridine-6'-thioamide (8) .....                          | 198 |
| 7.1.7 Synthesis of 2-( $\alpha$ -bromoacetyl)pyridine (10).....                              | 199 |
| 7.1.8 Synthesis of L <sup>1</sup> .....  | 200 |
| 7.1.9 Synthesis of L <sup>2</sup> .....  | 201 |
| 7.1.10 Synthesis of 1,3-di( $\alpha$ -bromoacetyl)benzene (13) .....                         | 202 |
| 7.1.11 Synthesis of 2-pyridine thioamide (15) .....  | 203 |
| 7.1.12 Synthesis of py-tz-phy bidentate bromoacetyl (16) .....                               | 204 |
| 7.1.13 Synthesis of L <sup>3</sup> .....   | 205 |
| 7.1.14 Synthesis of 1,3-diacetyl cresol (18).....  | 206 |
| 7.1.15 Synthesis of 1,3-( $\alpha$ -bromoacetyl)cresol (19).....                             | 207 |
| 7.1.16 Synthesis of L <sup>4</sup> .....   | 208 |

|  |     |
|--|-----|
| 7.2 Preparation of $L^5$ , $L^6$ and $L^7$ .....                                     | 209 |
| 7.2.1 Synthesis of 2,2'-bipyridine thioamide (20) .....                              | 209 |
| 7.2.2 Synthesis of $L^5$ .....   | 210 |
| 7.2.3 Synthesis of $L^6$ .....   | 211 |
| 7.2.4 Preparation of $L^7$ .....   | 212 |
| 7.2.5 Synthesis of $L^7$ .....   | 213 |
| 7.3 Preparation of $L^8$ .....   | 214 |
| 7.3.1 Synthesis of 1,3-diacetyl pyrene (23) .....                                    | 214 |
| 7.3.2 Synthesis of 1,3-dibromo-diacetyl pyrene (24) .....                            | 215 |
| 7.3.3 Preparation of $L^8$ .....   | 216 |
| 7.3.4 Synthesis of $L^8$ .....   | 218 |
| 7.4 Synthesis of complexes .....   | 220 |
| 7.4.1 Synthesis of complex $[Cu(L^1)(ClO_4)_2(sol)]$ .....                           | 220 |
| 7.4.2 Synthesis of complex $[Ni_2(L^2)_2]^{4+}$ .....                                | 220 |
| 7.4.3 Synthesis of complex $[Cu_2(L^3)_2]^{4+}$ .....                                | 220 |
| 7.4.4 Synthesis of complex $[Co_4(L^4)_4]^{8+}$ .....                                | 220 |
| 7.4.5 Synthesis of complex $[Zn_4(L^5)_4]^{8+}$ .....                                | 220 |
| 7.4.6 Synthesis of complex $[Ag_2(L^6)_2]^{2+}$ .....                                | 220 |
| 7.4.7 Synthesis of complex $[Cd(L^6)_2(MeCN)_2]^{2+}$ and $[Cd_2(L^6)_2]^{3+}$ ..... | 221 |
| 7.4.8 Synthesis of complex $[Co_2(L^7)_2]^{3+}$ .....                                | 221 |
| 7.4.9 Synthesis of complex $[Zn(L^7)_2]^{2+}$ and $[Zn_2(L^7)_2]^{3+}$ .....         | 221 |
| 7.4.10 Synthesis of complex $[Cu_4(L^8)_4]^{8+}$ .....                               | 221 |
| 7.4.11 Synthesis of complex $[Cd(DPC)_2]^{2+}$ .....                                 | 221 |
| 7.4.12 Synthesis of complex $[Cu_3OH(OH_2)_3(DPTO)_3]^{5+}$ .....                    | 222 |
| 7.4.13 Synthesis of 2,3-diphenyltetrazolium-5-olate .....                            | 222 |
| 7.4.14 Synthesis of complex $[Hg(DPTC)_2]^+$ .....                                   | 222 |
| 7.4.15 Synthesis of complex $[Hg_2Ag_2(DPTC)_4(acetone)_2(ClO_4)_2]$ .....           | 222 |
| 7.4.16 Synthesis of complex $K_2[Cu_8(DPTC)_8(ClO_4)_2]^{2+}$ .....                  | 222 |
| 7.4.17 Synthesis of complex $K_2[Cu_8(DPTC)_8(BF_4)_2]^{2+}$ .....                   | 223 |
| 7.4.18 Synthesis of complex $[Cu_2(DPTC)_2(DPTO)]$ .....                             | 223 |
| 8. References .....  | 224 |
| Appendix 1: Crystal Data Tables .....  | 231 |
| Table A1. Crystallographic data of $L^1$ complex $[Cu(L^1)(ClO_4)_2(sol)]$ .....     | 232 |
| Table A2. Crystallographic data of $L^2$ complex $[Ni_2(L^2)_2]^{4+}$ .....          | 233 |
| Table A3. Crystallographic data of $L^3$ complex $[Cu_2(L^3)_2]^{4+}$ .....          | 234 |

|   |     |
|---|-----|
| Table A4. Crystallographic data of $L^4$ complex $[Co_4(L^4)_4]^{8+}$ .....                               | 235 |
| Table A5. Crystallographic data of $L^5$ complex $[Zn_4(L^5)_4]^{8+}$ .....                               | 236 |
| Table A6. Crystallographic data of $L^6$ complex $[Ag_2(L^6)_2]^+$ .....                                  | 237 |
| Table A7. Crystallographic data of $L^6$ complex $[Cd(L^6)_2(MeCN)_2]^{2+}$ .....                         | 238 |
| Table A8. Crystallographic data of $L^6$ complex $[Cd_2(L^6)_2]^{3+}$ .....                               | 239 |
| Table A9. Crystallographic data of $L^7$ complex $[Co_2(L^7)_2]^{3+}$ .....                               | 240 |
| Table A10. Crystallographic data of $L^7$ complex $[Zn(L^7)_2]^{2+}$ .....                                | 241 |
| Table A11. Crystallographic data of $L^7$ complex $[Zn_2(L^7)_2]^{3+}$ .....                              | 242 |
| Table A12. Crystallographic data of $L^8$ complex $[Cu_4(L^8)_4]^{8+}$ .....                              | 243 |
| Table A13. Crystallographic data of <b>DPC</b> complex $[Cd(DPC)_2]^{2+}$ .....                           | 244 |
| Table A14. Crystallographic data of <b>DPC</b> complex $[Cu_3OH(OH_2)_3(DPTO)_6]^{5+}$ .....              | 245 |
| Table A15. Crystallographic data of 2,3-diphenyltetrazolium-5-olate (DPTO) .....                          | 246 |
| Table A16. Crystallographic data of <b>DPTC</b> complex $[Hg(DPTC)_2]$ .....                              | 247 |
| Table A17. Crystallographic data of <b>DPTC</b> complex $[Hg_2Ag_2(DPTC)_4(acetone)_2(ClO_4)_2]$<br>..... | 248 |
| Table A18. Crystallographic data of <b>DPTC</b> complex $[Cu_8(DPTC)_8(ClO_4)_2]^{8+}$ .....              | 249 |
| Table A19. Crystallographic data of <b>DPTC</b> complex $[Cu_8(DPTC)_8(BF_4)_2]^{8+}$ .....               | 250 |
| Table A20. Crystallographic data of <b>DPTC</b> complex $[Cu_2(DPTC)_2(DPTCO)]$ .....                     | 251 |
| Appendix 2: Publications .....  | 252 |

## List of Abbreviations

|           |   |
|-----------|---|
| $\alpha$  | Alpha                                     |
| Å         | Angstroms                                 |
| (aq)      | Aqueous                                   |
| $\beta$   | Beta                                      |
| COSY      | Correlation Spectroscopy                  |
| $J$       | Coupling constant                         |
| $\delta$  | Delta (chemical shift)                    |
| DNA       | Deoxyribonucleic acid                     |
| DMSO      | Deuterated dimethyl sulfoxide             |
| DCM       | Dichloromethane                           |
| d         | Doublet                                   |
| dd        | Doublet of doublets                       |
| ddd       | Doublet of doublets of doublets           |
| dt        | Doublets of triplets                      |
| ESI-MS    | Electrospray ionisation mass spectrometry |
| $\gamma$  | Gamma                                     |
| (g)       | Gas                                       |
| g         | gram                                      |
| <i>HH</i> | Head-to-head                              |
| <i>HT</i> | Head-to-tail                              |
| Hz        | Hertz                                     |
| $m/z$     | Mass/charge                               |

|                    |   |
|--------------------|---|
| MS                 | Mass Spectrometry                                   |
| MHz                | Megahertz   |
| <i>m</i> CPBA      | <i>meta</i> -chloroperoxybenzoic acid               |
| M-L                | Metal-ligand  |
| mg                 | Milligram   |
| ml                 | Millilitre  |
| mol                | Moles   |
| mmol               | Millimoles  |
| M                  | Molar   |
| m                  | Multiplet   |
| N-donor            | Nitrogen donor                                      |
| <sup>1</sup> H NMR | Nuclear Magnetic Resonance                          |
| O-donor            | Oxygen donor  |
| ppm                | Parts per million, $\delta$ (delta), chemical shift |
| Py                 | Pyridyl   |
| PyO                | Pyridyl-N-oxide                                     |
| RT                 | Room temperature                                    |
| s                  | Singlet   |
| THF                | Tetrahydrofuran                                     |
| Tz                 | Thiazole  |
| TLC                | Thin Layer Chromatography                           |
| TMS-CN             | Trimethylsilyl cyanide                              |
| t                  | Triplet   |

## **Acknowledgements**

I would like to thank my supervisor Prof. Craig Rice for his excellent guidance, advice and support throughout my PhD and also for solving the numerous crystal structures. I would like to thank Dr. Roger Jewsbury for all his support. My thanks also goes to past and present members of the Rice research group, in particular Rebecca Fennessy, all of whom have been a delight to work with over the years.

The following people have given their assistance and support with various aspects of the research I would therefore like to thank them; Dr. Thomas Riis-Johannessen for crystallographic analysis, Dr. Neil McLay for NMR, Dr. Lindsay Harding for Mass Spectrometry and Robert Faulkner for assistance with Mass Spectrometry.

I would like to thank the University of Huddersfield for providing this great opportunity and the necessary funding to perform this research. I would also like to thank other members within the Department of Chemical and Biological Sciences.

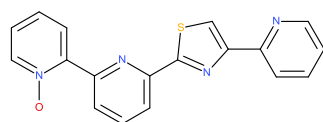
Most importantly I would like to thank my family; especially my Mum and Mark, my Dad and Carol, my sister and brother, my Nanna and John and finally my late Grandad for their support both emotionally and financially. Without their constant and unconditional support none of my achievements would have been possible. Special thanks to my Mum; for knowing exactly what to say, for answering the phone when all I do is cry, for listening to me rant and for always being there no matter what, you really are the best mum in the world.

My thanks also go to my friends; particularly Amy, Leanne, Lucy, Nikki and a special mention for Heidi without whom I guarantee I would be insane.

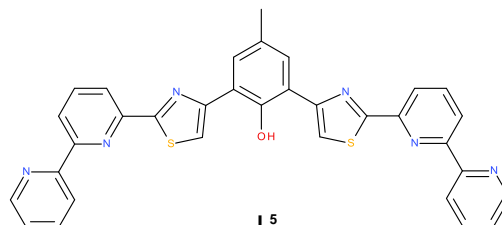
Lastly, I would like to thank my boyfriend Matt; for being my rock, for wiping my tears and making me laugh and most importantly for never giving up.

## Abstract

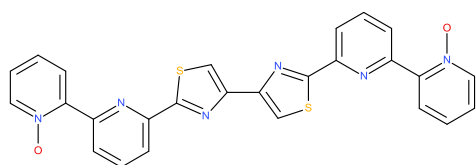
Described herein, is the synthesis and coordination chemistry of eight novel ligands **L**<sup>1</sup>-**L**<sup>8</sup>, and the solid state studies of diphenylcarbazide and dithizone. These ligands form metallosupramolecular assemblies upon coordination of transition metal ions resulting in a wide range of architectures.



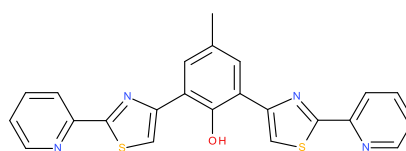
**L**<sup>1</sup>



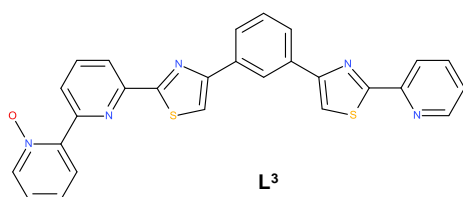
**L**<sup>5</sup>



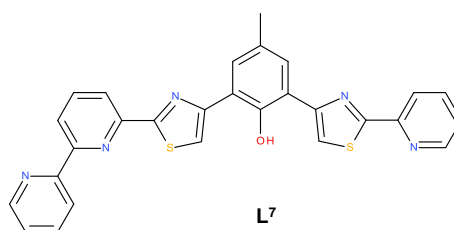
**L**<sup>2</sup>



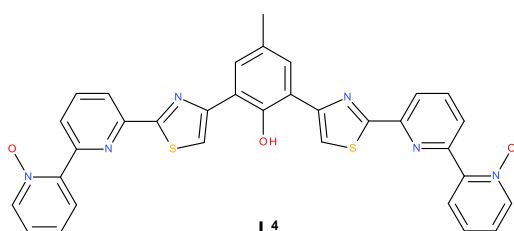
**L**<sup>6</sup>



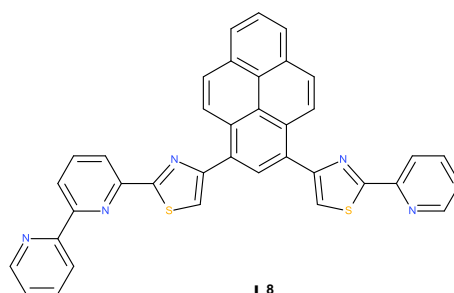
**L**<sup>3</sup>



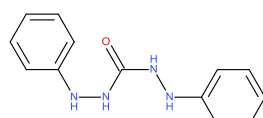
**L**<sup>7</sup>



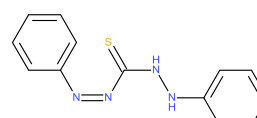
**L**<sup>4</sup>



**L**<sup>8</sup>



Diphenylcarbazide (DPC)



Dithizone (DPTC)

Described in chapter two is a series of ligands that contain both N-donor and N-oxide donor atoms,  $L^1$ - $L^4$ . Reaction of  $L^1$  with  $Cu^{2+}$  results in the formation of a mononuclear complex  $[Cu(L^1)(ClO_4)_2(sol)]$  (solvent = MeCN or  $H_2O$ ), whereas  $L^2$  forms the dinuclear double helicate  $[Ni_2(L^2)_2]^{4+}$  with  $Ni^{2+}$ . Reaction of  $L^3$  with  $Cu^{2+}$  results in the formation of a head-to-tail dinuclear double helicate  $[Cu_2(L^3)_2]^{4+}$ . The N-oxide units imparts flexibility in the ligand strand and where the unoxidised ligand strand forms a circular helicate, the incorporation of an N-oxide unit allows the formation of the dinuclear double helicate. Reaction of  $L^4$  with  $Co^{2+}$  results in the formation of a tetranuclear circular helicate  $[Co_4(L^4)_4]^{8+}$ . Analogous complexes that contain ligands with a 1,3-phenyl spacer unit give pentanuclear circular helicates, whereas with a 1,3-phenol spacer the lower tetranuclear species is observed. The difference in the nuclearity of the circular helicates is due to the steric bulk of the methyl group on the central phenol spacer. In the dinuclear double complex formed with  $L^3$  the N-oxide unit allows the ligand to flex, whereas the steric bulk of the  $-OH$  unit in  $L^4$  is sufficiently large that even with the added flexibility that the N-oxide units imparts a double helicate cannot be formed.

Chapter three introduces a new class of polydentate ligands,  $L^5$ - $L^7$ , these ligands consist of N-donor domains separated by a 1,3-phenol unit. The ligand  $L^5$  contains two identical tridentate N-donor domains, reaction of  $L^5$  with  $Zn^{2+}$  results in a tetranuclear circular helicate  $[Zn_4(L^5)_4]^{8+}$ . Within the structure all four  $Zn^{2+}$  ions are six-coordinate, arising from the coordination of two tridentate domains from two different ligand strands. Reaction of  $L^6$  with  $Ag^+$  results in the formation of the dinuclear double *meso*-helicate  $[Ag_2(L^6)_2]^{2+}$ . Reaction of  $L^6$  with  $Cd^{2+}$  produces a crystalline material that consists of both colourless and orange species. The colourless crystals correspond to the mononuclear complex  $[Cd(L^6)_2(MeCN)_2]^{2+}$ , whereas the orange crystals produce the dinuclear double *meso*-helicate  $[Cd_2(L^6)_2]^{2+}$ . This variation in self-assembly is a direct result of the  $-OH$  unit on the 1,3-phenol spacer; if the  $-OH$  unit is protonated the oxygen atom can only coordinate once and therefore the mononuclear complex forms, however deprotonation of one of the  $-OH$  unit results in the oxygen coordinating twice as a bridging donor to form the dinuclear complex. Both the  $[Cd(L^6)_2(MeCN)_2]^{2+}$  and  $[Cd_2(L^6)_2]^{2+}$  species are present in solution, under equilibrium conditions, varying the stoichiometry alters the predominant species. The ligand  $L^7$  is unsymmetrical, upon reaction with  $Co^{2+}$  the ligand partitions into two different binding sites; a tridentate N-donor domain and a tridentate domain consisting of the bidentate N-donor domain and the O-donor atom from the central 1,3-phenol spacer. The resulting dinuclear *HH*- $[Co_2(L^7)_2]^{3+}$  complex demonstrates that the two cobalt metal centres occupy different binding sites. Examining the solid state X-ray crystallographic data suggests that the two cobalt metal centres in the  $[Co_2(L^7)_2]^{3+}$  complex occupy different oxidation states;  $Co^{2+}$  and  $Co^{3+}$  to give a mixed valence helicate. In an analogous fashion

to  $\mathbf{L}^6$ , reaction of  $\mathbf{L}^7$  with  $\text{Zn}^{2+}$  produces a crystalline material that consists of both colourless and orange species. The colourless crystals correspond to the mononuclear complex  $[\text{Zn}(\mathbf{L}^7)_2]^{2+}$ , whereas the orange crystals produce the dinuclear double helicate  $[\text{Zn}_2(\mathbf{L}^6)_2]^{3+}$ . In the mononuclear  $[\text{Zn}(\mathbf{L}^7)_2]^{2+}$  species the  $\text{Zn}^{2+}$  metal centre is coordinated by the tridentate N-donor domain of two different ligands. In the dinuclear  $[\text{Zn}_2(\mathbf{L}^6)_2]^{3+}$  species each  $\text{Zn}^{2+}$  metal centres is coordinated by the tridentate N-donor domain of one ligand and the tridentate domain, consisting of the bidentate N-donor and the O-donor from the central 1,3-phenol spacer, from another different ligand. The variation in the self-assembly is a direct result of the stoichiometry of the reaction; the formation of these two complexes is under the same equilibrium conditions of the previous  $\mathbf{L}^6$  structures.

Described in chapter four is the potentially pentadentate N-donor ligand  $\mathbf{L}^8$ , which comprises of a bidentate and tridentate binding domains separated by a 1,3-pyrene spacer. Reaction of  $\mathbf{L}^8$  with  $\text{Cu}^{2+}$  results in the formation of a tetranuclear circular helicate  $[\text{Cu}_4(\mathbf{L}^8)_4]^{8+}$ . Each of the  $\text{Cu}^{2+}$  ions adopts a 5-coordinate geometry formed by the coordination of the bidentate domain of one ligand strand and the tridentate domain of a different ligand strand, resulting in a head-to-tail tetranuclear circular helicate. The formation of this head-to-tail circular helicate is a result of the 1,3-pyrene spacer preventing the formation of the linear double stranded assemblies and secondly the stereoelectronic preference of  $\text{Cu}^{2+}$ .

Chapter five reports the solid state studies of diphenylcarbazide and dithizone, which are both useful reagents for the colorimetric determination of a variety of different metal ions. Examination of the scientific literature over the past 100 years shows that the coordination chemistry of DPC and DPTC is inconsistent, with literature sources proposing contradictory and non-definitive explanations, this chapter aims to extend the knowledge surrounding these reagents by isolating crystals. DPC reacts with  $\text{Cd}^{2+}$  to form the mononuclear species  $[\text{Cd}(\text{DPC})_2]^{2+}$  the two ligands are coordinating through both the N-donor and O-donor domains. The discrepancies surrounding the DPC reaction is whether the redox reactions between the metal and ligand occur, upon reaction of DPC and  $\text{Cd}^{2+}$  the metal does not oxidise the ligand. Reaction of DPC and  $\text{Cu}^{2+}$  is more complex than the previous  $\text{Cd}^{2+}$  reaction, the resulting  $[\text{Cu}_3\text{OH}(\text{OH}_2)_3(\text{DPTO})_6]^{5+}$  structure comprises of six ligands and three metal ions. DPC undergoes oxidative intramolecular cyclisation to form the nitrogen containing heterocycle 2,3-diphenyltetrazolium-5-olate (DPTO) and coordinates the  $\text{Cu}^{2+}$  metal centre in two different modes: via both the oxygen and amide nitrogen atoms or by the bridging carbonyl unit. The  $[\text{Cu}_3\text{OH}(\text{OH}_2)_3(\text{DPTO})_6]^{5+}$  structure is also generated when reacting DPCO with  $\text{Cu}^{2+}$ . Unfortunately a crystal of a chromium or vanadium complex with DPC was not achieved; however the cyclised ligand was isolated,

highlighting that the oxidation and cyclisation of DPC is important in the coordination chemistry of these ions. Reaction of the sulphur derivative DPTC with various metal ions results in the deprotonation of the ligand to form the monoanionic species, which coordinates the metal ions via the S-donor and azo N-donor atoms. Reaction of DPTC with  $\text{Hg}^{2+}$  to form the mononuclear complex  $[\text{Hg}(\text{DPTC})_2]$ . The simple mononuclear complex involves two DPTC ligands coordinating the four-coordinate  $\text{Hg}^{2+}$  ion as a bidentate donor via the N-donor and S-donor atoms. The reaction of DPTC with both  $\text{Hg}^{2+}$  and  $\text{Ag}^+$  results in an interesting structure containing two  $\text{Ag}^+$ , two  $\text{Hg}^{2+}$  and four DPTC ligands. The DPTC appears to first react with  $\text{Hg}^{2+}$  to form the previous  $[\text{Hg}(\text{DPTC})_2]$  complex, this then acts as a bidentate ligand, coordinating via the S-donor atom and the  $\text{Hg}^{2+}$  itself to form the  $[\text{Hg}_2\text{Ag}_2(\text{DPTC})_4(\text{acetone})_2(\text{ClO}_4)_2]$  complex. The reaction of DPTC with  $\text{Cu}^{2+}$ , whether the anion is perchlorate or tetrafluoroborate, results in a very interesting structure, which comprises of eight DPTC ligands and eight  $\text{Cu}^+$  metal ions. The reaction of  $\text{Cu}^{2+}$  with DPTC results in the metal ion reducing to  $\text{Cu}^+$  and simultaneously the DPTC deprotonates to form the monoanionic form. The counter-anion acts as a template and the formation of the “ $\text{Cu}_8$ ” is a result of the presence of the anion. Reaction of copper (II) acetate with DPTC results in the  $[\text{Cu}_2(\text{DPTC})_2(\text{DPTCO})]$  complex. The structure contains three ligands and two reduced distorted tetrahedral  $\text{Cu}^+$  ions. Each  $\text{Cu}^+$  ion has four-coordinate geometry arising from the coordination of two different forms of the DPTC ligands. Two of the ligands present are the monoanionic DPTC, coordinating via the S-donor and terminal N-donor azo atoms. Whereas the third ligand has completely oxidised to form DPTCO, coordinating via both the terminal N-donor azo N-donor atoms, the sulphur atom bridges both of the metal ions.

# 1. Introduction

## 1.0 Supramolecular chemistry

Supramolecular chemistry has been defined by many chemists since its discovery, the most widely used definition is 'chemistry of molecular assemblies and of the intermolecular bond', described by Jean-Marie Lehn in 1995.<sup>1</sup> This definition can be further expressed as 'chemistry beyond the molecule' in which the most important factor is the method with which the components are held together. In contrast to molecular chemistry, which is predominantly based on the covalent bonding of atoms, supramolecular chemistry is based on reversible intermolecular interactions.<sup>2</sup>

Supramolecular chemistry is a multidisciplinary field, encompassing aspects of physical, organic, inorganic and biochemistry. The nature of supramolecular chemistry has allowed collaborations between a variety of specialists in a range of fields since its discovery by the groups of J-M. Lehn and C. J. Pederson in the late 1960's.

### 1.1 Origin of supramolecular chemistry

Supramolecular chemistry is a relatively new field of chemistry, although some concepts can be dated back to the beginning of modern chemistry it wasn't until the pioneering research by Pederson, Lehn and Cram on macrocyclic ligands that the foundations of this discipline were built.

Charles J. Peterson furthered the macrocyclic research conducted by the groups of Curtis, Busch and Jäger<sup>3-5</sup> and discovered the breakthrough in supramolecular chemistry, the synthesis of crown ethers.<sup>6, 7</sup> The development of this discipline was added to by the work of Donald Cram in 1986 on spherands<sup>8</sup> and the discovery of cryptands in 1967 by Jean-Marie Lehn.<sup>9</sup> In 1987, Cram, Lehn and Pederson received the Nobel Prize for their contributions within supramolecular chemistry, investigating the "host-guest" chemistry of three novel macrocyclic ligands for the coordination with metal ions (figure 1.1).

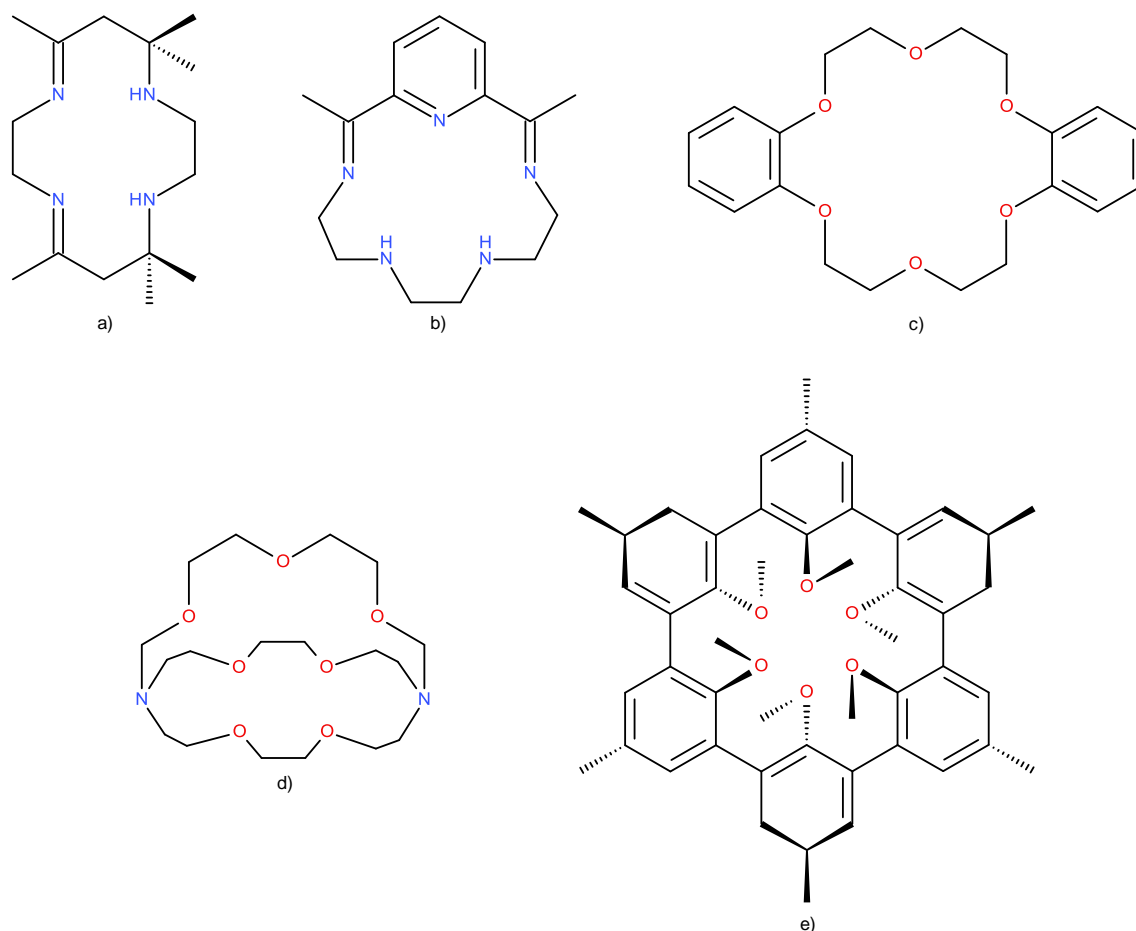


**Figure 1.1** Early macrocyclic ligands produced in supramolecular chemistry; a) Curtis 1962<sup>3</sup>, b) Busch 1964<sup>4</sup>, c) Pederson 1967<sup>6, 7</sup>, d) Lehn 1969<sup>9</sup> and e) Cram 1986<sup>8</sup>

Since the ground breaking work of Pederson, Lehn and Cram, supramolecular chemistry has become one of the fastest growing areas of modern day experimental chemistry, with recent research focussing on the design of increasingly complex systems.

## 1.2 Supramolecular interactions

The predominant feature of supramolecular chemistry is that the molecules are held together by noncovalent bonding interactions. The term 'noncovalent' includes a vast range of attractive and repulsive forces between the host, the guest and their surrounding environments.<sup>10</sup> These interactions may include; electrostatic forces, hydrogen bonding and  $\pi$ - $\pi$  stacking interactions.

The bond energy for a typical covalent bond is  $\sim 350 \text{ kJmol}^{-1}$ , whereas noncovalent interactions are generally weaker, these are summarised in table 1.1 below:

| Interaction      | Strength (kJmol <sup>-1</sup> )         |
|------------------|---|
| Ion-ion          | 200-300                                 |
| Ion-dipole       | 50-200                                  |
| Dipole-dipole    | 5-50                                    |
| Hydrogen bonding | 4-120                                   |
| Cation- $\pi$    | 5-80                                    |
| $\pi$ - $\pi$    | 0-50                                    |
| Van der Waals    | <5 (variable depending on surface area) |
| Hydrophobic      | Related to solvent-solvent energy       |

**Table 1.1** Summary of supramolecular interactions<sup>11</sup>

Although noncovalent bonds are generally weaker than covalent bonds, the strength of supramolecular chemistry lies in the combination of a number of weaker interactions.<sup>2</sup>

### 1.2.1 Ion-ion interactions

Ionic bonding is formed through an electrostatic attraction between two oppositely charged ions, although fairly uncommon in interactions in supramolecular chemistry, it is possible. Ionic bonds are formed due to the attraction between an atom that has lost an electron(s), forming a cation, and an atom that has gained an electron(s), forming an anion. The atoms are then attracted to each other by electrostatic attraction, forming an ionic bond. Usually the cation is a metal atom and the anion is a non-metal atom, the most commonly used example is sodium chloride (figure 1.2).

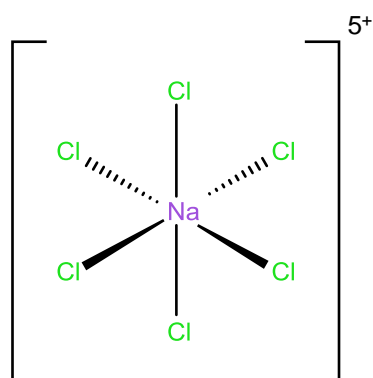


**Figure 1.2** Example of an ion-ion interaction

### 1.2.2 Ion-dipole interactions

Despite not being as strong as ion-ion interactions, ion-dipole interactions are extremely valuable for achieving strong bonds, a good example of ion-dipole interaction is when a crown ether and a metal ion are involved. An ion-dipole force results from the electrostatic attraction between an ion and a neutral molecular, in the case of potassium and [18]crown-6 (figure 1.3) the positively charged potassium cation attracts the polar lone pairs of the oxygen atoms in the crown ether receptor forming an ion-dipole interaction.

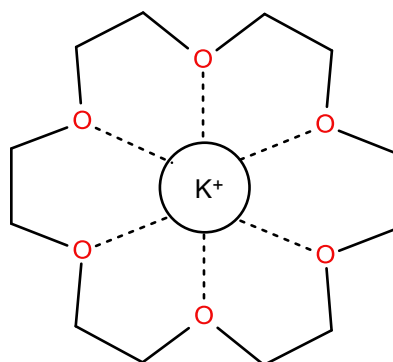


**Figure 1.3** Ion-dipole interactions between a metal cation and the oxygen lone pairs from the crown ether

### 1.2.3 Dipole-dipole interactions

Molecular dipoles occur when electrons are shared unequally in an atom, with the more electronegative atom pulling the bonding electrons closer, creating a partial negative charge and a partially positive charge on the other atom(s). Dipole-dipole interactions are formed when one dipole aligns with another dipole resulting in an attractive force between the pair of poles on adjacent molecules. This type of interaction is frequently observed in organic carbonyl compounds (figure 1.4).

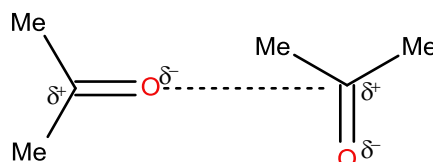


**Figure 1.4** Dipole-dipole interaction between two acetone molecules

### 1.2.4 Hydrogen bonding

Hydrogen bonding is a specific type of dipole-dipole interaction, which occurs between a hydrogen atom that is directly attached to an electronegative atom (usually F, N or O) and a dipole on an adjacent molecule or functional group (figure 1.5). The hydrogen bond has a range of geometries, lengths and strengths and is therefore crucial in supramolecular chemistry and nature. Hydrogen bonding plays an important role in determining the shape adopted by proteins and nucleic bases, the most famous example of hydrogen bonding occurs in DNA, where there are many hydrogen bond donors and acceptors holding the base pairs together.

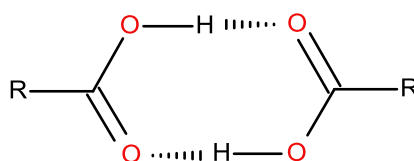


**Figure 1.5** An example of hydrogen bonding

### 1.2.5 $\pi$ - $\pi$ stacking interactions

$\pi$ - $\pi$  stacking interactions have a large influence on the molecule-based crystal structures of aromatic compounds.  $\pi$ - $\pi$  stacking forces occur between systems of aromatic rings, the intermolecular overlapping of the  $p$ -orbitals in the  $\pi$  conjugated system becomes stronger as the number of  $\pi$  electrons increase. Attractive forces can occur in two ways; 'face-to-face' whereby interactions occur between parallel aromatic rings (figure 1.6a) and 'edge-to-face' whereby a hydrogen atom from one ring interacts in a perpendicular orientation with the respect to the centre of another ring (figure 1.6b).

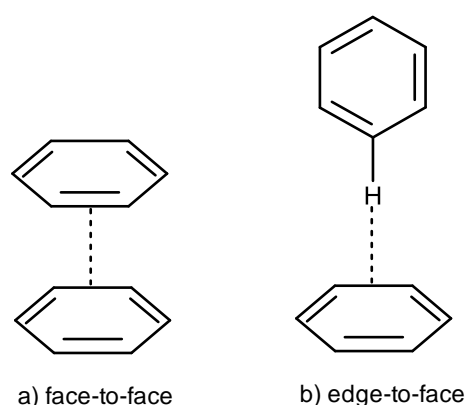


**Figure 1.6**  $\pi$ - $\pi$  stacking interactions

### 1.3 Host guest chemistry

Modern coordination chemistry has been expanding to mimic the complexity of biological systems such as the 'lock and key' principle described in 1894 by Emil Fischer. Emil Fischer's 'lock and key' principle can be summarised as 'the catalytic activity of enzymes is a result from the fact that the substrate fits tightly into a pocket in the surface of the enzyme, once the substrate is inside this pocket it is held in close proximity to the reactant which converts it to its product'.<sup>12</sup> Since the 'lock and key' principle was described in 1984 a great deal of attention has been spent on designing molecules that recognise and selectively bind each other, becoming known as host-guest chemistry.

In supramolecular chemistry the term host-guest chemistry is used to describe complexes that are composed of two or more molecules or ions that are held together by intermolecular interactions. Typically the host possessed a cavity which has the ability to recognise and bind specific guest species. Hosts can be separated into two categories; *Cavitands* and *Clathrands* (figure 1.7). *Cavitands* hosts usually have a large intermolecular cavity capable of completely enclosing the guest. Whereas, *Clathrands* possess extramolecular cavities and the guest is coordinated outside the host, usually in a cavity created between two or more molecules.<sup>10</sup>

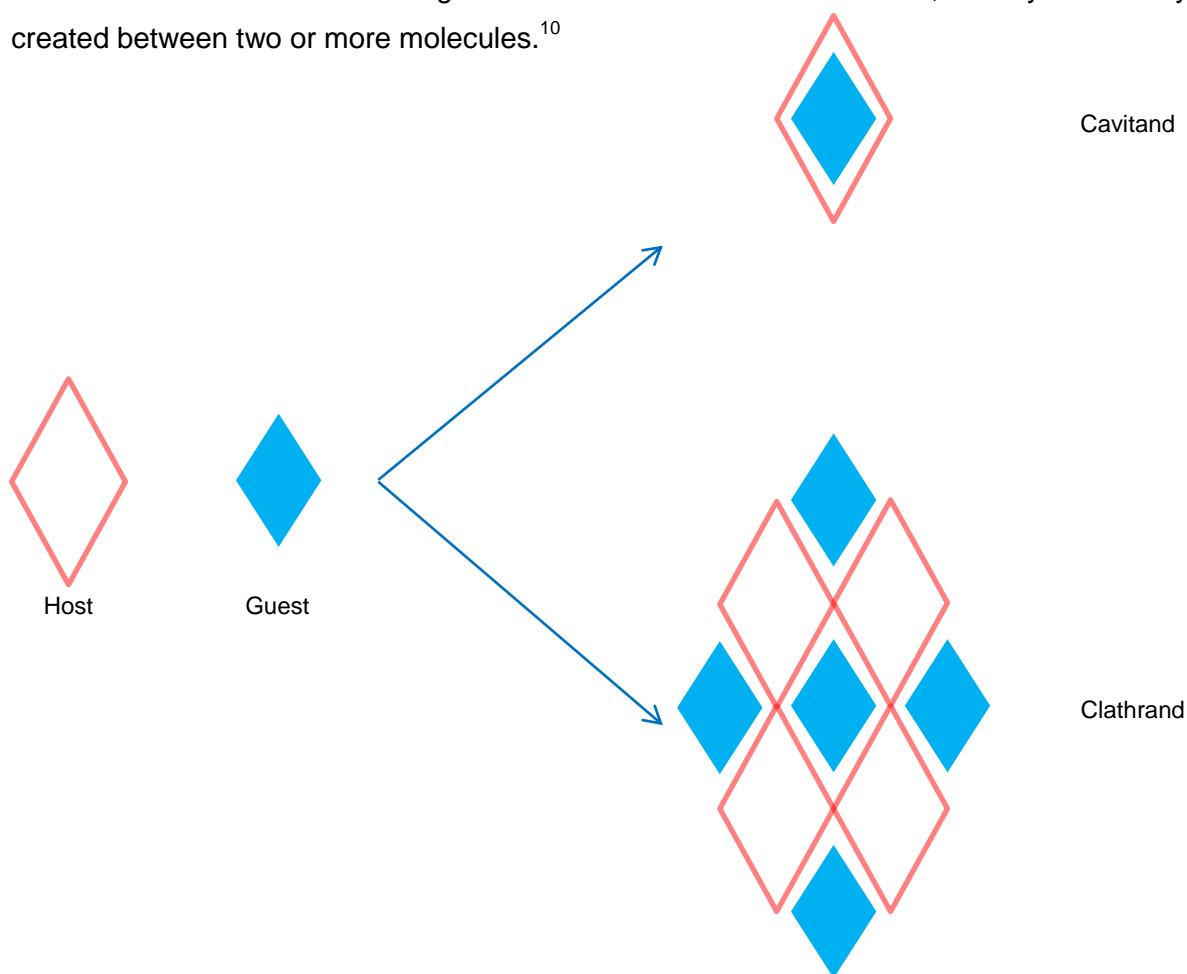


**Figure 1.7** Diagram illustrating the difference between a *Cavitand* and a *Clathrand* host molecules

Host guest chemistry encompasses the idea of molecular recognition, interacting via non-covalent bonding to sustain the three dimensional structures of proteins and other large molecules. For host guest interactions to occur the host molecule must not only be large enough to wrap around the guest molecule, but it must also possess the appropriate binding sites for the guest to bind to. If a host has a certain type of donor site for the guest to bind, it must contain an equal number of appropriate acceptor sites in a position which is practical for the intermolecular interactions between the host and guest to occur. If a host molecule is designed so that it possesses the required appropriate binding sites, geometry and size to accommodate a particular guest, then it is described as having selectivity towards that species. This in turn allows for so called 'designer molecules' to be created more simply and specifically.<sup>11</sup>

In 1986, Donald J. Cram defined host guest chemistry as 'the host is a molecule or ion whose binding sites converge in the complex and the guest component is any molecule or ion whose binding sites diverge in the complex'.<sup>13</sup> Common host molecules are cyclodextrins, calixarenes, carcerands and crown ethers.

### 1.3.1 Crown Ethers

Crown ethers are amongst the most simple and possible the most appealing macrocyclic ligands used in supramolecular chemistry due to their ability to act as hosts for cations and neutral molecules. They consist of a cyclic arrangement of alternating ether units linked by organic spacer groups, typically ethylene units and can exist in varying ring size. The series of O-donor atoms generates cavity suitable for coordination with guest species, usually s-block metal cations.

In 1967 Pederson accidentally discovered crown ethers whilst attempting to synthesis a linear di-ol, using the catethol (1,2-dihydroxybenzene) derivative as a starting material. Unbeknown to Pederson, his starting material was contaminated by some free catethrol (figure 1.8).<sup>10</sup>

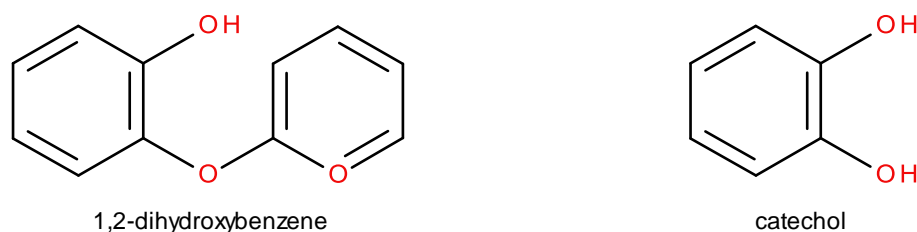


**Figure 1.8** Pederson's starting materials

The resulting product was a mixture of Pederson's desired compound along with a small amount of dibenzo[18]crown-6 (0.4% yield). Pederson was interested in the solubility properties of this unexpected compound, which was found to be sparingly soluble in methanol, the presence of a phenolic compound was confirmed by UV-spectroscopy. The addition of sodium hydroxide to the solution significantly enhanced the solubility.<sup>7</sup> Elemental analysis and mass spectroscopy confirmed the presence of the macrocycle dibenzo[18]crown-6 (figure 1.9)

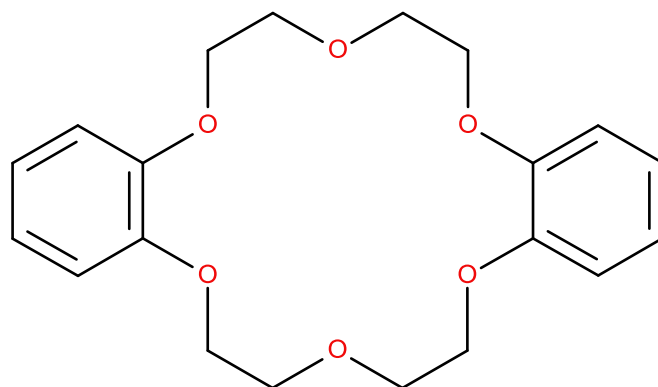


**Figure 1.9** Structure of dibenzo[18]crown-6

Pederson observed from a space filling model of dibenzo[18]crown-6 that a sodium cation can sit in the cavity of the crown, held together by the six oxygen donor atoms on the polyether rings holding the alkali metal cation by attractive electrostatic ion-dipole interactions. This fundamental result led to the rapid synthesis of a family of related macrocyclic species (figure 1.10). Pederson named his new macrocyclic structures crown ethers, due to their crown-like conformation when free in solution and when coordinated to a metal ion.<sup>14</sup> The first number, in the square brackets, refers to the number of atoms in the macrocycle and the second to the number of oxygen atoms in the ring.

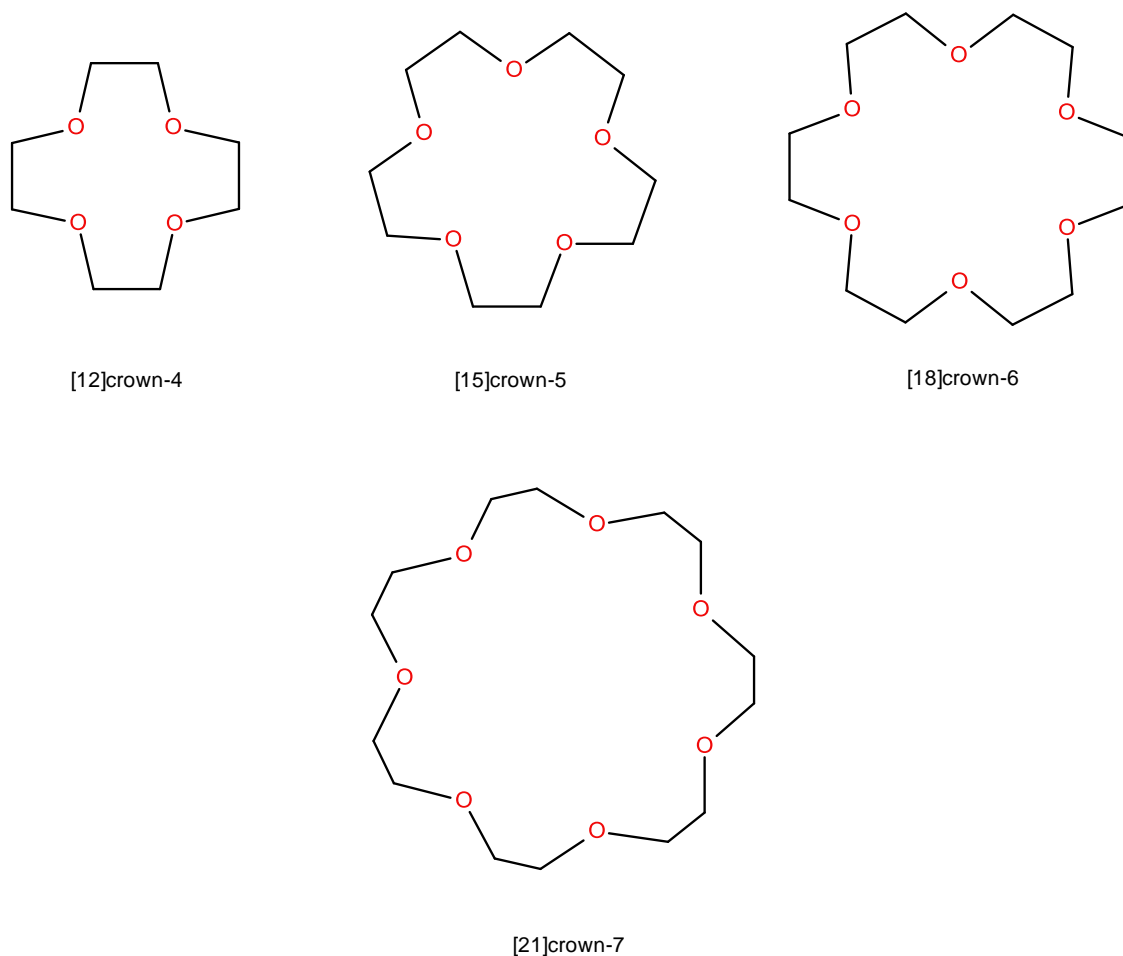


**Figure 1.10** Structures of crown ethers

The family of crown ethers consists of a cyclic array of differing numbers of ether oxygen atoms which generates different sized cavities which are suitable to bind alkali metal ions selectively. This selective binding of a particular guest by a host molecule forms the basis of molecular recognition and complementarity. A stronger complex is formed when there is a good match between the internal cavity volume of the host and the ionic size of the guest. Varying the number of O-donor or organic spacers within the macrocyclic unit changes the size of the cavity thus changing the most suitable cation for coordination with the host.

| Crown ether | Cavity diameter (Å) | Cation           | Diameter (Å) |
|-------------|---------------------|------------------|--------------|
| [12]crown-4 | 1.20-1.50           | Li <sup>+</sup>  | 1.36         |
| [15]crown-5 | 1.70-2.20           | Na <sup>+</sup>  | 1.90         |
| [18]crown-6 | 2.60-3.20           | K <sup>+</sup>   | 2.66         |
| [21]crown-7 | 3.40-4.30           | Cs <sup>+</sup>  | 3.38         |
|             |                     | Cu <sup>+</sup>  | 1.92         |
|             |                     | Ag <sup>+</sup>  | 2.52         |
|             |                     | Mg <sup>2+</sup> | 1.44         |
|             |                     | Ca <sup>2+</sup> | 2.20         |
|             |                     | La <sup>3+</sup> | 2.34         |
|             |                     | Lu <sup>3+</sup> | 2.00         |
|             |                     | Zr <sup>4+</sup> | 1.72         |

**Table 2** Comparison of different crown ethers and compatible cations<sup>10</sup>

For instance [12]crown-4 has an internal cavity of 1.20-1.50 Å, which is a perfect match for the coordination of Li<sup>+</sup> cations (diameter 1.36), whereas, it is not suitable for the larger K<sup>+</sup> ion (diameter 2.66). However, K<sup>+</sup> ions are complementary to [18]crown-6.

This relationship between cavity size, cationic radius and the stability of the resulting complex is well established and it was initially proposed that there is an optimal special fit between crown ethers and particular cations; this has been updated to include the flexibility of the crown ether unit. For example, although [15]crown-5 has a cavity diameter of 1.70-2.20 Å which is much smaller than the diameter of K<sup>+</sup> ions (2.66 Å), coordination still occurs as such macrocycles possess a certain degree of flexibility. Table 3 summarises the binding constants obtained for a selection of cations with various crown ethers:

| Crown ether      | Na <sup>+</sup> | K <sup>+</sup> | Rb <sup>+</sup> | Cs <sup>+</sup> | Ca <sup>2+</sup> | NH <sub>4</sub> <sup>+</sup> |
|------------------|-----------------|----------------|-----------------|-----------------|------------------|------------------------------|
| [12]crown-4      | 1.70            | 1.30           |                 |                 |                  |                              |
| [15]crown-5      | 3.24            | 3.43           |                 | 2.18            | 2.36             | 3.03                         |
| [18]crown-6      | 4.35            | 6.08           | 5.32            | 4.70            | 3.90             | 4.14                         |
| [21]crown-7      | 2.52            | 2.35           |                 | 5.02            | 2.80             | 3.27                         |
| Benzo[18]crown-6 | 4.30            | 5.30           | 4.62            | 3.66            | 3.50             |                              |

**Table 3** Binding constants obtained for various cations and a selection of crown ethers (log *K*, methanol, 20°C)<sup>11</sup>

Over recent years macrocycle developments have led to important roles in modern tools such as sensors<sup>15, 16</sup>, molecular switches<sup>10</sup> and dyes for spectrophotometric detection.<sup>17, 18</sup>

Following the discovery of crown ethers by Pederson in 1967 macrocyclic compounds can be extended to cryptands and Lariat ethers, as three dimensional analogues to the crown ether. In 1969 Lehn designed the first cryptand named after 'crypt' as the compound 'entombs' the guest cation.<sup>19</sup> Cryptands are cyclic or polycyclic assemblies that contain three or more binding sites held together by covalent bonds and are capable of encapsulating a metal ion entirely with a crown-like host enhancing cation selectivity.<sup>20</sup> Lariat ethers are a crown type macromolecule that contain a single podland side arm, contributing to the environment of the guest cation. Combining higher rigidity and preorganisation of the macrocyclic compounds with the addition of stability and flexibility of the podland complexation.<sup>21</sup>

#### **1.4 Self-assembly**

Supramolecular self-assembly has been described by many chemists over recent years; Steed, Turner and Wallace defined it as "the spontaneous and reversible association of molecular species to form larger, more complex supramolecular entities, according to the intrinsic information contained in the components".<sup>22</sup> The term self-assembly can only be applied to systems in which the assembly process is kinetically rapid and both completely reversible and replicable. Of paramount importance to this approach is the ability of the self-assembling species to correct their 'mistakes' during assembly to form the most thermodynamically stable product.<sup>20</sup>

Self-assembling species can be thought of as a dynamic combinatorial library in which that when several molecules join together many products are capable of forming; these will assemble, disassemble and reassemble until the most thermodynamically stable product is reached. The different molecules in the reaction are carefully and appropriately designed so that when they are placed together in solution the intermolecular interactions between the molecules control their orientation and spontaneously form a self-assembled structure.

The ultimate goal in supramolecular chemistry is to mimic the achievements of biological systems, there are many examples of self-assembly in nature, the two most impressive are the tobacco mosaic virus and DNA.

The tobacco mosaic virus (figure 1.11) is composed of 2130 identical subunits, each comprising 158 amino acids, which self-assemble and form a helical structure around a central strand of RNA, 6390 base pairs in length. The remarkable part about this virus is that if it was broken down into its component parts and mixed together the virus particle is correctly reassembled and regains full functionality.<sup>21</sup>

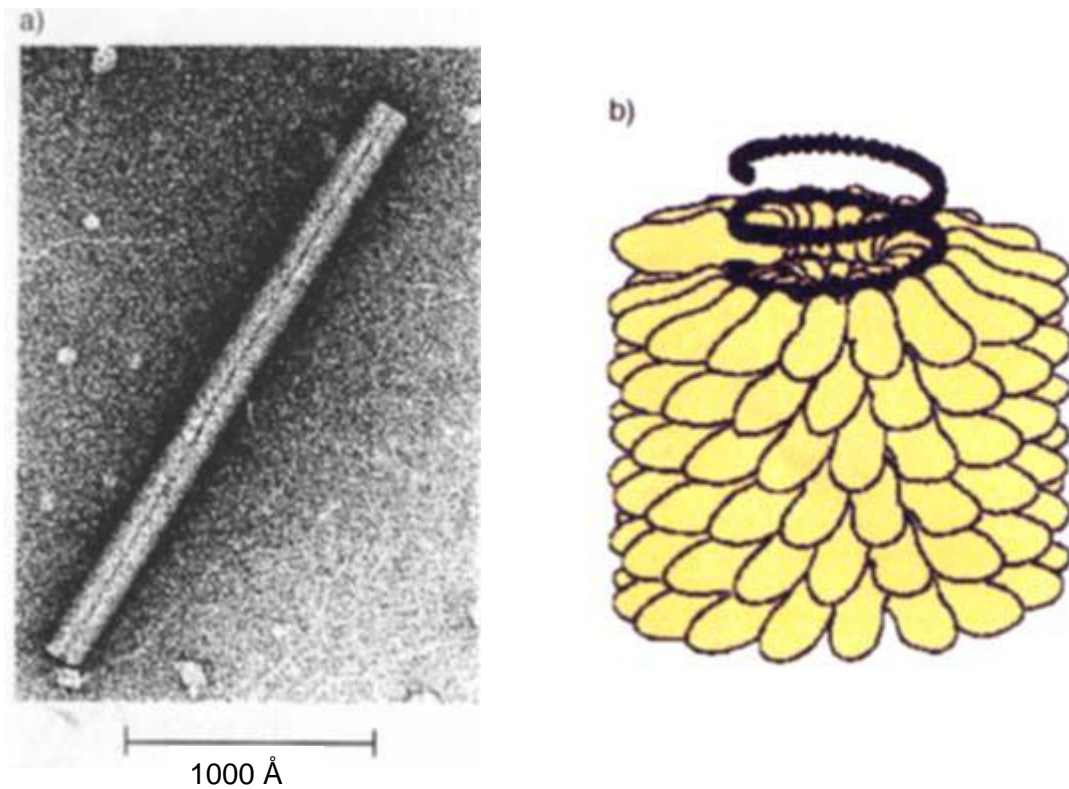


**Figure 1.11** The tobacco mosaic virus a) electron micrograph, b) schematic representation (the protein subunits are coloured yellow)<sup>22</sup>

The most famous example of self-assembly is the double helical structure of deoxyribonucleic acid (DNA). DNA consists of two right handed polynucleotide chains wind around a central axis defined by the hydrogen bonded complementary nucleic acids.<sup>13</sup> The two polynucleotide chains are held together by the attractive hydrogen bonding interactions between the base pairs resulting in the supramolecular structure. The base pairs adenine (A) and thymine (T), guanine (G) and cytosine (C) are complementary to each other and so the strands of DNA are programmed to only form in one particular way (figure 1.12).

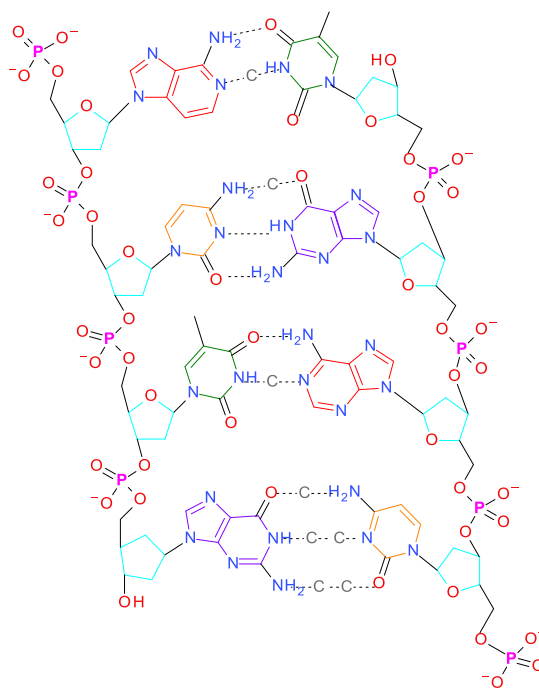


**Figure 1.12** The hydrogen bonding between the complementary base pairs of DNA

An extensive review into self-assembly in natural and unnatural systems by Philip and Stoddart in 1996 highlights the importance of establishing efficient synthetic routes for the construction of nanoscale architectures. To achieve this aim the chemist must have an understanding of the self-assembly of biological system; this goal can be accomplished by taking advantage and utilising the self-assembly between metal ions and ligands. With manipulation of these M-L interactions it is possible to produce a diverse array of supramolecular structures, termed metallosupramolecular chemistry.<sup>21</sup>

### 1.5 Metallosupramolecular chemistry

In 1994 Edwin Constable introduced the term metallosupramolecular chemistry to describe supramolecular assemblies that utilise the use of metal ion centres in order to self-assemble structures.<sup>11</sup> Exploiting the interactions between metal ions and donor groups from organic ligands has led to all manner of shapes and structures being created. Utilising coordination chemistry between the metal ions and the ligands, the ligands are able to bind metal centres by metal to ligands dative bonds, acting as 'supramolecular glue', holding the structures together.

The use of transition metal ions to direct assembly in metallosupramolecular chemistry is beneficial. Transition metals have very specific geometric requirements, allowing the chemist to program the coordination arrangement of a complex based on the different transition metal ions used to direct the assembly. Also, the dative bonds formed between



metal ion.<sup>25</sup> The potentially hexadentate ligand,  $L^a$ , used in the assembly contains a central pyrimidine ring with a bipyridine unit either side, meaning the ligand can partition into two bis-tridentate domains. Reaction of  $L^a$  with  $Ru^{II}(tpy)Cl_3$  results in the formation of a [2]-rack structure (figure 1.14).

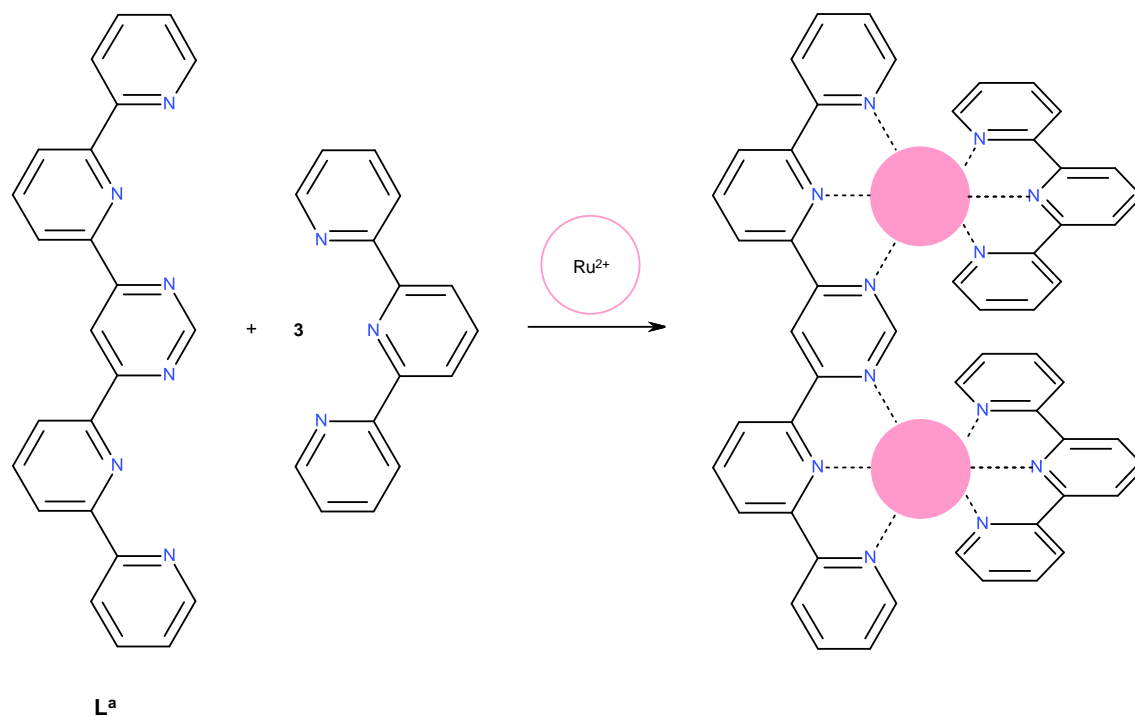


**Figure 1.14** Formation of a [2]-rack complex  $[Ru^{II}_2(L^a)(tpy)_2]^{4+}$

Each ruthenium metal centre has distorted octahedral geometry and is coordinated by the tridentate domain of ligand,  $L^a$  and a tridentate domain from a terpy unit. This results in the plane of the ligands being at right angles to each other, producing a structure that resembles a rack.

The trinuclear rack species based on similar components was reported in 1996 by Lehn and co-workers and is based on similar components.<sup>26</sup> Rack architectures can also be formed from bidentate ligands such as 2,2'-bipyridine and 1,10-phenanthroline with tetrahedral metal ions.<sup>27, 28</sup>

### 1.5.2 Ladders

Ladders are very similar to racks, the only difference is the addition of a second polytopic ligand, the auxiliary ligands are no longer protruding they are coordinated to another metal-backbone ligand unit. The nomenclature for ladders is  $[2n]L$ , when  $n$  is the number of 'rings' and the number 2 refers to the two sides which the rings connect.

The use of two linear polytopic ligands, auxiliary ligands and appropriate metal ions results in the formation of a ladder type complex. In 1996 Lehn and co-workers described ladder type complexes using the multidentate ligand,  $L^b$  which contains of a series of bidentate bipyridine domains.<sup>29</sup> Reaction of this ligand with the ditopic ligand bipyridinium,  $L^c$  and copper (I) ions in the correct stoichiometric amounts results in the formation of a ladder type complex (figure 1.15).

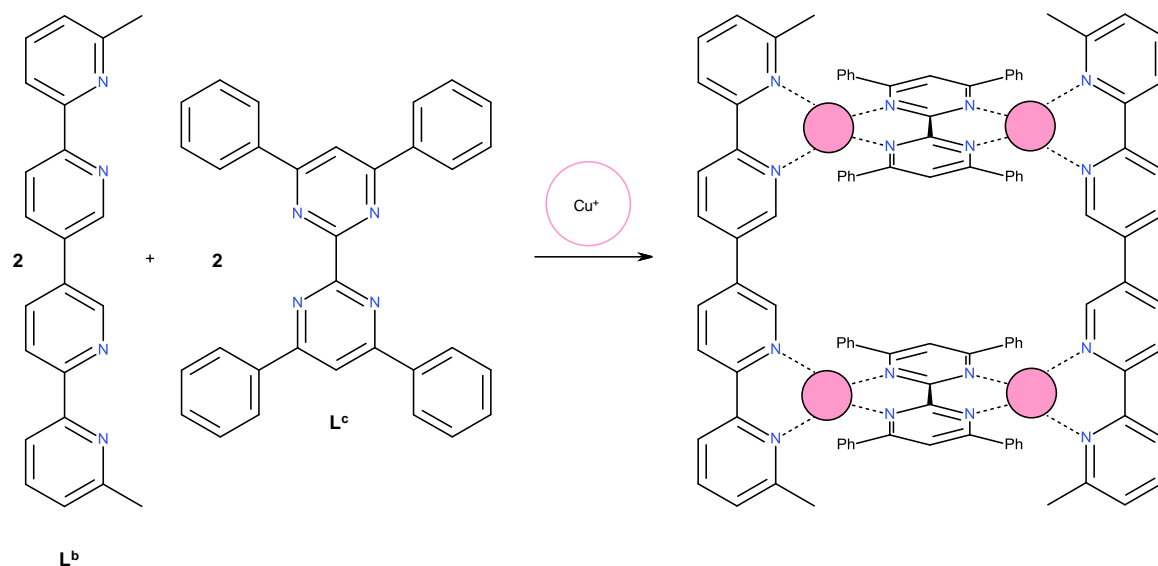


**Figure 1.15** Ladder type complex  $[Cu_4(L^b)_2(L^c)_2]^{4+}$

Each copper (I) metal ion has distorted tetrahedral geometry and is coordinated by two different bidentate binding domains, one from the bipyridinium ligand ( $L^c$ ) and the second from the multidentate ligand ( $L^b$ ). The bipyridinium ligand is then coordinated in exactly the same way to a second copper (I)-multidentate ligand unit, resulting in a structure that resembles a ladder. Many other examples of ladder complexes have been reported over recent years.<sup>30, 31</sup>

### 1.5.3 Grids

The molecular grid  $[m \times n]G$  consists of a square or rectangular matrix of metal centres and are formed from several polytopic ligand chains, the ligands self-assemble around the metal ion forming multiple coordination's to other ligand chains, resulting in a structure that resembles a grid. There are two types of grids; square grids occur when  $m$  and  $n$  are equal and rectangular grids when they are not. Square grids,  $[n \times n]$  are constructed from  $n$ -topic ligands with tetrahedral metal ions; much research has been carried out on  $[2 \times 2]$  square grid systems.<sup>32-35</sup> Polytopic ligands with octahedral coordination sited may generate grid architectures upon interaction with octahedral metal ions; however, the metallo-assembly is dependent on both the selection of metal ions and the organic component(s) employed.

Lehn and co-workers describe the potential for grid assemblies to be used in molecular scale information storage and processing, by preparing individual systems and researching the mechanistic aspect.<sup>36</sup> In 1994 Lehn and co-workers obtained one of the first grids, by combining a rigid tritopic ligand with  $\text{Ag}^+$  ions resulting in a 15-component reaction, comprising of six 6,6'-bis[2-(6-methylpyridyl)]-3,3-bipyridazine ligands and nine  $\text{Ag}^+$  ions resulting in a  $[3 \times 3]$  grid.<sup>37</sup> Lehn suggested that the arrangement of metal ions present could be used for information storage in the future, imagining that each metal ion corresponds to a 'bit' of information, allowing the storage of large amounts of information in very small volumes of material.

Hanan and co-workers reported the direct synthesis of a  $[2 \times 2]$ -grid array of octahedral metal ions with a potentially hexadentate ligand ( $\text{L}^a$ ).  $\text{L}^a$  comprises of two bipyridine units separated by a central pyrimidine ring, allowing the ligand to partition into two bis-tridentate domains. A  $[2 \times 2]$  grid type structure is generated upon reaction of  $\text{L}^a$  with cobalt (II) acetate in a 1:1 ligand-to-metal ratio, resulting in a complex consisting of four ligand strands and four cobalt cations (figure 1.16). Each metal centre occupies a distorted octahedral geometry formed by the coordination of two tridentate domains, one from each ligand, with the two ligands lying perpendicular to each other.<sup>38</sup> Further results have been reported showing that other metal ions displaying octahedral coordination geometry ( $\text{Ni}^{2+}$ ,  $\text{Zn}^{2+}$ ,  $\text{Cd}^{2+}$  and  $\text{Cu}^{2+}$ ) result in this  $[2 \times 2]$ -grid type array.

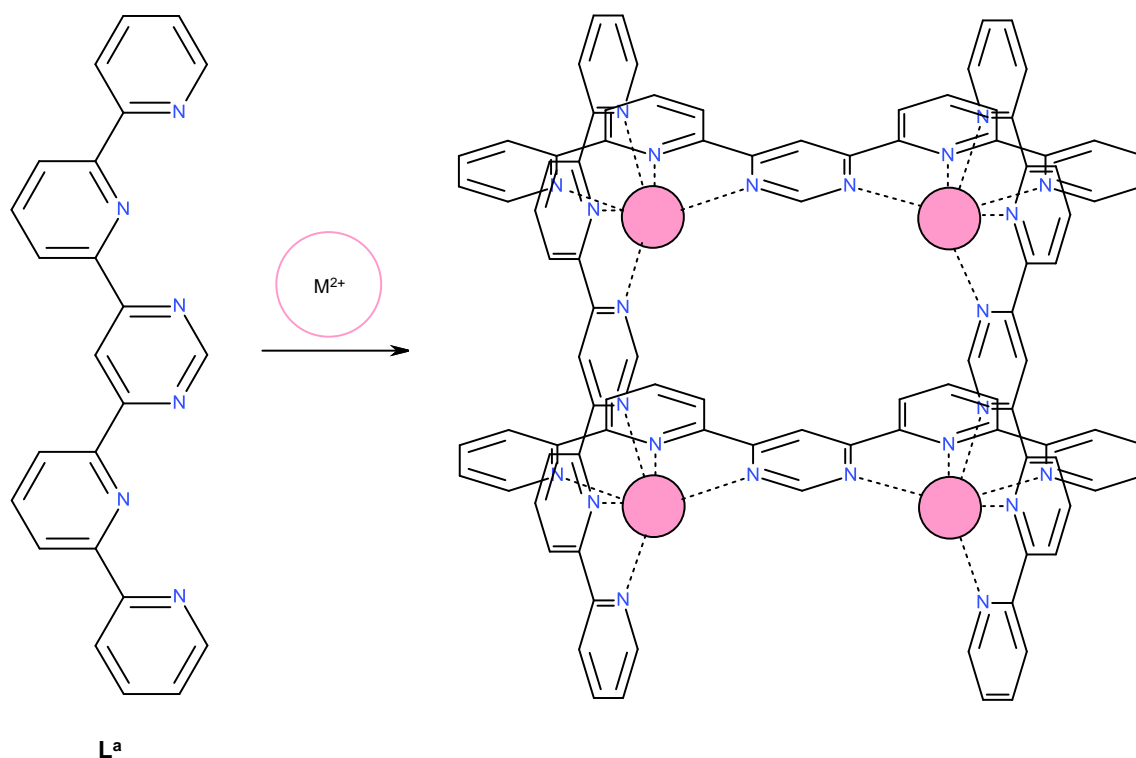


**Figure 1.16** Square [2 x 2] grid structure formed upon reaction of various metal cations with  $L^a$ . Where M could be  $Ni^{2+}$ ,  $Zn^{2+}$ ,  $Cd^{2+}$  or  $Cu^{2+}$

#### 1.5.4 Cages

Metallosupramolecular cage structures are formed spontaneously by metal directed self-assembly of several ligand strands to form a 3-dimensional cage structure with an internal cavity. Cages are slightly more complex than grid type architectures and have received a great deal of attention over recent years, not only for the self-assembly process that generates them, but also for the host-guest chemistry associated with their internal cavities. The central cavity within a cage structure is often large in size and are suitable for coordination of a range of guest species, including counter ions and solvent molecules, some of which act as templates directing the cage assembly.<sup>39</sup> Careful design of the ligand strands controls the cage assembly, altering the size and shape of the internal cavity can be achieved by modifying the position of the binding domain on the ligand. Furthermore, the size and shape of the cages can be modified by functionalising the ligands and using specific metal ions.

Fujita and co-workers have prepared many supramolecular cage structures in recent years, utilising the ability of the central cavity within the cage to encapsulate several guest species.<sup>40-46</sup> One particular example assembles from six metal ions and four ligands and has been shown to strongly bind a variety of neutral guests; from small aromatic guests such as benzene to large hydrophobic molecules such as *o*-carborane and adamantane

derivatives.  $L^d$  is a triangular molecular panel consisting of three binding sites, incorporation with an ethylene diamine protected  $Pd^{2+}$  complex, in the ratio of 2:3, successfully produced the  $M_4L_6$  cage. In the complex the four triangular  $L^d$  ligands are linked together at the corners of the triangles by a  $Pd^{2+}$  metal ion, resulting in every alternate face of the octahedron containing a molecular panel.<sup>47, 48</sup>

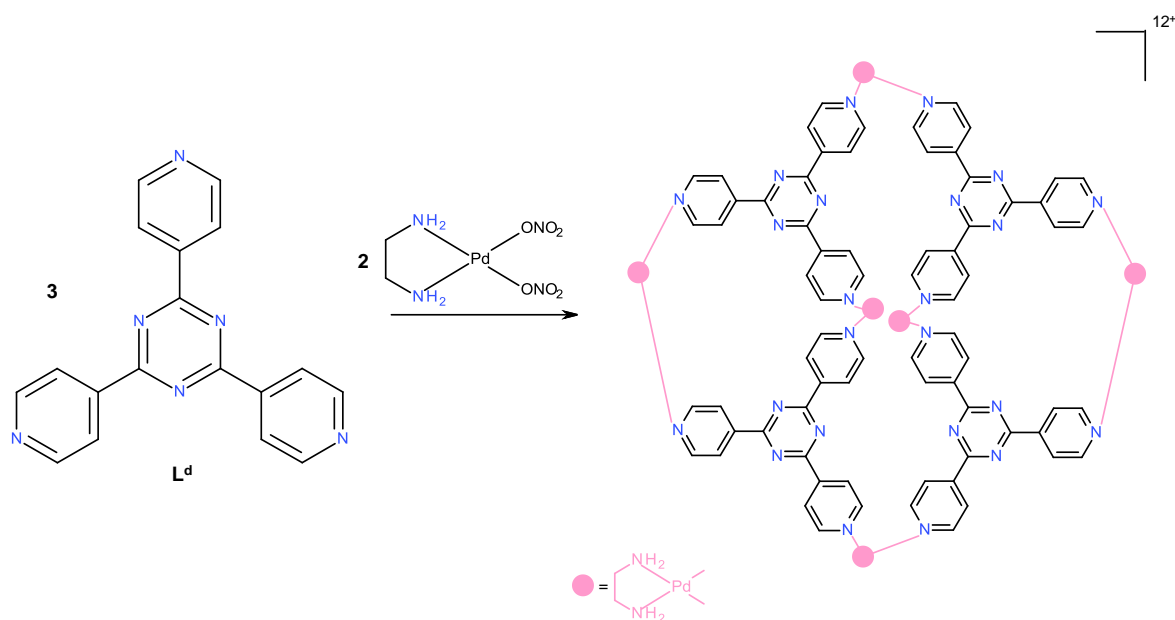


**Figure 1.17** Formation of the cage complex  $M_4L_6$

Ward and co-workers have published numerous examples of coordination cages in recent years, demonstrating that well designed molecules can self-assemble into many complex cage structures.<sup>49-56</sup> In 2006 a tetradentate ligand,  $L^e$ , containing two bidentate pyrazolyl-pyridine donor units connected to a 1,8 naphthyl spacer was synthesised. Reaction of  $L^e$  with various metal ions resulting in the formation of the dodecanuclear coordination cages  $[M_{12}(L^e)_{18}]X_{24}$  ( $M = Co^{2+}$ ,  $Cu^{2+}$  or  $Cd^{2+}$ ) ( $X^- = ClO_4^-$  or  $BF_4^-$ ) (Figure 1.18).<sup>57</sup> Each metal ion is coordinated by three bidentate pyrazolyl-pyridine units, in meridonal arrangement, resulting in a distorted octahedral geometry. In the complex the 12 metal ions occupy the vertices of a truncated tetrahedron and a bridging ligand spans each of the 18 edges. The central cavity of each cage can accommodate four counterions.

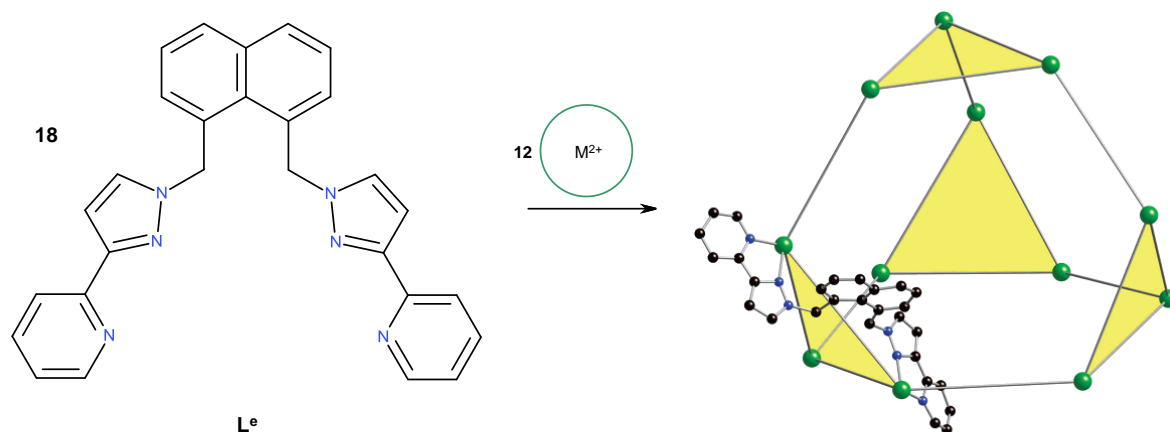


**Figure 1.18** Dodecanuclear cage  $[M_{12}(L^e)_{18}]X_{24}$ .<sup>57</sup>

Ward and co-workers furthered this work by preparing the ligand,  $L^f$ , similar to the previous ligand, only the pyrazolyl-pyridine units are connected to the naphthyl spacer in the -1,5 position. Reaction of  $L^f$  with cobalt (II) tetrafluoroborate in a 3:2 ratio results in an octahedral cubic coordination cage  $[Co_8(L^f)_{12}][BF_4]_{16}$  (figure 1.19) consisting of a cubic array of metal ions with a bis-bidentate ligand spanning each cage.<sup>55, 58, 59</sup>

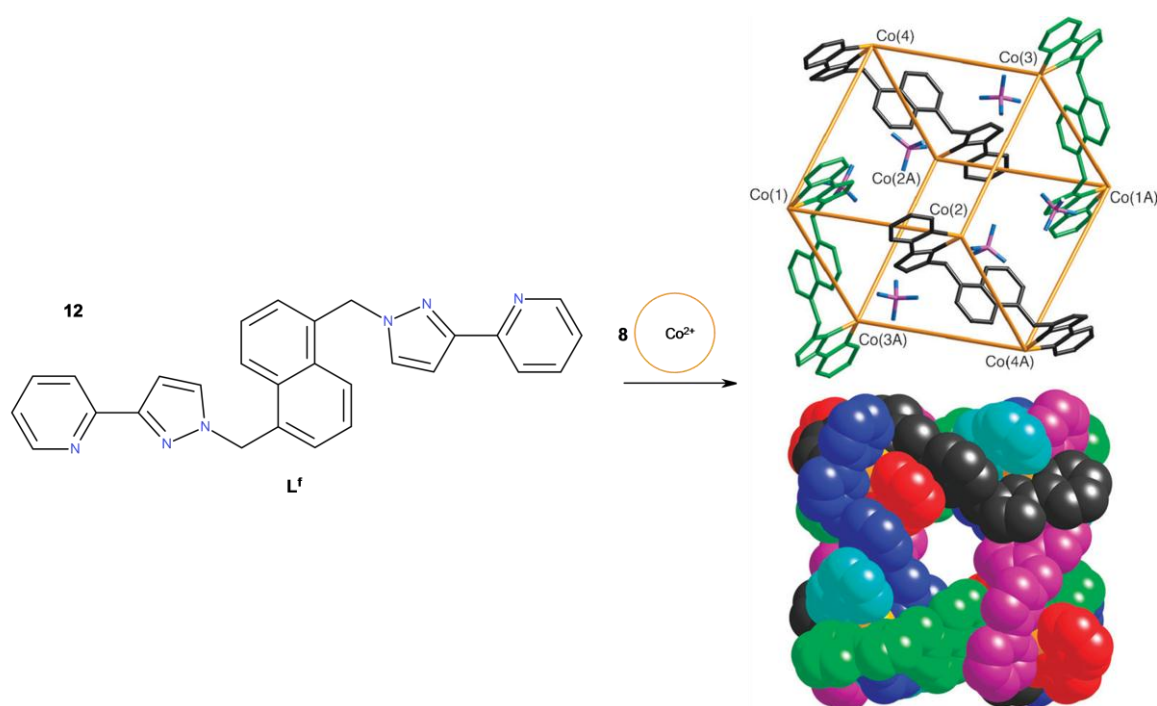


**Figure 1.19** Octahedral cubic cage  $[Co_8(L^f)_{12}]^{6+}$ . Top right: a partial view showing only four of the  $L^f$  ligands (the  $BF_4^-$  anions shown are those that occupy the spaces in the centre of each of the six faces of the cube). Bottom right: space filling view of the complete cage<sup>55, 58, 59</sup>

The cubic cage encloses a central cavity with a volume of 407 Å<sup>3</sup>; importantly the crystal structure shows that the central cavity is occupied by solvent (MeOH) molecules, not counter ions, meaning that the guest will not have to compete with anions for occupation in the central cavity. The interaction between the cubic cage and 23 compounds was investigated, binding coumarin with a higher selectivity compared to other potential guest of similar size and shape. The cubic cage binds guests via a combination of hydrogen bonding, non-polar interactions and solvophobic interactions. Importantly in the formation of this cage is the geometric isomerism of the eight metal centres, six have *mer* coordination geometry, whereas the other two have *fac* coordination geometry. The presence of the *fac* isomers 'opens' the cage as the metal ions are exposed to the interior cavity of the cage, meaning that the bulky naphthyl substitutes lie stacked to a chelating pyrazolyl-pyridine fragment. This leaves the protons from the three methylene groups orientated so to define a pocket for CH---X interactions, relatively close to the metal centre.<sup>60</sup> Further work included the addition of hydroxy groups to the para position of the pyridine units, rendering the octahedral cubic cage water soluble.<sup>61</sup>

### **1.6 Helicates**

The self-assembling double helical structure of DNA, where two right handed polynucleotide chains wind around a central axis defined by the hydrogen bonded complementary nucleic acids,<sup>62</sup> has directly inspired one of the most fascinating areas of supramolecular chemistry, the helicate. Helicates are oligonuclear coordination complexes where linear polydentate ligands wrap around metal ion(s). The term helicate was first introduced in 1987 by Lehn and co-workers to describe a polynuclear helical double strand.<sup>63</sup> Alternatively helicates can be defined as compounds that are characterised by a helical axis that possesses chirality associated with a screw like sense about a fixed axis. The pitch of the screw is the distance between the turns of the helix.<sup>10</sup>

Since the discovery of helicates in 1987 by Jean-Marie Lehn a vast amount of research into the principles of self-assembly and recognition has been conducted.<sup>64, 65</sup> These studies have demonstrated that the formation of a helicate is dependent on the design principle of both the ligand and the metal ion used. The ligand may vary in number and position of the binding sites and in turn be capable of coordination with specific coordination geometry, or be flexible enough to form a variety of metallosupramolecular architectures. The metal ion may have preferred coordination geometry, vary in size, and vary in binding strength and stability.<sup>64</sup> Resulting in careful preprogramming of the system in order to achieve the desired result.

### 1.6.1 Helicate Nomenclature

There are a wide variety of different types of helicate species; due to this the nomenclature can become quite complicated. To differentiate between the different types of helicates certain aspects need to be taken into account; (a) number of ligands, (b) number of metal centres and (c) number of binding sites. A simple helicate will be named in terms of number of metal centres and the number of ligand strands involved, for instance *mononuclear*, *dinuclear*, *trinuclear*, *tetranuclear*...etc., refer to; one, two, three and four metal centres respectively. The helicate can be made up from two ligand strands resulting in a *double* helicate or three ligand strands resulting in a *triple* helicate. For example a *dinuclear double* helicate refers to a helicate species consisting of two metal centres and two ligand strands. The assembly of the ligand strands leads to another classification, identical coordinated strands are termed *homostranded* helicates and a helicate made from different ligand strands leads to *heterostranded* helicates, the resulting helicates are termed *homoleptic* and *heteroleptic* respectively. Two key types of isometric forms can exist within helicates made from asymmetric ligands possessing different binding domains, resulting in directionality within the strands, according to the orientations of the coordinated ligand strands, termed head-to-head (*HH*) and head-to-tail (*HT*). The terms *homo* and *hetero* are also introduced when helicates consist of different metal centres; for example a helicate consisting of two identical ligand strands coordinated by both  $\text{Zn}^{2+}$  and  $\text{Hg}^{2+}$  ions would be termed a *heterometallic dinuclear double* helicate.

Each category of classification can be further divided according to whether the stereochemical requirements of the metal centres are fulfilled by the ligands. *Saturated* helicates occur when the donor atoms of the ligand strands fulfil the stereochemical requirements of the metal centres. The term *unsaturated* helicate results when the stereochemical requirements of the metal centre have not been fulfilled by the ligand strands, leading to the combination of ligand strands and supplementary counter anions or solvent molecules. Helicates may also be termed *meso-helicates* or *mesocates* when the ligand strands coordinate the metals in a side-by-side fashion and not a helical fashion, the metal ions in these species have different stereochemistry ( $\Lambda\Delta$  or  $\Delta\Lambda$ ) and result in an achiral assembly.

### 1.6.2 Homonuclear Helicates

Homoleptic helicates are assembled from identical ligand strands and have been studied extensively by numerous research groups.<sup>63, 66</sup> Constable and co-workers have over the years used oligopyridines in the construction of helical complexes; for example the potentially sexidentate ligand  $\text{L}^9$ .<sup>67</sup> They demonstrated that sexipyridine,  $\text{L}^9$ , formed homoleptic binuclear complexes of the type  $[\text{M}_2(\text{L}^9)_2]^{4+}$  ( $\text{M} = \text{Mn}^{2+}$ ,  $\text{Fe}^{2+}$ ,  $\text{Cu}^{2+}$  or  $\text{Cd}^{2+}$ ). The

metal centres are in identical six coordinate environments and are coordinated to three nitrogen atoms from a terpyridyl group from each ligand (figure 1.20).<sup>68, 69</sup>

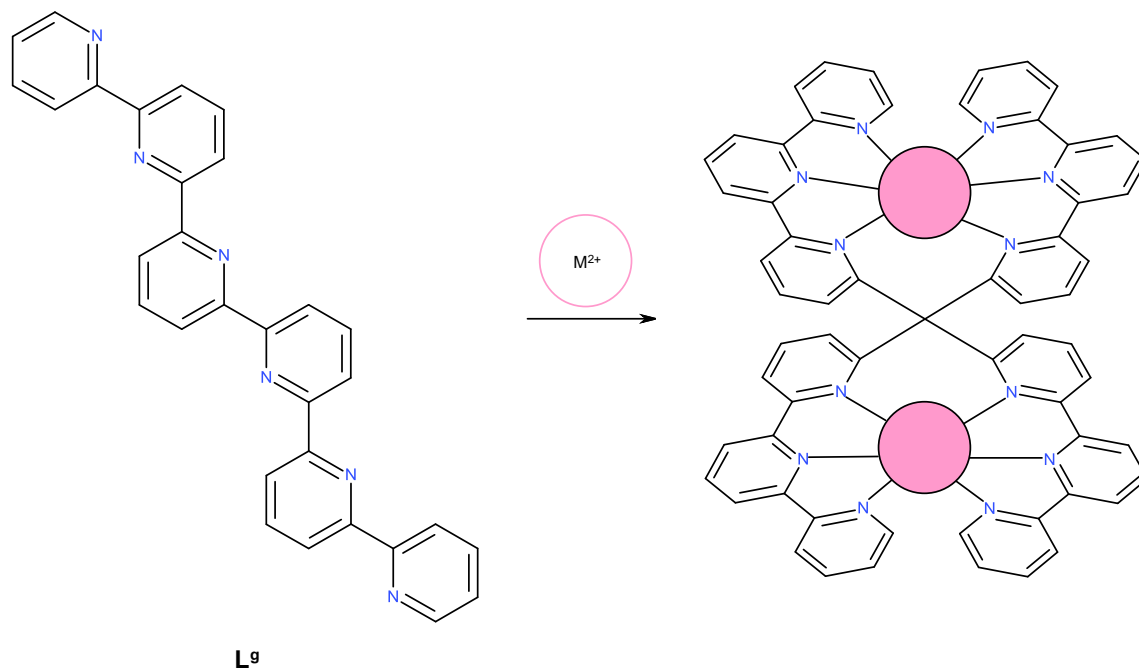


**Figure 1.20** Formation of the homoleptic helicate  $[M_2(L^9)_2]^{4+}$  ( $M = Mn^{2+}, Fe^{2+}, Cu^{2+}$  or  $Cd^{2+}$ )

However, reaction of **L<sup>9</sup>** with a tetrahedral metal ion, results in the formation of a different complex of the type  $[M_3(L^9)_2]^{3+}$  ( $M = Cu^+$  or  $Ag^+$ ). The tetrahedral metal centres have distorted tetrahedral geometry and are coordinated to a pair of adjacent pyridyls from each ligand (figure 1.21).

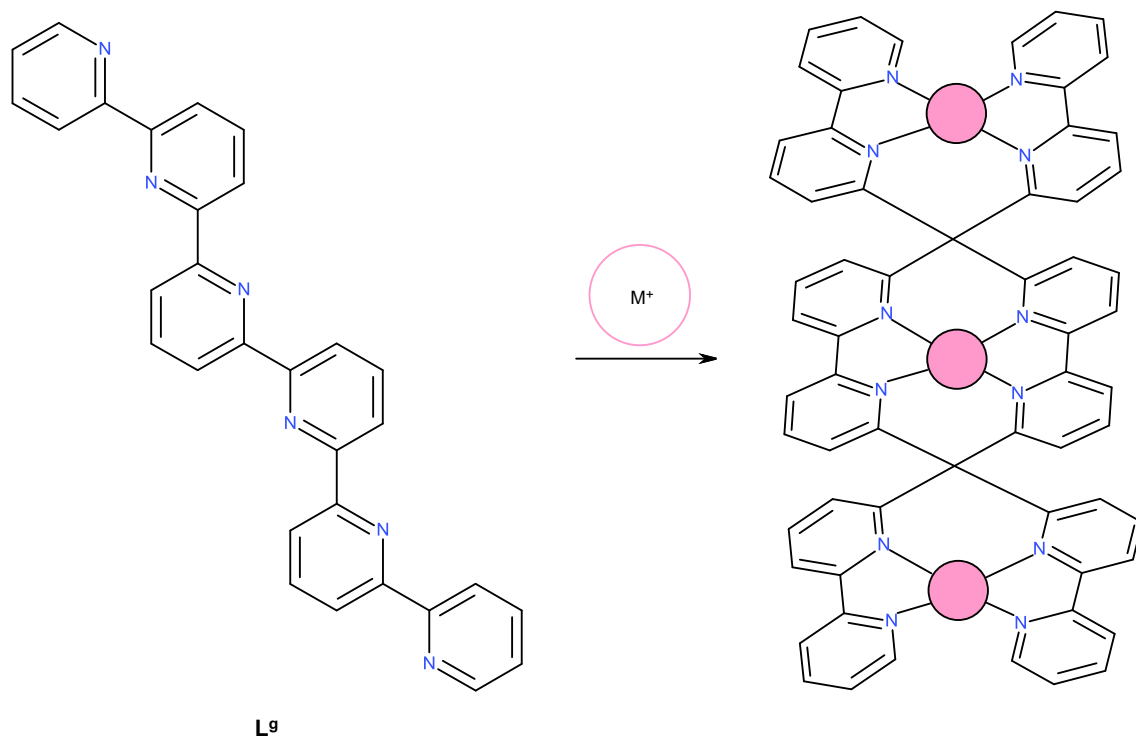


**Figure 1.21** Formation of the homoleptic helicate  $[M_3(L^9)_2]^{3+}$  ( $M = Cu^+$  or  $Ag^+$ )

In a double stranded helical polymetallic complex derived from oligopyridines the number of metal centres can vary depending on the coordination geometry of the transition metal. Figure 1.22 demonstrates the different coordination patterns of sexipyridine.<sup>70</sup>

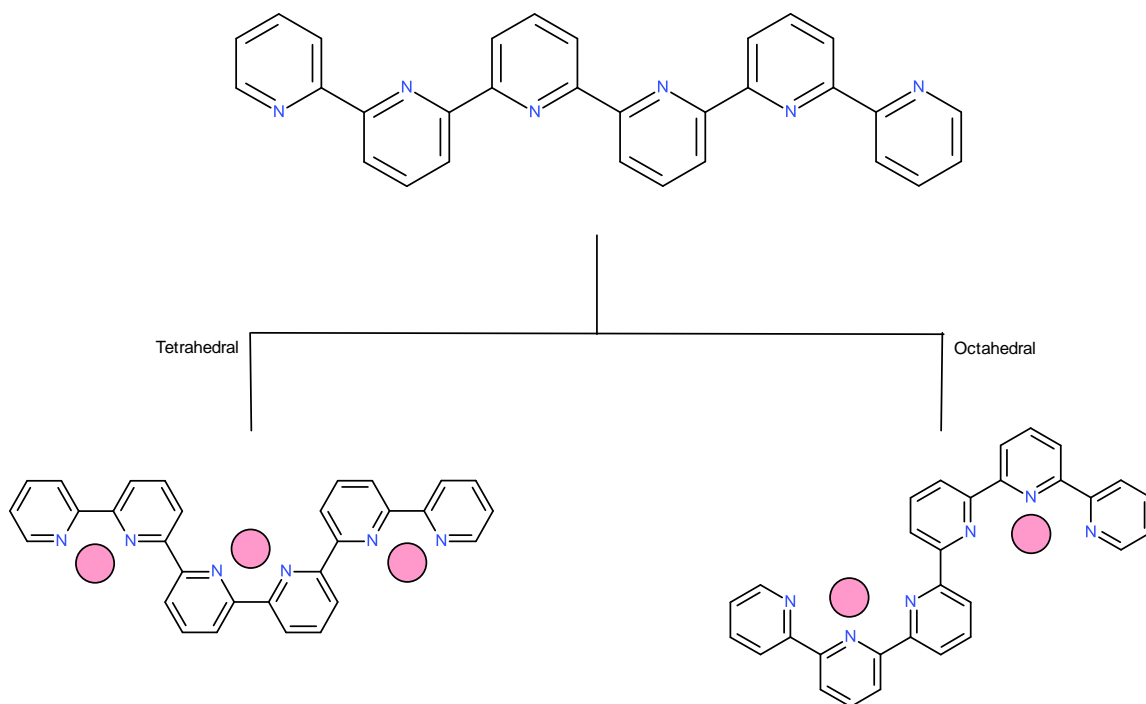


**Figure 1.22** Tetrahedral and octahedral recognition by sexipyridine

### 1.6.3 Heteroleptic Helicates

Heteroleptic helicates are not as common as the previous homoleptic helicates; however complexes composed of different ligand strands have been reported.<sup>71, 72</sup> In 1996 Lehn and co-workers prepared two similar ligands,  $L^h$  containing three bipyridine units linked via a methylene spacer and the other,  $L^i$ , containing three terpyridine units. Reaction of a mixture of these ligands with  $Cu^{2+}$  ions results in a heteroleptic trinuclear double helicate. The  $Cu^{2+}$  metal centres are pentacoordinated; however they display two different geometries; the central  $Cu^{2+}$  ion occupies distorted trigonal bipyramidal coordination, where the two terminal  $Cu^{2+}$  ions are square pyramidal. One bipyridine  $L^h$  strand and one terpyridine unit  $L^i$  strand are wrapped around each other and held together by three  $Cu^{2+}$  ions. Each  $Cu^{2+}$  metal centre is coordinated by one bipyridine unit from  $L^h$  and a terpyridine unit from  $L^i$ .<sup>73, 74</sup>

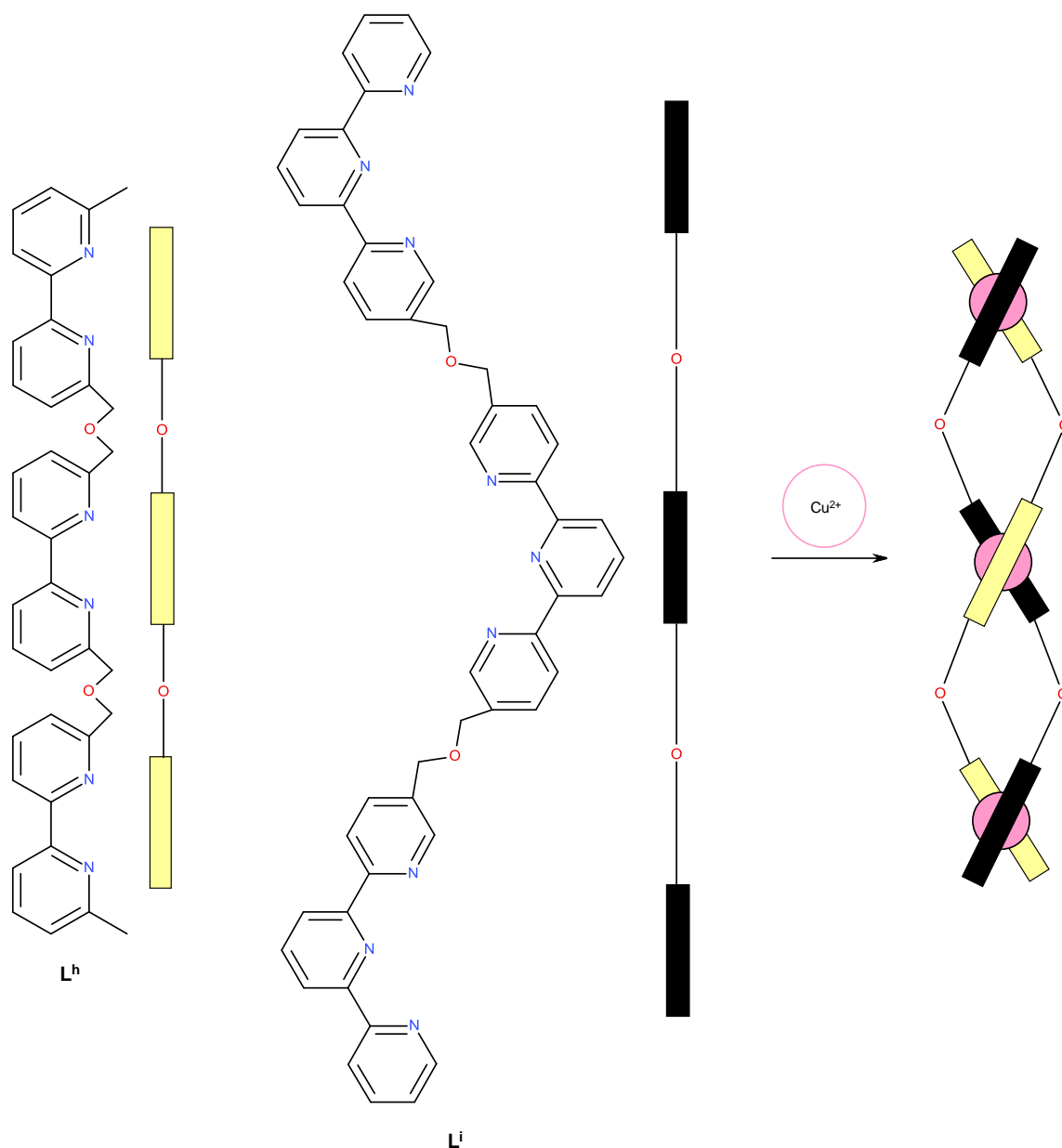


**Figure 1.23** Representation of the formation of the heteroleptic helicate  $[Cu_3(L^h)(L^i)]^{6+}$

#### 1.6.4 Unsaturated Helicates

Unsaturated helicates arise when the stereochemical requirements of the metal centres are not fulfilled by the ligands, resulting in incomplete coordination. This occurs as a result of a discrepancy between the intrinsic information encoded in the components of the complex and results in the metal cation completing its coordination sphere by coordinating to anions or solvent molecules.<sup>71, 75, 76</sup> The most studied unsaturated helicates are those derived from the quinquipyridine ligand,  $L^j$ , an example of this has been demonstrated by Constable and co-workers.<sup>77</sup> Reaction of quinquipyridine with  $Cu^{2+}$  results in a dinuclear double helicate  $[Cu_2(L^j)_2(OAc)]^{3+}$ . The quinquipyridine ligands partition into bipyridine and terpyridine subunits and coordinate the  $Cu^{2+}$  metal centres in a head-to-head assembly.

The  $\text{Cu}^{2+}$  metal centres occupy different binding domains: one is pseudooctahedrally coordinated by the terpyridine unit from two different ligands and the second  $\text{Cu}^{2+}$  is five-coordinate arising from the coordination of a bipyridine unit from two different ligands together with a monodentate acetate anion (figure 1.24).

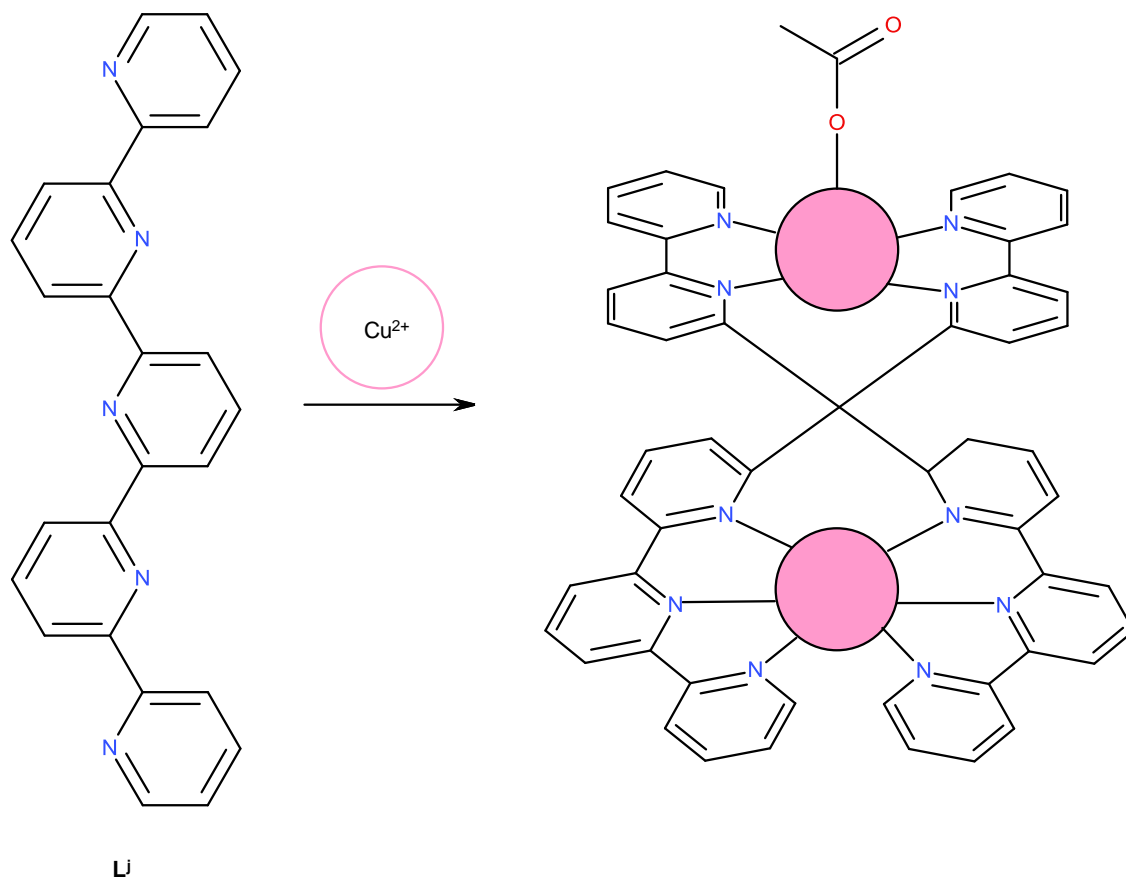


**Figure 1.24** Illustration of the formation of the unsaturated helicate  $[[\text{Cu}_2(\text{L}^1)_2(\text{OAc})]^{3+}$

### 1.6.5 Directional Helicates

A heteroleptic helicate occurs when an asymmetric ligand reacts with a metal cation resulting in the formation of two helical isomers; head-to-head (*HH*) and head-to-tail (*HT*). The lack of symmetry in the ligand strand gives it directionality and allows for a 'head' and a 'tail' to be designated on the strand. The directionality depends on the coordination geometry of the metal centre and whether the 'heads' or 'tails' of the ligand strands are coordinated to the opposite or same metal centre. In a head-to-head heteroleptic helicate the identical binding units of each ligand strands are coordinated to the same metal ion, where in a head-to-tail helicate different binding units of each ligand strands coordinate the same metal ion.<sup>78, 79</sup> In 1996 Constable and co-workers reported two asymmetric ligands  $\text{L}^k$  and  $\text{L}^l$ , consisting of an ortho-linked quaterpyridine ligand with different attachments, a methyl unit and tert-butyl substituent respectively, which show selectivity for the two

possible isomers.<sup>80</sup> Reaction of both of these ligands with  $\text{Cu}^+$  ions results in a dinuclear double helicate, but only one of the ligands show directionality in which isomer forms.

Upon reaction of  $\text{L}^k$ , the methyl substituent, with  $\text{Cu}^+$  ions results in the formation of both conformation helical isomers in a 1:1 mixture, and reaction of  $\text{L}^l$ , the tert-butyl substituent, with  $\text{Cu}^+$  ions; only the *HH* isomer forms. The  $\text{Cu}^+$  metal ions in all of the helicates occupy distorted tetrahedral coordination geometry, resulting from the coordination of two bidentate bipyridine units from each ligand (figure 1.25). The directionality in  $\text{L}^l$  arises from the short contacts between the tert-butyl substituents in the *HT* isomer, therefore only the *HH* $[\text{Cu}_2(\text{L}^l)_2]^{2+}$  isomer is formed.

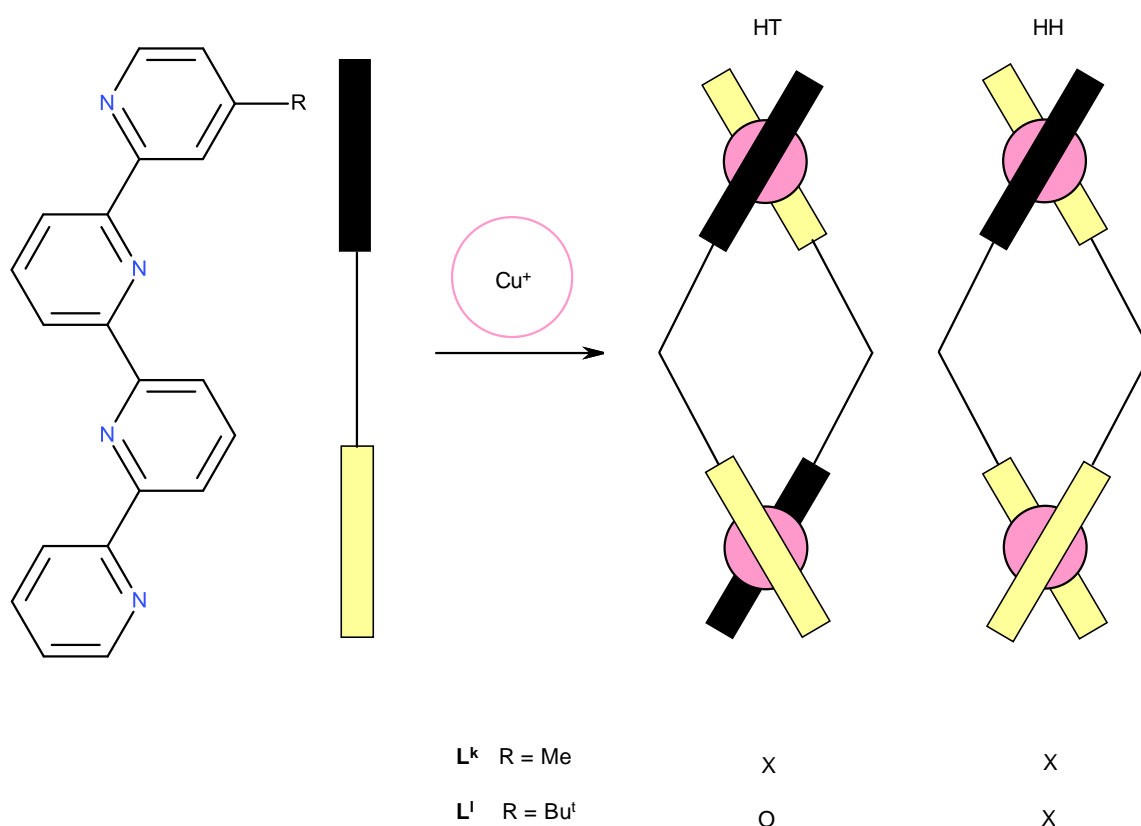


**Figure 1.25** Formation of *HH* and *HT*- $[\text{Cu}_2(\text{L}^k)_2]^{2+}$  and *HH*- $[\text{Cu}_2(\text{L}^l)_2]^{2+}$

The asymmetrical ligand  $\text{L}^m$  was reported in 2003 by Rice and co-workers, upon reaction with  $\text{Cu}^{2+}$ , in a 1:1 ratio the head-to-tail dinuclear helicate  $[\text{Cu}_2(\text{L}^m)_2]^{4+}$  formed.<sup>81</sup> Each ligand splits into a tridentate domain and a bidentate domain, twisting along the thiazole-pyridyl bond and coordinates the metal ion via the nitrogen donor atoms. Both of the  $\text{Cu}^{2+}$  metal ions are five coordinate and display square-based pyramidal geometry, resulting from the coordination of a bidentate (pyridyl-thiazole) unit from one ligand and a tridentate (terpyridyl) unit from the other (figure 1.26).

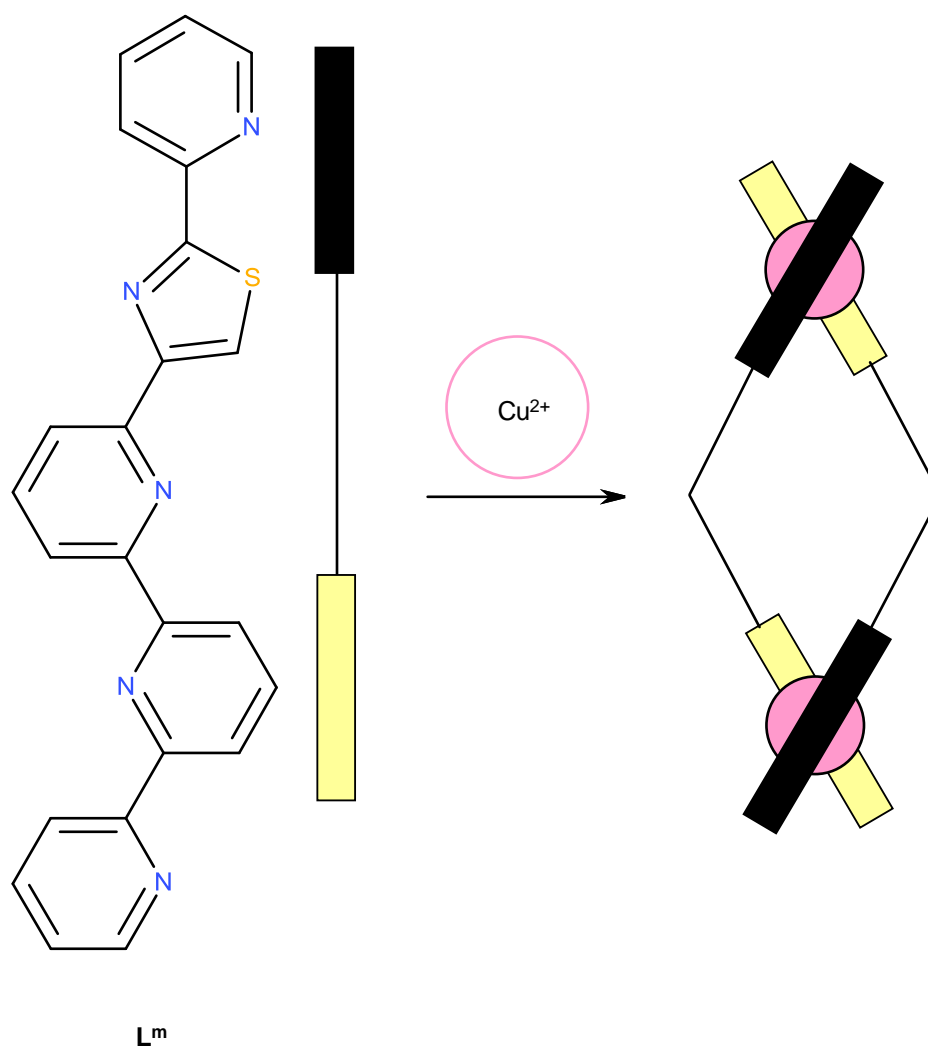


**Figure 1.26** Head-to-tail dinuclear double helicate  $[Cu_2(L^m)_2]^{4+}$

### 1.6.6 Heteronuclear Helicates

A heteronuclear helicate species is another type of helicate, where the metal ions involved in the complex are different.<sup>82-84</sup> An elegant example of heteronuclear helicate has been demonstrated by and co-workers in 2009, where a ligand containing two isomeric tridentate nitrogen donor domains produces a heteroditopic ligand capable of selectively binding  $Hg^{2+}$  and  $Zn^{2+}$  metal ions in a double stranded helicate.<sup>85</sup>

$L^n$  comprises of two isomeric tridentate domains connected via a flexible oxo-propylene bridge, containing a pyridyl-thiazole-pyridyl (py-tz-py) binding domain and a thiazole-pyridyl-pyridyl (tz-py-py) binding domain. Upon reaction of  $L^n$  with both  $Hg^{2+}$  and  $Zn^{2+}$ , in the ratio of 2:1:1, a heteronuclear dinuclear double helicate of  $[HgZn(L^n)_2]^{4+}$  forms (figure 1.27). The ligand strands in the helicate are aligned in a *HH*-manner; the  $Hg^{2+}$  ion displays pseudo-octahedral coordination geometry and is coordinated by the py-tz-py binding domain from both ligands. The  $Zn^{2+}$  metal ion displays pseudo-octahedral coordination

geometry and is coordinated by the other isomeric tz-py-py binding domain from both ligands. However, this domain is just for a  $\text{Zn}^{2+}$  metal ion in only 70% of the crystal, for the remainder the site is occupied by another  $\text{Hg}^{2+}$  metal ion.

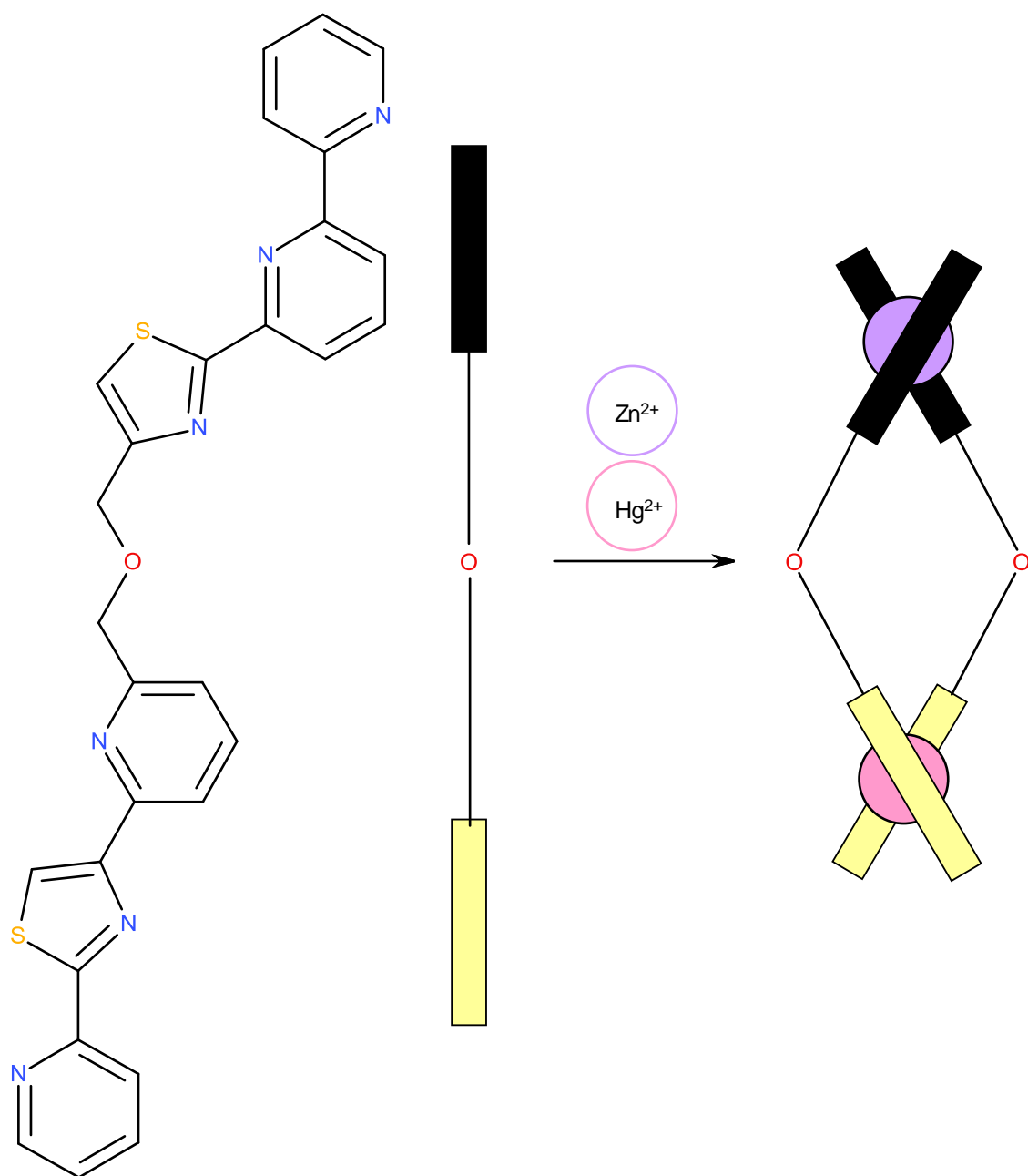


**Figure 1.27** Representation of the heteronuclear helicate  $[\text{HgZn}(\text{L}^n)_2]^{4+}$

The metal specificity is accredited to the bite angles of the tridentate binding domains; varying the position of the thiazole ring has a pronounced effect on the respective bite angle. The py-tz-py domain is more divergent and binds the larger ( $1.02 \text{ \AA}$ )  $\text{Hg}^{2+}$  ion, whereas the convergent tz-py-py binding domain coordinates the smaller ( $0.74 \text{ \AA}$ )  $\text{Zn}^{2+}$  ion.

### 1.6.7 Enantioselective and Diastereoselective Helicates

Many of the important biological and medicinal molecules exist as enantiomers, highlighting the importance of this section, as some supermolecules can exist in enantiomeric and diastereomeric forms. As discussed previously helicates can be defined as compounds that are characterised by a helical axis that possess chirality associated with the screw like sense about a fixed axis. The pitch of the screw is the distance between the turns of the helix. The helicate can travel in two directions; right-handed (plus, P) or left-handed (minus, M), according to whether the rotation of the screw is clockwise or anticlockwise (figure 1.28).<sup>86</sup>

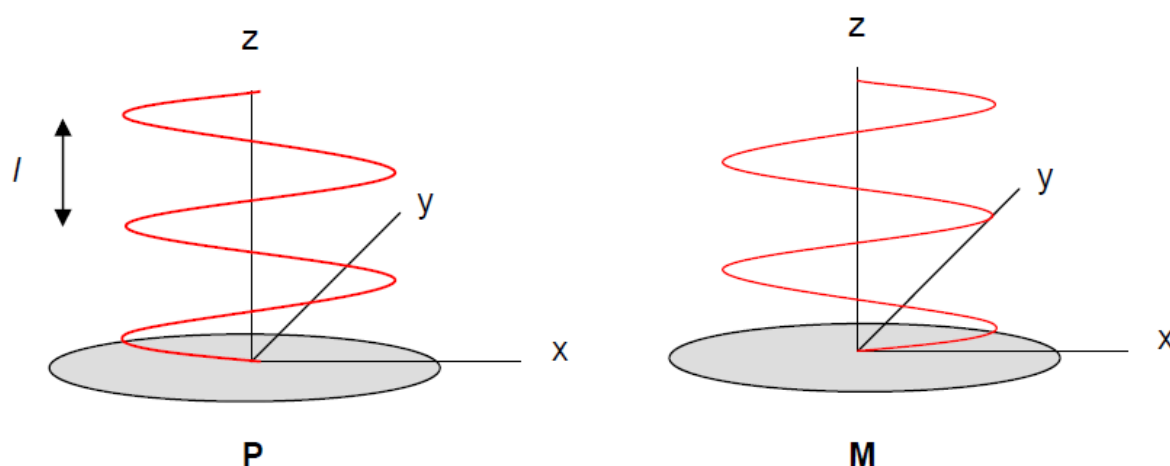


**Figure 1.28** Diagram illustrating both the right-handed (plus, P) and the left-handed (minus, M) rotations of helix.  $L$  is the pitch and  $z$  is the helical axis

The stereochemistry of the metal centres within the P and M helicates are also different. In a P helicate all of the metal centres are right-handed ( $\Delta$ ) and for M helicates all of the metal centres are left handed ( $\Lambda$ ) (figure 1.29). If in a helicate the stereochemistry of the metal centres are different then side-by-side helicates, known as meso-helicates are formed.<sup>64</sup>

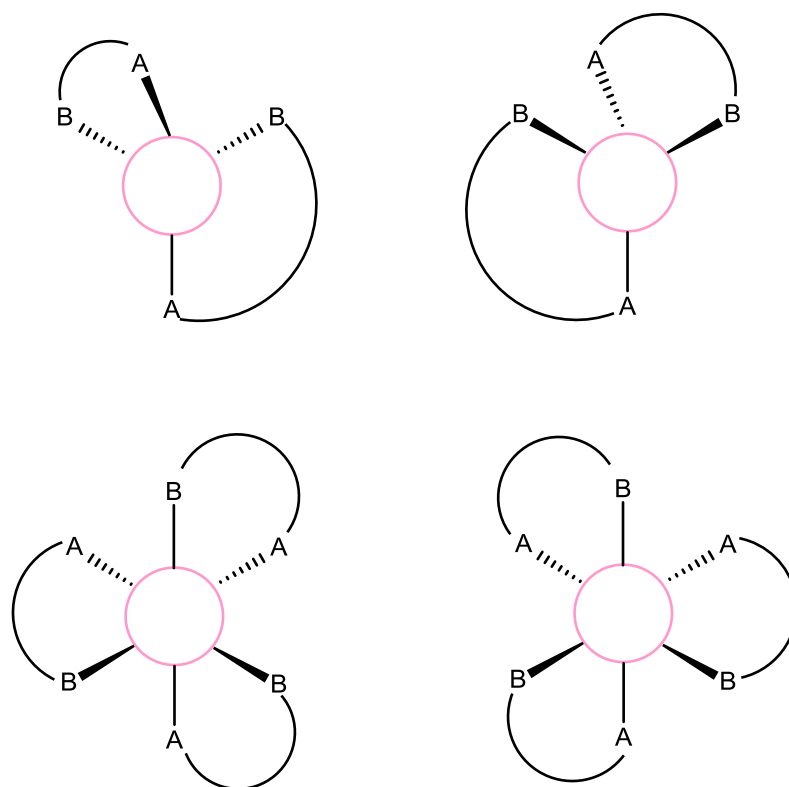


**Figure 1.29** Absolute configurations of both  $\Delta$  and  $\Lambda$  stereoisomers of a tetrahedral and octahedral metal ion

The work published by Constable and co-workers demonstrate how quaterpyridine ( $L^O$ ) and sexipyridine ( $L^P$ ) both form the right handed (P) left handed (M) helicate.<sup>87</sup> Reaction of quaterpyridine ( $L^O$ ) with an equimolar amount of  $Cu^+$  results in the formation of the dinuclear double helicate  $[Cu_2(L^O)_2]^{2+}$ . The distorted tetrahedral coordination geometry of the metal ions is coordinated by the bipyridine strands, the quaterpyridine ligands partition and coordinates another different metal (figure 1.30). As seen previously, reaction of sexipyridine ( $L^P$ ) with a range of metal ions in a equimolar fashion also results in the formation of a dinuclear double helicate  $[M_2(L^P)_2]^{4+}$  ( $M = Fe^{2+}, Mn^{2+}, Cu^{2+}$  or  $Cd^{2+}$ ). The sexipyridine ligand partitions into two tridentate binding domains and coordinates the distorted octahedral metal centres (figure 1.30). In all of the helicates the metal centres have the same configurations resulting in the formation of both (P) and (M) helicates.

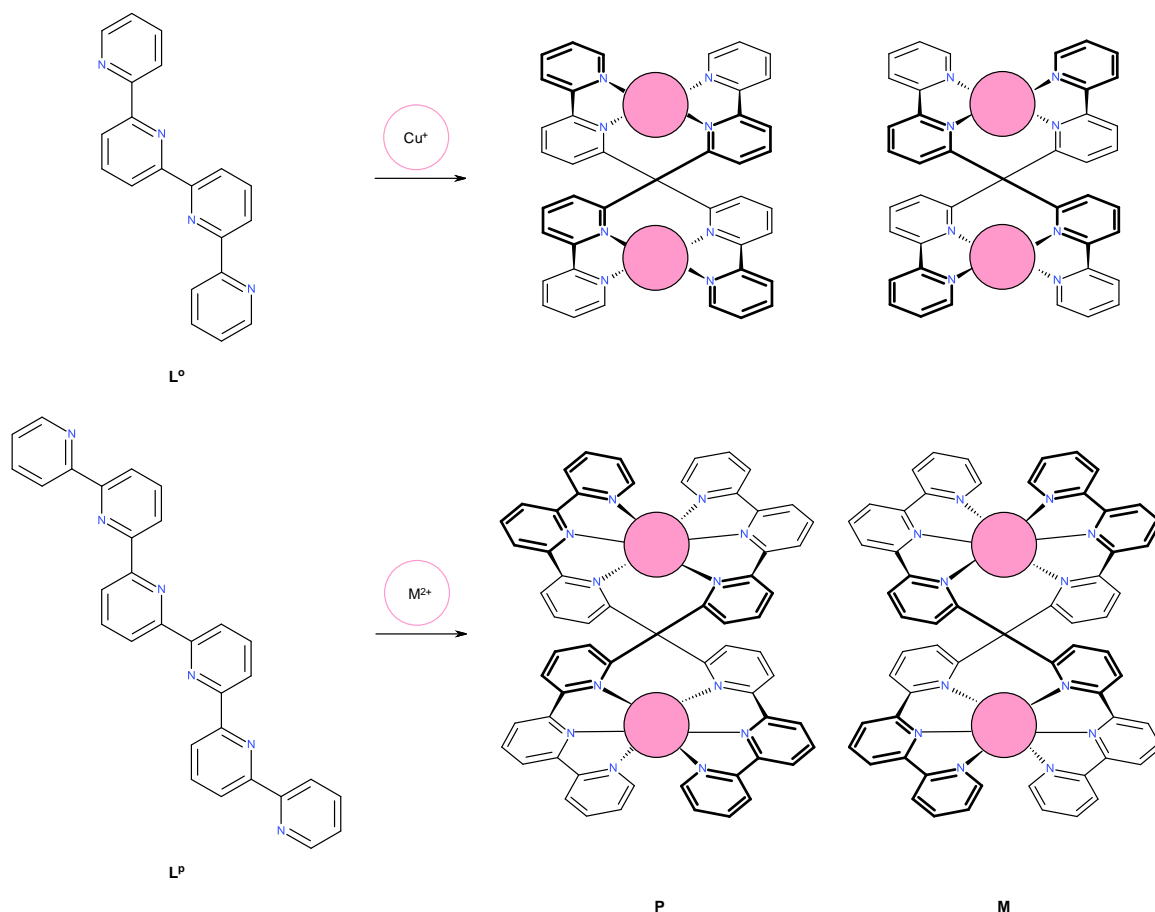


**Figure 1.30** Stereoselective complexes  $[Cu_2(L^O)_2]^{2+}$  (top) and  $[M_2(L^P)_2]^{4+}$  (bottom) ( $M = Fe^{2+}$ ,  $Mn^{2+}$ ,  $Cu^{2+}$  or  $Cd^{2+}$ )

The self-assembly of helicates are generally not enantioselective, therefore a racemic mixture of the two enantiomers is observed. However, over recent years many research groups including Constable<sup>88</sup> and Von Zelewsky<sup>89</sup>, have demonstrated how enantioselectivity in helicates can be controlled. The incorporation of a chiral pinene unit into an oligopyridine ligand strand allowed Constable and Von Zelewsky to programme the ligands to result in only one type of helical enantiomer; this is due to the steric bulk of the chiral substituent interacting with the oligopyridine strands (figure 1.31).

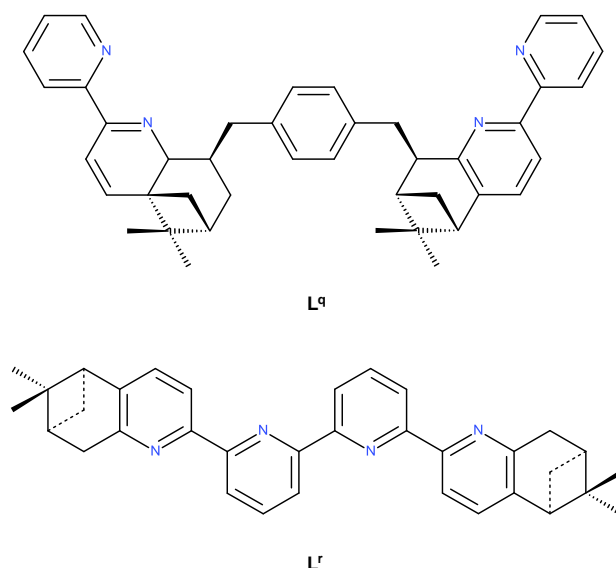


**Figure 1.31** Structures of Von Zelewsky's ligand  $L^Q$  and Constable's ligand  $L^r$

Von Zelewsky synthesised  $L^Q$ , a bis-bidentate ligand with pinene units separated by a phenyl spacer, upon reaction of either the (+)- or (-)- $L^Q$  enantiomer with either  $Cd^{2+}$  or  $Zn^{2+}$  (metal: ligand ratio of 2:3) results in the formation of a dinuclear triple helicate preferential of one stereoisomer. Constable prepared a similar ligand,  $L^r$ , upon reaction of either (S,S) or (R,R)  $L^r$  with one equimolar amount results in the formation of the dinuclear double helical complex (P)- $[Cu_2(L^r)_2]^{2+}$ .<sup>90</sup>

### 1.6.8 Meso Helicates

As discussed in the previous section, in order to be classed as a 'true' helicate all of the metal centres involved in the complex must have the same stereochemistry, heterochiral coupling ( $\Delta\Delta$  or  $\Lambda\Lambda$ ) of the metal centres results in the assembly of the achiral meso-helicate or mesocate. Unlike in the conventional helicate where the ligands wrap around the metal centres in an 'over-and-under' conformation, a meso-helicate describes a complex where two ligands are lying 'side-by-side' instead of being twisted around one another. The preferential synthesis of the meso-helicate instead of the traditional helicate appears to be controlled by a variety of factors: variation of the metal<sup>91, 92</sup>, modification of the spacer unit<sup>93, 94</sup> or by the incorporation of a guest molecule<sup>95</sup>.

A recent example has been demonstrated by Rice and co-workers who prepared a ligand that forms either a dinuclear double helicate or a dinuclear double meso-helicate dependent upon the size of the metal ion or the steric bulk of the ligand strand.<sup>96</sup> The ligand  $L^s$  is potentially hexadentate and consists of two tridentate tz-py-py binding domains separated by a central substituted triphenyl spacer unit. Upon reaction of  $L^s$  with  $Cd^{2+}$  produces a dinuclear double helicate  $[Cd_2(L^s)_2]^{4+}$ . The metal centres adopt a 6-coordinate

distorted-octahedral geometry by coordination of two tz-py-py domains, one from each ligand strand. The ligands wrap around the  $\text{Cd}^{2+}$  metal ions in an 'over-and-under' arrangement, twisting about the central triphenyl spacer. However, reaction of  $\text{L}^s$  with  $\text{Co}^{2+}$  produces the dinuclear double meso-helicate  $[\text{Co}_2(\text{L}^s)_2]^{4+}$ . The metal centres adopt six-coordinate geometry and are coordinated by the tz-py-py binding domains of two different ligand strands. Unlike the previous  $\text{Cd}^{2+}$  structure the ligands do not twist around the metal ion, they coordinate in a 'side-by-side' arrangement, resulting in the two  $\text{Co}^{2+}$  having opposite chirality (figure 1.32).

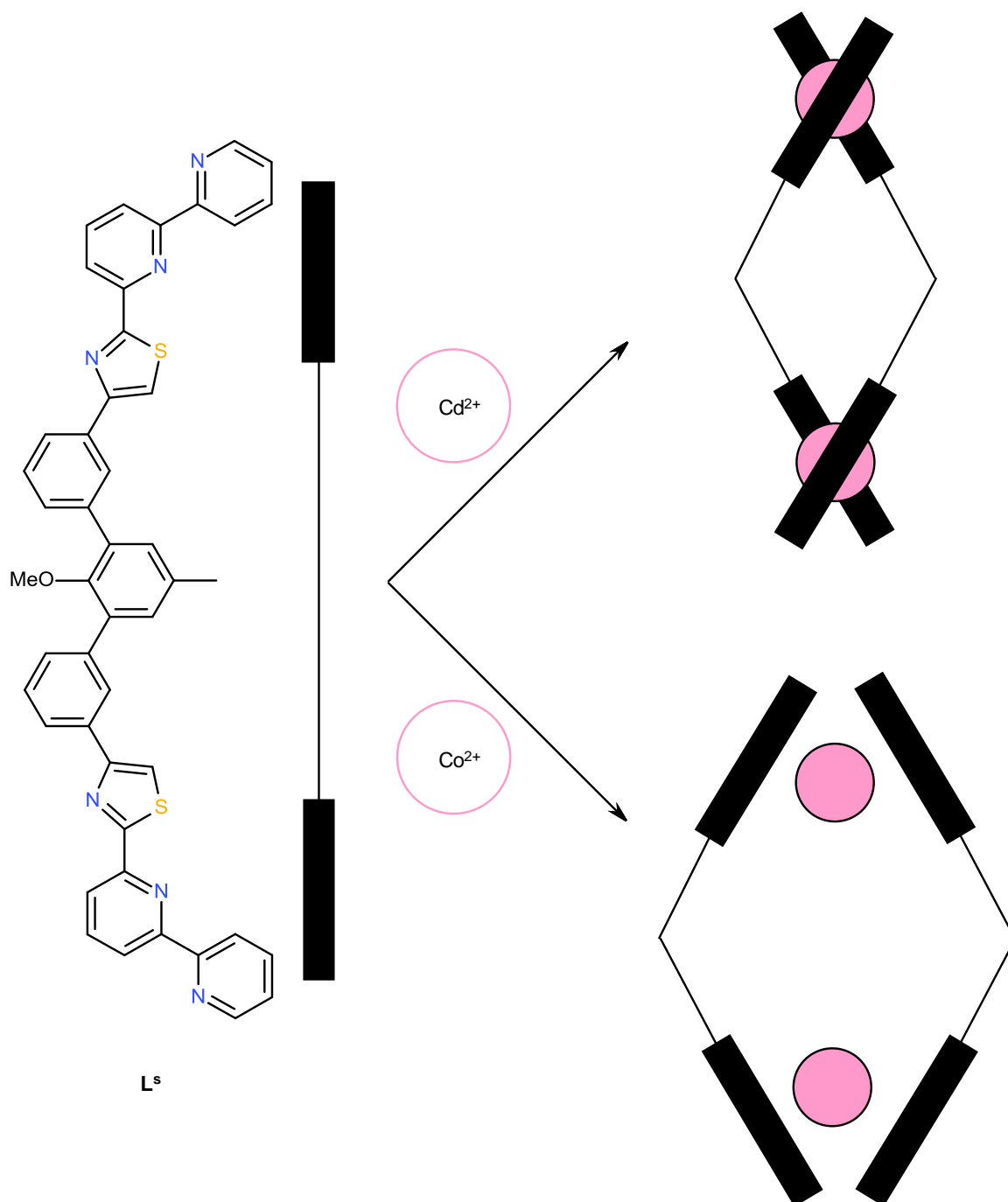


**Figure 1.32** Controlling the formation of the dinuclear double meso-helicate  $[\text{Co}_2(\text{L}^s)_2]^{4+}$

Rice and co-workers explained that the formation of a dinuclear double helicate with  $\text{Cd}^{2+}$  but a dinuclear double meso-helicate with  $\text{Co}^{2+}$  is accredited to the central methoxy group on the triphenyl spacer. In the  $[\text{Cd}_2(\text{L}^{\text{s}})_2]^{4+}$  double helicate the two oxygen atoms are brought into close proximity, the smaller  $\text{Co}^{2+}$  ion reduces the metal-nitrogen bond by 20%, resulting in an increase in the electrostatic repulsion between the methoxy units. The formation of the dinuclear double meso-helicate  $[\text{Co}_2(\text{L}^{\text{s}})_2]^{4+}$  destabilises the unfavourable steric interactions as the methoxy units are pointing away from each other.

### 1.7 Circular Helicates

In the field of supramolecular chemistry the spontaneous and selective self-assembly of metal ions with well-designed ligands producing a variety of inorganic entities is an area of intense activity. Since Jean-Marie Lehn introduced the term helicate a large number of metallosupramolecular helicates have been characterised, involving the spontaneous self-assembly of two or more multidentate ligands that helically wrap around a central array of metal ions, becoming a fascinating aspect of supramolecular chemistry. Through careful consideration of ligand topology and metal stereoelectronic preferences a wide variety of polynuclear double, triple and quadruple helicates have been reported, programming ligands with further information has allowed the resulting helicates to express certain structural features of higher order complexity. Helicates that express higher order complexity can be achieved by elaborating on the basic design principles of helicate formation, allowing: 1) directional control over ligand alignment, 2) selective incorporation of different metal centres and 3) selective incorporation of different ligand strands resulting in head-to-tail, heterometallic and heteroleptic helicates.

The ability to control the formation of polynuclear helical complexes is well established; however, the formation of the circular helicate is less understood. Circular helicates are related to conventional linear helicates in that the ligands wrap around the metal centres, the difference relates to the positioning of the metal ions. In linear helicates the ligands wrap around the metal ions in a linear arrangement whereas in a circular helicate the metals are located in a cyclic arrangement. Although examples of circular helicates exist they are quite rare, the main reason being is that they are subjected to the same construction method that applies to helicate formation *i.e.* using a ligand that contain two or more binding domains that coordinate different metal ions. For the higher nuclearity circular helicate to preside in solution the formation of the entropically favoured linear helicate must be prevented, chemists have stabilised the formation of the circular species by intermolecular or intramolecular interactions.

A striking example of circular helicates has been demonstrated by Lehn and co-workers, where the nuclearity of the self-assembled species is controlled by the nature of the counter anions. The reaction of the tris-2,2'-bipyridine ligand  $L^t$  and  $FeCl_2$  resulting in a pentanuclear circular helicate, which encloses a strongly bound chloride anion that tightly fits into the central cavity (figure 1.33).<sup>97</sup>

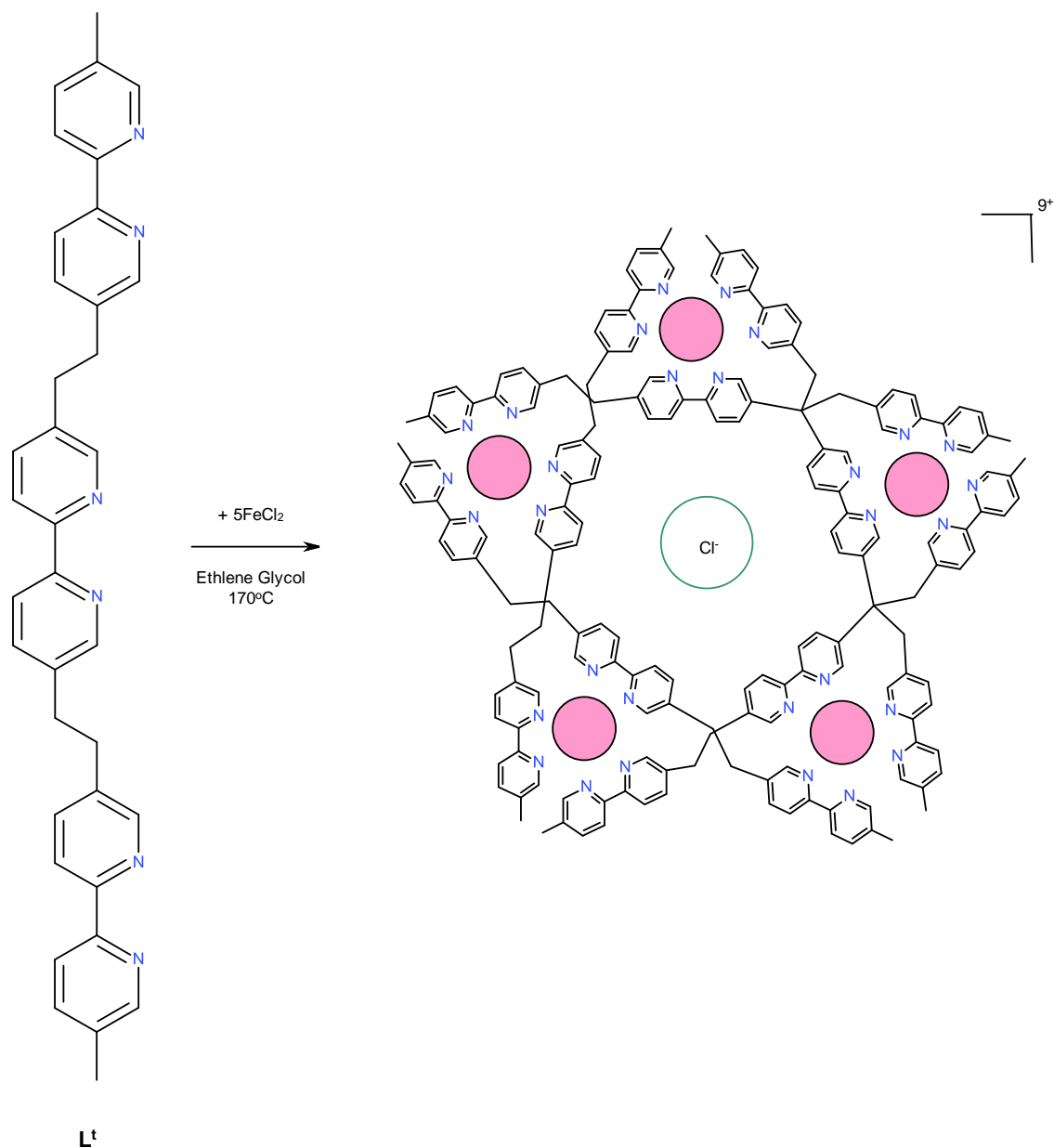


**Figure 1.33** Self-assembly of the pentanuclear circular helicate from five  $L^t$  ligands and five  $Fe^{2+}$  ions in the presence of a chloride anion

The resulting  $[Fe_5(L^t)_5Cl]^{9+}$  complex consists of five  $Fe^{2+}$  ions, five  $L^t$  ligands and a chloride ion. Each  $Fe^{2+}$  ion has distorted octahedral geometry occupied by three bipyridine groups, two terminal and one central, belonging to three different ligand strands. Due to the short linkers between the bipyridine units the central and terminal bipyridine N-donors cannot be

arranged around the same metal ion. The central cavity is occupied by a strongly bound chloride anion which templates the assembly, this cannot be exchanged for other anions such as  $\text{PF}_6^-$  or  $\text{CF}_3\text{SO}_3^-$  demonstrating the selectivity of the pentanuclear circular helicate for  $\text{Cl}^-$ . Lehn and co-workers investigated the kinetic and thermodynamic control of the pentanuclear circular helicate  $[\text{Fe}_5(\text{L}^t)_5\text{Cl}]^{9+}$  in a later study.<sup>98</sup> Following the reaction of  $\text{L}^t$  with  $\text{Fe}^{2+}$  by NMR and ESI MS studies indicates that initially a trinuclear helical structure forms before disassembling and generating the pentanuclear circular helicate. The self-assembly of the ligand  $\text{L}^t$  and  $\text{FeCl}_2$  yields the triple linear helicate over a relatively short reaction time, whereas the circular helicate is obtained after prolonged heating at 170 °C. The formation of both architectures obtained from the reaction of  $\text{L}^t$  with  $\text{Fe}^{2+}$  is explained as the triple helicate is a kinetic product and is formed fast and reversibly, thereafter disassembles and transforms into the thermodynamic product. The higher stability of the pentanuclear circular helicate is attributed to several factors; strain in the bound ligand and/or coordination centres and the electrostatic with the included chloride anion.

To explore the self-assembly of circular helicates in more detail it was of interest to Lehn and co-workers to investigate controlling the formation of such circular helicate architectures by examining the importance of the metal salt.<sup>99</sup> The reaction of  $\text{L}^t$  with  $\text{Fe}(\text{BF}_4)_2$  does not generate the pentanuclear circular helicate, instead the resulting structure is the hexanuclear circular helicate  $[\text{Fe}_6(\text{L}^t)_6\text{BF}_4]^{12+}$ . The resulting complex possesses six  $\text{Fe}^{2+}$  centres arranged as a hexagon with ligands wrapping around those centres. The coordination geometry of the  $\text{Fe}^{2+}$  is very similar to that described previously for the pentanuclear circular helicate, with each  $\text{Fe}^{2+}$  binding to two terminal and one central bipyridine units of three different ligands. In the presence of the smaller  $\text{Cl}^-$  anion the self-assembly of  $\text{L}^t$  with  $\text{Fe}^{2+}$  produces a pentanuclear circular helicate. However, with larger anions, such as  $\text{SO}_4^{2-}$ ,  $\text{BF}_4^-$  and  $\text{SiF}_6^-$  the resulting structure is the hexanuclear circular helicate. Reaction of  $\text{L}^t$  with  $\text{FeBr}_2$  gave a nearly equimolar amount of both pentanuclear and hexanuclear circular helicates as the  $\text{Br}^-$  anion is of an intermediate size. The charge of the anion has little influence on the resulting structure as the hexanuclear circular helical architecture is obtained by both mono- and divalent anions. Lehn summarised the findings as the nuclearity of the circular helicate depends on the size of the anion to be included in the central cavity of the circular helicates.

Another example of the self-assembly of circular helicates that relies on anion templation is demonstrated by Ward and co-workers.<sup>57</sup> The tetradentate ligand  $\text{L}^u$  consists of two pyrazole-pyridine arms connected to a 1,8-naphthlenediyl spacer *via* methylene linkers. Reaction of  $\text{L}^u$  with  $[\text{Cu}(\text{MeCN})_4](\text{OTf})$  or  $[\text{Ag}(\text{MeCN})_4](\text{BF}_4)$  in a 1:1 ratio resulted in a mononuclear complex, with both the pyrazole-pyridine arms of  $\text{L}^u$  coordinating the sole

metal ion. In the  $[\text{Cu}(\text{L}^{\text{u}})](\text{OTf})$  structure the  $\text{Cu}^+$  metal centre is four coordinate geometry between planar and tetrahedral. There is no evidence of close contact between the  $\text{Cu}^+$  metal centre and the triflate anions. The structure of  $[\text{Ag}(\text{L}^{\text{u}})](\text{BF}_4)$  is generally similar, with exception that the two ligand arms are essentially coplanar providing a planar array of four N-donor atoms around the  $\text{Ag}^+$  centre. The  $\text{Ag}^+$  ion is two coordinate with two additional weak interactions (figure 1.34).

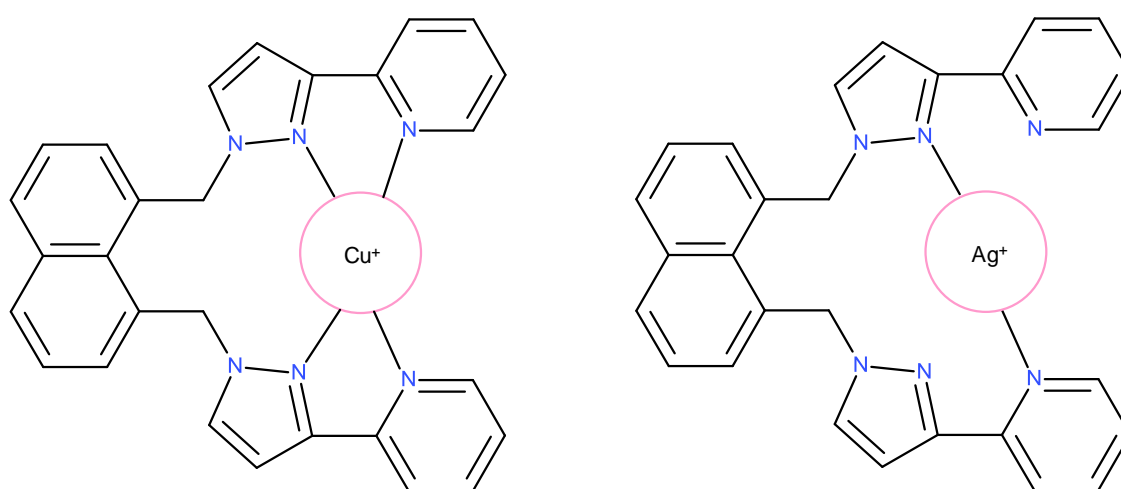


**Figure 1.34** Structure of the complex cations  $[\text{Cu}(\text{L}^{\text{u}})](\text{OTf})$  and  $[\text{Ag}(\text{L}^{\text{u}})](\text{BF}_4)$

The  $\text{Cu}^+$  and  $\text{Ag}^+$  complexes were examined by electrospray mass spectrometry which showed the presence of strong ions corresponding to both the mono cations  $[\text{M}(\text{L}^{\text{u}})]^+$  ( $\text{M} = \text{Cu}^+$  or  $\text{Ag}^+$ ). For the  $\text{Cu}^+$  species there was no evidence for the formation of higher nuclearity species. However, for the  $\text{Ag}^+$  species the spectra also contained weaker signals corresponding to traces of the oligomers  $\{[\text{Ag}_2(\text{L}^{\text{u}})_2](\text{BF}_4)\}^+$ ,  $\{[\text{Ag}_3(\text{L}^{\text{u}})_3](\text{BF}_4)_2\}^+$  and  $\{[\text{Ag}_4(\text{L}^{\text{u}})_4](\text{BF}_4)_3\}^+$ , suggesting a templating role played by the  $\text{BF}_4^-$  anion as these minor components are not present in the  $\text{Cu}^+$  triflate species. To determine whether the  $\text{BF}_4^-$  anion could act as a template for circular helicates; this work was extended, Ward and co-workers prepared a complex of  $[\text{Cu}(\text{MeCN})_4](\text{BF}_4)$ . The resulting complex was  $[\text{Cu}_4(\text{L}^{\text{u}})_4][\text{BF}_4]$ , a tetranuclear circular helicate (figure 1.35).

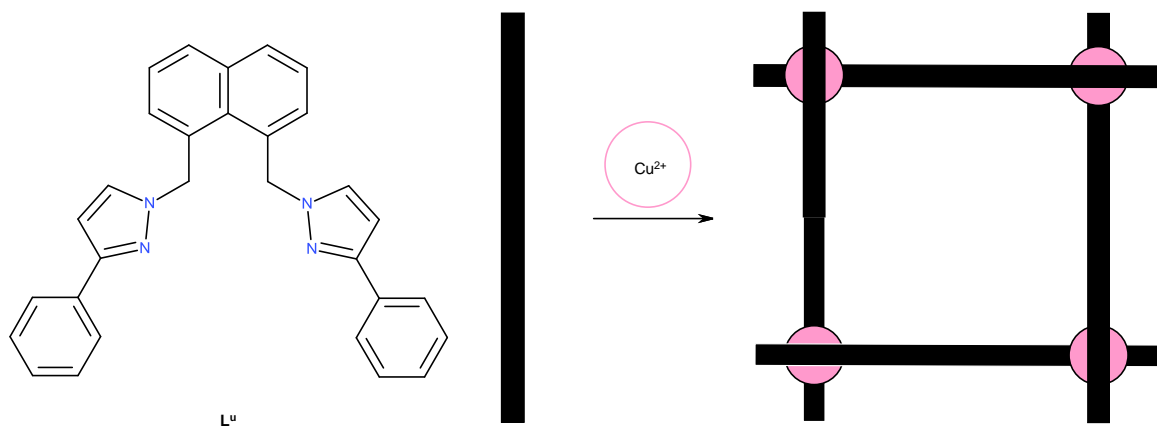


**Figure 1.35** Representation of the tetranuclear circular helicate  $[\text{Cu}_4(\text{L}^u)_4][\text{BF}_4]$

The four metal ions and four ligand strands have assembled into a cyclic helical array, with a  $\text{BF}_4^-$  anion occupying the central cavity. All  $\text{Cu}^+$  ions are four coordinate, arising from the coordination of two pyrazolyl-pyridine units from two different ligand strands. The four  $\text{L}^u$  ligands wrap around the metal ions in an 'over and under' conformation. The stability of the tetranuclear circular helicate is accredited to three favourable features: firstly the aromatic stacking that exists, secondly the tetrahedral coordination geometry of each  $\text{Cu}^+$  ion and finally the encapsulated  $\text{BF}_4^-$  anion which is a perfect fit for the central cavity. The role of the  $\text{BF}_4^-$  anion as a template is highlighted as no such tetranuclear species occurs with the triflate salt.

Gloe and co-workers recently added to the area with their research on a series of bis-bidentate ligands containing bis-pyridylimine units, differing from each other in the linking element (-S-,  $-\text{CH}_2-$ , -O-) (figure 1.36).<sup>100</sup>

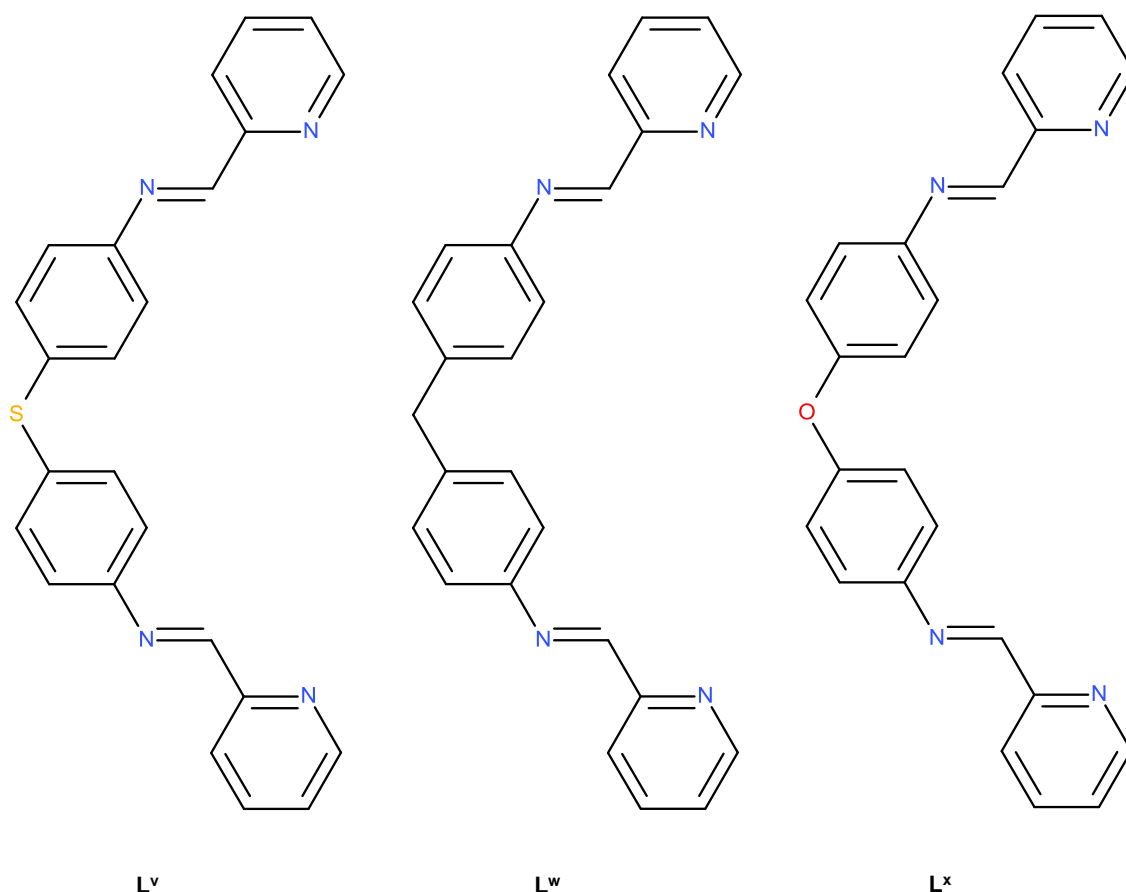


**Figure 1.36** Bis-pyridylimine ligands,  $L^V$ ,  $L^W$  and  $L^X$  produced by Gloe and co-workers in 2010

The variation of the linking element makes a significant change to the angle of the pyridylimine strands, but surprisingly it has little influence on the resulting structures. Reaction of  $L^{V-X}$  with  $\text{CuSO}_4 \cdot \text{H}_2\text{O}$  afforded the hexanuclear circular helical complex  $[\text{Cu}(L^{V-X})(\text{SO}_4)]_6$  in almost quantitative yields. Each  $\text{Cu}^{2+}$  ion has distorted octahedral coordination spheres, resulting from interactions with two bidentate pyridylimine strands of different ligands and one bidentate sulphate ion. The six  $\text{Cu}^{2+}$  ions have alternative  $\Lambda$  and  $\Delta$  configurations, leading to overall meso-centrosymmetry. The coordination of the sulphate anions play a crucial role in the formation of the hexanuclear meso-helicate, as upon changing the anions to  $\text{SO}_4^{2-}$ ,  $\text{ClO}_4^-$  or  $\text{NO}_3^-$  only the cationic non-cyclic triple helicate  $[\text{Cu}_2(L^{V-X})_3]^{4+}$  forms. The reaction in changing the anions but maintaining the same conditions demonstrates that the topological control of the self-assembly process is associated with the bidentate coordination of the sulphate anions, which directs the assembly towards a double rather than triple stranded structure around the six  $\text{Cu}^{2+}$  metal centres.

The formation of a circular helicate can also be assisted by intramolecular interactions, which stabilise the formation of the circular species relative to its double stranded alternative. An example of this approach is the work carried out by Williams and co-workers using ligands containing the bis(oxazoline)pyridine unit with slightly different substituents (figure 1.37).<sup>101</sup>

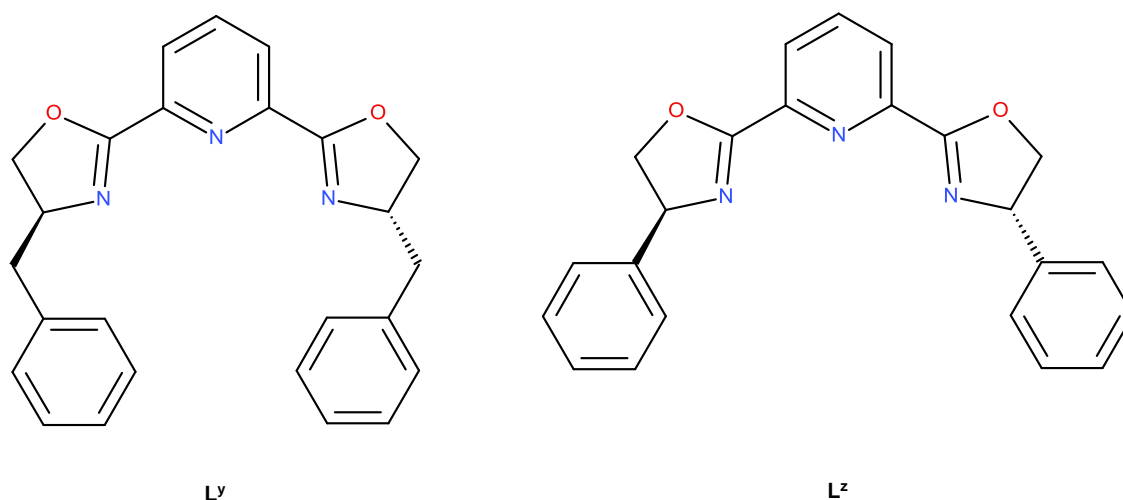
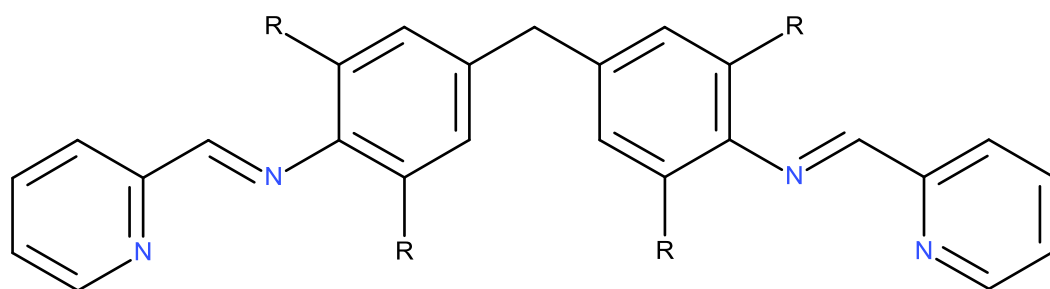


**Figure 1.37** The bis(oxazoline) pyridine ligands  $L^y$  and  $L^z$  reported by Williams and co-workers

Both  $L^y$  and  $L^z$  form helicate complexes with  $Ag^+$ , but the type of helix differs. Reaction of  $L^y$  with  $Ag^+$  results in the dinuclear double helicate  $[Ag_2(L^y)_2]^{2+}$  with the  $L^y$  ligands acting as a monodentate chelate coordinating the  $Ag^+$  by two oxazoline N-donor atoms. The phenyl substituents may be regarded as extending the ligand strands and are slightly inclined to the helical axis. Removing the methylene attachment in  $L^z$  generates a different helical structure, upon reaction of  $L^z$  with  $Ag^+$  a trinuclear circular helicate forms. The complex  $[Ag_3(L^z)_3]^{3+}$  consists of an equilateral triangle of silver ions with the ligands bridging the sides of the triangle, binding through oxazoline N-donor atoms. In the double helical structure of  $[Ag_2(L^y)_2]^{2+}$  with methylene group linking the phenyl substituents to the oxazoline ring is directed roughly along the helical axis, but in the triple circular helicate  $[Ag_3(L^z)_3]^{3+}$  the bond is equatorial and therefore perpendicular to the helical axis. This allows a strong stacking interaction between the pyridine group of one ligand and the phenyl rings of the other two. The explanation of the remarkable difference in the two structures is the existence of the stacking interactions in  $[Ag_3(L^z)_3]^{3+}$ , the absence or presence of these stacking interactions modifies the resulting structure.

Hannon and co-workers demonstrated that inter-strand  $CH\cdots\pi$  interactions are the principal driving force for the preferential formation of high complexity cyclic assemblies over their dimeric counterparts. This was achieved by introducing alkyl substituents onto the spacers of readily prepared bis(pyridylimine) ligands  $L^{aa-cc}$  (figure 1.38).<sup>102, 103</sup>



$L^{aa}$  R = H

$L^{bb}$  R = Me

$L^{cc}$  R = Et

**Figure 1.38** M. J. Hannon and co-workers bis(pyridylimine) ligands  $L^{aa-cc}$

Reaction of  $L^{aa}$  with metal ions capable of tetrahedral coordination leads to a solution equilibrium of two dimeric isomers; a helicate and a meso-helicate. In attempt to prevent the equilibrium ligands  $L^{bb-cc}$  were designed, where the introduction of alkyl groups onto the spacer with the goal of twisting the phenyl rings out of planarity with the iminopyridine units and thus disfavouring the meso-helicate. Reaction of  $L^{bb}$  with  $Cu^+$  did not result in a helicate/meso-helicate equilibrium but instead the trinuclear circular  $[Cu_3(L^{bb})_3]^{3+}$  formed. The metal ions assemble on the three vertices of a triangle with each ligand wrapping 'over and under'. Each  $Cu^+$  centre is four coordinate in a distorted tetrahedral coordination geometry bound to two pyridylimine units from two different ligands. The methyl groups have favoured a trimeric species as there are six  $CH\cdots\pi$  interactions. They believed that  $\pi$ - $\pi$  interactions were the reason for the structure obtained but that one  $\pi$ - $\pi$  interaction alone wouldn't be effective enough to force the cyclic nature of the structure. It was concluded therefore that whilst one  $\pi$ - $\pi$  interaction alone might not be sufficient enough to have an effect, the combination of all six of the  $\pi$ - $\pi$  interactions together acted as the driving force behind the formation of this compact cyclic compound. Four of the bowl shaped  $[Cu_3(L^{bb})_3]^{3+}$  complexes assemble in a tetrahedral fashion through 12  $CH\cdots\pi$  interactions to form a tetrameric bowl shaped architecture consisting of 12  $Cu^+$  ions, 12  $L^{bb}$  ligands stabilised by 12  $CH\cdots\pi$  interactions. Reaction of  $L^{cc}$  with  $Cu^+$  ions results in a dinuclear double helicate, with each  $Cu^+$  metal centre occupying distorted tetrahedral geometry coordinating to a pyridylimine binding unit of each ligand. The twisting of the ligand to coordinate the metal ions is an 'over and under' conformation confirms the presence of conventional helicate architecture and not the meso-helicate equilibrium observed with  $L^{aa}$ . There are four  $CH\cdots\pi$  interactions that occur between the ethyl unit of one ligand and the phenyl rings of the opposite ligand. In contrast to the methyl ligand  $L^{bb}$  the longer ethyl substituent  $L^{cc}$  forms the entropically favoured dinuclear double helicate,

the CH... $\pi$  interactions are not as effective because the ethyl substituents are too long. The formation of a trinuclear circular helicate with  $L^{bb}$  with  $Cu^+$  can be accredited to the CH... $\pi$  interactions which stabilise the complex, playing an important role in determining the classification of the supramolecular architecture.

Ligand  $L^{dd}$  prepared by Constable and co-workers uses an ethyl spacer to split two bipyridine sites, reaction of this ligand with  $Cu^+$  results in helicates and circular helicates simultaneously existing as a mixture. The reaction was monitored by ESI MS and NMR studies, with solid state structures confirming both the *P* and *M* helical diastereoisomers (figure 1.39).<sup>104</sup>

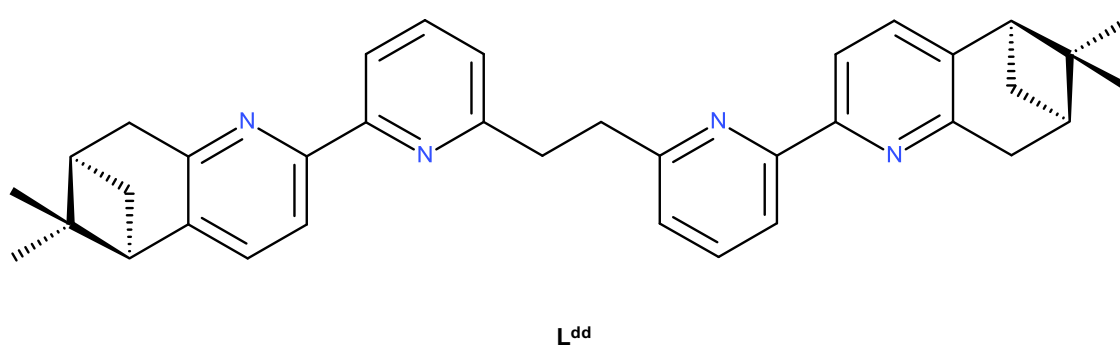


**Figure 1.39** Ligand  $L^{dd}$  prepared by Constable and co-workers

The solid state structural determination of the reaction between  $L^{dd}$  and  $Cu^+$  confirmed a 1:1 mixture of both dinuclear double helicate  $[Cu_2(L^{dd})_2]^{2+}$  and the trinuclear circular helicate  $[Cu_3(L^{dd})_3]^{3+}$ . Investigating this reaction by NMR spectroscopy suggested that the spectra contained between three and five species, depending on the concentration of the sample. ESI MS studies revealed the existence of a library of compounds which revealed the tri-, tetra- and pentanuclear circular helicates in addition to the dinuclear double helicate. Concentration studies of the mixture revealed an increase in the higher nuclearity species at higher concentration, suggesting that the formation of the circular helicate was strongly influenced by entropic factors.

Several helical structures have been reported by Von Zelewsky using the pinene-2,2'-bipyridine species linked by different bridging isomers (figure 1.40). Upon reaction with metal ions the ligands behave differently and generate various helical structures.<sup>105, 106</sup>

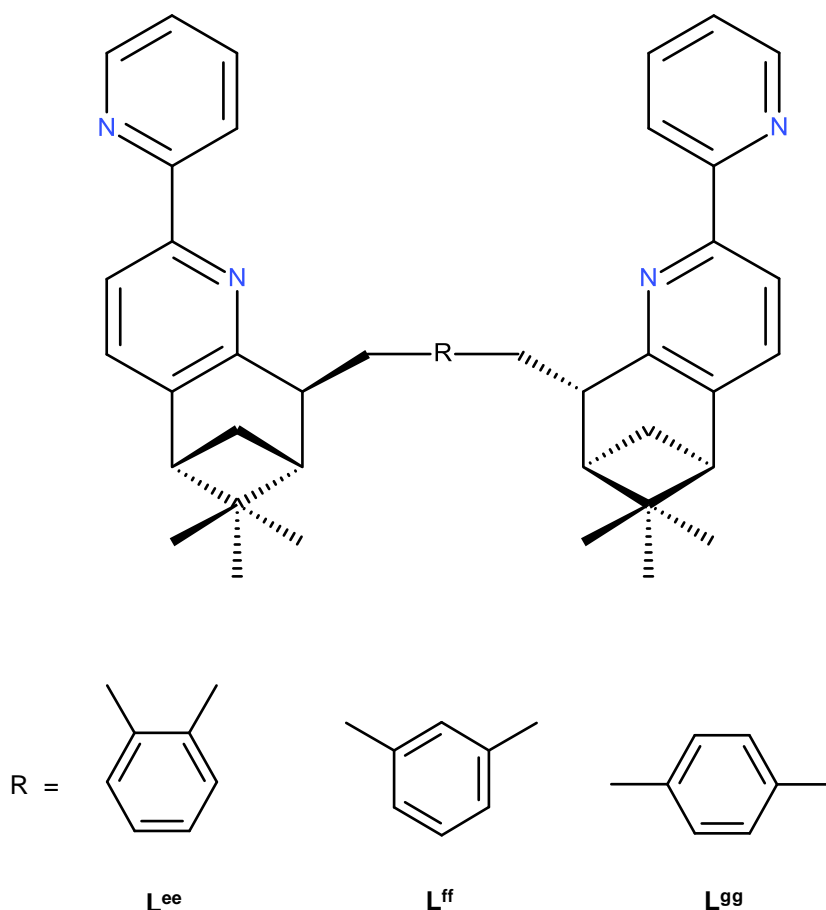


**Figure 1.40** The chiragen type ligands reported by Von Zelewsky

Reaction of the ortho-linked ligand  $L^{ee}$  and  $Ag^+$  reveals mainly the presence of the mononuclear complex  $[Ag(L^{ee})]^+$  in the ESI MS. Molecular modelling shows that  $L^{ee}$  occupies all four sites of the tetrahedrally coordinated  $Ag^+$  centre. The ESI MS spectra of  $L^{ff}$ , the meta-substituted ligand, with  $Ag^+$  indicate the formation of polynuclear species. The most abundant species corresponds to the dinuclear complex  $[Ag_2(L^{ff})_2]^{2+}$ , but signals of lower intensity corresponding to  $[Ag_3(L^{ff})_3]^{3+}$  and  $[Ag_5(L^{ff})_5]^{5+}$  were detected. Ligand  $L^{gg}$ , the para substituted linker shows a completely different behaviour to that of ligand  $L^{ee}$  and  $L^{ff}$ . The spontaneous formation of a hexanuclear circular helicate with  $Ag^+$  ions is characterised by X-ray diffraction, NMR and ES MS spectroscopy. The  $Ag^+$  ions in the  $[Ag_6(L^{gg})_6]^{6+}$  complex are tetrahedrally coordinated by four N-donor atoms from two different ligands. In the reaction with the ligand prepared from (-)- $\alpha$ -pinene, a circular helicate of *P*-handedness was obtained. The corresponding reaction with the ligand prepared from (+)- $\alpha$ -pinene delivered the *M* analogue. The hexanuclear species  $[Ag_6(L^{gg})_6]^{6+}$  self-assembles from the metal ion and the ligand alone there is no central element, for example an anion, acting as a template. Von Zelewsky and co-workers showed that related ligands could be tuned by using small variations in the structure of the bridging unit, therefore varying the resulting self-assembled species.

A study reported by Zhang and co-workers on the tetradentate Schiff base ligand  $L^{hh}$  demonstrates the metal dependant assembly of either a dinuclear double helical complex or a trinuclear circular helicate. Ligand  $L^{hh}$  exists as three isomers; cis-cis, cis-trans and trans-trans, but only the first two are characterised in the study (figure 1.41).<sup>107</sup>

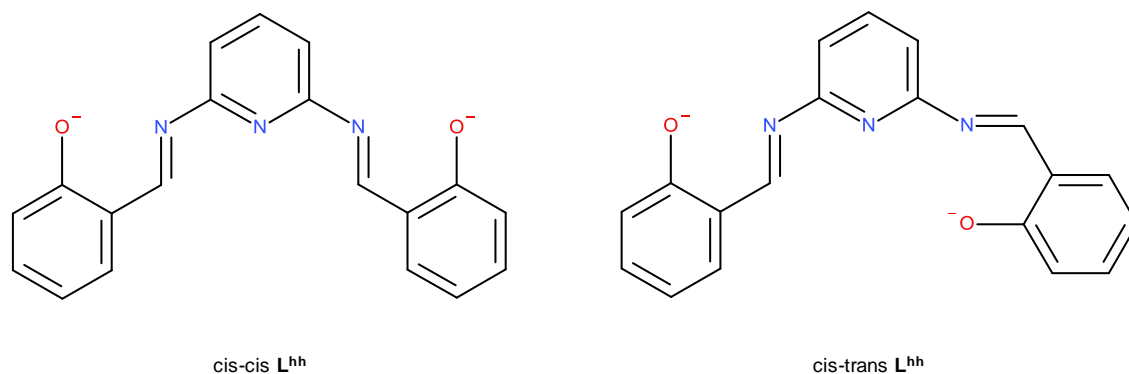


**Figure 1.41** The two conformation of the ligand  $L^{hh}$  prepared by Zhang and co-workers

When  $L^{hh}$  is reacted with  $Cu^{2+}$  a dinuclear double meso-helicate was obtained, owing to the cis-cis conformation of the ligand. The  $Cu^{2+}$  centres are between square planar and tetrahedral geometry arising from the coordination of the phenolic oxygen and imino N-donor atoms from two adjacent ligands. The reaction of  $L^{hh}$  with  $Co^{2+}$  generates a trinuclear circular helicate, with the ligand adopting a cis-trans conformation. The resulting complex consists of an approximately equilateral triangle of  $Co^{2+}$  metal on the apexes of the triangle with the ligands being the sides of the triangle. Each  $Co^{2+}$  ion is coordinated by two dehydrogenated phenolic oxygen atoms and two imine N-donor atoms from two different ligands to form tetrahedral coordination geometry. The difference in the structures formed from the  $L^{hh}$  ligand is due to the coordination spheres on the metal ions involved. The assembly is controlled by the weaker Jahn-Teller effect in  $Co^{2+}$  than that of  $Cu^{2+}$ , corresponding to tetrahedral and square planar coordination in the trinuclear circular helicate and dinuclear double helicate complexes are obtained, respectively.

Hannon and co-workers demonstrated that a metal ions preference for different coordination geometries could affect with self-assembly outcome. The bis-bidentate ligand  $L^{ii}$ , separated by a 1,3-bis(aminomethyl)phenyl spacer, formed linear dimers with tetrahedral metal ions and trinuclear circular helicates with octahedral metal ions (figure 1.42).<sup>108</sup>

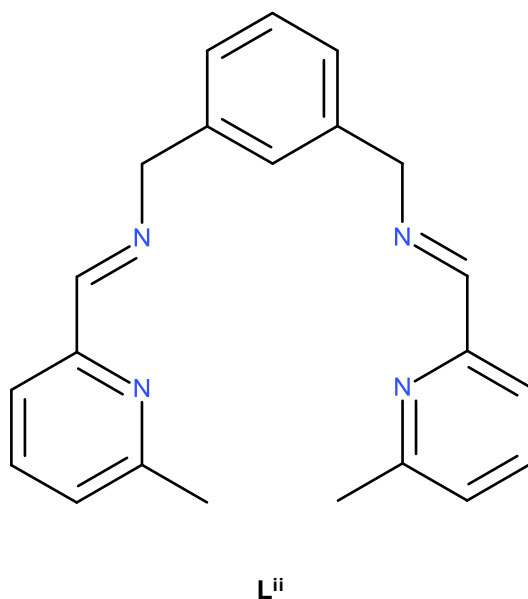


**Figure 1.42** The pyridylimine ligand system reported by Hannon and co-workers

Coordination of  $L^{ii}$  to tetrahedral monocations such as  $Cu^+$  and  $Ag^+$  gave a dinuclear double helicate of the type  $[M_2(L^{ii})_2]^{2+}$  ( $M = Cu^+$  or  $Ag^+$ ), which was characterised by NMR and ESI MS spectroscopy. Changing the metal ions coordination preference to octahedral had a dramatic influence on the self-assembly. Coordination of  $L^{ii}$  to  $Ni^{2+}$  generated a trinuclear circular helicate  $[Ni_3(L^{ii})_3(OAc)_3]^{3+}$ . The  $Ni^{2+}$  metal centres adopt a six coordinate distorted square pyramidal geometry bound to two pyridylimine binding sites and a bidentate acetate molecule. The  $Ni^{2+}$  circular helicate pack together in a hexagonal array to give channels in which the remaining anions and solvent molecules are located. Reaction of  $L^{ii}$  with five coordinate  $Cu^{2+}$  results in a mixture of dinuclear double helicate and trinuclear circular helicate and results in the formation of solvent dependent mixtures of dimer and trimer. Hannon and co-workers demonstrated that changes in the metal ions coordination geometry can directly affect the angles at the connection points of the ligands and thus the nuclearity of the supramolecular helical system.

Rice and co-workers showed another approach to creating circular helicates by displaying how the use of the metal ionic radii could be manipulated in order to form circular structures. The ligand  $L^{jj}$  containing two tridentate N-donor domains separated by a 1,3-phenylene spacer was reacted with two metal ions of differing ionic radii to produce two very different helical architectures. Ligand  $L^{jj}$  was first reacted with  $Cd^{2+}$  to produce a dinuclear double helicate  $[Cd_2(L^{jj})_2]^{4+}$ , on the other hand a pentanuclear circular helicate  $[Zn_5(L^{jj})_5]^{10+}$  is formed when  $L^{jj}$  was reacted with  $Zn^{2+}$  (figure 1.43).<sup>109</sup>

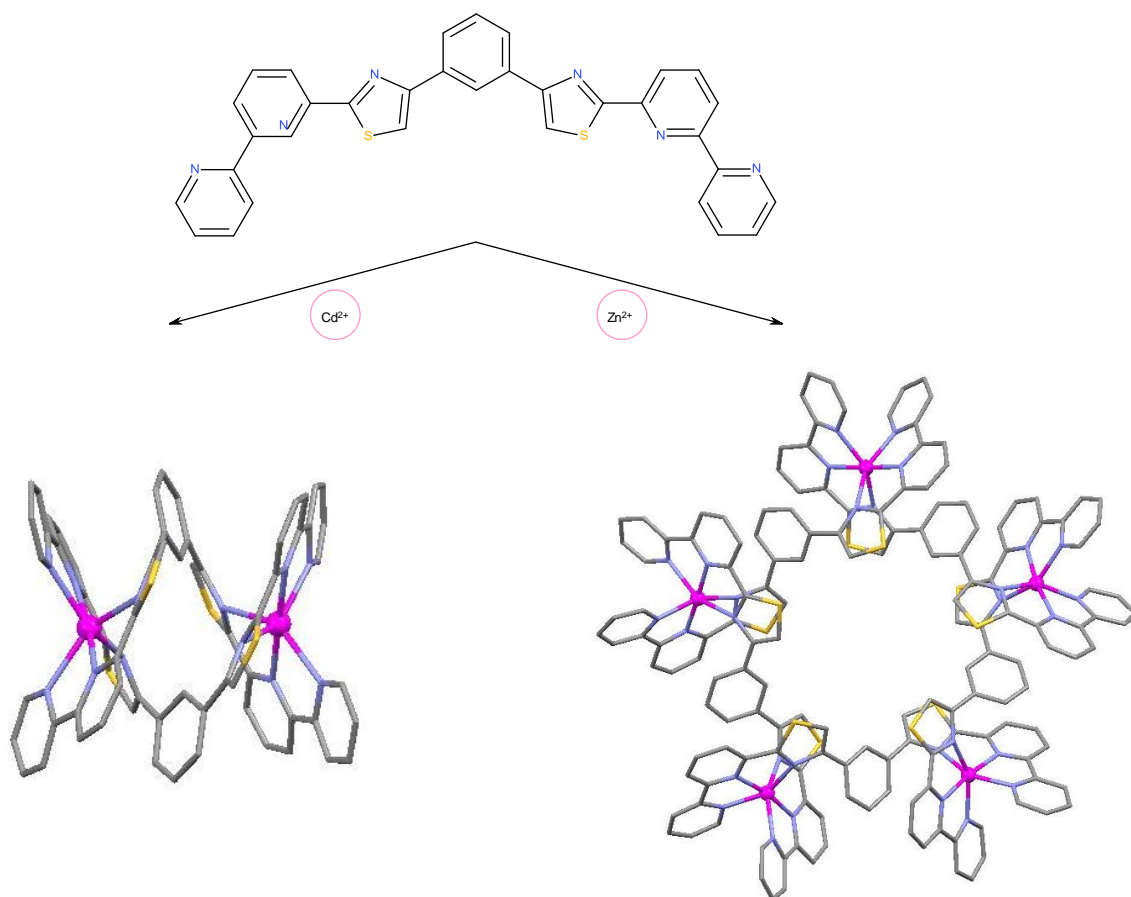


**Figure 1.43** The dinuclear double helicate  $[\text{Cd}_2(\text{L}^{\text{ij}})_2]^{4+}$  and the pentanuclear circular helicate  $[\text{Zn}_5(\text{L}^{\text{ij}})_5]^{10+}$  <sup>109</sup>

In the dinuclear double helicate the ligand partitions into two tridentate domains, each comprising a thiazole-pyridyl-pyridyl unit linked by the 1,3-phenylene spacer. The  $\text{Cd}^{2+}$  centres have distorted octahedral geometries, imparted by coordination of one tridentate thiazole-pyridyl-pyridyl domain from each ligand. The ESI-MS of the pentanuclear circular helicate showed a number of low nuclear fragments corresponding to  $\{[\text{Zn}_2(\text{L}^{\text{ij}})](\text{ClO}_4)_3\}^+$ ,  $\{[\text{Zn}(\text{L}^{\text{ij}})](\text{ClO}_4)\}^+$  and  $\{[\text{Zn}_2(\text{L}^{\text{ij}})_2](\text{ClO}_4)_3\}^+$ , but also a peak corresponding to the pentanuclear species  $\{[\text{Zn}_5(\text{L}^{\text{ij}})_5](\text{ClO}_4)_8\}^{2+}$ . In the solid state all five  $\text{Zn}^{2+}$  are six coordinate, arising from the coordination of two tridentate thiazole-pyridyl-pyridyl domains in an ‘over and under’ conformation. The formation of either dinuclear double helicate or pentanuclear circular helicate is controlled by inter-ligand steric interactions which, in turn, are governed by the size of the metal ion. It was concluded that the use of the larger  $\text{Cd}^{2+}$  metal ion (0.95 Å) brought the protons on the central phenylene units into close proximity, but sufficient distance away to form the dinuclear double helicate. However, the smaller  $\text{Zn}^{2+}$  metal (0.75 Å) and corresponding shorter Zn-N bonds forced the protons into a much closer proximity and so the steric interactions of the phenylene spacers forced the complex to find its most stable form, the pentanuclear cyclic helicate. The results produced by Rice and co-workers demonstrate how subtle changes in the metal-ligand bond distances, caused by the ionic

radii of the metal, can influence the inter-ligand steric interactions and have a pronounced effect on the outcome of the supramolecular self-assembly.

Rice and co-workers then furthered the understanding of how to form these higher nuclearity species by producing the first reported circular helicates that express certain structural features of higher order complexity. Formation of the circular helicates was driven by repulsion between the central phenylene groups of  $L^{jj}$ , as discussed previously. Since this approach appeared to be a robust path for generating circular helicates Rice and co-workers explored  $L^{jj}$  and its variants  $L^{kk}$  and  $L^{ll}$  to see whether further structural complexity could be obtained (figure 1.44).<sup>110</sup>

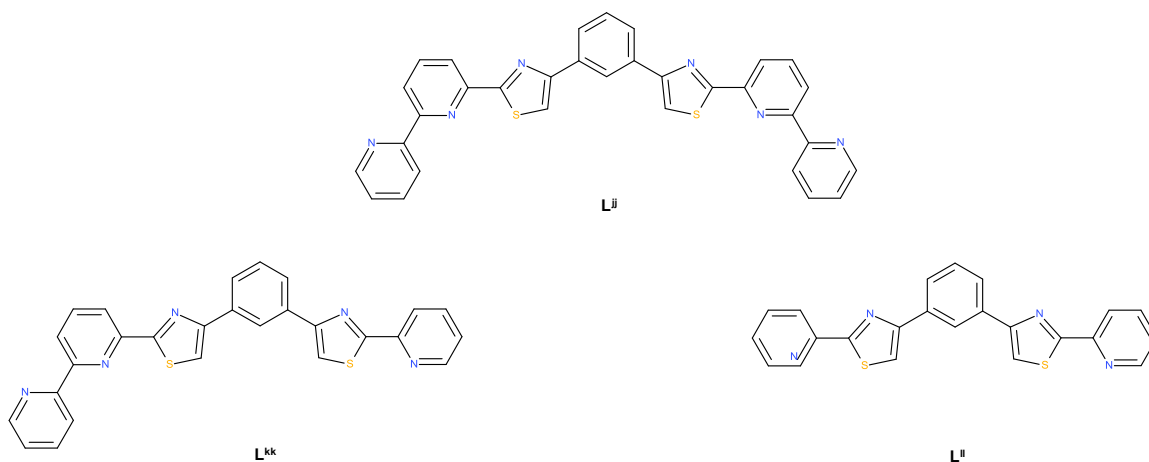


**Figure 1.44** The previously ligand  $L^{jj}$  reported by C. R. Rice and co-workers and two new ligands  $L^{kk}$  and  $L^{ll}$

Using the reasoning that a five coordinate metal ion would combine with a ditopic “3+2” dentate ligand Rice and co-workers designed the head-to-tail ligand  $L^{kk}$ . Reaction of  $L^{kk}$  with an equimolar amount of  $Cu^{2+}$  resulted in a head-to-tail pentanuclear circular helicate  $HT-[Cu_5(L^{kk})_5]^{10+}$  (figure 1.45). In the complex the ligands adopt the anticipated “3+2” binding mode, wherein the bidentate and tridentate N-donor atoms span two different  $Cu^{2+}$  centres. The ligands are arranged so that each  $Cu^{2+}$  ion is coordinated by the bidentate domain of one ligand and the tridentate domain of the next. All  $Cu^{2+}$  centres display distorted square based pyramidal geometries. The two different binding sites on ligand  $L^{kk}$  allowed for the directionality of the head-to-tail circular helicate to be achieved whilst also satisfying the coordination desires of  $Cu^{2+}$ . Coupling this with the steric interactions of the phenyl spacer ensured that when the self-assembly formed it was cyclic.

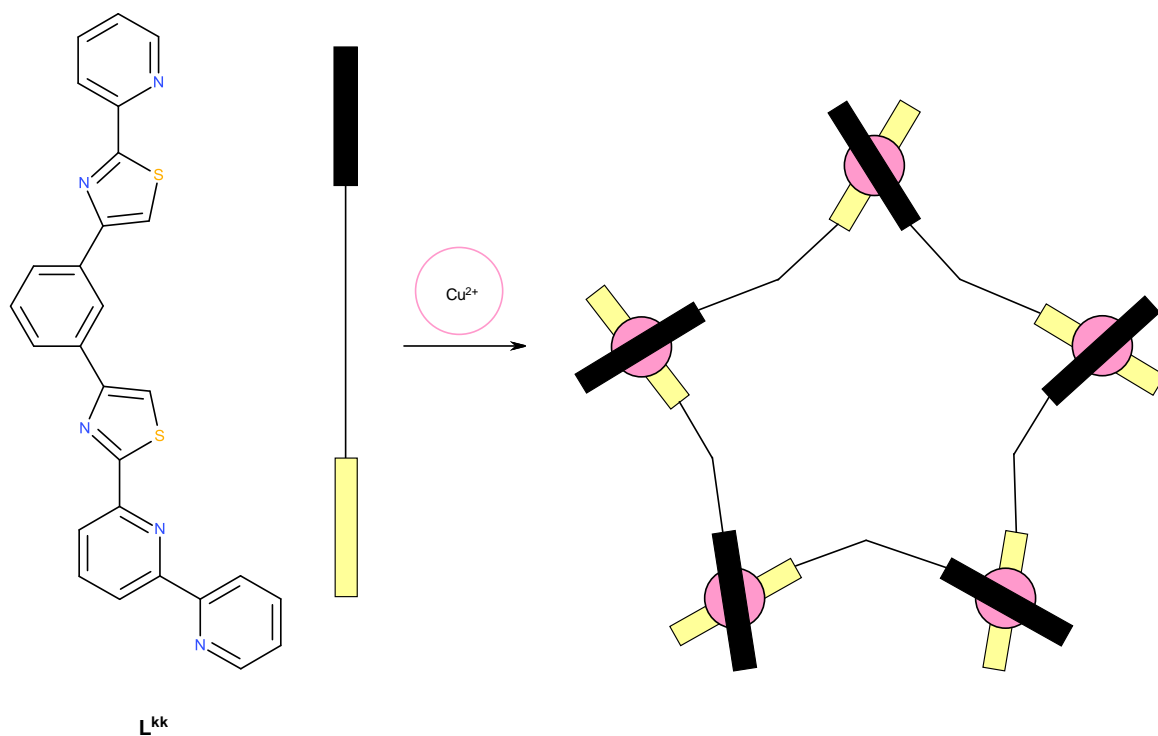


**Figure 1.45** Schematic representation of the  $HT-[Cu_5(L^{kk})_5]^{10+}$  circular helicate

Rice and co-workers focussed next on forming the heteroleptic circular helicate. The combination of the two different ligands  $L^j$  and  $L^i$  allowed for the formation of  $[Cu_5(L^{kk})_3(L^i)_2]^{10+}$  upon reaction with  $Cu^{2+}$  (figure 1.46).  $Cu^{2+}$ ,  $L^j$  and  $L^i$  appear in a 5:3:2 ratio, respectively. One of the metal centres occupies an octahedral binding site coordinated by two tridentate donors from  $L^j$ , whilst the remaining four are five-coordinate bound by one tridentate domain of  $L^j$  and one bidentate domain from  $L^i$ . Rice and co-workers have established that the basic algorithms for programming structural complexity in linear helicates can also be applied to related cyclic counterparts. The formation of these head-to-tail and heteroleptic circular helicates is a result of the steric interactions on the phenylene spacers and the versatile coordination of  $Cu^{2+}$ .

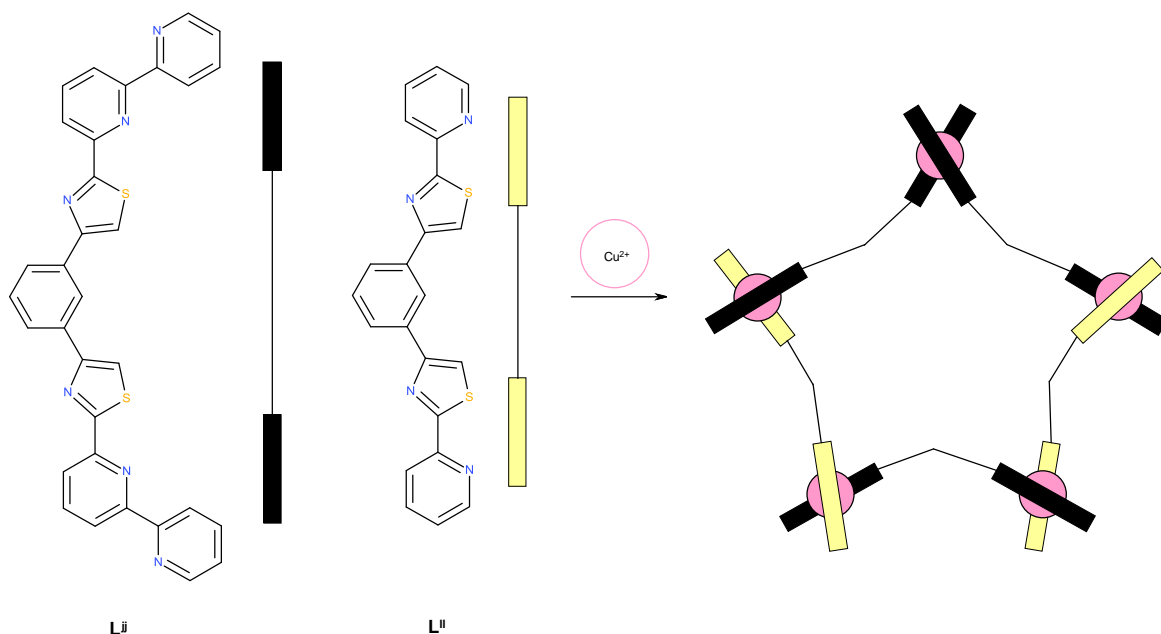


**Figure 1.46** Schematic representation of the heteroleptic circular helicate  $[\text{Cu}_5(\text{L}^{\text{kk}})_3(\text{L}^{\text{ll}})_2]^{10+}$

### 1.8 Ligand Recognition

The challenge of helicate chemistry is to understand the fundamental principles of recognition, self-assembly and self-organisation, along with searching for new functional devices, comprehensive research is being conducted to achieve these goals. As stated in section 1.6.2 a large proportion of the helicates produced are prepared from identical ligand strands and are known as homoleptic helicates. The use of a mixture of ligands can lead to mixtures of heteroleptic and homoleptic oligonuclear coordinating helical complexes. If such a mixture is formed then there is no recognition between the ligand strands and the self-assembly process is unspecific.<sup>65</sup>

In 2000 Cohen and co-workers demonstrated how structurally related ligands are not sufficiently instructed to form the heteroleptic helicate and instead form a mixture of both homoleptic and heteroleptic helicates.<sup>71, 72</sup>  $\text{L}^{\text{mm}}$  consists of three bipyridine units linked via a methylene spacer,  $\text{L}^{\text{nn}}$  consists of two bipyridine units either side of a 1,10-phenanthroline spacer. Reaction of a mixture of  $\text{L}^{\text{mm}}$ ,  $\text{L}^{\text{nn}}$  and  $\text{Cu}^+$  ions results in the formation of a mixture of homoleptic and heteroleptic helicates (figure 1.47).

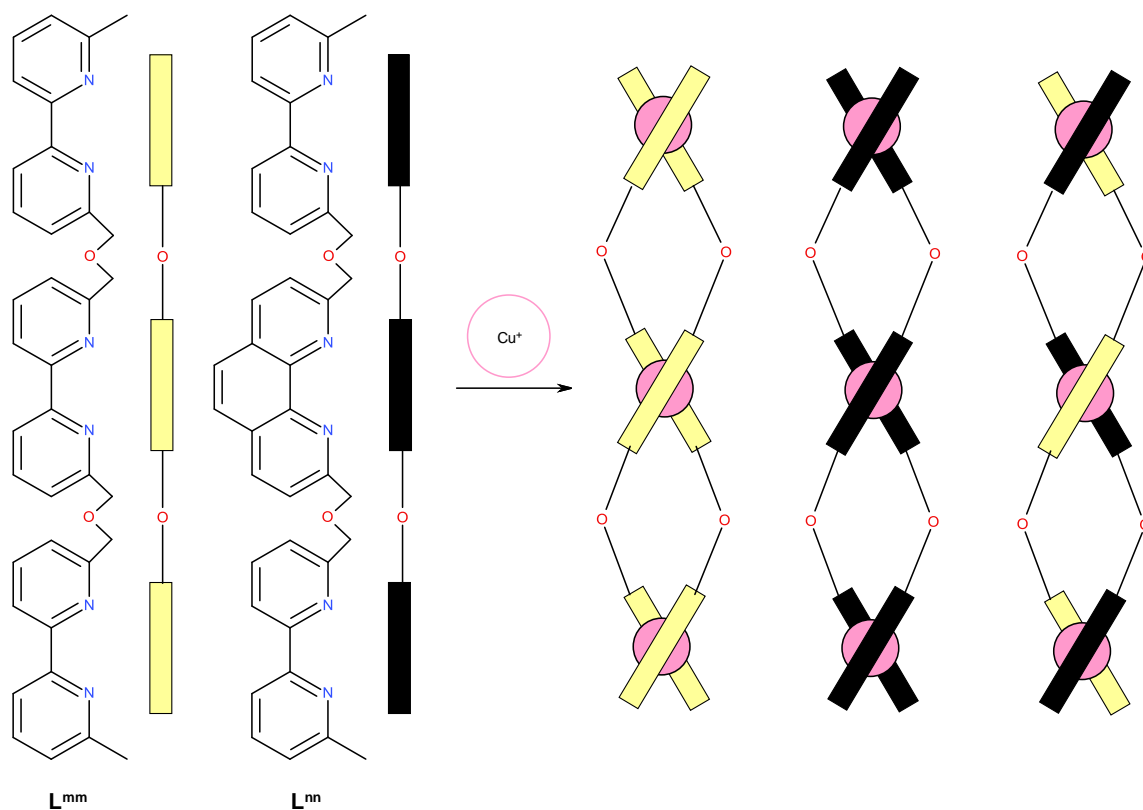


**Figure 1.47** Illustration representation of the formation of a mixture of both homo- and heteroleptic helicates upon reaction of  $L^{mm}$  and  $L^{nn}$  with  $Cu^+$  ions

Cohen and co-workers established that the importance of self-recognition in the self-assembly of helicates relies on the specific preprogramming of the instructions within the ligand strands.

Successful self-recognition in the formation of helicates is demonstrated by Lehn and co-workers and their oligo(2,2'-bipyridine) ligands of different lengths, which upon reaction of four different ligands ( $L^{oo-r}$ ) with  $Cu^+$  results in the spontaneous formation of only homoleptic helicates (figure 1.48).<sup>111</sup>

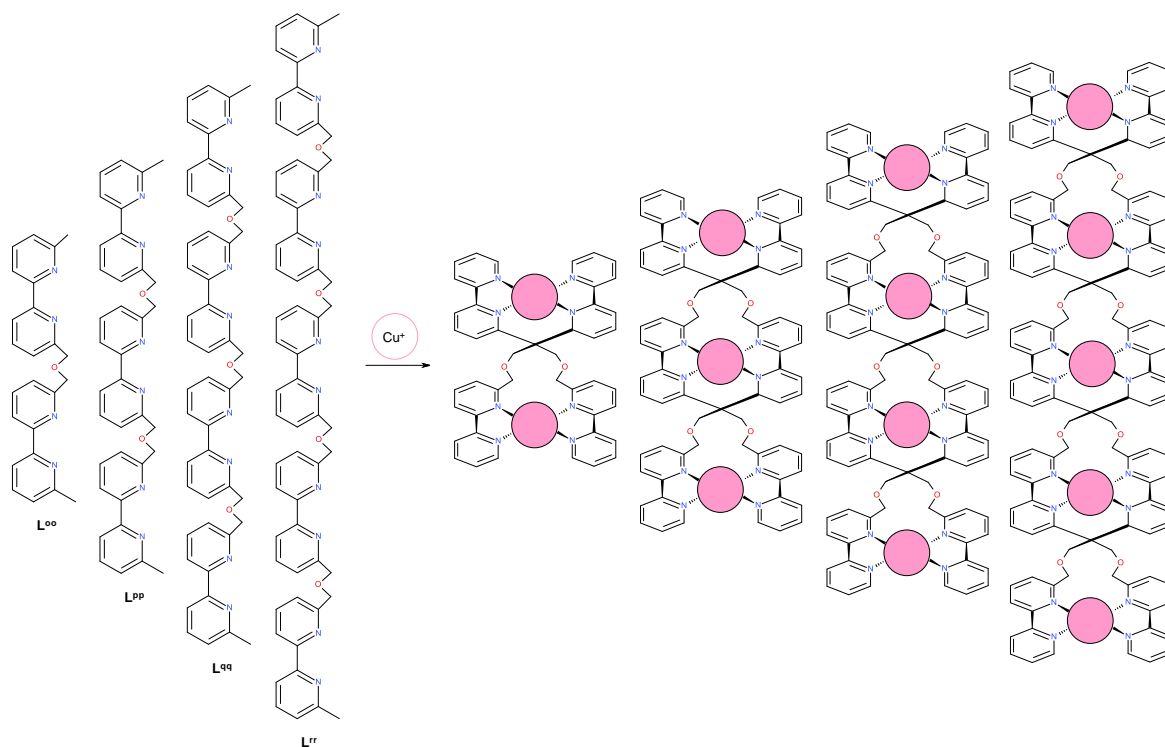


**Figure 1.48** Self-recognition in the self-assembly of the double helicates from a mixture of oligopyridine ligands ( $L^{oo-rr}$ ) with  $Cu^+$

Ligands  $L^{oo-rr}$  consist of varying lengths of 2,2'-bipyridine units separated by methylene spacers, which partition the ligands into separate bidentate binding domains which coordinate the  $Cu^+$  ions, resulting in the metal centres occupying a distorted tetrahedral geometry. The formation of a heteroleptic species with the ligands would be unfavourable as uncoordinated bipyridine binding domains would exist.

Lehn furthered this work by reporting two ligands strands  $L^{ss}$  and  $L^{tt}$ , which both contain three bipyridine units separated by a different spacer. Reaction of a mixture of  $L^{ss}$ ,  $L^{tt}$ ,  $Cu^+$  and  $Ni^{2+}$  ions in a stoichiometric amount concludes in the formation of only homoleptic species  $[Cu_3(L^{ss})_2]^{3+}$  and  $[Ni_3(L^{tt})_3]^{6+}$ . The copper centres within  $[Cu_3(L^{ss})_2]^{3+}$  occupy distorted tetrahedral geometry arising from the coordination of two bipyridine domains, one from each 6'6'-linked tritopic bipyridine ligand. The nickel centres within  $[Ni_3(L^{tt})_3]^{6+}$  occupy distorted tetrahedral geometry arising from the coordination of three bipyridine domains, one from each 5,5'-linked tris(bipyridine) ligand (figure 1.49).

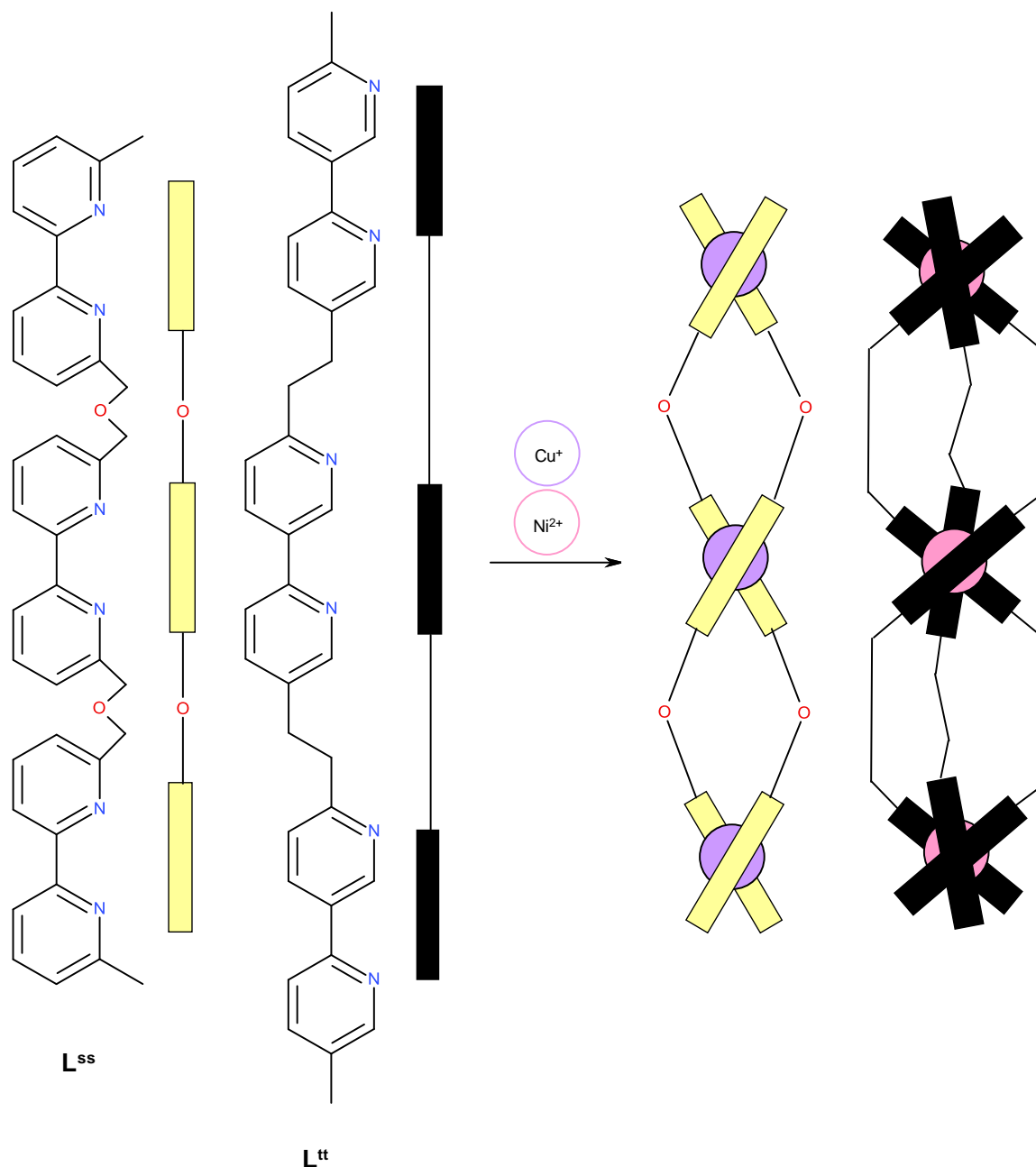


**Figure 1.49** Representation of the work reported by Lehn and co-workers on ligand recognition between two tri-bidentate ligands  $L^{ss}$  and  $L^{tt}$  with  $Cu^+$  and  $Ni^{2+}$  ions

### 1.8.1 Ligand Programming

The ligands used in the construction of metallosupramolecular helicate complexes often contain multiple coordination sites and are able to self-assemble around metal ions. Utilising the diversity of the metal ions and by exploiting the interactions between these metal ions and the ligands has led to the production of a wide range of aesthetically pleasing helicates and has allowed this field to be explored. Understanding the chemical requirements behind the molecular building blocks (size, shape, symmetry and electronic properties) allows for the system to be pre-programmed to contain all the specific

information needed to produce fascinating well-defined and controllable structures.<sup>10</sup> Ligand programming involves designing ligands that contain precise molecular instructions so that upon reaction of a specific metal ion leads to the generation of a desired metallosupramolecular complex. The programming nature of helicate complexes has attracted a lot of attention over the years with researchers designing individual molecular components that self-assemble to produce a more outstanding complicated aggregate.

The well-studied use of oligopyridines as helicing ligands by Constable demonstrated specifically designed ligands which when reacted with various metal ions of a preferred geometry results in the production of the desired superstructure. An example of this research was undertaken with sexipyridine ( $L^{uu}$ ) and a range of different metal ions possessing different coordination geometries imposed by the electronic preferences.<sup>112, 113</sup>  $L^{uu}$  is able to partition into various sets of binding domains, rotating about the pyridyl-pyridyl bonds to accommodate the required coordination of the metal ion. Therefore partitioning sexipyridine into potentially a tri-bidentate, bis-tridentate or a hexadentate binding domain. Reaction of  $L^{uu}$  with various transition metal ions leads to the formation of double helical systems, either existing as dinuclear complexes or trinuclear depending on the preferred coordination geometry of the metal ion involved. However, reaction of  $L^{uu}$  with the lanthanide cation  $Eu^{3+}$  results in the formation of a hexadentate mononuclear system  $[Eu(L^{uu})(NO_3)_2]^+$ , where all of the nitrogen donors from one sexipyridine ligand coordinate a single metal centre. Upon reaction of  $L^{uu}$  with  $Cd^{2+}$  the dinuclear double helical complex  $[Cd_2(L^{uu})_2]^{4+}$  forms. The  $Cd^{2+}$  metal ions adopt distorted octahedral geometry and binds to the tridentate domain of two different ligand strands. The reaction of with  $Cu^+$  results in the sexipyridine ligand acting as a tri-bidentate binding donor coordinating to the metal ions via three separate bipyridine units, resulting in a trinuclear double helicate  $[Cu_3(L^{uu})_2]^{3+}$ . The metal ions complete their coordination sphere by coordinating to another bipyridine unit from a different strand (figure 1.50).

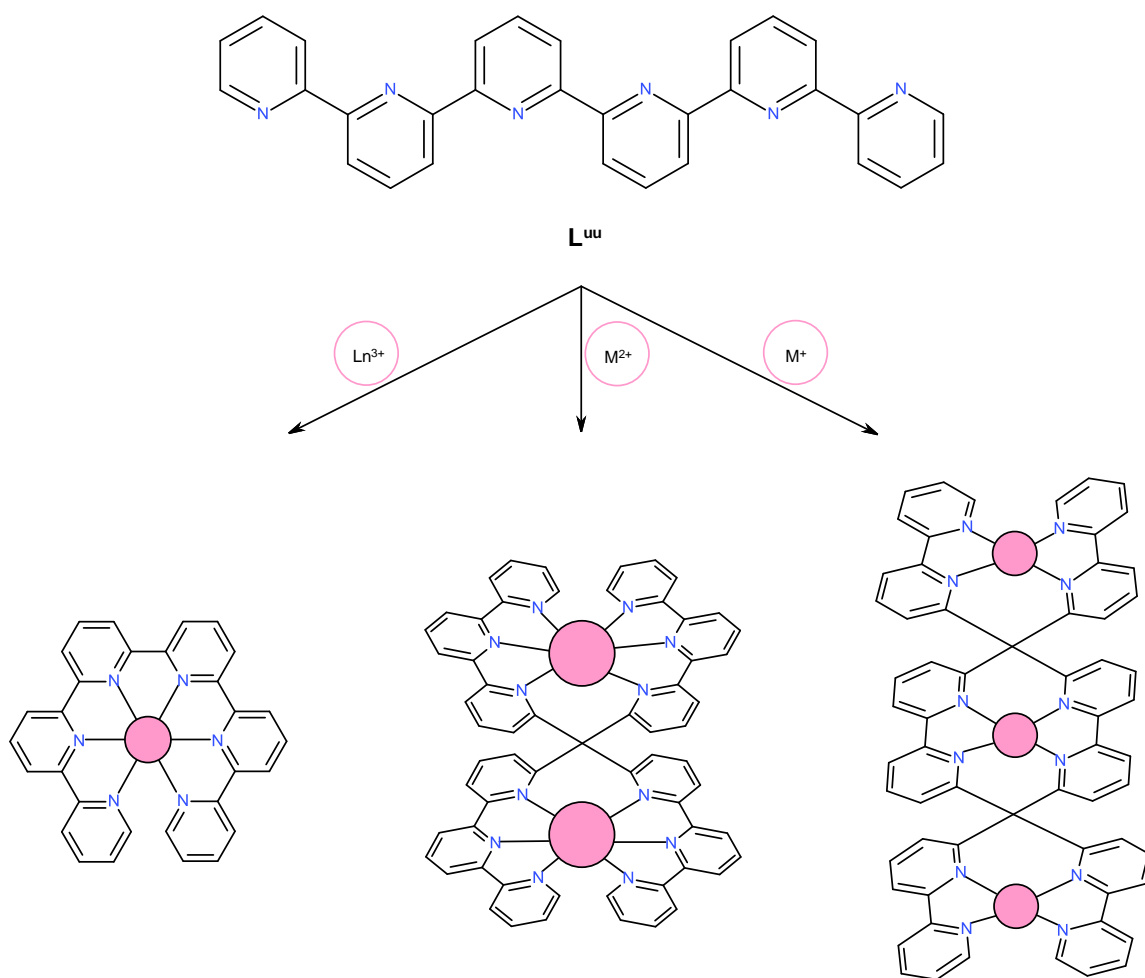


**Figure 1.50** Possible helical complexes of sexipyridine

The information stored within the ligands associated with the successful assembly of metal helicates is vital, without this pre-programmed information of large number of different species would exist; this has been demonstrated further by Rice and co-workers.<sup>114-116</sup> The research performed at the University of Huddersfield on a new class of ligands for the assembly of helicates established the synthesis and coordination of a series of polydentate N-donor ligands based on pyridyl and thiazole domains. The inclusion of the five-membered thiazole unit into a ligand chain results in the natural portioning of the ligand strands into separate binding domains, as opposed to partitioning controlled by the coordination preference of the metal cation. The natural partitioning of these pyridyl-thiazole ligands into distinct binding domains by twisting about the central C-C bond is due to the inability of the thiazole units to coordinate the same metal ion. The pre-programmed instructions of the position of these thiazoles, therefore the portioning of the binding domains plays a crucial role in the formation of different helical complexes (figure 1.51).

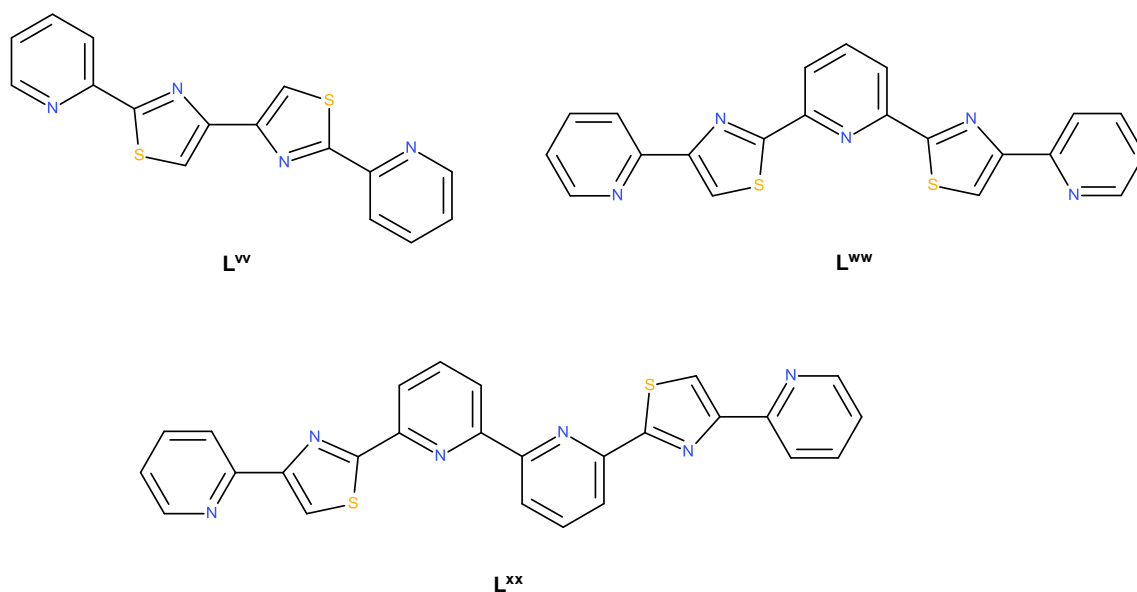


**Figure 1.51** Pyridyl thiazole ligands produced by Rice and co-workers

Reaction of the potentially tetradentate ligand  $L^v$  with either  $Co^{2+}$ ,  $Cu^{2+}$  or  $Zn^{2+}$  results in the formation of a dinuclear triple helical species of the type  $[M_2(L^v)_2]^{4+}$ . All three complexes are similar to one another; the metal ions involved have distorted octahedral geometry arising from the coordination of three thiazole-pyridyl units, one from each ligand.

Molecular modelling of the  $L^{wv}$ , the potentially pentadentate ligand suggests that a py-tz-py unit cannot easily act as a tridentate chelate as the two terminal pyridyl units are not sufficiently convergent.<sup>116</sup> Instead this ligand partitions into two bidentate py-tz units and coordinates  $Cu^{2+}$  in a dinuclear double helical array. Each of the  $Cu^{2+}$  centres in  $[Cu_2(L^{wv})_2]^{4+}$  are four coordinate and are coordinated by the py-tz unit from two different ligands, the central pyridine unit is uncoordinated and acts as an innocent spacer group separating the two py-tz binding domains.

Addition of another pyridine unit into the centre creates a new ligand which forms three different helical arrangements.  $L^{xx}$  does not act as a potentially hexadentate donor when reacted with  $Cu^{2+}$  or  $Zn^{2+}$ , but instead like  $L^{xx}$  acts as a bis-bidentate py-tz chelate and the central bipyridyl unit is uncoordinated forming the dinuclear double helicate  $[M_2(L^{xx})_2]^{4+}$  ( $M = Cu^{2+}$  or  $Zn^{2+}$ ). Upon reaction with  $Ni^{2+}$  a dinuclear double helicate is also formed, however the ligand acts as a bis-tridentate donor. Coordination through the py-tz-py domains of two ligand strands leads to octahedral geometry of the  $Ni^{2+}$  ion. When  $L^{xx}$  is reacted with  $Cd^{2+}$  it partitions into a tridentate py-tz-py and a bidentate py-tz domain resulting in a dinuclear double helicate of  $[Cd_2(L^{xx})_2]^{4+}$  where the terminal pyridine units are not coordinated.

### 1.8.2 Allosteric Interactions

Allosteric interactions involve a link between two or more coordination sites, if the event of an interaction at one coordination site affects the binding of a second connected coordination site then the ligand is termed allosteric.<sup>1</sup> This type of interaction plays an important role in biology, particularly in enzymes, where the binding of the effector often induces a conformational change that can influence the activity. In supramolecular chemistry ligands are designed to contain specific donor units of varying nature and number with the ability to partition into different binding domains which are capable of coordinating metal cations, resulting in a particular disposition of the binding sites.

Rebek and co-workers first demonstrated the allosteric effect in 1979 with macrocyclic polyethers, incorporating two remote but independent sites involving a crown ether unit for binding alkali or ammonium ions and a bipyridyl unit for the binding of transition metal ions (figure 1.52). The transport of alkali metal ions by the crown ether unit was subject to the simple control by binding a transition metal at the bipyridyl site.<sup>117, 118</sup>

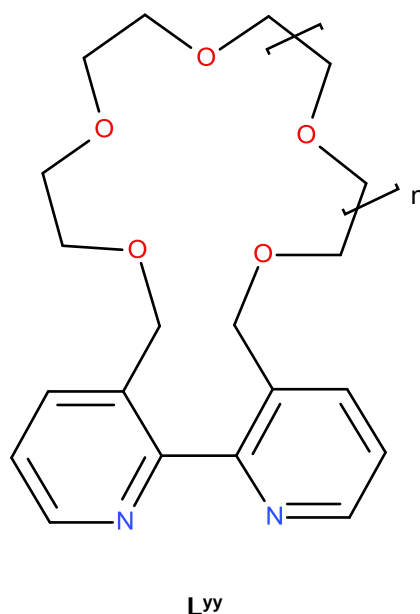


**Figure 1.52** Structure of Rebek's macrocyclic polyether ligand  $L^y$

The reactivity of the crown ether receptor is dramatically affected by the coordination of the bipyridyl units. Coordination of metal ions at the bipyridyl sites forces the aromatic groups towards each other restricting the conformation of the crown ether receptor as the benzylic oxygen atoms are directed away from each other in such a manner that they cannot be part of the ether cavity. Binding of the crown ether unit to an alkali earth metal brings the oxygen atoms closer together fixing the position of the benzylic oxygen atoms. The approach by Rebek and co-workers is related to the allosteric effect in which the ability of

the crown ether unit to coordinate group I metal ions is influenced by the coordination of the remote bipyridyl binding domains.

### 1.8.3 Ditopic Ligands

The synthesis and characterisation of ditopic ligands that possess two guest binding sites that are capable of coordinating various or specific guest species has received substantial attention over the years.<sup>119-121</sup> Ditopic ligands often contain a macrocyclic unit attached to another metal-ion binding unit that are capable of coordinating two different guest species. A well designed example of a ditopic ligand has been demonstrated by Ward and co-workers, who prepared a series of ligands containing a phenanthroline binding unit attached to an adjacent crown ether unit of various sizes (figure 1.53).<sup>122</sup>

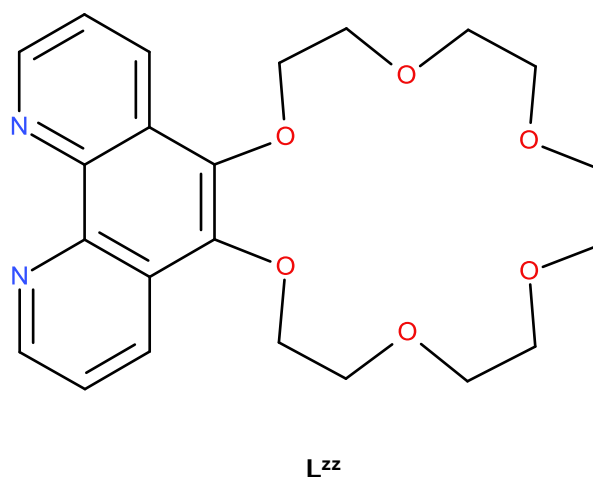


**Figure 1.53** Ditopic ligand  $L^{Zz}$  containing a phenanthroline N-donor domain attached to an adjacent [18]crown-6 unit

This simple example of a ditopic phenanthroline-crown ether ligand contains two metal binding sites that are directly fused. The bidentate N-donor domain provided by the phenanthroline is capable of coordinating transition metal cations, and the crown ether fragment is capable of binding group I and II metal ions. Reaction of this ditopic ligand with  $[Ru^{II}(bipy)_2Cl_2] \cdot 2H_2O$  resulted in a range of complexes of the type  $[Ru^{II}(bipy)_2(L^{Zz})][PF_6]_2$  and their redox potentials were investigated upon addition of barium.  $[Ru^{II}(bipy)_2(L^{Zz})][PF_6]_2$  shows a typical redox property of  $[Ru(bipy)_3]^{2+}$  derivative, with a  $Ru^{II}/Ru^{III}$  couple at -0.89 V vs. ferrocene/ferrocenium ( $Fc/Fc^+$ ) and three ligand centres couples at -1.74, -.193 and 2.17 V vs.  $Fc/Fc^+$  in MeCN. Upon addition of  $Ba^{2+}$  the ligand centre becomes broader but the  $Ru^{II}/Ru^{III}$  couple undergoes a gradual positive shift to +0.94 V. This clearly demonstrated that the barium ions are coordinated to the crown ether unit causing a slight electrostatic destabilisation of the  $Ru^{III}$  state.

Rice and co-workers have also incorporated a crown ether unit into a ligand strand, which contains a thiazole-pyridyl-pyridyl-thiazole chain to produce the ditopic ligand  $L^{aaa}$  (figure 1.54).<sup>123</sup>

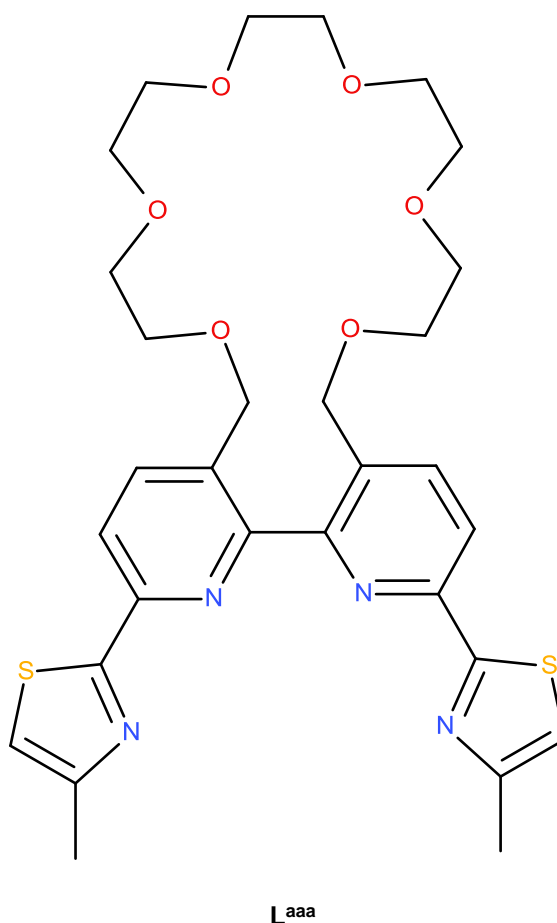


**Figure 1.54** Structure of the ditopic ligand  $L^{aaa}$

In theory  $L^{aaa}$  could act as a tetradentate donor or a bis-bidentate donor, twisting along the tz-tz bond. Reaction of  $L^{aaa}$  with  $Hg^{2+}$  resulted in the exclusive formation of a dinuclear double helicate corresponding to  $[Hg_2(L^{aaa})_2]^{4+}$ . Treatment of  $[Hg_2(L^{aaa})_2]^{4+}$  with an excess of  $NaClO_4$  afforded a complex of  $[Hg_2(L^{aaa})_2Na_2]^{6+}$ , a dinuclear double helicate. The X-ray crystal structure demonstrates that the ligand splits into two bis-bidentate domains with the two  $Hg^{2+}$  ions coordinated by two bridging ligands in a double helical arrangement. Each of the  $Hg^{2+}$  metal centres have distorted tetrahedral geometry formed by the coordination of two thiazole-pyridyl bidentate N-donor units, one from each of the two ligands involved. The sodium ions are coordinated within the crown ether unit, one is seven coordinate and binds to five oxygen atoms, leaving both the benzylic oxygen atoms uncoordinated. Solvent and anion molecules complete the  $Na^+$  coordination. The inability for the [18]crown-6 to fulfil the coordination preference of the  $Na^+$  ions is due to the size of the unit. The reaction of  $[Hg_2(L^{aaa})_2]^{4+}$  with the larger  $Ba(ClO_4)_2$  results in the formation of a

mononuclear species where the  $\text{Hg}^{2+}$  is coordinated by the tetradentate ligand in the equatorial plane and two perchlorate anions in the axial sites. The  $\text{Ba}^{2+}$  is coordinated within the crown ether unit by all six of the oxygen donor atoms available, reflecting the complementarity in size between the ionic radius of  $\text{Ba}^{2+}$  and the cavity volume of [18]crown-6. In the mononuclear complex both of the benzylic oxygen atoms are coordinating the  $\text{Ba}^{2+}$  ions, therefore restricting the mobility of the ligand, preventing it from partitioning into two bidentate domains. The system generated by Rice and co-workers demonstrates the reprogrammable nature of the ditopic ligand  $\mathbf{L}^{\text{aaa}}$ , where the initial programmed formation of a dinuclear double helicate with  $\text{Na}^+$  can be reprogrammed upon introduction of  $\text{Ba}^{2+}$  to form a mononuclear complex.

## 2. Self-assembly of helicates and circular helicates using N-oxide containing ligands

There are a large number of self-assembled species resulting from the coordination of ligands containing many different donor units, but surprisingly the use of the N-oxide donor unit has received little attention in self-assembly and its ability to control the formation of metallosupramolecular species has largely been overlooked.

In 2001 Amoroso and co-workers undertook a comparative study of the coordination complexes of a series of  $[\text{NiL}_2][\text{ClO}_4]$  complexes (L = terpyridine 1,1',1''-N-trioxide, terpyridine 1,1''-N-dioxide or terpyridine 1-N-oxide) to determine how the variation in ligand geometry affects the resulting complex.<sup>124</sup> Their results are summarised in table 2.1:

| Complex                          | Average Ni-O bond length (Å) | Arrangement |
|----------------------------------|------------------------------|-------------|
| $[\text{Ni}(\text{terpyO}_3)_2]$ | 2.056                        | facial      |
| $[\text{Ni}(\text{terpyO}_2)_2]$ | 2.026                        | meridonal   |
| $[\text{Ni}(\text{terpyO})_2]$   | 2.055                        | meridonal   |

**Table 2.1** Results from the study conducted by Amoroso and co-workers<sup>124</sup>

Amoroso and co-workers observed the greater flexibility of the terpyridine tris-N-oxide in its ability to facially co-ordinate the metal centre. In 2002 the group furthered their work on N-oxides in focussing upon the oxidation of 4',4''-diphenyl-2,2':6',2'':6,2''-quaterpyridine, both the bis-N-oxide and tetra-N-oxide quaterpyridines co-ordinate to a variety of metal ions. The results show that the tetra-N-oxide is a more flexible donor, arranging itself in numerous ways (allowing cubic geometry). However, the bis-N-oxide ligand has the central bipyridyl fragment which makes the ligand tend towards a more linear form of co-ordination and favours the eight coordinate geometry.<sup>125</sup>

The complexes reported by Amoroso and co-workers all have mononuclear structures e.g. only one metal ion is present. However, in 2007 Rice and co-workers incorporated the N-oxide donor unit within the middle of the ligand strand ( $\text{L}^{\text{bbb}}\text{-L}^{\text{ccc}}$ ) and formed dinuclear double helicates of the type  $[\text{M}_2\text{L}_2]^{n+}$  (Figure 2.1).<sup>126</sup>

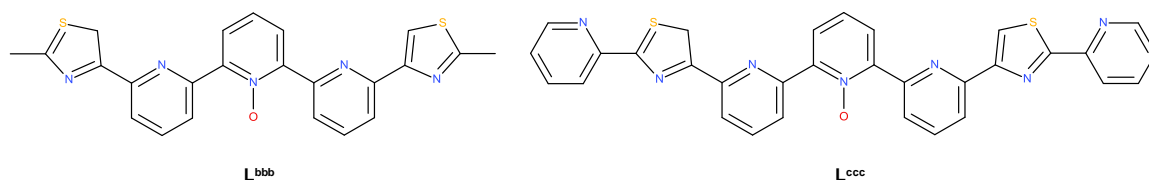


**Figure 2.1** The two symmetrical polydentate pyridyl-thiazole ligands reported by Rice and co-workers in 2007<sup>126</sup>

Reaction of either of these ligands with  $\text{Cd}(\text{ClO}_4) \cdot 6\text{H}_2\text{O}$  results in the formation of a dinuclear double helicate, the N-oxide unit partitions the ligands into two separate binding domains. Both ligands in the  $[\text{Cd}_2(\text{L}^{bbb})_2(\text{ClO}_4)_2]^{2+}$  complex are partitioned into two tridentate binding domains with the N-oxide unit acting as a bridging donor to both cadmium ions. Studies carried out in 2000, by Rice and co-workers, on a similar ligand containing a pyridyl-thiazole-pyridyl-thiazole-pyridyl chain forms a mononuclear complex with cadmium.<sup>114</sup> A direct comparison cannot be made but it is reasonable to assume that the steric constraints of the N-oxide unit prevent the ligand from efficiently coordinating one metal ion.

Each of the metals in the  $[\text{Cd}_2(\text{L}^{ccc})_2]^{4+}$  solid state structure are coordinated via the central N-oxide unit and the two terminal bidentate pyridyl-thiazole domains from each ligand. The interactions between the pyridyl unit adjacent to the N-oxide and the cadmium are considered too long to be bonding. As with  $L^{bbb}$ , the N-oxide coordinates both cadmium ions, acting as a bridging bidentate donor. The incorporation of the N-oxide unit changes the partitioning of the ligand as reaction of a ligand strand identical to  $L^{ccc}$ , but without the central N-oxide unit, results in the formation of a trimetallic double helicate with cadmium.<sup>81</sup> Here the ligand partitions into three different binding domains, the two terminal pyridyl-thiazole donors and a central tridentate terpyridine unit. Whereas,  $L^{ccc}$  cannot act as a tridentate unit due to the N-oxide unit forcing the ligand into two different binding domains.

Described in this chapter is the synthesis and coordination chemistry of four polydentate N-oxide ligands  $L^1$ - $L^4$  (Figure 2.2) which assemble into helical supramolecular arrays upon coordination with transition metal ions. These particular ligands comprise of polydentate donor domains (pyridyl-thiazole-pyridyl-N-oxide) where the N-oxide unit has been incorporated into the terminal domains of the ligand strand. The simplest of these ligands  $L^1$ , contains a tetradentate donor domain consisting of pyridyl-N-oxide-pyridyl-thiazole-pyridyl donor units. The ligand  $L^2$ , contains two identical thiazole-pyridyl-pyridyl-N-oxide (tz-py-pyO) binding domains. The head-to-tail ligand  $L^3$ , contains two different binding domains, which consist of a bidentate thiazole-pyridyl (tz-py)  $\text{N}_2$  binding domain and a tridentate thiazole-pyridyl-pyridyl-N-oxide (tz-py-pyO) binding domain separated by a 1,3-

phenylene unit.  $L^4$ , contains two identical thiazole-pyridyl-pyridyl-N-oxide (tz-py-pyO)  $N_3$  binding domains separated by a 1,3-phenol spacer.

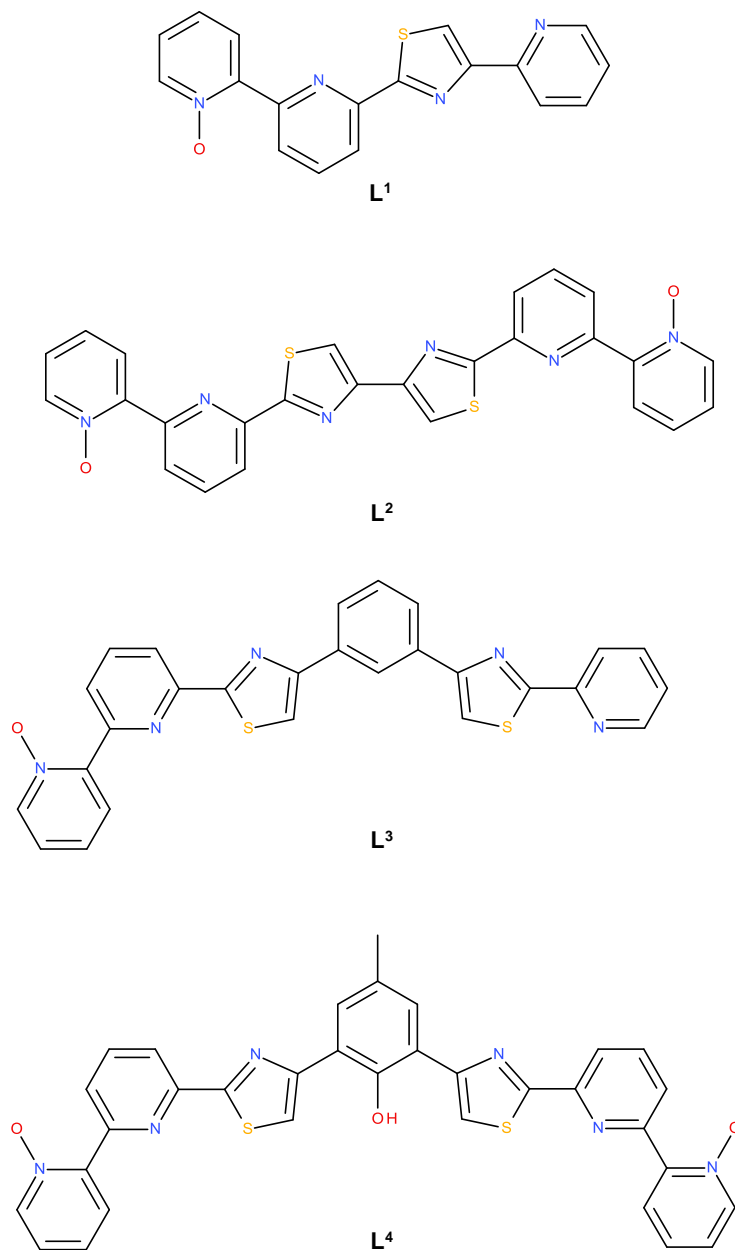
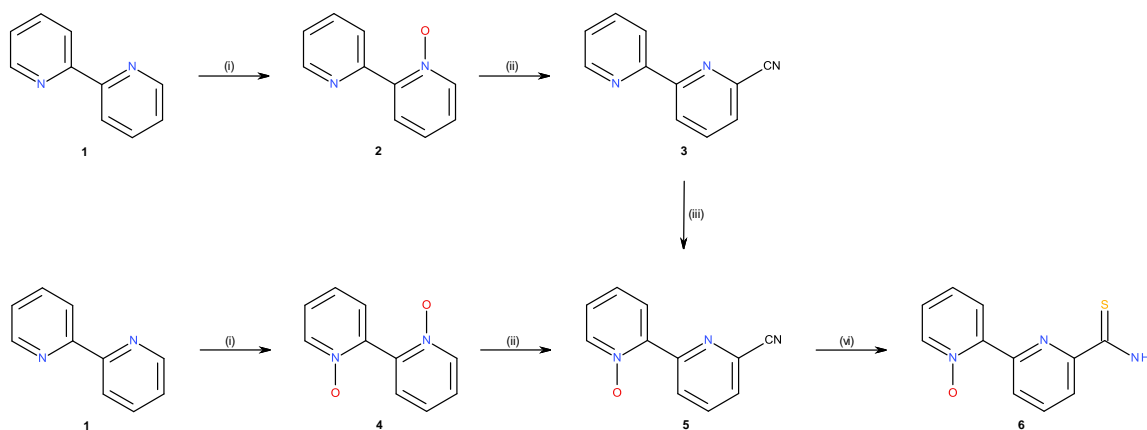


Figure 2.2 Ligands  $L^1$ - $L^4$

## 2.1 Ligand synthesis

### 2.1.1 Synthesis of 1-*N*-oxide-2,2'-bipyridine-6'-thioamide (6)

The principal material in the formation of these *N*-oxide ligands is 6'-cyano-2,2'-bipyridine-*N*-1-oxide (5) which can be prepared via two different routes (Scheme 2.1).



**Scheme 2.1** Synthesis of 1-*N*-oxide-2,2'-bipyridine-6'-thioamide (6). Reagents and conditions: (i) *m*CBPA, DCM, RT; (ii) TMS-CN, BzCl, DCM, reflux; (iii) *m*CBPA, DCM, RT; (iv) H<sub>2</sub>O<sub>2</sub>, CH<sub>3</sub>COOH, heat at 80 °C; (v) TMS-CN, BzCl, DCM, reflux; (vi) H<sub>2</sub>S, Et<sub>3</sub>N, EtOH, RT.

The first route involves a four-step synthesis starting from the reaction of 2,2'-bipyridyl (1) with a stoichiometric amount *m*CBPA, giving the mono-*N*-oxide (2). The reaction was carefully monitored by TLC and the reaction stopped before the formation of the bis-*N*-oxide started to occur, purification by column chromatography gave (2) as white solid. Reaction of the mono-*N*-oxide (2) with trimethylsilylcyanide in the presence of benzoyl chloride gave 6'-carbonitrile-2,2'-bipyridine (3).<sup>127</sup> Complete conversion of (3) to 6'-cyano-2,2'-bipyridine-1-oxide (5) using a slight excess of *m*CBPA, gave a sandy solid after purification by column chromatography. The presence of an ion at *m/z* 220 (*M* + Na<sup>+</sup>) in the ESI-MS confirmed the presence of 6'-cyano-2,2'-bipyridine-1-oxide (5).

The second route involved reaction of 2,2'-bipyridine-bis-1,1'-*N*-oxide. Specifically, a solution of 2,2'-bipyridyl (1) in hydrogen peroxide and glacial acetic acid was heated at 80 °C for 7 hours. The resulting yellow solution was cooled to room temperature, slowly added to acetone and placed in a fridge for 2 days during which time a precipitate formed, which was isolated by filtration to give 2,2'-bipyridine-bis-1,1'-*N*-oxide (4). The reaction of (4) with benzoyl chloride and trimethylsilylcyanide in DCM, was monitored by TLC until it was judged that the maximum quantity of the product (5) had formed. Purification by column chromatography gave 6'-cyano-2,2'-bipyridine-1-*N*-oxide (5) resulting in a three-step synthesis.

6'-cyano-2,2'-bipyridine-1-*N*-oxide (5) was converted to 1-*N*-oxide-2,2'-bipyridine-6'-thioamide (6) by reaction with H<sub>2</sub>S gas in a similar manner to Rice and co-workers in 2007.<sup>127</sup> The reaction produced a yellow solid when purging hydrogen sulphide through a solution of (5) in ethanol in the presence of triethylamine. The appearance of two singlets, corresponding to the thioamide at 9.4 and 7.7 ppm in the <sup>1</sup>H NMR confirmed the complete conversion of the carbonitrile derivative. Furthermore, in the ESI-MS an ion was observed at *m/z* 254 (M + Na<sup>+</sup>).

The first route was the desired method of synthesis as although it requires more synthetic steps, it is the most reliable method of preparation as the yields from the second step were variable, with a maximum recovery of 60% compared to the 98% obtained from the first route. The main difficulty with the second route is due to the insoluble nature of 2,2'-bipyridine-bis-1,1'-*N*-oxide, and the reaction resulted in the formation of varying amounts of the unwanted 6,6''-dicyano derivative.

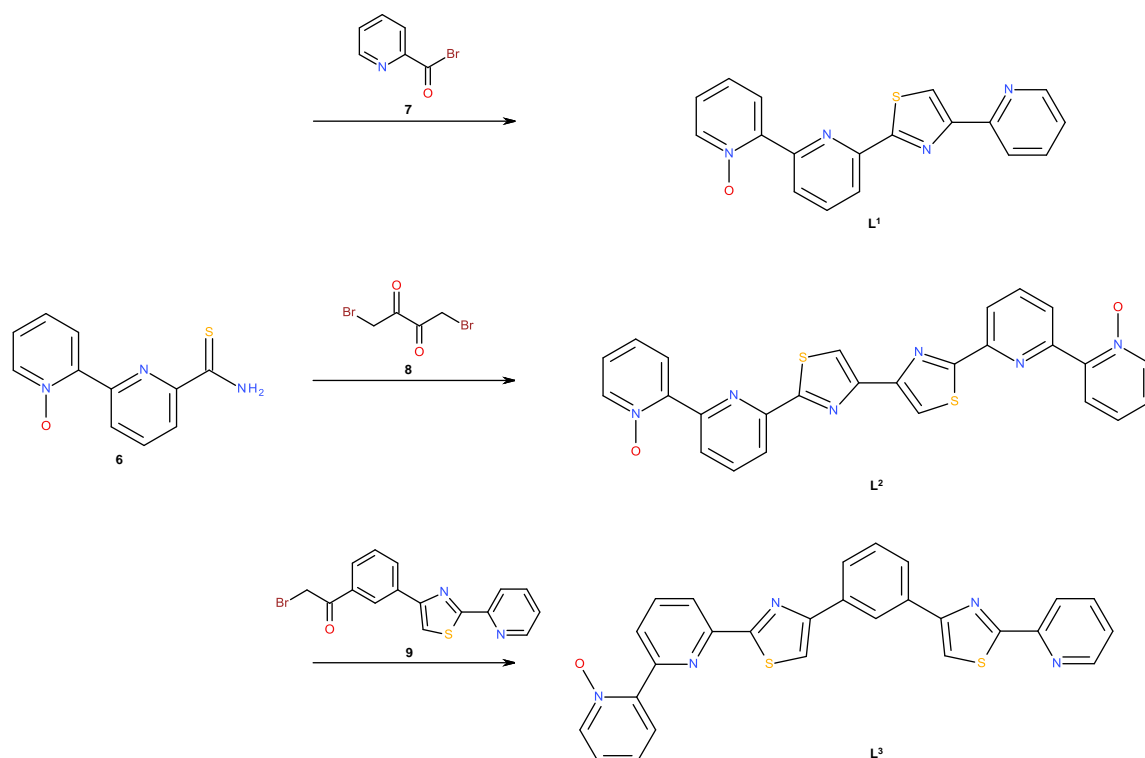
### 2.1.2 Synthesis of Ligands **L**<sup>1</sup>-**L**<sup>3</sup>

The three *N*-oxide ligands **L**<sup>1</sup>, **L**<sup>2</sup> and **L**<sup>3</sup> were synthesised in an analogous fashion, outlined in scheme 2.2, reaction of the thioamide (6) with  $\alpha$ -bromoacetyl derivatives (7)-(9) in EtOH gave the corresponding ligands **L**<sup>1</sup>-**L**<sup>3</sup>.

The 2-( $\alpha$ -bromoacetyl)pyridine (7) used in the synthesis of **L**<sup>1</sup> was prepared in a similar manner to the procedure detailed by Rice and co-workers in 2007.<sup>128</sup> To a suspension of 1-*N*-oxide-2,2'-bipyridine-6'-thioamide (6) in EtOH was added 2-( $\alpha$ -bromoacetyl)pyridine (7) and the reaction was refluxed for 8 hours, during which time all reactants dissolved. The reaction was allowed to stand at room temperature for 12 hours and the resulting precipitate was filtered and suspended in concentrated ammonia to give **L**<sup>1</sup> as a pale yellow solid. The formation of **L**<sup>1</sup> was confirmed by <sup>1</sup>H NMR which showed 12 different aromatic proton environments and contained, amongst others, a singlet at 8.5 ppm, corresponding to the thiazole ring. ESI-MS also confirms the formation of **L**<sup>1</sup> with an ion observed at *m/z* 333 (M + H<sup>+</sup>).

The synthesis for **L**<sup>2</sup> is outlined in scheme 2.2 and was carried out in a similar manner to that of **L**<sup>1</sup>. The synthesis of 1,4-dibromo-2,3-dione (8) was carried out according to the procedure outlined by Rice and co-workers in 2000.<sup>114</sup> Reaction of this  $\alpha$ -bromoacetyl derivative (8) with 1-*N*-oxide-2,2'-bipyridine-6'-thioamide (6) in EtOH for 8 hours, during which time a precipitate formed. Filtration, washing and neutralisation gave the ligand **L**<sup>2</sup> as a pale yellow solid. ESI-MS confirmed the successful formation of **L**<sup>2</sup> as an ion at *m/z* 509 (M + H<sup>+</sup>) was observed. <sup>1</sup>H NMR was uninformative as the solubility of the ligand was very poor, even in d<sup>6</sup>-DMSO at 80 °C.

The synthesis of the  $\alpha$ -bromoacetyl (9) was carried out in a similar manner to the procedure described by Rice and co-workers.<sup>110</sup> Reaction of the thioamide (6) and the thiazole-containing  $\alpha$ -bromoacetyl derivative (9) in EtOH at reflux for 8 hours resulted in a precipitate. Filtration followed by washing and suspension in concentrated ammonia gave  $L^3$  as a light yellow solid. Confirmation of the successful formation of  $L^3$  was obtained by  $^1H$  NMR which showed a total of 17 different aromatic protons which would be expected for the unsymmetrical ligand. Additionally an ion in the ESI-MS was observed at  $m/z$  492 ( $M + H^+$ ).

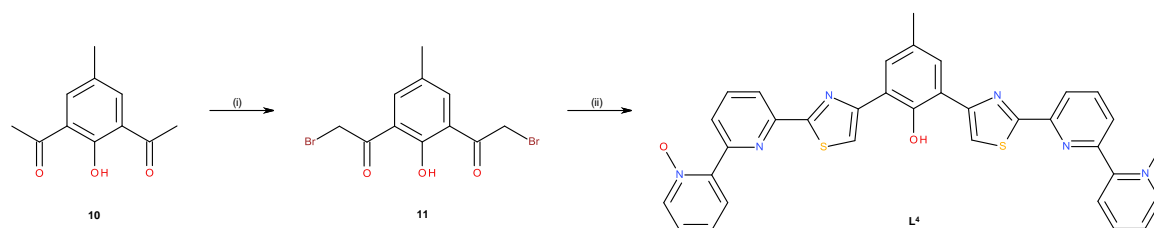


**Scheme 2.2** Synthesis of ligands  $L^1$ - $L^3$ . Reagents and conditions: EtOH, reflux

### 2.1.3 Synthesis of $L^4$

The synthesis of  $L^4$  is outlined in scheme 2.3. The Friedel-Crafts acylation of *p*-cresol was carried out in a similar manner to the procedure described by Mandal & Nag in 1983.<sup>129</sup> Reaction of the diketone (10) with bromine in acetic acid gave the mono, di, tri and tetra-brominated species, purification of the crude material via column chromatography gave the dibrominated product (11). A shift in ppm and change in integration in the  $^1H$  NMR spectra from 2.7 ppm for  $-COCH_3$ , that integrates to 6H, to 4.6 ppm for  $-CH_2Br$ , that integrates to 4H, confirms the formation of the 1,3-di( $\alpha$ -bromoacetyl)cresol (11). Furthermore, in the ESI-MS an ion is observed at  $m/z$  373 corresponding to ( $M + Na^+$ ). Reaction of the dibromo-ketone (11) and the thioamide (6) in EtOH resulted in the thioamide attaching once to form a thiazole, with one of the  $-CH_2Br$  units left unreacted. This is due to the

solubility; once the thioamide (6) has reacted with one of the  $\alpha$ -bromoacetyls it becomes insoluble in EtOH and precipitates. However, reaction of the thioamide (6) with the  $\alpha$ -bromoacetyl (11) in DMF for 18 hours at 80 °C results in a precipitate. Filtration followed by deprotonation with concentrated ammonia gave the ligand  $L^4$  as a pale yellow solid. As with  $L^2$  the solubility of the ligand is very poor, even in  $d^6$ -DMSO at 80 °C and precluded  $^1H$  NMR analysis. ESI-MS confirms the successful formation of  $L^4$ , showing an ion at  $m/z$  616 ( $M + H^+$ ).



**Scheme 2.3** Synthesis of  $L^4$ . Reagents and conditions: (i)  $Br_2$ ,  $CH_3COOH$ , heat at 80 °C; (ii) thioamide (6), DMF, heat at 80 °C

## 2.2 Coordination Chemistry

### 2.2.1 Complexes of $L^1$ with copper (II)

The reaction of  $L^1$  with an equimolar amount of  $Cu(ClO_4)_2 \cdot 6H_2O$  in MeCN results in a green solution. ESI-MS of the resulting solution confirmed the formation of a mononuclear complex with an ion observed at  $m/z = 494$  corresponding to the complex  $\{[Cu(L^1)]ClO_4\}^+$ . Higher molecular weight ions at  $m/z = 1088$ , 1683, 2280 and 2873 which correspond to  $\{[Cu_n(L^1)_n](ClO_4)_{2n-1}\}^+$ , where  $n = 2, 3, 4$  and 5 are also observed. It is likely that these higher nuclearity ions are due to aggregation of the mononuclear species during the ESI-MS process. Slow diffusion of ethyl acetate vapour into the resulting green solution afforded pale green crystals of X-ray quality. Single crystal X-ray diffraction studies confirmed the formation of the mononuclear species  $[Cu(L^1)(ClO_4)_2(sol)]$  (figure 2.3).

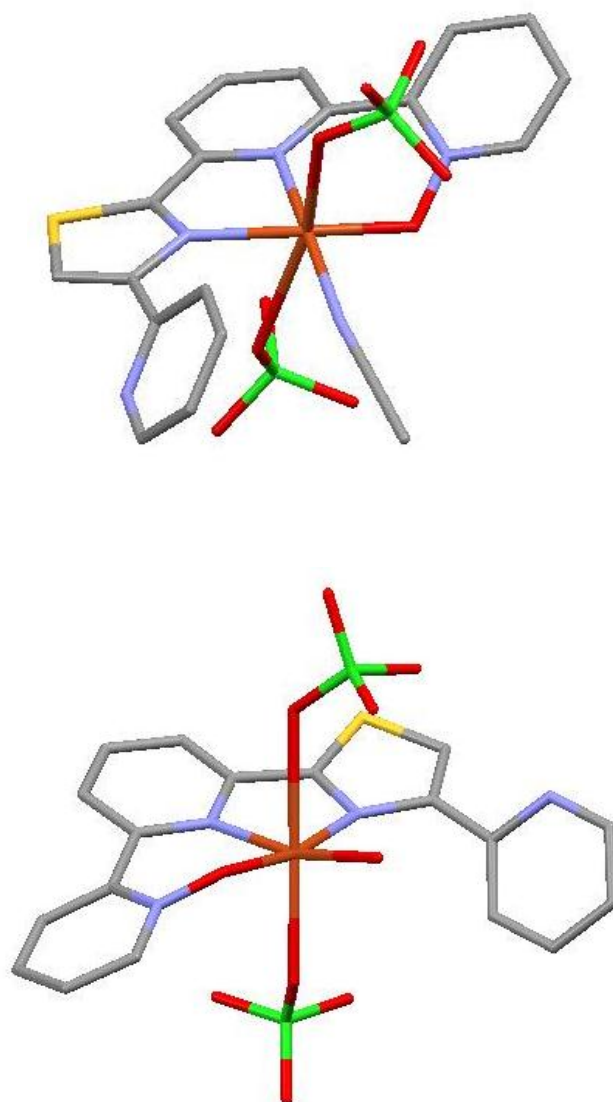


**Figure 2.3** X-ray crystal structure of  $[\text{Cu}(\text{L}^1)(\text{ClO}_4)_2(\text{MeCN})]$  (top) and  $[\text{Cu}(\text{L}^1)(\text{ClO}_4)_2(\text{H}_2\text{O})]$  (bottom)

In the solid state there are two different molecules in the unit cell, each of which contains a 6-coordination metal centre formed by coordination of one ligand strand, two perchlorate counter ions and either a molecule of MeCN (top) or a H<sub>2</sub>O molecule (bottom) giving the simple mononuclear species  $[\text{Cu}(\text{L}^1)(\text{ClO}_4)_2(\text{sol})]$ . In both cases the ligand acts as a tridentate donor, coordinating the copper metal centre by the thiazole and pyridine N-donor units and also the terminal O-donor N-oxide unit (Cu-N: 1.97-2.03 Å; Cu-ON: 1.92-2.36 Å).

| [Cu(L <sup>1</sup> )(ClO <sub>4</sub> ) <sub>2</sub> (MeCN)] |                 | Cu(L <sup>1</sup> )(ClO <sub>4</sub> ) <sub>2</sub> (H <sub>2</sub> O)] |                 |
|--|-----------------|---|-----------------|
| Bond   | Bond length (Å) | Bond  | Bond length (Å) |
| Cu(2)-N(6)   | 2.034(5)        | Cu(1)-N(2)  | 1.965(5)        |
| Cu(2)-N(7)   | 1.972(5)        | Cu(1)-N(3)  | 2.013(5)        |
| Cu(2)-N(9)   | 1.979(6)        | Cu(1)-O(7)  | 1.981(4)        |
| Cu(2)-O(13)  | 1.920(4)        | Cu(1)-O(8)  | 1.914(4)        |
| Cu(2)-O(24)  | 2.355(5)        | Cu(1)-O(21)   | 2.285(5)        |

**Table 2.2** Selected bond lengths (Å) for the complex [Cu(L<sup>1</sup>)(ClO<sub>4</sub>)<sub>2</sub>(sol)]

| [Cu(L <sup>1</sup> )(ClO <sub>4</sub> ) <sub>2</sub> (MeCN)] |                | Cu(L <sup>1</sup> )(ClO <sub>4</sub> ) <sub>2</sub> (H <sub>2</sub> O)] |                |
|--|----------------|---|----------------|
| Bond   | Bond angle (°) | Bond  | Bond angle (°) |
| N(6)-Cu(2)-O(24)   | 91.65(19)      | N(2)-Cu(1)-N(3)   | 82.7(2)        |
| N(7)-Cu(2)-N(6)  | 81.8(2)        | N(2)-Cu(1)-O(7)   | 165.4(2)       |
| N(7)-Cu(2)-N(9)  | 170.1(2)       | N(2)-Cu(1)-O(21)  | 101.08(19)     |
| N(7)-Cu(2)-O(24)   | 96.4(2)        | N(3)-Cu(1)-O(21)  | 104.24(18)     |
| N(9)-Cu(2)-N(6)  | 100.6(2)       | O(7)-Cu(1)-N(3)   | 95.86(19)      |
| N(9)-Cu(2)-O(24)   | 93.1(2)        | O(7)-Cu(1)-O(21)  | 93.40(17)      |
| O(13)-Cu(2)-N(6)   | 166.3(2)       | O(8)-Cu(1)-N(2)   | 89.6(2)        |
| O(13)-Cu(2)-N(7)   | 88.0(2)        | O(8)-Cu(1)-N(3)   | 168.00(19)     |
| O(13)-Cu(2)-N(9)   | 88.0(2)        | O(8)-Cu(1)-O(7)   | 89.30(18)      |
| O(13)-Cu(2)-O(24)  | 98.6(2)        | O(8)-Cu(1)-O(21)  | 86.20(18)      |

**Table 2.3** Selected bond angles (°) for the complex [Cu(L<sup>1</sup>)(ClO<sub>4</sub>)<sub>2</sub>(sol)]

### 2.2.2 Coordination chemistry of $L^2$ with nickel (II)

The reaction of  $L^2$  with  $Ni(ClO_4)_2 \cdot 6H_2O$  in  $MeNO_2$  produced a green solution. ESI-MS gave a remarkably simple spectrum with ions at  $m/z = 1433$ ,  $922$  and  $665$  corresponding to  $\{[Ni_2(L^2)_2](ClO_4)_3\}^+$ ,  $\{[Ni_2(L^2)](ClO_4)_3\}^+$  and  $\{[Ni_2(L^2)_2](ClO_4)_2\}^{2+}$  respectively, confirming the formation of a dinuclear double helicate. Slow diffusion of THF into the resulting solution afforded light green crystals of X-ray quality. Single crystal X-ray crystallographic analysis confirmed the formation of a dinuclear double helicate  $[Ni_2(L^2)_2]^{4+}$  (figure 2.4).

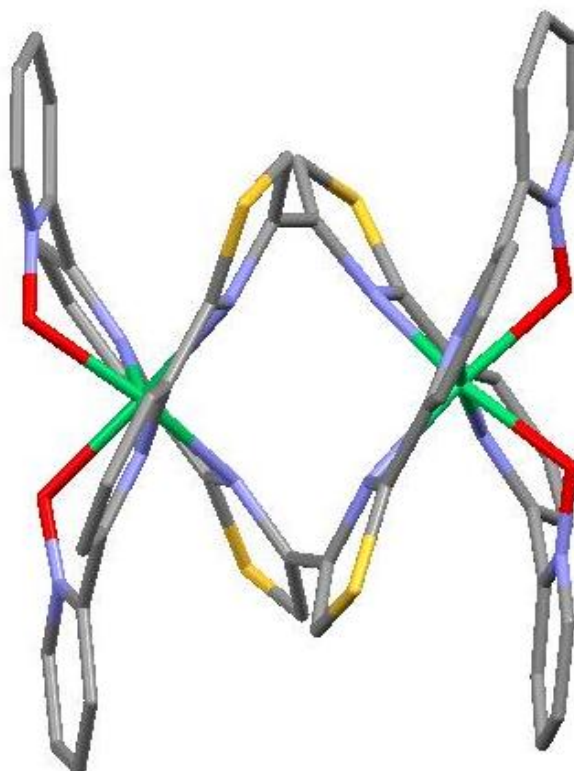


**Figure 2.4** X-ray crystal structure of  $[Ni_2(L^2)_2]^{4+}$

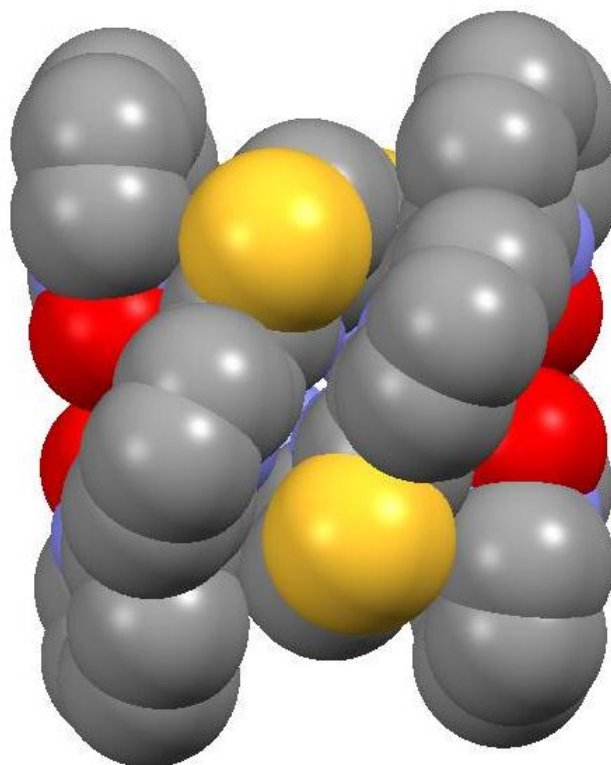


**Figure 2.5** X-ray crystal structure of  $[\text{Ni}_2(\text{L}^2)_2]^{4+}$  space filling model

The solid state structure (figure 2.4) shows that  $\text{L}^2$  partitions into two tridentate domains comprising of thiazole-pyridyl-pyridyl-N-oxide (tz-py-pyO) donor units. Each of the  $\text{Ni}^{2+}$  ions adopt a distorted octahedral geometry and are coordinated by two tridentate domains from different ligands (Ni-N: 2.04-2.10 Å; Ni-O: 2.02-2.06 Å).

| Bond        | Bond length (Å) |
|-------------|-----------------|
| Ni(1)-N(4)  | 2.091(3)        |
| Ni(1)-N(5)  | 2.049(3)        |
| Ni(1)-N(10) | 2.084(3)        |
| Ni(1)-N(11) | 2.043(3)        |
| Ni(1)-O(3)  | 2.046(3)        |
| Ni(1)-O(4)  | 2.017(2)        |
| Ni(2)-N(2)  | 2.051(3)        |
| Ni(2)-N(3)  | 2.075(3)        |
| Ni(2)-N(8)  | 2.045(3)        |
| Ni(2)-N(9)  | 2.101(3)        |
| Ni(2)-O(1)  | 2.024(3)        |
| Ni(2)-O(2)  | 2.043(3)        |

**Table 2.4** Selected bond lengths (Å) for the complex  $[\text{Ni}_2(\text{L}^2)_2]^{4+}$

| Bond              | Bond angle (°) | Bond            | Bond angle (°) |
|-------------------|----------------|-----------------|----------------|
| N(5)-Ni(1)-N(4)   | 78.61(12)      | N(2)-Ni(2)-N(3) | 79.50(12)      |
| N(5)-Ni(1)-N(10)  | 103.16(12)     | N(2)-Ni(2)-N(9) | 108.23(12)     |
| N(10)-Ni(1)-N(4)  | 105.20(11)     | N(3)-Ni(2)-N(9) | 104.98(11)     |
| N(11)-Ni(1)-N(4)  | 107.70(12)     | N(8)-Ni(2)-N(2) | 170.99(13)     |
| N(11)-Ni(1)-N(5)  | 172.34(12)     | N(8)-Ni(2)-N(3) | 104.05(11)     |
| N(11)-Ni(1)-N(10) | 79.66(11)      | N(8)-Ni(2)-N(9) | 79.08(12)      |
| N(11)-Ni(1)-O(3)  | 88.83(11)      | O(1)-Ni(2)-N(2) | 85.05(11)      |
| O(3)-Ni(1)-N(4)   | 159.66(11)     | O(1)-Ni(2)-N(3) | 162.71(11)     |
| O(3)-Ni(1)-N(5)   | 84.12(12)      | O(1)-Ni(2)-N(8) | 90.17(11)      |
| O(3)-Ni(1)-N(10)  | 89.06(11)      | O(1)-Ni(2)-N(9) | 87.12(12)      |
| O(4)-Ni(1)-N(4)   | 88.92(10)      | O(1)-Ni(2)-O(2) | 82.93(12)      |
| O(4)-Ni(1)-N(5)   | 90.88(11)      | O(2)-Ni(2)-N(2) | 87.49(12)      |
| O(4)-Ni(1)-N(10)  | 161.68(11)     | O(2)-Ni(2)-N(3) | 88.66(12)      |
| O(4)-Ni(1)-N(11)  | 84.99(11)      | O(2)-Ni(2)-N(8) | 84.35(12)      |
| O(4)-Ni(1)-O(3)   | 80.62(10)      | O(2)-Ni(2)-N(9) | 160.62(12)     |

**Table 2.5** Selected bond angles (°) for the complex  $[\text{Ni}_2(\text{L}^2)_2]^{4+}$

### 2.2.3 Coordination chemistry of $\text{L}^3$ with copper (II)

Reaction of  $\text{L}^3$  with  $\text{Cu}(\text{ClO}_4)_2 \cdot 6\text{H}_2\text{O}$  in  $\text{MeNO}_2$  gives a green solution from which green crystals were produced upon slow diffusion of DCM. The ESI-MS confirmed the formation of a dinuclear double helicate with ions at  $m/z = 1407$  and  $915$  corresponding to  $\{[\text{Cu}_2(\text{L}^3)_2](\text{ClO}_4)_3\}^+$  and  $\{[\text{Cu}_2(\text{L}^3)](\text{ClO}_4)_3\}^+$  respectively. Solid state analysis shows the formation of a head-to-tail dinuclear double helicate  $[\text{Cu}_2(\text{L}^3)_2]^{4+}$  (figure 2.6).

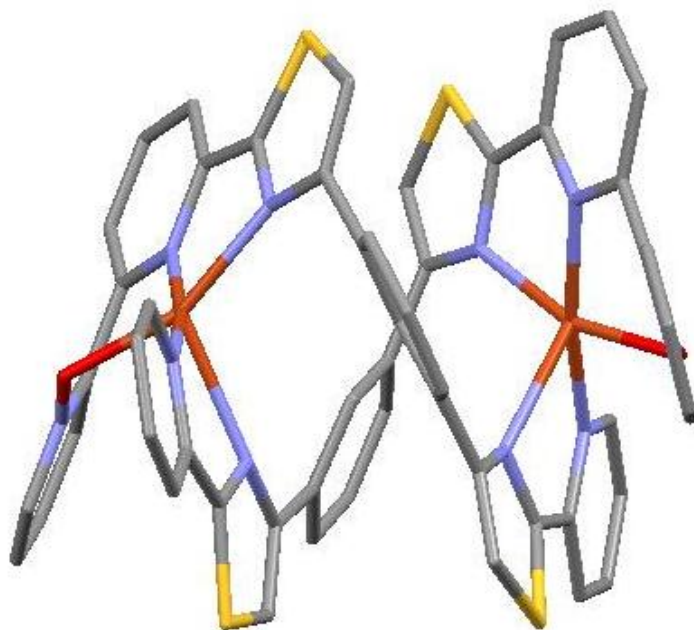


**Figure 2.6** X-ray crystal structure of [Cu<sub>2</sub>(L<sup>3</sup>)<sub>2</sub>]<sup>4+</sup>

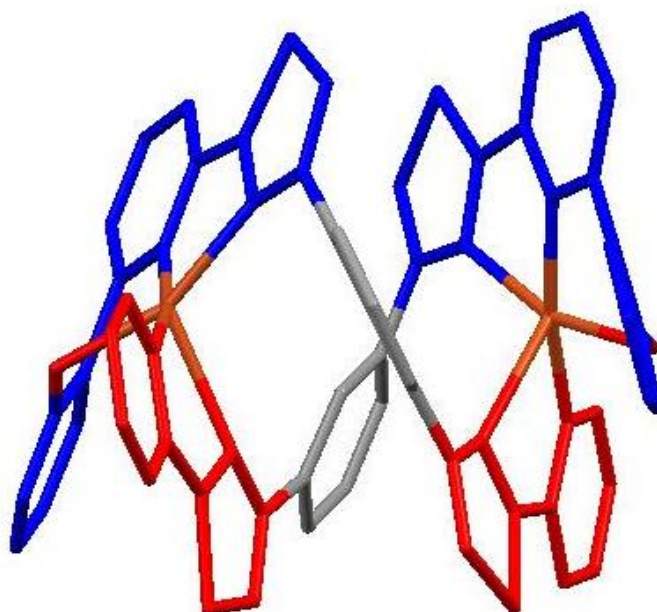


**Figure 2.7** X-ray crystal structure of [Cu<sub>2</sub>(L<sup>3</sup>)<sub>2</sub>]<sup>4+</sup> showing bidentate head (red) and tridentate tail (blue)

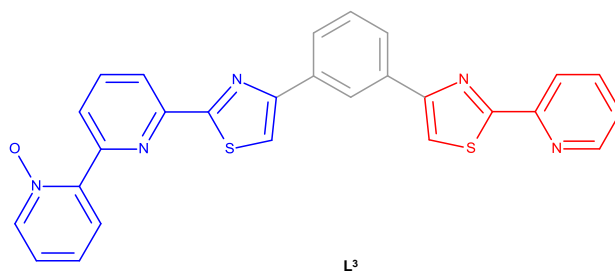


**Figure 2.8** The two different binding domains of  $L^3$  bidentate head (red) and tridentate tail (blue)

Solid state analysis shows that each ligand partitions into a tridentate (tail) and a bidentate (head) domain separated by a 1,3-phenylene spacer. Each of the copper ions is coordinated by the tz-py-pyO unit (tail) from one ligand strand and a tz-py (head) unit from a different ligand, giving a 5-coordinate metal centre (Cu-N: 1.99-2.43 Å; Cu-O; 1.96 Å).

| Bond        | Bond length (Å) |
|-------------|-----------------|
| Cu(1)-N(4)  | 2.431(2)        |
| Cu(1)-N(5)  | 1.998(2)        |
| Cu(1)-N(7)  | 2.001(2)        |
| Cu(1)-N(8)  | 2.041(2)        |
| Cu(1)-O(2)  | 1.962(2)        |
| Cu(2)-N(2)  | 1.983(3)        |
| Cu(2)-N(3)  | 2.026(2)        |
| Cu(2)-N(9)  | 2.364(3)        |
| Cu(2)-N(10) | 1.989(3)        |
| Cu(2)-(O1)  | 1.965(2)        |

**Table 2.6** Selected bond lengths (Å) for the complex  $[Cu_2(L^3)_2]^{4+}$

| Bond            | Bond angle (°) | Bond             | Bond angle (°) |
|-----------------|----------------|------------------|----------------|
| N(5)-Cu(1)-N(4) | 75.79(10)      | N(2)-Cu(2)-N(3)  | 81.30(10)      |
| N(5)-Cu(1)-N(7) | 167.50(10)     | N(2)-Cu(2)-N(10) | 170.36(11)     |
| N(5)-Cu(1)-N(8) | 96.98(10)      | N(2)-Cu(2)-N(9)  | 111.34(10)     |
| N(7)-Cu(1)-N(4) | 116.34(9)      | N(3)-Cu(2)-N(9)  | 116.49(9)      |
| N(7)-Cu(1)-N(8) | 80.74(9)       | N(10)-Cu(2)-N(3) | 98.89(10)      |
| N(8)-Cu(1)-N(4) | 115.59(9)      | N(10)-Cu(2)-N(9) | 77.30(10)      |
| O(2)-Cu(1)-N(4) | 81.55(8)       | O(1)-Cu(2)-N(2)  | 86.37(10)      |
| O(2)-Cu(1)-N(5) | 93.47(9)       | .O(1)-Cu(2)-N(3) | 158.48(10)     |
| O(2)-Cu(1)-N(7) | 85.80(9)       | O(1)-Cu(2)-N(9)  | 84.40(9)       |
| O(2)-Cu(1)-N(8) | 161.69(9)      | O(1)-Cu(2)-N(10) | 90.36(9)       |

**Table 2.7** Selected bond angles (°) for the complex  $[\text{Cu}_2(\text{L}^3)_2]^{4+}$

#### 2.2.4 Coordination chemistry of $\text{L}^4$ with cobalt (II)

The reaction of  $\text{L}^4$  with an equimolar amount of  $\text{Co}(\text{BF}_4)_2 \cdot 6\text{H}_2\text{O}$  in  $\text{MeNO}_2$  results in a pale orange solution. Analysis by ESI-MS gave an ion at  $m/z = 1607$  corresponding to  $\{[\text{Co}_4(\text{L}^4)_4](\text{ClO}_4)_6\}^{2+}$ , confirming the formation of a tetranuclear cyclic helicate. The presence of a lower nuclearity fragment at  $m/z = 2454$  corresponding to  $\{[\text{Co}_3(\text{L}^4)_3](\text{ClO}_4)_5\}^+$ , is probably an artefact of the ESI-MS process and has been observed in cyclic helicates reported by Rice and co-workers in 2010.<sup>110</sup> Slow diffusion of DCM into the resulting solution afforded pale orange crystals of X-ray quality. Single crystal X-ray diffraction studies confirmed the formation of the tetranuclear cyclic helicate  $[\text{Co}_4(\text{L}^4)_4]^{8+}$  (figure 2.9).

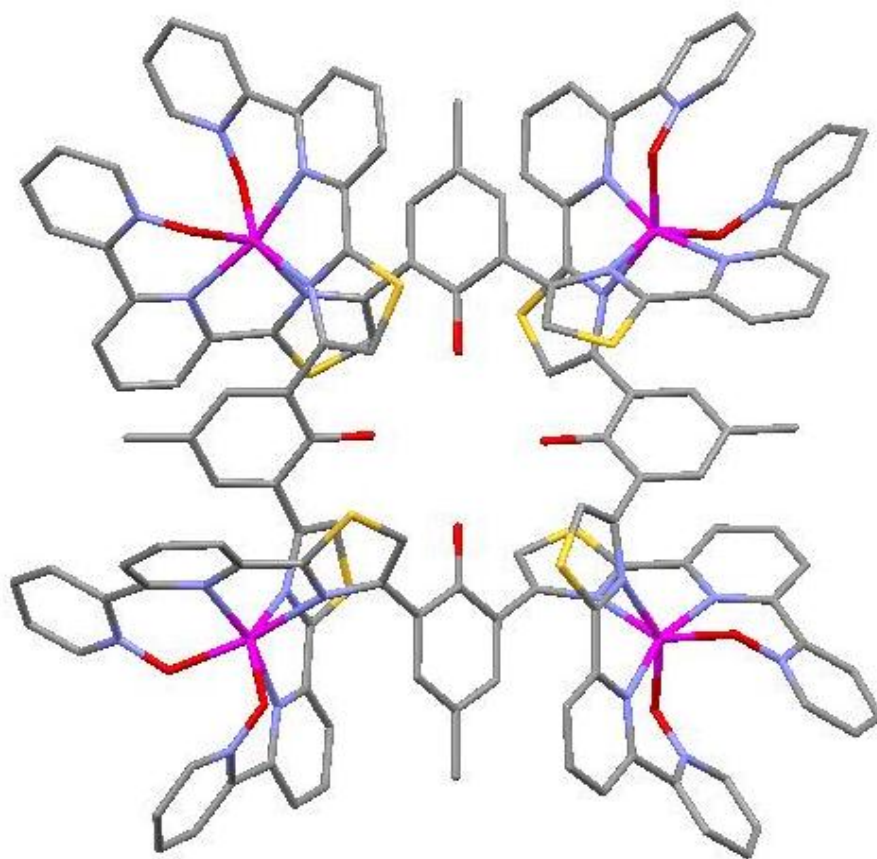


**Figure 2.9** X-ray crystal structure of [Co<sub>4</sub>(L<sup>4</sup>)<sub>4</sub>]<sup>8+</sup>

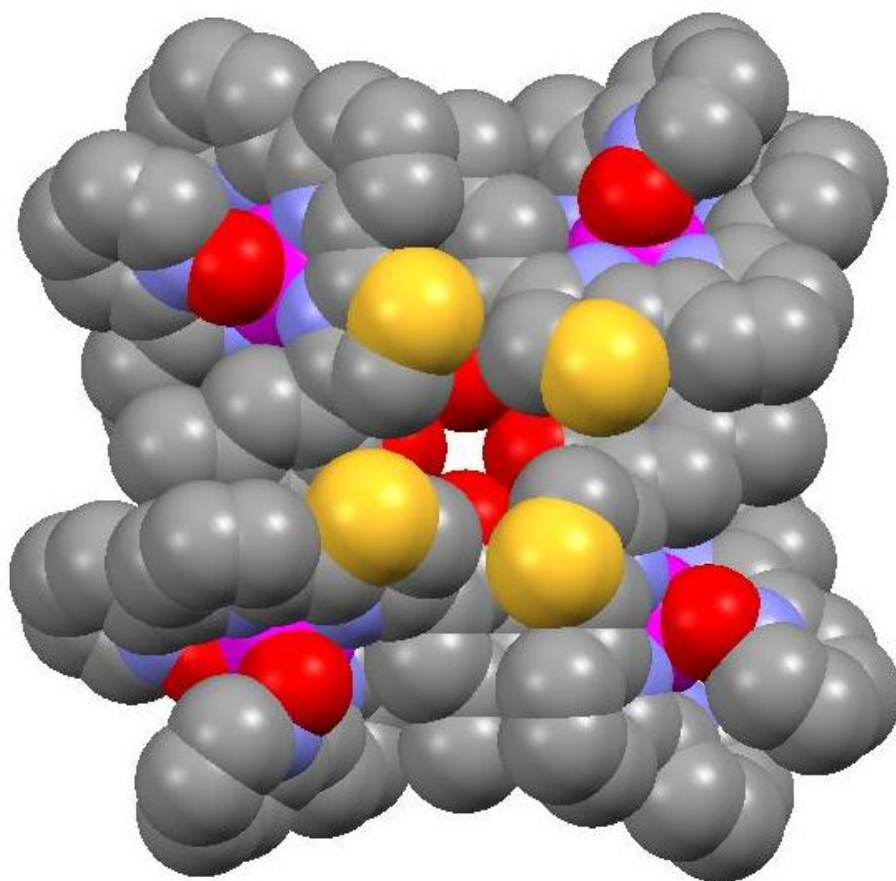


**Figure 2.10** X-ray crystal structure of  $[\text{Co}_4(\text{L}^4)_4]^{8+}$  space filling model

In the solid state there are four cobalt metal ions coordinated by four ligands with all  $\text{Co}^{2+}$  ions adopting a six-coordinate distorted octahedral geometry (Zn-N: 2.12-2.20 Å; Co-O: 2.00-2.07 Å). Each of the ligands has separated into two tridentate tz-py-pyO donor units partitioned by a 1,3-phenol spacer. The phenol spacers bridge each of the domains in an 'over and under' conformation. The four -OH units do not coordinate to the metal centres but hydrogen bond to one another.

| Bond        | Bond length (Å) | Bond        | Bond length (Å) |
|-------------|-----------------|-------------|-----------------|
| Co(1)-N(4)  | 2.157(5)        | Co(3)-N(10) | 2.137(5)        |
| Co(1)-N(5)  | 2.151(5)        | Co(3)-N(11) | 2.115(5)        |
| Co(1)-N(8)  | 2.144(5)        | Co(3)-N(14) | 2.125(5)        |
| Co(1)-N(9)  | 2.156(5)        | Co(3)-N(15) | 2.200(5)        |
| Co(1)-O(2)  | 2.029(4)        | Co(3)-O(4)  | 2.067(5)        |
| Co(1)-O(3)  | 2.000(4)        | Co(3)-O(5)  | 2.022(5)        |
| Co(2)-N(16) | 2.143(5)        | Co(4)-N(2)  | 2.128(6)        |
| Co(2)-N(17) | 2.130(5)        | Co(4)-N(3)  | 2.150(5)        |
| Co(2)-N(20) | 2.120(5)        | Co(4)-N(22) | 2.188(5)        |
| Co(2)-N(21) | 2.138(5)        | Co(4)-N(23) | 2.116(5)        |
| Co(2)-O(6)  | 2.026(5)        | Co(4)-O(1)  | 2.030(5)        |
| Co(2)-O(7)  | 2.016(5)        | Co(4)-O(8)  | 2.067(5)        |

**Table 2.8** Selected bond lengths (Å) for the complex  $[\text{Co}_4(\text{L}^4)_4]^{8+}$

| Bond              | Bond angle (°) | Bond              | Bond angle (°) |
|-------------------|----------------|-------------------|----------------|
| N(5)-Co(1)-N(4)   | 77.06(19)      | N(10)-Co(3)-N(15) | 80.19(19)      |
| N(5)-Co(1)-N(9)   | 114.01(19)     | N(11)-Co(3)-N(10) | 78.0(2)        |
| N(8)-Co(1)-N(4)   | 114.01(19)     | N(11)-Co(3)-N(14) | 166.0(2)       |
| N(8)-Co(1)-N(5)   | 166.30(19)     | N(14)-Co(3)-N(10) | 113.5(2)       |
| N(8)-Co(1)-N(9)   | 76.8(2)        | N(11)-Co(3)-N(15) | 112.37(19)     |
| N(9)-Co(1)-N(4)   | 81.58(18)      | N(14)-Co(3)-N(15) | 78.6(2)        |
| O(2)-Co(1)-N(4)   | 152.1(2)       | O(4)-Co(3)-N(10)  | 145.43(19)     |
| O(2)-Co(1)-N(5)   | 82.09(18)      | O(4)-Co(3)-N(11)  | 80.46(19)      |
| O(2)-Co(1)-N(8)   | 89.68(17)      | O(4)-Co(3)-N(14)  | 92.60(19)      |
| O(2)-Co(1)-N(9)   | 90.33(18)      | O(4)-Co(3)-N(15)  | 83.45(18)      |
| O(3)-Co(1)-N(4)   | 89.08(19)      | O(5)-Co(3)-N(10)  | 112.9(2)       |
| O(3)-Co(1)-N(5)   | 89.46(19)      | O(5)-Co(3)-N(11)  | 83.20(19)      |
| O(3)-Co(1)-N(8)   | 82.90(19)      | O(5)-Co(3)-N(14)  | 84.8(2)        |
| O(3)-Co(1)-N(9)   | 151.7(2)       | O(5)-Co(3)-N(15)  | 162.08(19)     |
| O(3)-Co(1)-O(2)   | 109.22(19)     | O(5)-Co(3)-O(4)   | 90.83(18)      |
| N(17)-Co(2)-N(16) | 77.8(2)        | N(2)-Co(4)-N(3)   | 77.2(2)        |
| N(17)-Co(2)-N(21) | 115.4(2)       | N(2)-Co(4)-N(22)  | 118.9(2)       |
| N(20)-Co(2)-N(16) | 116.4(2)       | N(3)-Co(4)-N(22)  | 82.19(19)      |
| N(20)-Co(2)-N(17) | 162.7(2)       | N(23)-Co(4)-N(3)  | 118.9(2)       |
| N(20)-Co(2)-N(21) | 77.8(2)        | N(23)-Co(4)-N(22) | 76.7(2)        |
| N(21)-Co(2)-N(16) | 82.4(2)        | O(1)-Co(4)-N(2)   | 80.8(2)        |
| O(6)-Co(2)-N(16)  | 87.77(19)      | O(1)-Co(4)-N(3)   | 147.8(2)       |

|                  |           |                  |           |
|------------------|-----------|------------------|-----------|
| O(6)-Co(2)-N(17) | 89.19(19) | O(1)-Co(4)-N(23) | 88.1(2)   |
| O(6)-Co(2)-N(20) | 81.9(2)   | N(23)-Co(4)-N(2) | 160.3(2)  |
| O(6)-Co(2)-N(21) | 150.5(2)  | O(1)-Co(4)-N(22) | 88.24(19) |
| O(7)-Co(2)-N(16) | 150.3(2)  | O(1)-Co(4)-O(8)  | 115.9(2)  |
| O(7)-Co(2)-N(17) | 81.7(2)   | O(8)-Co(4)-N(2)  | 89.4(2)   |
| O(7)-Co(2)-N(20) | 88.2(2)   | O(8)-Co(4)-N(3)  | 87.21(19) |
| O(7)-Co(2)-N(21) | 87.31(19) | O(8)-Co(4)-N(22) | 146.3(2)  |
| O(7)-Co(2)-O(6)  | 113.4(2)  | O(8)-Co(4)-N(23) | 80.8(2)   |

**Table 2.9** Selected bond angles (°) for the complex  $[\text{Co}_4(\text{L}^4)]^{8+}$

### 2.3 Discussion

From the single crystal X-ray crystallographic and ESI-MS studies it is clear that  $[\text{Cu}(\text{L}^1)(\text{ClO}_4)_2(\text{sol})]$ ,  $[\text{Ni}_2(\text{L}^2)]^{4+}$ ,  $[\text{Cu}_2(\text{L}^3)]^{4+}$  and  $[\text{Co}_4(\text{L}^4)]^{8+}$  are present both in the solid state and in solution.  $\text{L}^1$  acts as a tridentate donor upon reaction with  $\text{Cu}^{2+}$ , coordinating via the thiazole-pyridyl-pyridyl-N-oxide donor unit, two counter ions and a solvent molecule (acetonitrile or water) complete the geometry. The terminal N-donor unit does not coordinate the metal centre; this can be attributed to the divergent nature of the pyridyl-thiazole-pyridyl domains, which prevents the ligand acting as a tetradentate donor. Reaction of  $\text{L}^2$  with  $\text{Ni}^{2+}$  produces a dinuclear double helicate where each ligand strand partitions into two tridentate domains, twisting through the thiazole-thiazole bond. The binding domains of the ligands provide all six donor atoms required by the 6 coordinated metal ion centres to form a saturated dinuclear double-stranded helicate complex.

The head-to-tail ligand,  $\text{L}^3$ , forms a head-to-tail dinuclear double helicate when reacted with  $\text{Cu}^{2+}$ . The ligand partitions into two different domains, a tridentate tail and a bidentate head, separated by a 1,3-phenylene spacer (figure 2.8). Using the ability of  $\text{Cu}^{2+}$  to adopt a 5-coordinate geometry each  $\text{Cu}^{2+}$  is coordinated by the bidentate head of one ligand and the tridentate tail of another, different ligand. The sixth coordination site is occupied by a weak interaction with a perchlorate anion. It is somewhat surprising that this ligand forms a dinuclear double helicate with  $\text{Cu}^{2+}$ , as previous work reported by Rice and co-workers in 2010 shows that this type of ligand, containing a 1,3-phenylene spacer usually forms a pentanuclear circular helicate upon coordination with transition metals.<sup>110</sup> Upon reaction with copper (II),  $\text{L}^{\text{kk}}$  forms a head-to-tail pentanuclear circular helicate.

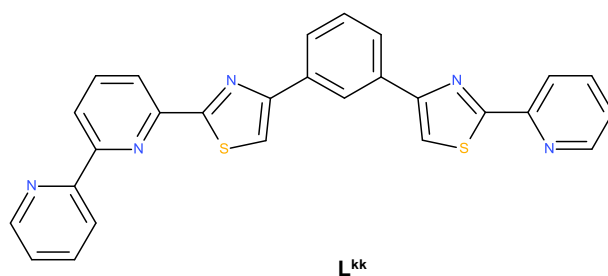


**Figure 2.11** Head-to-tail ligand,  $L^{kk}$  reported by Rice and co-workers in 2010

As discussed previously these cyclic helicates form due to unfavourable steric interactions between the protons on the central phenylene units. However, the inclusion of an N-oxide unit on the terminal pyridine must allow the ligand to flex so that the two phenyl units are more remote, reducing the steric interaction. As previously discussed in the introduction; reaction of  $L^{kk}$  with  $Cd^{2+}$  results in a dinuclear double helicate, the inter-ligand phenyl separation for  $[Cd_2(L^{kk})_2]^{4+}$  is 4.2 Å which is identical to the inter-ligand phenyl separation for  $[Cu_2(L^3)_2]^{4+}$  (4.2 Å) (figure 2.12).<sup>85</sup> The N-oxide unit allows more flexibility than an N-donor unit therefore allowing the formation of the entropically favoured dimer.

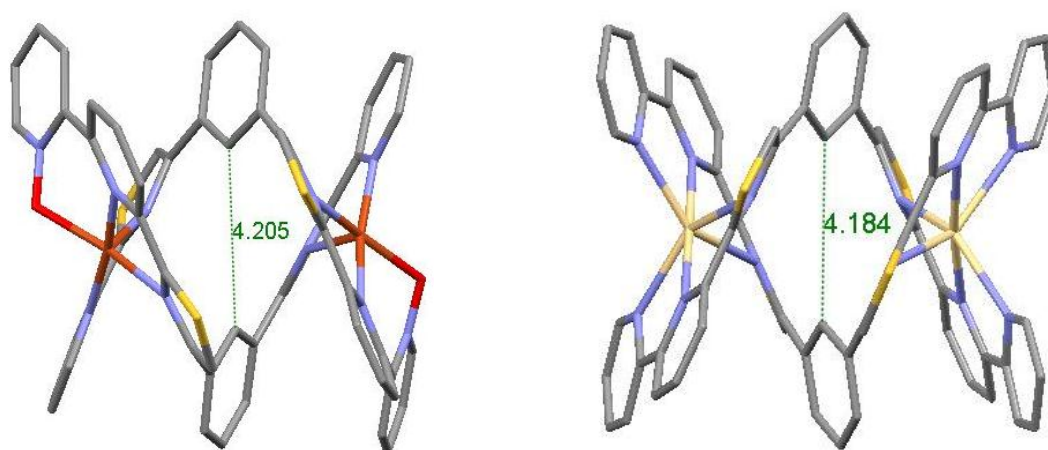


**Figure 2.12** Inter-ligand phenyl separation for  $[Cu_2(L^3)_2]^{4+}$  (right) and  $[Cd_2(L^{kk})_2]^{4+}$  (left)

It is clear that reaction of  $L^4$  with an equimolar amount of  $Co^{2+}$  gives a tetranuclear cyclic helicate, the formation of the entropically favoured dinuclear double helicate is prevented by the steric repulsion between the  $-OH$  units on the phenol spacer, as similarly reported by Rice and co-workers<sup>85, 110</sup> The 6 coordinate metal ions are coordinated by two tridentate tz-py-pyO donor units from different ligands. In each ligand the two tridentate domains are partitioned by a 1,3-phenol spacer, which bridge the domains in an 'over and under' conformation (figure 2.10), giving rise to a helical cyclic oligomer as opposed to a

face-to-face array associated with more grid-like architectures. The four –OH units do not coordinate to the metal centres but hydrogen bond to one another (Figure 2.13).

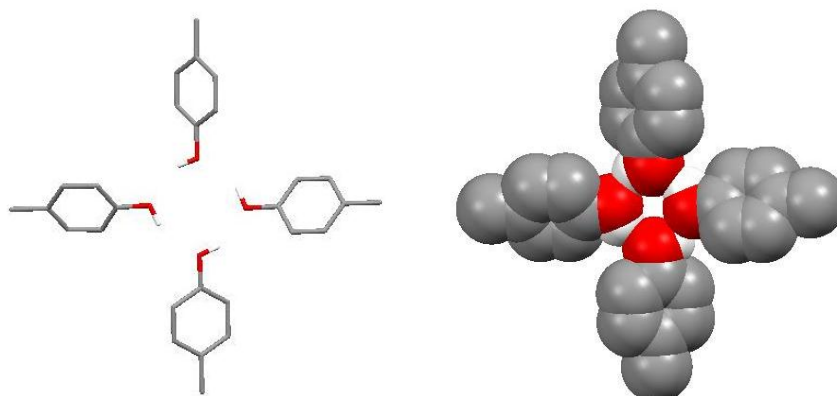


**Figure 2.13** The hydrogen bonding between the –OH units on the 1,3-phenol spacer

In an analogous fashion to the cyclic helicates discussed in the introduction, the formation of the cyclic species is controlled by the spacer unit as this prevents formation of the ‘simple’ dinuclear species due to intra-ligand steric repulsion. However, unlike the 1,3-phenylene analogous ( $L^j-L^k$  figure 1.44) which result in the pentanuclear species  $[M_5(L)_5]^{10+}$ , the 1,3-phenol spacer forms a tetranuclear species. As both the phenyl and phenol have the same substitution pattern (1,3-) the formation of the lower nuclearity species must be a consequence of the steric bulk of the methyl group on the central phenol spacer. In a tetranuclear assembly the distance between adjacent tridentate binding domains will be longer than the corresponding pentanuclear cyclic helicate and the steric demands of the methyl groups will therefore prevent the pentanuclear assembly. Measurement of the centroids of the central pyridine rings in adjacent ligand strands show that the distance is substantially longer in  $[Co_4(L^4)_4]^{8+}$  (average 8.0 Å) than the pentanuclear species  $[Zn_5(L^j)_5]^{10+}$  (average 7.0 Å) (figure 2.14).<sup>85</sup>

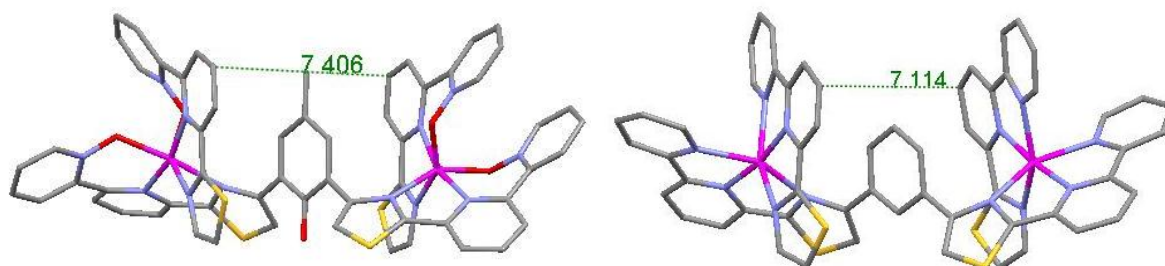


**Figure 2.14**  $[Co_4(L^4)_4]^{8+}$  (left) and  $[Zn_5(L^j)_5]^{10+}$  (right)

In this chapter we have developed a method that allows the incorporation of N-oxide donor units into the terminal position of a series of polydentate ligands which produce, upon coordinate with different d-block metal ions, a mononuclear single stranded complex, a dinuclear double stranded and a tetranuclear circular helicate. The incorporation of this unit within the ligand strand can change the behaviour of the ligand as it increases the flexibility of the donor units.

### 3. Polydentate ligands containing a central phenol unit and their self-assembly with metal ions

In recently reported work Rice and co-workers demonstrated a robust approach for generating circular helicates and extended it to investigate the formation of circular helicates with diverse structural complexity.<sup>109, 110</sup> In the previous chapter the 1,3-phenol spacer was used to generate a tetranuclear circular helicate  $[\text{Co}_4(\text{L}^4)_4]^{8+}$  (figure 2.9), in this chapter this spacer unit will be explored in more depth and extended to form helicates with higher order complexity. Described in this chapter is the synthesis and coordination chemistry of a potentially hexadentate N-donor ligand, a potentially tetradentate N-donor ligand and a potentially pentadentate N-donor ligand,  $\text{L}^5$ ,  $\text{L}^6$  and  $\text{L}^7$  respectively (figure 3.1).  $\text{L}^5$  contains two identical tridentate thiazole-pyridyl-pyridyl  $\text{N}_3$  binding domains separated by a 1,3-phenol unit.  $\text{L}^6$  contains two identical bidentate thiazole-pyridyl  $\text{N}_2$  binding domains separated by a 1,3-phenol unit.  $\text{L}^7$  is unsymmetrical and contains two different binding domains, which consist of a tridentate thiazole-pyridyl-pyridyl  $\text{N}_3$  binding domain and a bidentate thiazole-pyridyl  $\text{N}_2$  binding domain again separated by a 1,3-phenol unit.

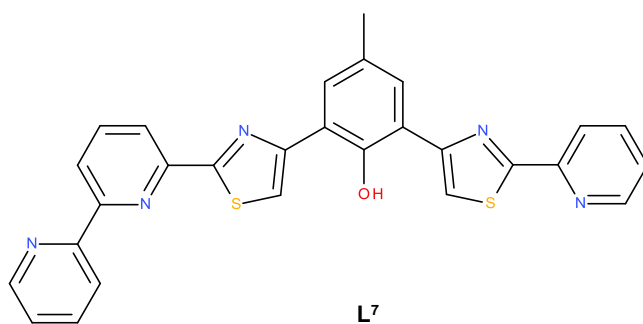
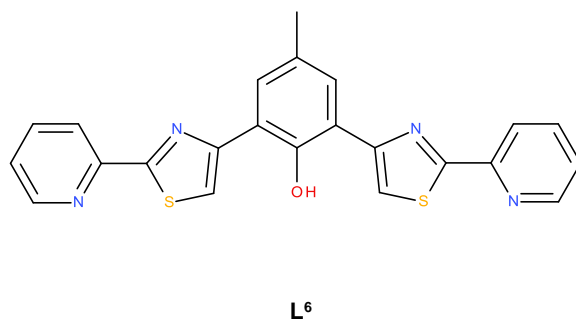
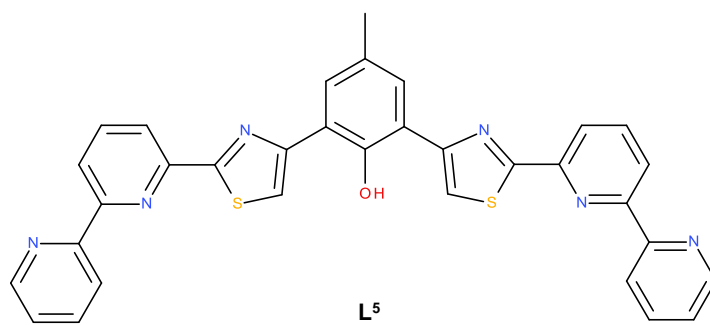
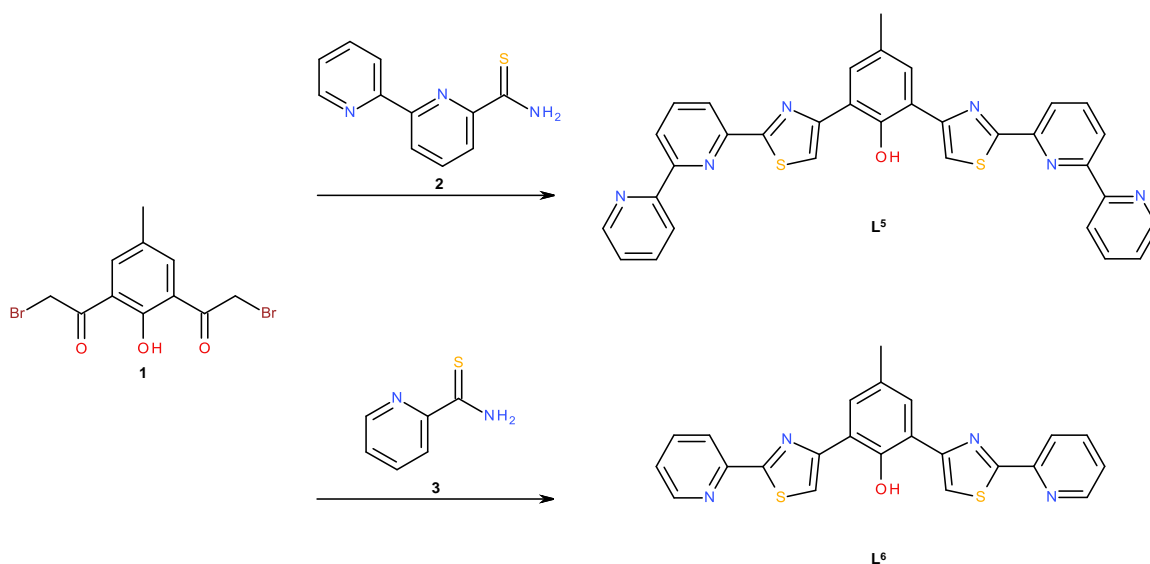


Figure 3.1 Ligands  $L^5$ - $L^7$

### 3.1 Ligand synthesis

#### 3.1.1 Synthesis of Ligands $L^5$ and $L^6$

The principal material in the formation of these polydentate ligands is the  $\alpha$ -bromoacetyl compound 1,3-di( $\alpha$ -bromoacetyl)phenol (1), previously discussed in chapter 2 (scheme 2.3).



**Scheme 3.1** Synthesis of ligands  $L^5$  and  $L^6$ . Reagents and conditions: DMF, heat at 80 °C.

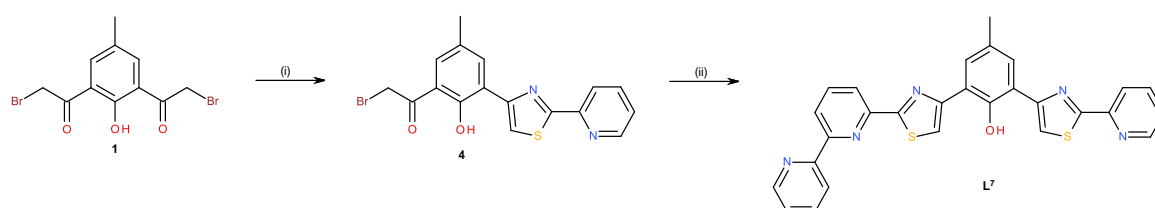
The synthesis of  $L^5$  is outlined in scheme 3.1, reaction of the dibromo-ketone (1) and 2,2'-bipyridine-6-thioamide (2)<sup>127</sup> in EtOH resulted in the formation of one thiazole ring with one of the  $-\text{CH}_2\text{Br}$  units left unreacted. This is due to the solubility; when the thioamide (2) has reacted once it forms the mono-thiazole product which is insoluble in EtOH and precipitates preventing further reaction. However, reaction of the thioamide (2) with the  $\alpha$ -bromoacetyl (1) in DMF for 24 hours at 80 °C results in a precipitate, which after filtration followed by deprotonation with concentrated ammonia gave the ligand  $L^5$  as a pale yellow solid. The formation of  $L^5$  was confirmed by  $^1\text{H}$  NMR which showed 9 different aromatic proton environments and contained, amongst others, a singlet at 8.51 ppm, corresponding to the thiazole ring. ESI-MS also confirms the formation of  $L^5$  with an ion observed at  $m/z$  583 ( $M + \text{H}^+$ ).

The synthesis for  $L^6$  is also outlined in scheme 3.1 and was carried out in a similar manner to that of  $L^5$ . Reaction of the  $\alpha$ -bromoacetyl (1) with pyridine-2-thioamide (3)<sup>127</sup> in DMF for 8 hours produces a precipitate. Filtration, washing and neutralisation gave the ligand  $L^6$  as a pale yellow solid. On analysis by  $^1\text{H}$  NMR spectroscopy, the ligand  $L^6$ , revealed a total of 6 different aromatic signals, with 2 singlet chemical shifts at 12.45 ppm and 2.41 ppm

corresponding to the spacer unit protons -OH and -CH<sub>3</sub>, respectively and also contained a singlet at 8.47 ppm, corresponding to the thiazole ring. ESI-MS also confirmed the successful formation of **L**<sup>6</sup> as an ion at *m/z* 429 (M + H<sup>+</sup>) was observed.

### 3.1.2 Synthesis of Ligands **L**<sup>7</sup>

The synthesis of **L**<sup>7</sup> is outlined in scheme 3.2 and was carried out in a similar manner to Rice and co-workers.<sup>110</sup> To a solution of 1,3-di( $\alpha$ -bromoacetyl)phenol (**1**) in DCM was added pyridine-2-thioamide (**3**) and the reaction was stirred at room temperature for 12 hours. The resulting precipitate was isolated by filtration and neutralised. Purification by column chromatography gave the mono-pyridylthiazole (**4**). Confirmation of the successful formation of (**4**) was obtained from <sup>1</sup>H NMR spectroscopy which showed seven different aromatic protons which included a singlet signal at 8.31 ppm that integrates to 1H, thus showing the tz unit was present. A singlet peak at 4.59 ppm that integrates to 2H showed a -CH<sub>2</sub>Br unit was still present; therefore (**4**) had successfully formed. ESI-MS also confirmed the successful formation of (**4**) as an ion at *m/z* 390 (M + H<sup>+</sup>) was observed. Reaction of (**4**) with 2,2'-bipyridine-6-thioamide (**2**) in EtOH at reflux for 8 hours resulted in a yellow precipitate which was isolated by filtration. Suspension in concentrated NH<sub>3</sub> followed by filtration and washing gave ligand **L**<sup>7</sup> as a pale yellow solid. Confirmation of the successful formation of **L**<sup>7</sup> was obtained from the <sup>1</sup>H NMR spectrum, which due to the unsymmetrical nature of the ligand showed a total of 15 signals including two different thiazole proton environments. ESI-MS also confirmed the successful formation of **L**<sup>7</sup> as an ion at *m/z* 506 (M + H<sup>+</sup>) was observed.



**Scheme 3.2** Synthesis of ligand **L**<sup>7</sup>. Reagents and conditions: (i) pyridine-2-thioamide (**3**), DCM, room temperature. (ii) 2,2'-bipyridine-6-thioamide (**2**), EtOH, reflux

## 3.2 Coordination Chemistry

### 3.2.1 Complexes of $L^5$ and zinc (II)

The reaction of  $L^5$  with an equimolar amount of  $Zn(CF_3SO_3)_2$  in MeCN results in a pale orange solution. Slow diffusion of diisopropyl ether vapour into the resulting orange solution afforded pale orange crystals of X-ray quality. Single crystal X-ray diffraction studies confirmed the formation of the tetranuclear circular species  $[Zn_4(L^5)_4]^{8+}$  (figure 3.2).

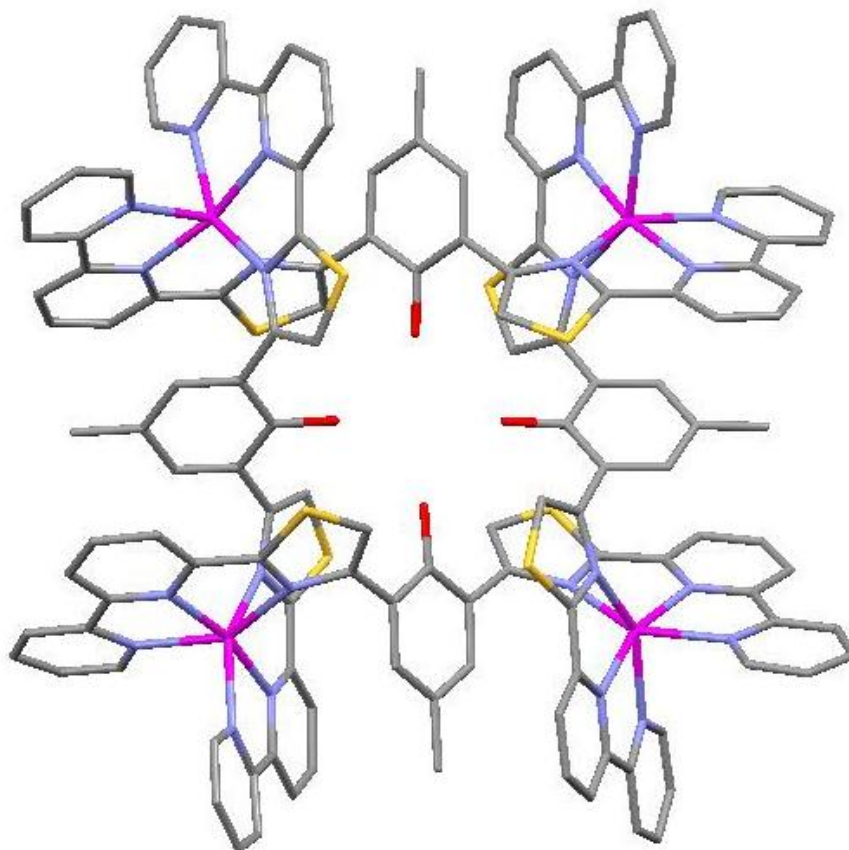


**Figure 3.2** X-ray crystal structure of  $[Zn_4(L^5)_4]^{8+}$

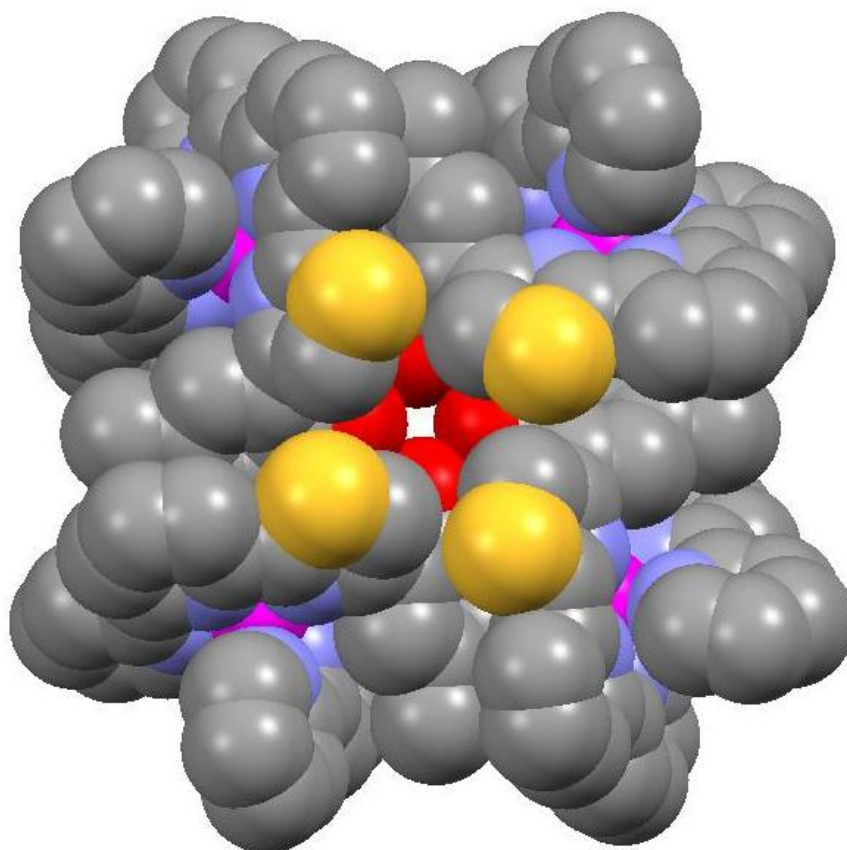


**Figure 3.3** X-ray crystal structure of  $[\text{Zn}_4(\text{L}^5)_4]^{8+}$  space filling model

In the solid state there are four  $\text{Zn}^{2+}$  metal ions coordinated by four ligands with all  $\text{Zn}^{2+}$  ions adopting a six-coordinate distorted octahedral geometry (Zn-N: 2.08-2.81 Å). Each of the  $\text{L}^5$  ligands has partitioned into two tridentate tz-py-py donor units separated by a 1,3-phenol spacer. The phenol spacers bridge each of the domains in an 'over and under' conformation. The four -OH units do not coordinate to the metal centres but hydrogen bond to one another.

| Bond       | Bond length (Å) | Bond        | Bond length (Å) |
|------------|-----------------|-------------|-----------------|
| Zn(1)-N(1) | 2.207(4)        | Zn(2)-N(7)  | 2.197(4)        |
| Zn(1)-N(2) | 2.083(4)        | Zn(2)-N(8)  | 2.092(4)        |
| Zn(1)-N(3) | 2.812(4)        | Zn(2)-N(9)  | 2.193(4)        |
| Zn(2)-N(4) | 2.231(4)        | Zn(3)-N(10) | 2.185(4)        |
| Zn(2)-N(5) | 2.099(3)        | Zn(3)-N(11) | 2.091(4)        |
| Zn(2)-N(6) | 2.194(4)        | Zn(3)-N(12) | 2.228(4)        |

**Table 3.1** Selected bond lengths (Å) for the complex  $[\text{Zn}_4(\text{L}^5)_4]^{8+}$

| Bond             | Bond angle (°) | Bond               | Bond angle (°) |
|------------------|----------------|--------------------|----------------|
| N(1)-Zn(1)-N(1)  | 91.20(2)       | N(8)-Zn(2)-N(4)    | 112.69(14)     |
| N(2)-Zn(1)-N(1)  | 74.86(14)      | N(8)-Zn(2)-N(5)    | 167.56(14)     |
| N(2')-Zn(1)-N(1) | 95.61(14)      | N(8)-Zn(2)-N(6)    | 98.23(14)      |
| N(2)-Zn(1)-N(2)  | 166.6(2)       | N(8)-Zn(2)-N(7)    | 74.53(14)      |
| N(2)-Zn(1)-N(3)  | 76.61(14)      | N(8)-Zn(2)-N(9)    | 75.70(14)      |
| N(2)-Zn(1)-N(3)  | 113.20(14)     | N(9)-Zn(2)-N(4)    | 86.06(14)      |
| N(2)-Zn(1)-N(3)  | 113.20(14)     | N(9)-Zn(2)-N(6)    | 98.83(14)      |
| N(3)-Zn(1)-N(1)  | 95.56(14)      | N(9)-Zn(2)-N(7)    | 147.74(14)     |
| N(3)-Zn(1)-N(1)  | 151.18(14)     | N(10)-Zn(3)-N(10)  | 87.02(18)      |
| N(3)-Zn(1)-N(3)  | 91.87(19)      | N(10)-Zn(3)-N(12)  | 99.46(14)      |
| N(5)-Zn(2)-N(4)  | 75.42(14)      | N(10')-Zn(3)-N(12) | 149.22(14)     |
| N(5)-Zn(2)-N(7)  | 95.95(14)      | N(11)-Zn(3)-N(10)  | 76.11(14)      |
| N(5)-Zn(2)-N(9)  | 115.14(14)     | N(11')-Zn(3)-N(10) | 118.06(14)     |

|                 |            |                    |           |
|-----------------|------------|--------------------|-----------|
| N(5)-Zn(2)-N(6) | 75.42(14)  | N(11)-Zn(3)-N(11)  | 161.70(2) |
| N(6)-Zn(2)-N(4) | 148.89(19) | N(11)-Zn(3)-N(12)  | 74.31(15) |
| N(6)-Zn(2)-N(7) | 97.46(19)  | N(11)-Zn(3)-N(12') | 92.66(15) |
| N(7)-Zn(2)-N(4) | 94.09(14)  | N(12)-Zn(3)-N(12)  | 90.20(5)  |

**Table 3.2** Selected bond angles (°) for the complex  $[\text{Zn}_4(\text{L}^5)_4]^{8+}$

### 3.2.2 Complexes of $\text{L}^6$ and silver (I)

The reaction of  $\text{L}^6$  with a stoichiometric amount of  $\text{AgClO}_4 \cdot 4\text{H}_2\text{O}$  in  $\text{MeNO}_2$  gives a yellow solution. Pale yellow crystals are produced after slow diffusion of chloroform into the resulting solution, producing crystals of X-ray quality. Single crystal X-ray diffraction studies confirmed the formation of the dinuclear species  $[\text{Ag}_2(\text{L}^6)_2]^{2+}$  (figure 3.4).

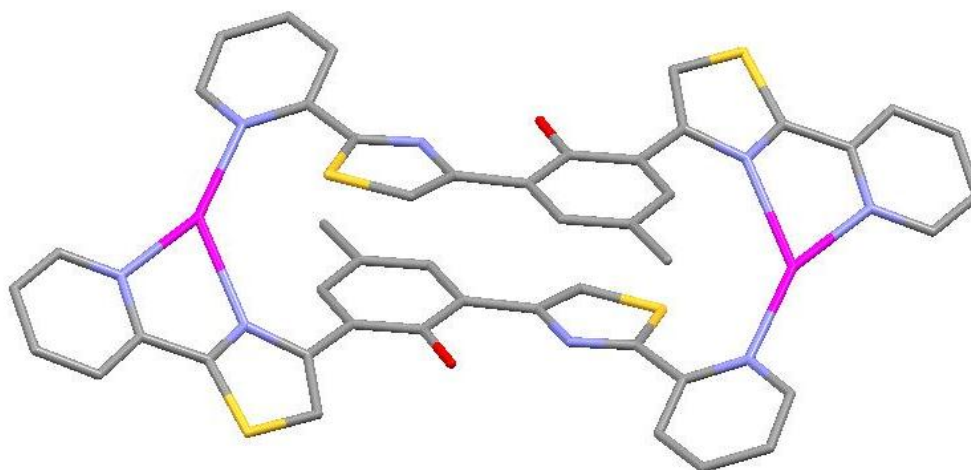


**Figure 3.4** X-ray crystal structure of  $[\text{Ag}_2(\text{L}^6)_2]^{2+}$

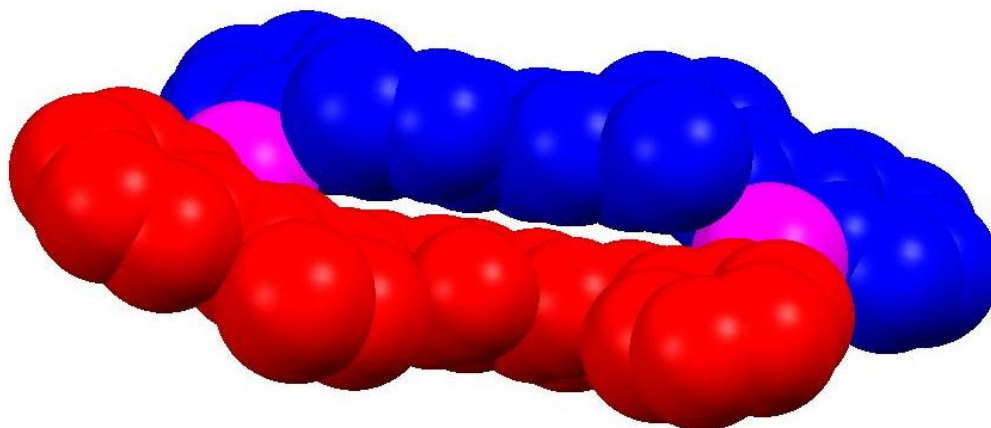


**Figure 3.5** Space filling side view of the X-ray crystal structure of  $[Ag_2(L^6)_2]^{2+}$

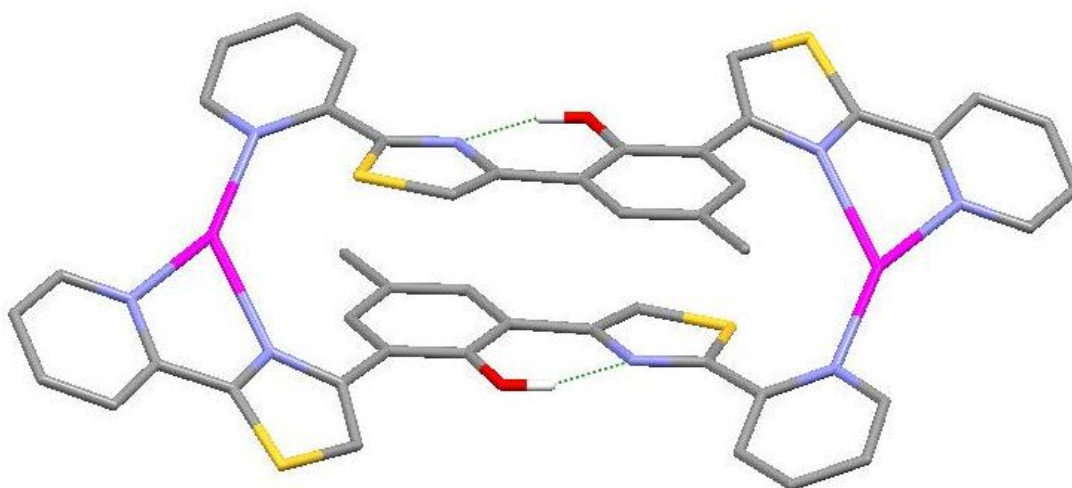


**Figure 3.6** The hydrogen bonding that exists in the X-ray crystal structure of  $[Ag_2(L^6)_2]^{2+}$

In the solid state crystal structure of the dinuclear  $[Ag_2(L^6)_2]^{2+}$  species each  $Ag^+$  ion adopts a three coordinate coordination geometry arising from the coordination of a tz-py N-donor domain from one ligand and a pyridyl N-donor domain from another different ligand (Ag-N: 2.20-2.36 Å). The uncoordinated thiazole N-donor atoms hydrogen bond to the central 1,3-phenol spacer units (figure 3.6). Figure 3.5 clearly shows the complex is a *meso*-helicate form of the complex, the two L<sup>6</sup> ligands lay 'side-by-side' instead of being twisted around one another.

| Bond       | Bond length (Å) |
|------------|-----------------|
| Ag(1)-N(1) | 2.198(3)        |
| Ag(1)-N(3) | 2.360(3)        |
| Ag(1)-N(4) | 2.294(3)        |

**Table 3.3** Selected bond lengths (Å) for the complex  $[\text{Ag}_2(\text{L}^6)_2]^{2+}$

| Bond            | Bond angle (°) |
|-----------------|----------------|
| N(1)-Ag(1)-N(3) | 132.03(11)     |
| N(1)-Ag(1)-N(4) | 154.40(12)     |
| N(4)-Ag(1)-N(3) | 72.23(11)      |

**Table 3.4** Selected bond angles (°) for the complex  $[\text{Ag}_2(\text{L}^6)_2]^{2+}$

### 3.2.3 Complexes of $L^6$ and cadmium(II)

The reaction of  $L^6$  with  $Cd(ClO_4)_2 \cdot 6H_2O$  produces a crystalline material upon slow diffusion of diethyl ether vapour. Examination of the crystalline species revealed two different species, with some of the material colourless and some orange. Single crystal X-ray diffraction analysis of the colourless crystals demonstrated the formation of the mononuclear species  $[Cd(L^6)_2(MeCN)_2]^{2+}$  (figure 3.7).

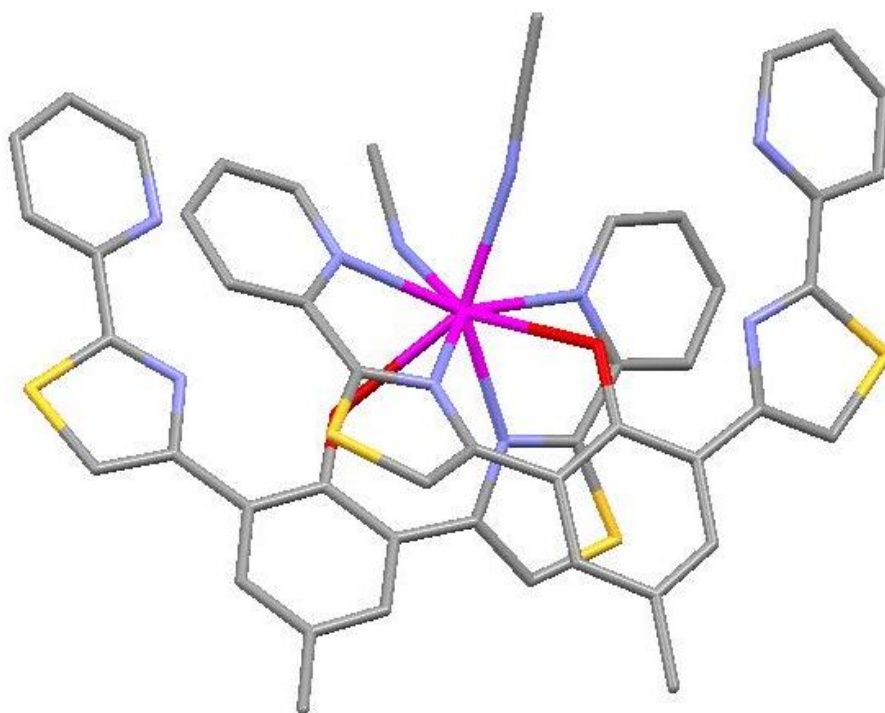


**Figure 3.7** X-ray crystal structure of the mononuclear species  $[Cd(L^6)_2(MeCN)_2]^{2+}$ , produced from the colourless crystals of  $L^6$  with  $Cd(ClO_4)_2 \cdot 6H_2O$

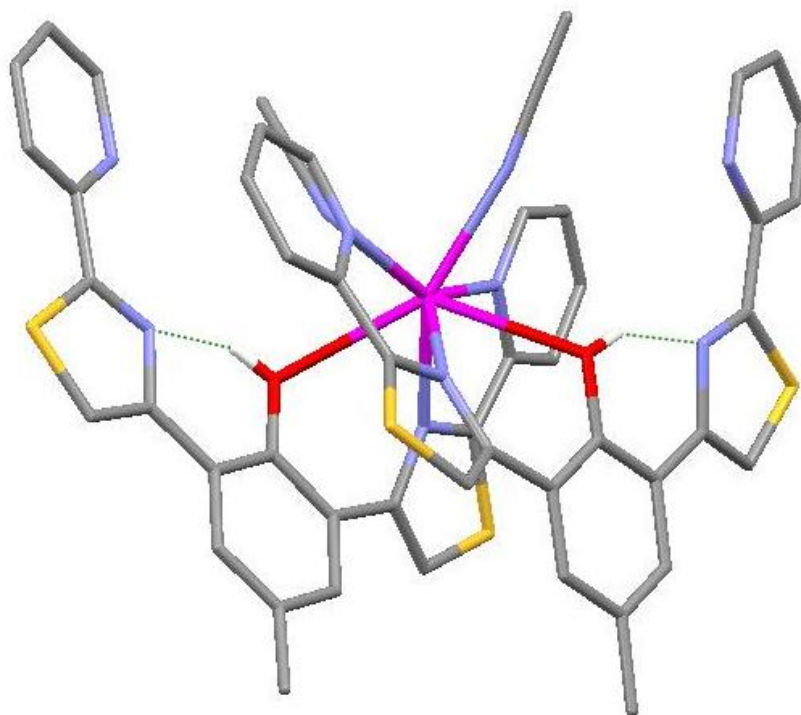


**Figure 3.8** Hydrogen bonding that exist in X-ray crystal structure of the mononuclear species  $[\text{Cd}(\text{L}^6)_2(\text{MeCN})_2]^{2+}$ , produced from the colourless crystals of  $\text{L}^6$  with  $\text{Cd}(\text{ClO}_4)_2 \cdot 6\text{H}_2\text{O}$

In the solid state crystal structure of the mononuclear  $[\text{Cd}(\text{L}^6)_2(\text{MeCN})_2]^{2+}$  complex the  $\text{Cd}^{2+}$  metal centre is coordinated by the bidentate N-donor domain and the O-donor domain from the 1,3-phenol spacer from two different ligands (Cd-N: 2.35-2.47 Å; Cd-O: 2.73-2.2.76 Å). Two acetonitrile solvent molecules complete the eight coordinate geometry (Cd-N: 2.44-2.47 Å). The uncoordinated thiazole N-donor atoms hydrogen bond to the central 1,3-phenol spacer units (figure 3.8).

| Bond       | Bond length (Å) | Bond        | Bond length (Å) |
|------------|-----------------|-------------|-----------------|
| Cd(1)-N(3) | 2.346(5)        | Cd(1)-N(9)  | 2.435(6)        |
| Cd(1)-N(4) | 2.427(5)        | Cd(1)-N(10) | 2.470(6)        |
| Cd(1)-N(5) | 2.394(6)        | Cd(1)-O(1)  | 2.761(5)        |
| Cd(1)-N(6) | 2.388(5)        | Cd(1)-O(2)  | 2.726(5)        |

**Table 3.5** Selected bond lengths (Å) for the complex  $[\text{Cd}(\text{L}^6)_2(\text{MeCN})_2]^{2+}$

| Bond             | Bond angle (°) | Bond             | Bond angle (°) |
|------------------|----------------|------------------|----------------|
| N(3)-Cd(1)-N(4)  | 69.44(19)      | N(5)-Cd(1)-N(9)  | 78.94(19)      |
| N(3)-Cd(1)-N(5)  | 135.58(19)     | N(5)-Cd(1)-N(10) | 80.62(19)      |
| N(3)-Cd(1)-N(6)  | 86.77(17)      | N(6)-Cd(1)-N(4)  | 137.61(18)     |
| N(3)-Cd(1)-N(9)  | 145.07(19)     | N(6)-Cd(1)-N(5)  | 69.93(18)      |
| N(3)-Cd(1)-N(10) | 101.19(18)     | N(6)-Cd(1)-N(9)  | 105.35(18)     |
| N(4)-Cd(1)-N(9)  | 80.33(19)      | N(6)-Cd(1)-N(10) | 144.1(2)       |
| N(4)-Cd(1)-N(10) | 76.76(18)      | N(9)-Cd(1)-N(10) | 88.00(2)       |
| N(5)-Cd(1)-N(4)  | 149.62(18)     |                  |                |

**Table 3.6** Selected bond angles (°) for the complex  $[\text{Cd}(\text{L}^6)_2(\text{MeCN})_2]^{2+}$

Examination by X-ray crystallography of the orange crystals produced from the reaction of  $L^6$  with  $Cd(ClO_4)_2 \cdot 6H_2O$  shows the formation of a dinuclear complex  $[Cd_2(L^6)_2]^{2+}$  (figure 3.9).

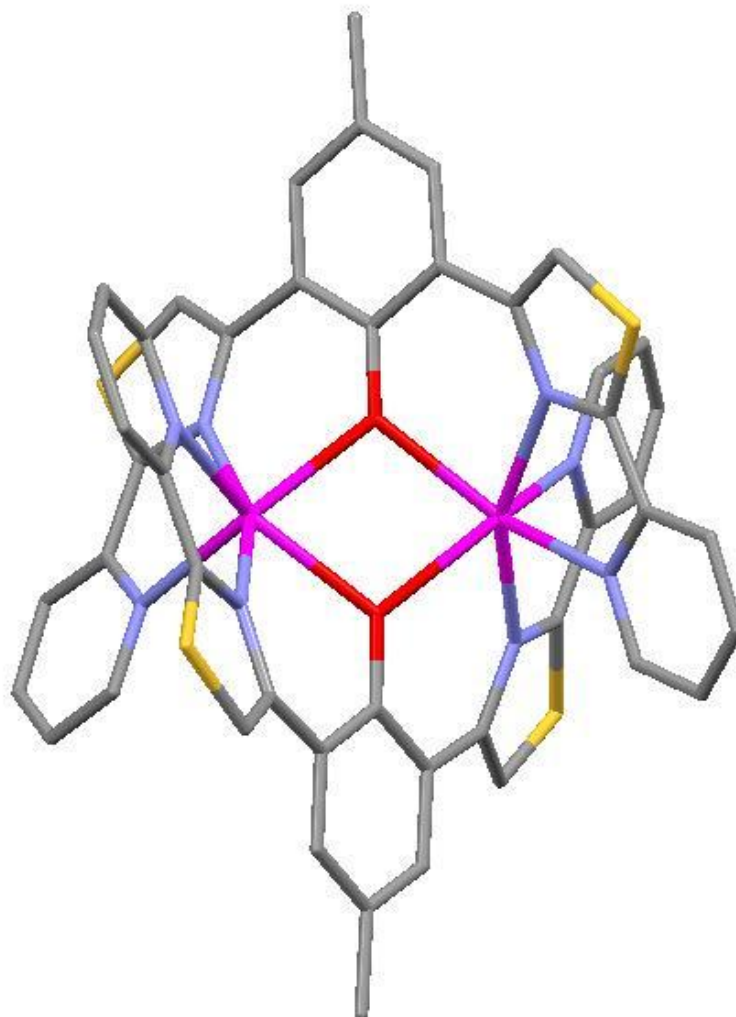


**Figure 3.9** X-ray crystal structure of the dinuclear species  $[Cd_2(L^6)_2]^{2+}$ , produced from the orange crystals of  $L^6$  with  $Cd(ClO_4)_2 \cdot 6H_2O$

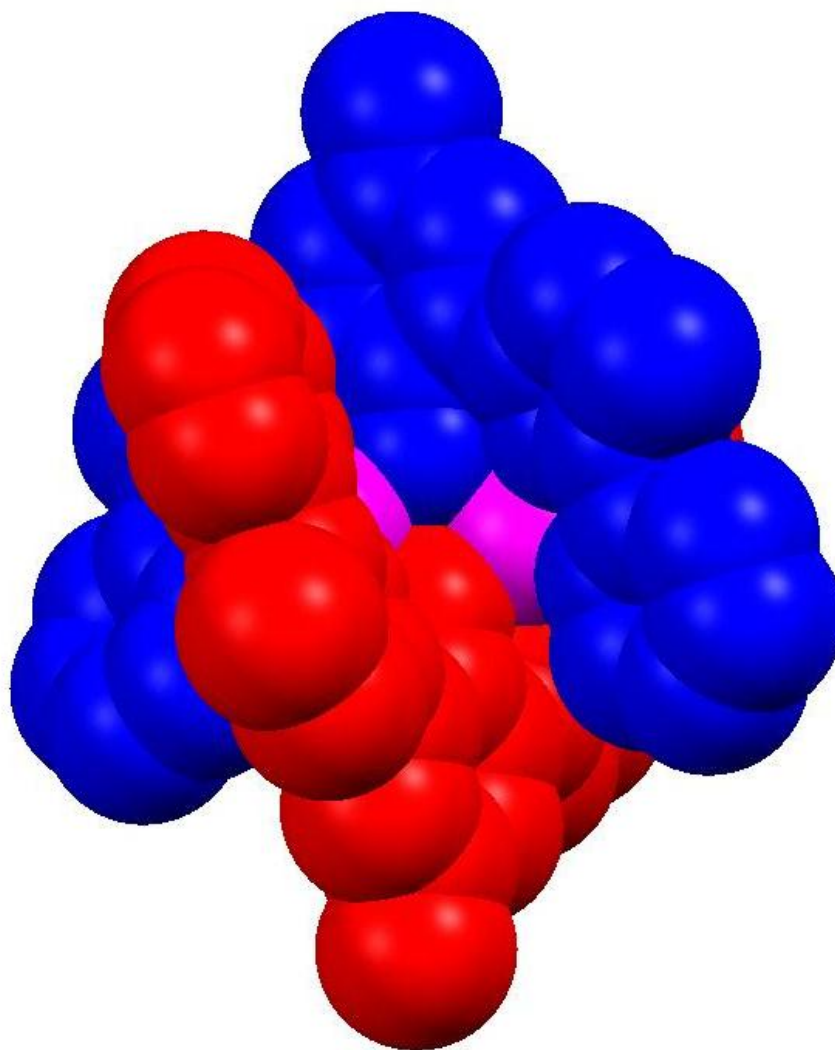


**Figure 3.10** Space fill of the X-ray crystal structure of the dinuclear species  $[\text{Cd}_2(\text{L}^6)_2]^{2+}$ , produced from the orange crystals of  $\text{L}^6$  with  $\text{Cd}(\text{ClO}_4)_2 \cdot 6\text{H}_2\text{O}$

In the solid state the ligand  $\text{L}^6$  acts as a bis-bidentate donor coordinating via the N-donor thiazole-pyridyl domains from two different ligand stands, the O-donor atom from the central 1,3-phenol spacer bridges the two octahedral  $\text{Cd}^{2+}$  metal centres (Cd-N: 2.35-2.43 Å; Cd-O: 2.73-2.76 Å).

| Bond       | Bond length (Å) | Bond       | Bond length (Å) |
|------------|-----------------|------------|-----------------|
| Cd(1)-N(3) | 2.272(17)       | Cd(2)-N(1) | 2.372(18)       |
| Cd(1)-N(4) | 2.378(18)       | Cd(2)-N(2) | 2.290(16)       |
| Cd(1)-N(5) | 2.398(17)       | Cd(2)-N(7) | 2.306(16)       |
| Cd(1)-N(6) | 2.282(17)       | Cd(2)-N(8) | 2.375(18)       |
| Cd(1)-O(1) | 2.253(14)       | Cd(2)-O(1) | 2.261(15)       |
| Cd(1)-O(2) | 2.268(14)       | Cd(2)-O(2) | 2.241(15)       |

**Table 3.7** Selected bond lengths (Å) for the complex  $[\text{Cd}_2(\text{L}^6)_2]^{2+}$

| Bond            | Bond angle (°) | Bond            | Bond angle (°) |
|-----------------|----------------|-----------------|----------------|
| N(3)-Cd(1)-N(4) | 71.29(6)       | O(1)-Cd(1)-N(6) | 125.94(6)      |
| N(3)-Cd(1)-N(6) | 96.31(6)       | O(1)-Cd(1)-O(2) | 77.00(5)       |
| N(3)-Cd(1)-N(5) | 155.34(6)      | O(2)-Cd(1)-N(3) | 123.78(6)      |
| N(4)-Cd(1)-N(5) | 107.26(6)      | O(2)-Cd(1)-N(4) | 99.53(6)       |
| N(6)-Cd(1)-N(4) | 91.85(6)       | O(2)-Cd(1)-N(5) | 137.41(6)      |
| N(6)-Cd(1)-N(5) | 71.02(6)       | O(2)-Cd(1)-O(6) | 75.69(6)       |
| N(1)-Cd(2)-N(8) | 104.28(7)      | O(1)-Cd(2)-N(1) | 134.97(6)      |
| N(2)-Cd(2)-N(1) | 71.62(6)       | O(1)-Cd(2)-N(2) | 74.54(6)       |
| N(2)-Cd(2)-N(7) | 153.73(6)      | O(1)-Cd(2)-N(7) | 127.49(6)      |
| N(2)-Cd(2)-N(8) | 90.31(6)       | O(1)-Cd(2)-N(4) | 138.31(6)      |
| N(7)-Cd(2)-N(1) | 94.23(6)       | O(1)-Cd(2)-N(6) | 125.94(6)      |
| N(7)-Cd(2)-N(8) | 71.40(6)       | O(2)-Cd(2)-N(1) | 101.28(6)      |
| O(1)-Cd(1)-N(3) | 74.52(6)       | O(2)-Cd(2)-N(2) | 75.53(6)       |

|                 |           |                 |           |
|-----------------|-----------|-----------------|-----------|
| O(1)-Cd(1)-N(4) | 138.31(6) | O(2)-Cd(2)-N(7) | 139.22(6) |
| O(1)-Cd(1)-N(5) | 101.93(6) | O(2)-Cd(2)-N(8) | 77.39(5)  |
| O(1)-Cd(1)-N(5) | 101.93(6) |                 |           |

**Table 3.8** Selected bond angles (°) for the complex  $[\text{Cd}_2(\text{L}^6)_2]^{2+}$

### 3.2.4 Complexes of $\text{L}^7$ and cobalt(II)

Reaction of  $\text{L}^7$  with  $\text{Co}(\text{BF}_4)_2 \cdot 6\text{H}_2\text{O}$  in  $\text{MeNO}_2$  produces a yellow solution, slow diffusion of dichloromethane vapour into the resulting solution afforded pale yellow crystals of X-ray quality. Single crystal X-ray diffraction studies confirmed the formation of the dinuclear species  $[\text{Co}_2(\text{L}^7)_2]^{3+}$  (figure 3.11).

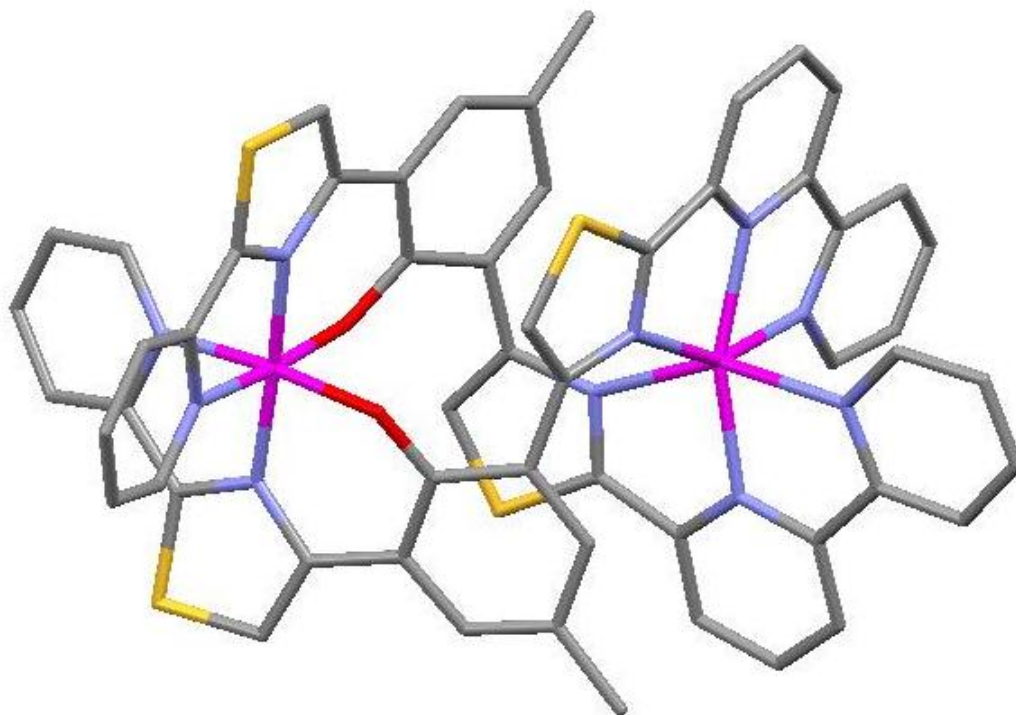


**Figure 3.11** X-ray crystal structure of the dinuclear double helicate  $[\text{Co}_2(\text{L}^7)_2]^{3+}$

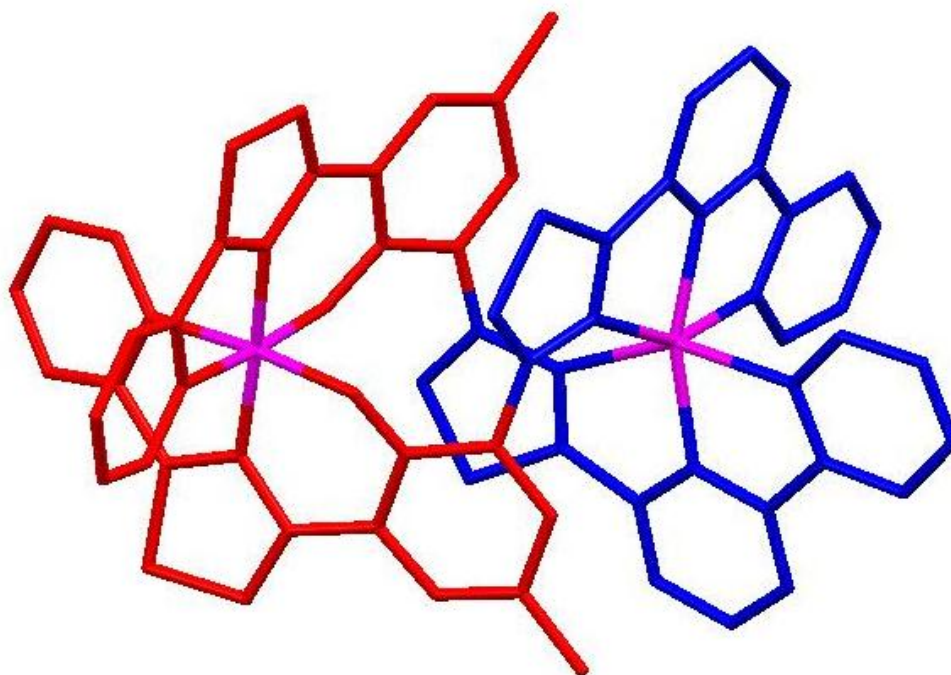


**Figure 3.12** X-ray crystal structure of the dinuclear double helicate  $[\text{Co}_2(\text{L}^7)_2]^{3+}$ ; red = tridentate head, blue = tridentate tail

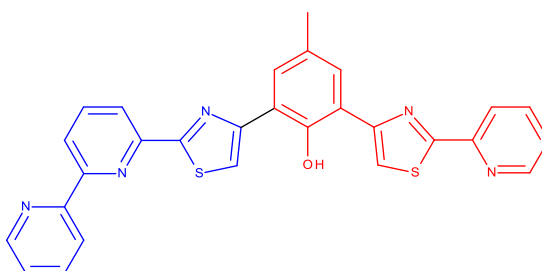


**Figure 3.13** The two different binding domains of  $\text{L}^7$ ; red = tridentate head and blue = tridentate tail

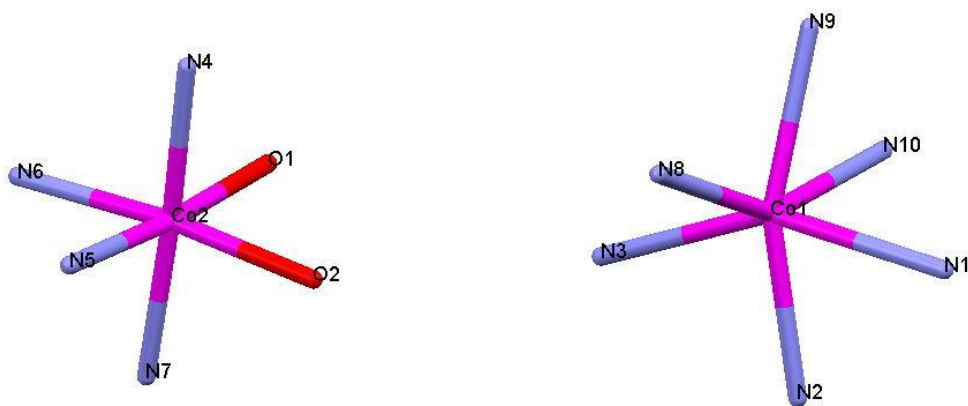


**Figure 3.14** The metal-ligand bonds in the X-ray crystal structure of the dinuclear double helicate  $[\text{Co}_2(\text{L}^7)_2]^{3+}$

In the solid state crystal structure of the dinuclear double helicate  $[\text{Co}_2(\text{L}^7)_2]^{3+}$  both the metal centres adopt six coordinate geometry arising from the coordination of a tridentate domain from two different ligand strands to give a head-to-head dinuclear double helicate. The two cobalt metal centres occupy different binding sites; one is coordinated by the N-donor tz-py-py donor atoms from the tridentate tail (blue) (Cd-N: 2.06-2.20 Å) and the other is coordinated by the bidentate N-donor tz-py head (red) and the O-donor atom from the central 1,3-phenol spacer unit (Cd-N: 1.88-1.98 Å; Cd-O: 1.86-1.87 Å).

| Bond        | Bond length (Å) | Bond       | Bond length (Å) |
|-------------|-----------------|------------|-----------------|
| Co(1)-N(1)  | 2.193(2)        | Co(2)-N(4) | 1.880(2)        |
| Co(1)-N(2)  | 2.061(2)        | Co(2)-N(5) | 1.980(2)        |
| Co(1)-N(3)  | 2.192(19)       | Co(2)-N(6) | 1.977(2)        |
| Co(1)-N(8)  | 2.196(2)        | Co(2)-N(7) | 1.879(2)        |
| Co(1)-N(9)  | 2.062(2)        | Co(2)-O(1) | 1.862(18)       |
| Co(1)-N(10) | 2.186(2)        | Co(2)-O(2) | 1.866(17)       |

**Table 3.9** Selected bond lengths (Å) for the complex  $[\text{Co}_2(\text{L}^7)_2]^{3+}$

| Bond             | Bond angle (°) | Bond            | Bond angle (°) |
|------------------|----------------|-----------------|----------------|
| N(2)-Co(1)-N(1)  | 75.49(8)       | N(6)-Co(2)-N(4) | 96.65(9)       |
| N(3)-Co(1)-N(1)  | 151.60(8)      | N(6)-Co(2)-N(5) | 90.67(9)       |
| N(3)-Co(1)-N(2)  | 76.61(8)       | N(7)-Co(2)-N(4) | 176.46(9)      |
| N(8)-Co(1)-N(1)  | 97.60(8)       | N(7)-Co(2)-N(5) | 94.16(9)       |
| N(8)-Co(1)-N(2)  | 118.58(8)      | N(7)-Co(2)-N(6) | 82.19(9)       |
| N(8)-Co(1)-N(3)  | 91.07(7)       | N(7)-Co(2)-N(6) | 82.17(11)      |
| N(9)-Co(1)-N(1)  | 90.26(8)       | O(1)-Co(2)-N(4) | 92.38(8)       |
| N(9)-Co(1)-N(2)  | 160.05(8)      | O(1)-Co(2)-N(5) | 174.87(8)      |
| N(9)-Co(1)-N(3)  | 118.10(8)      | O(1)-Co(2)-N(6) | 89.61(8)       |
| N(9)-Co(1)-N(8)  | 76.56(8)       | O(1)-Co(2)-N(7) | 90.96(8)       |
| N(10)-Co(1)-N(1) | 88.86(8)       | O(2)-Co(2)-N(4) | 89.50(8)       |
| N(10)-Co(1)-N(2) | 90.10(8)       | O(2)-Co(2)-N(5) | 89.06(8)       |
| N(10)-Co(1)-N(3) | 96.30(8)       | O(2)-Co(2)-N(6) | 173.75(8)      |
| N(10)-Co(1)-N(8) | 151.32(8)      | O(2)-Co(2)-N(7) | 91.61(8)       |
| N(10)-Co(1)-N(9) | 75.51(8)       | O(2)-Co(2)-O(1) | 91.22(8)       |
| N(5)-Co(2)-N(4)  | 82.50(9)       |                 |                |

**Table 3.10** Selected bond angles (°) for the complex  $[\text{Co}_2(\text{L}^7)_2]^{3+}$

### 3.2.3 Complexes of $L^7$ and zinc(II)

In a similar manner to  $L^6$  and  $Cd^{2+}$ , the reaction of  $L^7$  with  $Zn(ClO_4)_2 \cdot 6H_2O$  produces two different types of crystalline material upon diffusion of diethyl ether vapour into the resulting solution. Examination showed both colourless and yellow crystals present. Single crystal X-ray diffraction analysis of the colourless crystals demonstrated the formation of the mononuclear species  $[Zn(L^7)_2]^{2+}$  (figure 3.15).

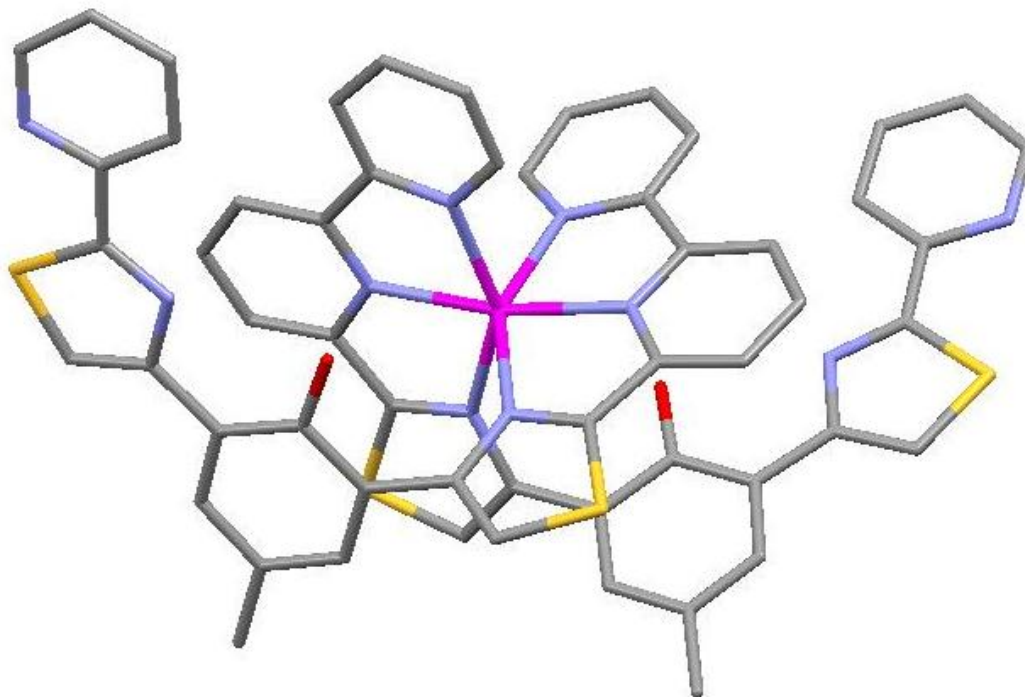


**Figure 3.15** X-ray crystal structure of the mononuclear species  $[Zn(L^7)_2]^{2+}$ , produced from the colourless crystals of  $L^7$  with  $Zn(ClO_4)_2 \cdot 6H_2O$

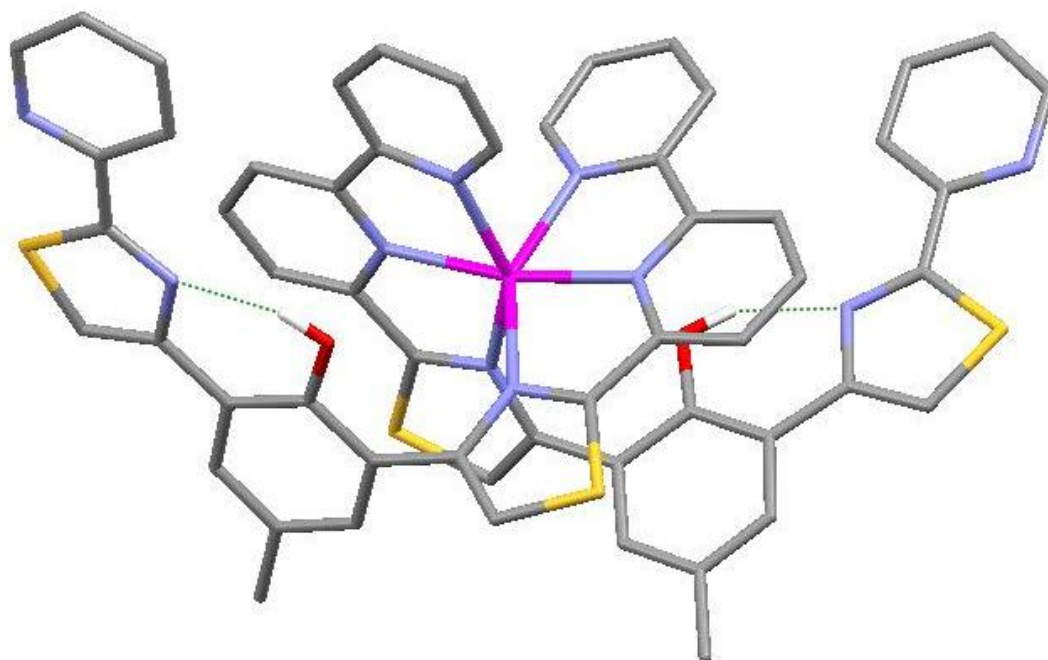


**Figure 3.16** The hydrogen bonding present in the X-ray crystal structure of the mononuclear species  $[Zn(L^7)]^{2+}$ , produced from the colourless crystals of  $L^7$  with  $Zn(ClO_4)_2 \cdot 6H_2O$

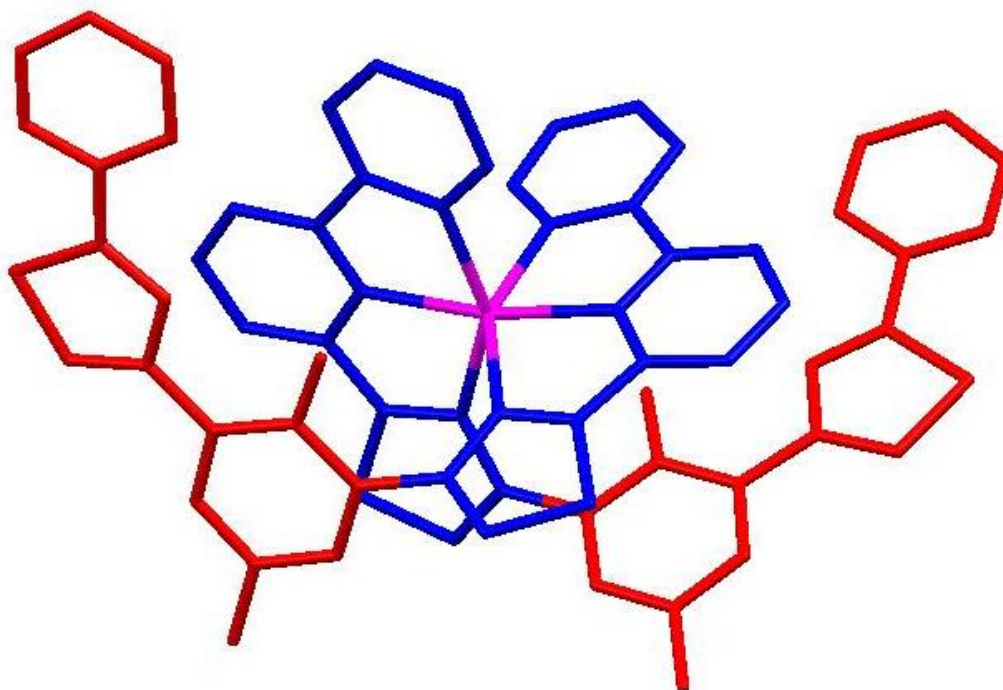


**Figure 3.17** X-ray crystal structure of the mononuclear species  $[Zn(L^7)]^{2+}$ , produced from the colourless crystals of  $L^7$  with  $Zn(ClO_4)_2 \cdot 6H_2O$ , red = head, blue = tridentate tail and pink =  $Zn^{2+}$

In the solid state crystal structure of the mononuclear  $[\text{Zn}(\text{L}^7)_2]^{2+}$  complex the  $\text{Zn}^{2+}$  metal centre is coordinated by the tridentate tail (blue) N-donor tz-py-py domain of two different ligands (Zn-N: 2.10-2.21 Å). The uncoordinated thiazole N-donor atoms hydrogen bond to the central 1,3-phenol spacer units (figure 3.16).

| Bond       | Bond length (Å) |
|------------|-----------------|
| Zn(1)-N(1) | 2.209(2)        |
| Zn(1)-N(2) | 2.102(2)        |
| Zn(1)-N(3) | 2.209(2)        |
| Zn(1)-N(6) | 2.203(2)        |
| Zn(1)-N(7) | 2.104(2)        |
| Zn(1)-N(8) | 2.190(2)        |

**Table 3.11** Selected bond lengths (Å) for the complex  $[\text{Zn}(\text{L}^7)_2]^{2+}$

| Bond           | Bond angle (°) | Bond           | Bond angle (°) |
|----------------|----------------|----------------|----------------|
| N(2)Zn(1)-N(1) | 74.51(8)       | N(7)Zn(1)-N(1) | 97.38(8)       |
| N(2)Zn(1)-N(3) | 75.37(8)       | N(7)Zn(1)-N(3) | 113.09(8)      |
| N(2)Zn(1)-N(6) | 96.91(8)       | N(7)Zn(1)-N(6) | 74.76(9)       |
| N(2)Zn(1)-N(7) | 168.45(8)      | N(7)Zn(1)-N(8) | 75.59(8)       |
| N(2)Zn(1)-N(8) | 113.38(8)      | N(8)Zn(1)-N(1) | 99.45(8)       |
| N(3)Zn(1)-N(1) | 149.59(8)      | N(8)Zn(1)-N(3) | 88.61(8)       |
| N(6)Zn(1)-N(1) | 90.88(8)       | N(8)Zn(1)-N(6) | 149.59(8)      |
| N(3)Zn(1)-N(3) | 96.83(8)       |                |                |

**Table 3.12** Selected bond angles (°) for the complex  $[\text{Zn}(\text{L}^7)_2]^{2+}$

However, examination of the orange crystals produced from the reaction of  $L^7$  with  $Zn(ClO_4)_2 \cdot 6H_2O$  shows a dinuclear complex  $[Zn_2(L^7)_2]^{3+}$  (figure 3.18).

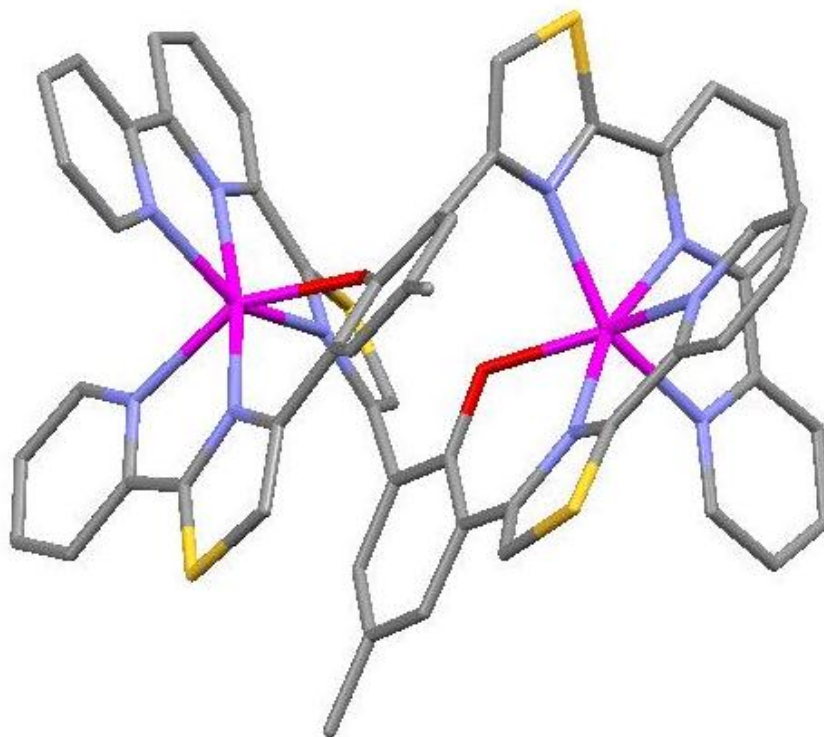


**Figure 3.18** X-ray crystal structure of the dinuclear species  $[Zn_2(L^7)_2]^{3+}$ , produced from the orange crystals of  $L^7$  with  $Zn(ClO_4)_2 \cdot 6H_2O$

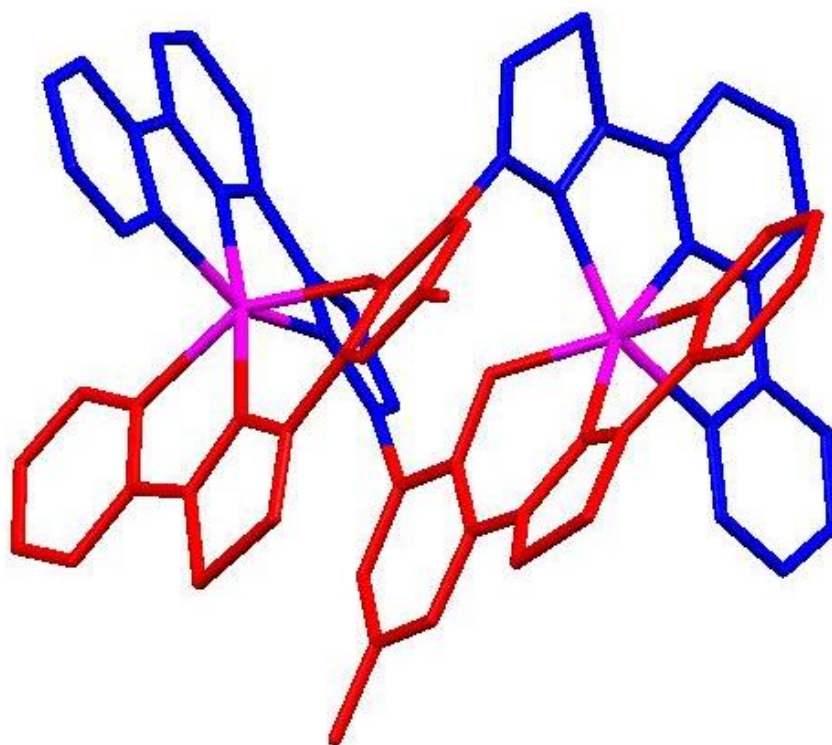


**Figure 3.19** X-ray crystal structure of the dinuclear species  $[\text{Zn}_2(\text{L}^7)_2]^{3+}$ , produced from the orange crystals of  $\text{L}^7$  with  $\text{Zn}(\text{ClO}_4)_2 \cdot 6\text{H}_2\text{O}$ , red = tridentate head, blue = tridentate tail and pink =  $\text{Zn}^{2+}$

$\text{L}^7$  acts as a head-to-tail ligand in the solid state complex of  $[\text{Zn}_2(\text{L}^7)_2]^{3+}$ , binding the octahedral  $\text{Zn}^{2+}$  metal centres in two different modes, each metal centre is coordinated by the N-donor tz-py-py donor domain from the tridentate tail (blue) (Zn-N: 2.11-2.23 Å). The coordination geometry is completed by the coordination of a bidentate N-donor py-tz and the O-donor atom from the central 1,3-phenol spacer unit from the tridentate head (red) (Zn-N: 2.10-2.22 Å; Zn-O: 2.08-2.12 Å).

| Bond        | Bond length (Å) | Bond       | Bond length (Å) |
|-------------|-----------------|------------|-----------------|
| Zn(1)-N(3)  | 2.225(7)        | Zn(2)-N(1) | 2.210(7)        |
| Zn(1)-N(4)  | 2.114(7)        | Zn(2)-N(2) | 2.101(8)        |
| Zn(1)-N(5)  | 2.199(7)        | Zn(2)-N(6) | 2.215(7)        |
| Zn(1)-N(9)  | 2.132(8)        | Zn(2)-N(7) | 2.107(7)        |
| Zn(1)-N(10) | 2.218(7)        | Zn(2)-N(8) | 2.231(7)        |
| Zn(1)-O(2)  | 2.082(5)        | Zn(2)-O(1) | 2.120(5)        |

**Table 3.13** Selected bond lengths (Å) for the complex  $[\text{Zn}_2(\text{L}^7)_2]^{3+}$

| Bond             | Bond angle (°) | Bond            | Bond angle (°) |
|------------------|----------------|-----------------|----------------|
| N(4)-Zn(1)-N(3)  | 74.10(3)       | N(1)-Zn(2)-N(6) | 93.20(3)       |
| N(4)-Zn(1)-N(5)  | 74.40(3)       | N(1)-Zn(2)-N(8) | 90.50(3)       |
| N(4)-Zn(1)-N(9)  | 166.80(3)      | N(2)-Zn(2)-N(1) | 75.90(3)       |
| N(4)-Zn(1)-N(10) | 97.00(3)       | N(2)-Zn(2)-N(6) | 94.90(3)       |
| N(5)-Zn(1)-N(3)  | 148.40(3)      | N(2)-Zn(2)-N(7) | 167.80(3)      |
| N(5)-Zn(1)-N(10) | 95.20(3)       | N(2)-Zn(2)-N(8) | 115.30(3)      |
| N(9)-Zn(1)-N(3)  | 115.70(3)      | N(2)-Zn(2)-O(1) | 81.40(3)       |
| N(9)-Zn(1)-N(5)  | 95.50(3)       | N(6)-Zn(2)-N(8) | 149.50(3)      |
| N(9)-Zn(1)-N(10) | 75.20(3)       | N(7)-Zn(2)-N(1) | 98.50(3)       |
| N(10)-Zn(1)-N(3) | 89.20(3)       | N(7)-Zn(2)-N(6) | 74.40(3)       |
| O(2)-Zn(1)-N(3)  | 86.40(2)       | N(7)-Zn(2)-N(8) | 75.20(3)       |
| O(2)-Zn(1)-N(4)  | 108.90(3)      | N(7)-Zn(2)-O(1) | 106.60(3)      |
| O(2)-Zn(1)-N(5)  | 103.40(2)      | O(1)-Zn(2)-N(1) | 152.30(3)      |

|                  |           |                 |           |
|------------------|-----------|-----------------|-----------|
| O(2)-Zn(1)-N(9)  | 81.30(3)  | O(1)-Zn(2)-N(6) | 104.60(3) |
| O(2)-Zn(1)-N(10) | 151.30(3) | O(1)-Zn(2)-N(8) | 84.90(3)  |

**Table 3.14** Selected bond angles (°) for the complex  $[Zn_2(L^7)_2]^{3+}$

### 3.3 Discussion

Reaction of  $L^5$  with  $Zn^{2+}$  results in the formation of a tetranuclear circular helicate, each  $L^5$  ligand acts as a bis-tridentate donor, coordinating via the tz-py-py donor unit from two different ligands. In an analogous fashion to the previous chapter the formation of the entropically favoured dinuclear double helicate is prevented by the steric repulsion between the  $-OH$  units on the phenol spacer, as similarly reported by Rice and co-workers.<sup>109, 110, 130</sup> In the previous chapter the 1,3-phenol spacer was used to generate a tetranuclear circular helicate  $[Co_4(L^4)_4]^{8+}$  (figure 2.9), reaction of the similar ligand  $L^5$  with an equimolar amount of  $Zn^{2+}$  also produced a tetranuclear circular helicate. The 6 coordinate metal ions are coordinated by two tridentate py-py-tz N-donor units from different ligands. In each ligand the two tridentate domains are partitioned by a 1,3-phenol spacer, which bridge the domains in an 'over and under' conformation (figure 3.2), giving rise to a helical cyclic oligomer as opposed to a face-to-face array associated with more grid-like architectures. The four  $-OH$  units do not coordinate to the metal centres but hydrogen bond to one another (Figure 3.20).

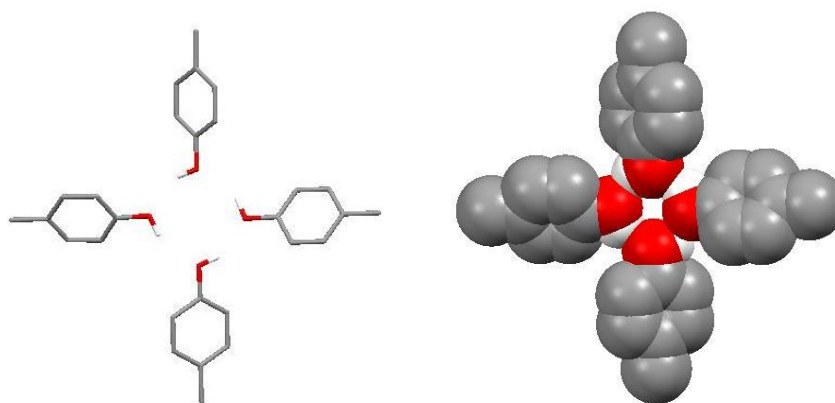


**Figure 3.20** – The hydrogen bonding between the  $-OH$  units on the 1,3-phenol spacer

As with the previous chapter the formation of the cyclic species is controlled by the spacer unit as this prevents formation of the 'simple' dinuclear species due to intra-ligand steric repulsion. However, unlike the 1,3-phenylene analogous ( $L^{jj}-L^{ll}$  figure 1.44) which result in the pentanuclear species  $[M_5(L)_5]^{10+}$ , the 1,3-phenol spacer forms a tetranuclear species. As both the phenyl and phenol have the same substitution pattern (1,3-) the formation of

the lower nuclearity species must be a consequence of the steric bulk of the methyl group on the central phenol spacer. In a tetranuclear assembly the distance between adjacent tridentate binding domains will be longer than the corresponding pentanuclear circular helicate and the steric demands of the methyl groups will therefore prevent the pentanuclear assembly. Measurement of the centroids of the central pyridine rings in adjacent ligand strands show that the distance is substantially longer in  $[\text{Zn}_4(\text{L}^4)_4]^{8+}$  (average 8.0 Å) than the pentanuclear species  $[\text{Zn}_5(\text{L}^j)_5]^{10+}$  (average 7.7 Å) (figure 3.21).<sup>109</sup>

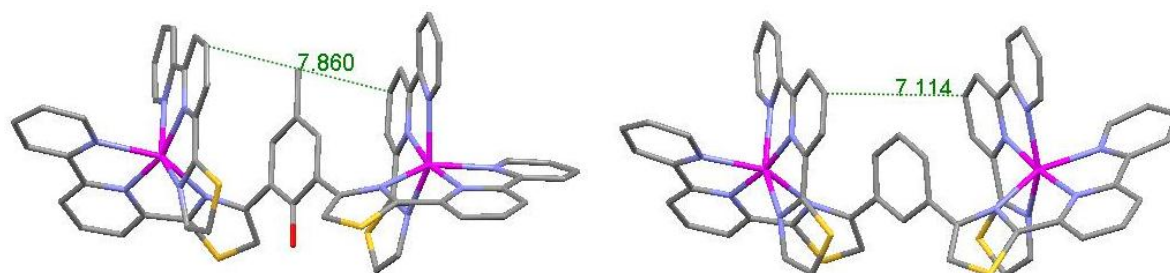


**Figure 3.21**  $[\text{Zn}_4(\text{L}^4)_4]^{8+}$  (left) and  $[\text{Zn}_5(\text{L}^j)_5]^{10+}$  (right)

Solution state studies confirm that the  $[\text{Zn}_4(\text{L}^5)_4]^{8+}$  tetranuclear helicate persists in both the solid state and solution. Reaction of  $\text{L}^5$  with an equimolar amount of  $\text{Zn}(\text{CF}_3\text{SO}_3)_2$  in  $\text{CD}_3\text{CN}$  shows the expected 9 aromatic responses in the  $^1\text{H}$  NMR. Analysis by ESI-MS gave an ion at  $m/z$  1742 corresponding to  $\{[\text{Zn}_4(\text{L}^5)_4](\text{CF}_3\text{SO}_3)_6\}^{2+}$ , confirming the formation of a tetranuclear cyclic helicate. The presence of lower molecular weight fragments at  $m/z$  797 and 1379 corresponding to  $\{[\text{Zn}(\text{L}^5)](\text{CF}_3\text{SO}_3)\}^+$  and  $\{[\text{Zn}(\text{L}^5)_2](\text{CF}_3\text{SO}_3)_6\}^+$ , respectively is probably an artefact of the ESI-MS process.

Reaction of  $\text{L}^6$  with  $\text{Ag}^+$  produces a dinuclear double *meso*-helicate, where the two  $\text{L}^6$  ligands are lying side-by-side and do not helically wrap around the  $\text{Ag}^+$  metal centres in an 'over and under' conformation (figure 3.5). The three coordinate  $\text{Ag}^+$  metal ions are coordinated by  $\text{L}^6$  in two different modes: via the tz-py unit of one ligand and the pyridyl unit only of another different ligand. The -OH unit on the 1,3-phenol spacer from both of the ligands in the complex have not deprotonated, giving a total charge for the complex as  $2^+$ , which is confirmed by the presence of two  $\text{ClO}_4^-$  counter-anions in the solid state. The  $\text{Ag}^+$  metal ions in  $[\text{Ag}_2(\text{L}^6)_2]^{2+}$  adopt a three coordinate trigonal geometry, the  $\text{Ag}-\text{L}^6$  bond lengths are similar to those reported by Zhong-Lu and co-workers on their work on the formation of three tricoordinate dinuclear  $\text{Ag}^+$  complexes, with each  $\text{Ag}^+$  ion coordinated to three methyl-substituted aminopyridines with terephthalic acid.<sup>131</sup> One thiazole N-donor unit does not coordinate the  $\text{Ag}^+$  metal centres; this can be attributed to the size of the metal ion (1.2 Å) and the divergent nature of the ligand; caused by the five-membered

thiazole ring, preventing the ligand acting as a bis-bidentate donor. Hydrogen bonding exists between the uncoordinated thiazole N-donor atoms and the -OH from the central 1,3-phenol spacer, stabilising the formation of the dinuclear double mesocate  $[\text{Ag}_2(\text{L}^6)_2]^{2+}$  (figure 3.6). As previously stated in the introduction the hydrogen bond has a range of geometries, lengths and strengths and is therefore crucial in supramolecular chemistry and nature.<sup>10</sup> Further evidence for the formation of  $[\text{Ag}_2(\text{L}^6)_2]^{2+}$  was gained through  $^1\text{H}$  NMR and ESI-MS studies. Due to the two  $\text{L}^6$  ligands coordinating in two different modes the one-dimensional spectrum of  $[\text{Ag}_2(\text{L}^6)_2]^{2+}$  should show 10 peaks, but examination of the  $^1\text{H}$  NMR spectrum showed only 5 broad peaks. The likely explanation of this is that the solution in the  $[\text{Ag}_2(\text{L}^6)_2]^{2+}$  solution is fluxional, with the ligands undergoing intramolecular rearrangement and interchanging between the two different coordination modes (figure 3.22).

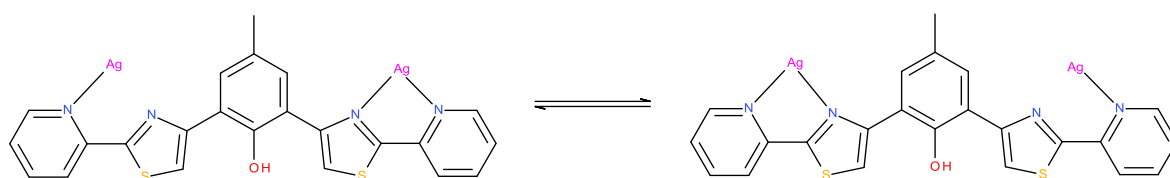


**Figure 3.22** The fluxional arrangement of the two ligand coordination modes in the  $[\text{Ag}_2(\text{L}^6)_2]^{2+}$  complex

The presence of ions in ESI-MS spectrum at  $m/z$  743, 965 and 1379 corresponding to  $\{[\text{Ag}(\text{L}^6)(\text{ClO}_4)]\}^+$ ,  $\{[\text{Ag}(\text{L}^6)_2]\}^+$  and  $\{[\text{Ag}_3(\text{L}^6)_2](\text{ClO}_4)_2\}^+$  respectively, are due to aggregation during the ESI-MS progress. A molecular ion at  $m/z$  1171 corresponding to  $\{[\text{Ag}_2(\text{L}^6)_2](\text{ClO}_4)\}^+$  confirms the presence of the dinuclear species.

Reaction of  $\text{L}^6$  with  $\text{Cd}^{2+}$  produces two different coloured crystals which result in the formation of two different supramolecular assemblies. The colourless crystals produced from the reaction of  $\text{L}^6$  with  $\text{Cd}^{2+}$  resulted in the formation of the mononuclear complex  $[\text{Cd}(\text{L}^6)_2(\text{MeCN})_2]^{2+}$ , whereas the orange crystals produced from the same reaction of  $\text{L}^6$  with  $\text{Cd}^{2+}$  resulted in the formation of the dinuclear complex  $[\text{Cd}_2(\text{L}^6)_2]^{2+}$ . The eight coordinate  $\text{Cd}^{2+}$  metal centre in  $[\text{Cd}(\text{L}^6)_2(\text{MeCN})_2]^{2+}$  is coordinated by the tridentate domain of two different ligands, which comprises of the bidentate tz-py N-donor domain and the O-donor from the central spacer unit and two acetonitrile solvent molecules complete the coordination geometry. The ligands in the  $[\text{Cd}(\text{L}^6)_2(\text{MeCN})_2]^{2+}$  complex have not deprotonated, with both the 1,3-phenol spacers containing an -OH unit, this is confirmed by the presence of two perchlorate anions in the solid state and by ESI-MS. The eight M-L ( $\text{L} = \text{L}^6$  or MeCN) bonds formed around the  $\text{Cd}^{2+}$  metal centre is a result of the size of the 2<sup>nd</sup> row  $\text{Cd}^{2+}$  metal ion (0.95 Å), allowing more interactions with ligands. Hydrogen bonding

exists between the uncoordinated thiazole N-donor atoms and the -OH unit from the central 1,3-phenol spacer, stabilising the formation of the mononuclear complex  $[\text{Cd}(\text{L}^6)_2(\text{MeCN})_2]^{2+}$ . The six coordinate  $\text{Cd}^{2+}$  metal centres in the  $[\text{Cd}_2(\text{L}^6)_2]^{2+}$  structure are coordinated by the bidentate py-tz N-donor domains from two different ligands, the O-donor atom from the central 1,3-phenol unit bridges the two metal centres to give a dinuclear double meso-helicate. The O-donor domain bridges the two  $\text{Cd}^{2+}$  metal centres to form two tridentate domains; this type of bridging O-donor atom was shown previously in ligands  $\text{L}^{\text{bbb}}$  and  $\text{L}^{\text{ccc}}$  reported by Rice and co-workers in 2007, in this work the central N-oxide atom of both ligands bridges the  $\text{Cd}^{2+}$  metal centres partitioning the ligands into two distinct binding domains (figure 2.1).<sup>126</sup> As there are only two perchlorate anions present in the solid state  $[\text{Cd}_2(\text{L}^6)_2]^{2+}$  structure it is assumed that both of the  $\text{L}^6$  ligands have deprotonated, giving an overall charge of 2+. Figure 3.9 shows the solid state structure of the  $[\text{Cd}_2(\text{L}^6)_2]^{2+}$  complex; this self-assembly is a dinuclear double *meso*-helicate in which the two bidentate domains of each ligand coordinate two different metal ions in a 'side by side' conformation. Each of the ligands coordinates via a C-type arrangement giving rise to metal centres of opposite chirality, as opposed to a "true" helicate where the ligands twist and adopt an S-type arrangement resulting in the two metal centres having the same chirality.<sup>96</sup>

Thus the colourless crystals correspond to the mononuclear complex whereas the orange crystals produced the dinuclear double *meso*-helicate. This difference is a direct result of the -OH unit on the 1,3-phenol spacer. If the -OH unit is protonated the oxygen atom can only coordinate once and therefore the mononuclear  $[\text{Cd}(\text{L}^6)_2(\text{MeCN})_2]^{2+}$  complex forms, however deprotonation of one of the -OH unit results in the oxygen coordinating twice as a bridging donor to form the dinuclear double *meso*-helicate  $[\text{Cd}_2(\text{L}^6)_2]^{2+}$  (figure 3.23).



**Figure 3.23** The different coordination modes of the OH on the 1,3-phenol spacer unit (right protonated and left deprotonated)

The  $^1\text{H}$  NMR of a solution of  $\text{L}^6$  and  $\text{Cd}^{2+}$  contains very broad peaks, which again can be explained by the equilibrium between the two distinct species ( $[\text{Cd}(\text{L}^6)_2(\text{MeCN})_2]^{2+} + \text{L} \leftrightarrow [\text{Cd}_2(\text{L}^6)_2]^{2+} + 2\text{MeCN}$ ).

The ESI-MS of a solution of  $\text{L}^6$  and  $\text{Cd}^{2+}$  shows three main ions at  $m/z$  969, 1069 and 1178 corresponding to  $\{[\text{Cd}(\text{L}^6)_2]\}^+$ ,  $\{[\text{Cd}(\text{L}^6)_2](\text{ClO}_4)\}^+$  and  $\{[\text{Cd}_2(\text{L}^6)_2](\text{ClO}_4)\}^+$ , respectively. Altering the metal-ligand stoichiometry has a pronounced effect on the ratio of the peaks, in a solution containing a 1:2 metal-ligand ratio the most predominant species is the

mononuclear complex  $\{[\text{Cd}(\text{L}^6)_2](\text{ClO}_4)\}^+$ . Adding more metal ion, to give an equimolar amount of metal-ligand, resulted in the lower molecular weight ions significantly reducing in intensity and correspondingly the ion at  $m/z$  1178 corresponding to  $\{[\text{Cd}_2(\text{L}^6)_2](\text{ClO}_4)\}^+$  was the most predominant species. ESI-MS also supports the deprotonation of two -OH units in the dinuclear structure; the molecular formula for the ion at  $m/z$  1179, corresponding to  $\{[\text{Cd}_2(\text{L}^6)_2](\text{ClO}_4)\}^+$ , is consistent with the deprotonation of both -OH units.

Although the formation of either the mononuclear or dinuclear species is dependent on stoichiometry, the formation of either  $[\text{Cd}(\text{L}^6)_2(\text{MeCN})_2]^{2+}$  or  $[\text{Cd}_2(\text{L}^6)_2]^{2+}$  must be in equilibrium as both structures are proposed when equimolar amounts of  $\text{L}^6$  and  $\text{Cd}^{2+}$  are used (figure 3.24).

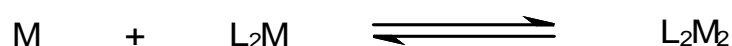


**Figure 3.24** The equilibrium present in the reaction of  $\text{L}^6$  with  $\text{Cd}^{2+}$  that forms either the mononuclear  $[\text{Cd}(\text{L}^6)_2(\text{MeCN})_2]^{2+}$  complex or the dinuclear double helical  $[\text{Cd}_2(\text{L}^6)_2]^{2+}$  complex

Ligand  $\text{L}^7$  is an unsymmetrical head-to-tail ligand which when reacted with transition metal cations forms either a *HT* or *HH* complex. The ligand partitions into two different domains, a tridentate tail (blue) and a tridentate head (red), separated by a 1,3-phenol spacer (figure 3.25). Reaction of  $\text{L}^7$  with  $\text{Co}^{2+}$  results in the *HH*-dinuclear double helicate  $[\text{Co}_2(\text{L}^7)_2]^{3+}$ , in the solid state structure there are three  $\text{BF}_4^-$  counter ions present indicating that the complex has an overall charge of 3+. If we assume that both -OH units have deprotonated then this suggests that the complex contains one  $\text{Co}^{2+}$  and one  $\text{Co}^{3+}$  metal ions. This is supported by the different coordination environments of the two cobalt metal centres; one is coordinated by the N-donor tz-py-py domain (Cd-N: 2.06-2.20 Å) and the other is coordinated by the bidentate N-donor tz-py domain and the O-donor atom from the central 1,3-phenol spacer unit (Cd-N: 1.88-1.98 Å; Cd-O: 1.86-1.87 Å). The bond lengths support the idea that the two cobalt metal centres have different oxidation states, with the longer M-L bond length occupying the  $\text{Co}^{2+}$  metal centre. This suggests that  $\text{Co}^{2+}$  coordinates to the tridentate tz-py-py N-donor domain (blue) with an average bond length of 2.15 Å. Whereas the  $\text{Co}^{3+}$  is coordinated by the tridentate head (red) which consists of the bidentate tz-py N-donor domain and the O-donor domain from the 1,3-phenol spacer, with an average N-donor bond length of 1.93 Å and an average O-donor bond length of 1.86 Å.

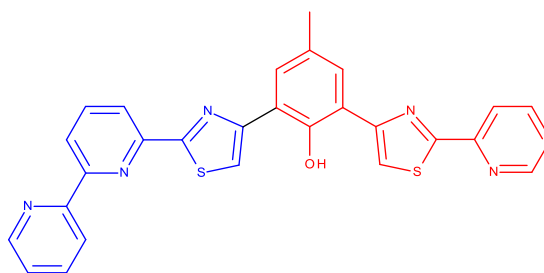


**Figure 3.25** The two different binding domains of  $L^7$ , red = tridentate head, blue = tridentate tail

Previous work has shown that the different oxidation states of cobalt can be distinguished by the M-L bond lengths. In 1994 Williams and co-workers produced a bis-bidentate ligand  $L^{ddd}$  that upon reaction with  $Co^{2+}$  results in a dinuclear triple helicate with  $Co^{2+}$ -N bond lengths ranging from 2.15-2.20 Å (figure 3.26).<sup>132</sup>

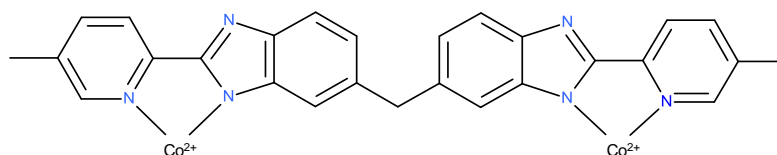


**Figure 3.26** The ligand  $L^{ddd}$  produced by A. F. Williams and co-workers in 1994

Hannon and co-workers formed a dinuclear  $Co^{3+}$  structure by reacting one equivalent bis-pyridylimine ligand  $L^{eee}$  with an equimolar amount of  $Co^{2+}$  (figure 3.27).<sup>133</sup> M. J. Hannon indicate that the formation of the helical complex is due to the  $Co^{2+}$  oxidising in the air to form  $Co^{3+}$ . The resulting structure was a dinuclear structure with each  $L^{eee}$  ligand coordinating to one metal centre with an average  $Co^{3+}$ -N bond lengths ranging from 1.90-1.92 Å, the dinuclear structure is supported by a triple-bridge formed by one acetate anion and two hydroxide ligands.

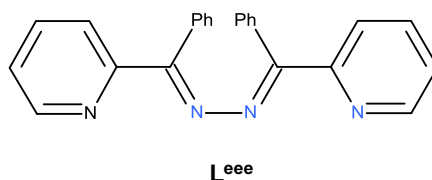


**Figure 3.27** The ligand  $L^{eee}$  produced by M. J. Hannon and co-workers in 2003

In 2004 Yan and co-workers reported a mixed-valence molecular square that contained both  $Co^{2+}$  and  $Co^{3+}$ . The  $Co^{2+}$ -N bond lengths are 2.09-2.13 Å, compared to the  $Co^{3+}$ -N bond lengths 1.88-1.94 Å and  $Co^{3+}$ -O 1.91 Å. This correlates to the bond lengths obtained for the  $[Co_2(L^7)_2]^{3+}$  structure:  $Co^{2+}$ -N 2.06-2.20 Å,  $Co^{3+}$ -N 1.88-1.98 Å and  $Co^{3+}$ -O 1.86-1.87 Å.<sup>134</sup> The reason for the shorter bond distances to the  $Co^{3+}$  ion is due to the higher charge

of this cation resulting in shorter M-L bond lengths. Furthermore the harder  $\text{Co}^{3+}$  ion is coordinated by the harder of the two ligand domains (two O-donor and four N-donor atoms) whereas the  $\text{Co}^{2+}$  ion is coordinated by the softer domain (six N-donor atoms). Reaction of  $\text{L}^7$  with  $\text{Co}^{2+}$  results in a head-to-head helicate, however reaction of  $\text{L}^7$  with  $\text{Zn}^{2+}$  results in a head-to-tail helicate; this provides further support for the mixed valence cobalt helicate as the two cobalt metal ions are occupying different binding sites. In the  $HH[\text{Co}_2(\text{L}^7)_2]^{3+}$  structure the two cobalt metal ions are coordinated to the same domain, whereas in the  $[\text{Zn}_2(\text{L}^7)_2]^{3+}$  structure each zinc metal ion is coordinated by the head of one ligand and the tail of another different ligand resulting in both  $\text{Zn}^{2+}$  ions coordinated by one O-donor and five N-donor atoms.

Reaction of the similar ligand prepared by Rice and co-workers in 2010 and  $\text{Cu}^{2+}$  results in the head-to-tail pentanuclear circular helicate  $HT[\text{Cu}_5(\text{L}^{\text{kk}})_5]^{10+}$  (figure 1.45), the 1,3-phenylene spacer results in a pentanuclear circular helicate whereas the 1,3-phenol spacer results in the dinuclear double helicate.<sup>110</sup> The O-donor atom in the 1,3-phenol  $HH[\text{Co}_2(\text{L}^7)_2]^{3+}$  complex is involved in the coordination with the metal ions therefore twisting the ligands so the inter-ligand steric interactions between the spacer units do not exist and the entropically favoured dimer is produced.

Due to the paramagnetic nature of the  $d^7$   $\text{Co}^{2+}$  metal ion analysis by  $^1\text{H}$  NMR spectroscopy is precluded. The ESI-MS of a solution of  $\text{L}^7$  and  $\text{Co}^{2+}$  shows ions at  $m/z$  1213 and 1301 corresponding to  $\{[\text{Co}_2(\text{L}^7)_2](\text{BF}_4)\}^+$  and  $\{[\text{Co}_2(\text{L}^7)_2](\text{BF}_4)_2\}^+$ . Both of the -OH units on the 1,3-phenol spacer of the ligands have deprotonated in the ion at  $m/z$  1213, whereas only one -OH unit has deprotonated in the ion at  $m/z$  1301. Unfortunately the ESI-MS studies do not reinforce the theory suggested by solid state characterisation; in the solution studies both of the peaks correspond to  $\text{Co}^{2+}$ , suggesting that the oxidation process occurs over a long period of time.

In an identical manner to that of  $\text{L}^6$ ,  $\text{L}^7$  reacts with  $\text{Zn}^{2+}$  to produce two different coloured crystals which results in the formation of two different supramolecular assemblies. The colourless crystals produced from the reaction of  $\text{L}^7$  with  $\text{Zn}^{2+}$  resulted in the formation of the mononuclear complex  $[\text{Zn}(\text{L}^7)_2]^{2+}$ , whereas the orange crystals produced from the same reaction resulted in the formation of the dinuclear complex  $[\text{Zn}_2(\text{L}^7)_2]^{3+}$ . The  $\text{Zn}^{2+}$  metal centre in the mononuclear  $HH[\text{Zn}(\text{L}^7)_2]^{2+}$  complex has octahedral geometry arising from the coordination of the tridentate tz-py-py (tail) domain of two different ligands forming a head-to-head or tail-to-tail complex. The ligands in the  $[\text{Zn}(\text{L}^7)_2]^{2+}$  complex have not deprotonated, with both the 1,3-phenol spacers containing an -OH unit, this is confirmed by the presence of two perchlorate anions in the solid state and by ESI-MS studies. Hydrogen bonding exists between the uncoordinated thiazole N-donor atoms and the -OH

from the central 1,3-phenol spacer, stabilising the formation of the mononuclear complex  $[\text{Zn}(\text{L}^7)_2]^{2+}$  (figure 3.16).

In the  $[\text{Zn}_2(\text{L}^7)_2]^{3+}$  complex each of the  $\text{Zn}^{2+}$  metal centres are coordinated by the tridentate head (red) of one ligand and the tridentate tail (blue) of another different ligand to give a head-to-tail dinuclear double helicate. The octahedral coordination geometry of the  $\text{Zn}^{2+}$  metal centres arises from the coordination of the tz-py-py N-donor domains from the tridentate tail (blue) and the tridentate head (red) which consists of the bidentate tz-py N-donor domain and the O-donor domain from the 1,3-phenol spacer. As there three perchlorate anions present in the solid state  $[\text{Zn}_2(\text{L}^7)_2]^{3+}$  structure it is assumed that one of the  $\text{L}^7$  ligands has deprotonated, giving an overall charge of 3+. The protonated -OH unit can be distinguished by the longer M-L bond lengths (2.12 Å) compared to the shorter deprotonated M-L bond lengths (2.08 Å). Unlike the previous  $[\text{Cd}_2(\text{L}^6)_2]^{2+}$  structure the O-donor atom from the spacer unit in the  $[\text{Zn}_2(\text{L}^7)_2]^{3+}$  is coordinating as a monodentate ligand, with each O-donor atom coordinating a different metal centre. The formation of these two complexes is under the same equilibrium conditions of the previous  $[\text{Cd}(\text{L}^6)_2(\text{MeCN})_2]^{2+}$  and  $[\text{Cd}_2(\text{L}^6)_2]^{2+}$  structures (figure 3.24). Thus the colourless crystals correspond to the mononuclear complex whereas the orange crystals are the dinuclear double helicate; this difference is a direct result of the stoichiometry of the reaction. In the mononuclear complex the  $\text{Zn}^{2+}$  is coordinated by the N-donor tridentate domain from two different ligands, the soft  $\text{Zn}^{2+}$  metal centre prefers the softer N-donor atom, however changing the stoichiometry forces the oxygen atoms to coordinate and the dinuclear complex forms. In an analogous manner to the previous  $HH[\text{Co}_2(\text{L}^7)_2]^{3+}$  structure reported previously, the formation of the entropically favoured dimer instead of the pentanuclear circular helicate reported on the head-to-tail  $\text{L}^{\text{kk}}$  ligand is a result of the central 1,3-phenol spacer. The O-donor atom from the spacer is involved in the coordination with the metal ions, therefore the ligands are twisted and the inter-ligand steric interactions between the spacer units do not exist.

The  $^1\text{H}$  NMR of the solution is of a solution of  $\text{L}^7$  with  $\text{Zn}^{2+}$  is uninformative as in both the mononuclear and dinuclear helicates the  $\text{L}^7$  ligand is unsymmetrical and shows 15 aromatic responses. A slight shift in ppm of the dinuclear double helical  $[\text{Zn}(\text{L}^7)_2]^{2+}$  complex occurs if the metal-ligand ratio is changed from 2:1 to 1:1, the minor peaks present in the  $[\text{Zn}(\text{L}^7)_2]^{2+}$  complex become the major peaks in the  $[\text{Zn}_2(\text{L}^6)_2]^{3+}$  complex, therefore the dinuclear double complex is becoming more apparent. The ESI-MS of a solution of  $\text{L}^7$  and  $\text{Zn}^{2+}$  shows four main ions at  $m/z$  1073, 1175, 1239 and 1338 corresponding to  $\{[\text{Zn}(\text{L}^7)_2]\}^+$ ,  $\{[\text{Zn}(\text{L}^7)_2](\text{ClO}_4)\}^+$ ,  $\{[\text{Zn}_2(\text{L}^7)_2](\text{ClO}_4)\}^+$  and  $\{[\text{Zn}_2(\text{L}^7)_2](\text{ClO}_4)_2\}^+$ , respectively. In a similar manner to the previous  $\text{L}^6$  and  $\text{Cd}^{2+}$  spectrum altering the metal-ligand stoichiometry has a

pronounced effect on the ratio of the peaks, in a solution containing a 1:2 metal-ligand ratio the most predominant species is the mononuclear complex  $\{[\text{Zn}(\text{L}^7)_2](\text{ClO}_4)\}^+$  at  $m/z$  1175. Adding more metal ion changed the ratio of the peaks; the most predominant species in a solution of 1:1 metal-ligand ratio is the ion at  $m/z$  1239, corresponding to the dinuclear species, a reduction in intensity for the other three peaks is also observed. ESI-MS also supports the deprotonation of one -OH units in the dinuclear structure; the molecular formula for the ion at  $m/z$  1239, corresponding to  $[\text{Zn}_2(\text{L}^7)_2](\text{ClO}_4)\}^+$  is consistent with the deprotonation of one -OH unit.

In summary, three novel polydentate ligands  $\text{L}^5$ - $\text{L}^7$ , consisting of N-donor domains separated by a 1,3-phenol spacer unit were successfully synthesised.  $\text{L}^5$  has been shown to self-assemble into a tetranuclear circular helicate upon reaction with  $\text{Zn}^{2+}$  metal ions and this structure persists in both the solid and solution state. This high nuclearity species forms as a result of unfavourable steric interaction between the -OH units of the 1,3-phenol spacer, preventing the formation of the dinuclear complex. Formation of a tetranuclear assembly, instead of the pentanuclear obtained with the 1,3-phenylene spacer, is a consequence of the steric bulk of the methyl group on the central 1,3-phenol spacer. Variation of the ligand allowed the formation of the *meso*-helicate  $[\text{Ag}_2(\text{L}^6)_2]^{2+}$  with  $\text{Ag}^+$ . Reaction of a pentadentate ligand  $\text{L}^7$  with  $\text{Co}^{2+}$  results in the oxidation of the metal ion in the air to form  $\text{Co}^{3+}$ ; allowing the formation of a mixed valence dinuclear double helicate, where the two different metal cations can be distinguished by their M-L bond lengths. The formation of the entropically favoured dimer instead of the a circular helicate is a result of the central 1,3-phenol spacer; the ligands are twisted and the inter-ligand steric interactions between the spacer units do not exist due to the O-donor atom coordinating to the metal ions. We have demonstrated that subtle changes caused by both the central -OH unit and the stoichiometry of the reaction have a pronounced effect on the resulting structure. These changes modify the self-assembly outcome; both the mononuclear and dinuclear complexes are present in solution, with variation in intensity depending on the stoichiometry, however the formation of either complex in the solid state is in equilibrium as both structures are proposed when equimolar amounts of metal and ligand are used.

## 4. Formation of a head-to-tail tetranuclear circular helicate

In a recent study Rice and co-workers reported that the inclusion of a 1,3-phenylene spacer unit between two identical tridentate tz-py-py N<sub>3</sub> binding domains allows the formation of a pentanuclear circular helicate, these systems can be further controlled to form heteroleptic and head-to-tail circular helicates.<sup>109, 110</sup> Work reported by M. Whitehead in 2010 describes the synthesis and coordination chemistry of the potentially hexadentate N-donor ligand **L<sup>fff</sup>**, which contains two identical tridentate thiazole-pyridyl-pyridyl N-donor domains separated by a 1,3-pyrene unit (figure 4.1).<sup>135</sup>

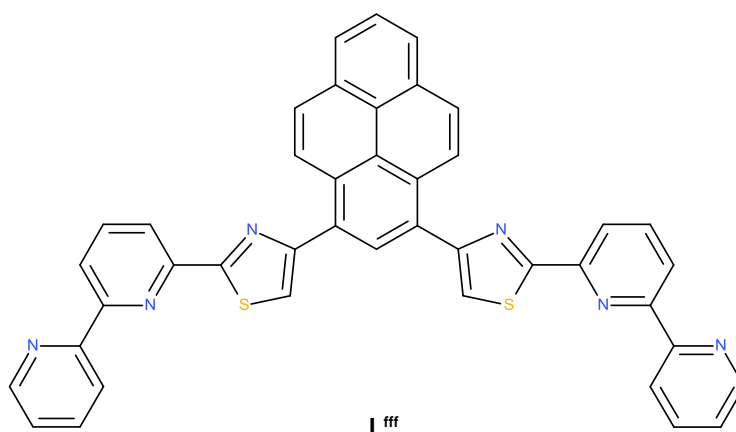


**Figure 4.1** The potentially hexadentate ligand reported by M. Whitehead in 2010

Analysis by ESI-MS of the reaction of this ligand with an equimolar amount of Zn<sup>2+</sup> show a number of low nuclearity fragments, but also a peak at 1931 which corresponds to the tetranuclear circular helicate  $\{[Zn_4(L^{fff})_4](CF_3SO_3)_6\}^{2+}$ , but despite exhaustive attempts suitable crystals for X-ray diffraction could not be grown. It was reported that heating the resulting solution at 60 °C overnight produced crystals suitable for X-ray crystallography. Structural analysis confirmed the formation of the tetranuclear circular helicate  $[Zn_4(L^{fff})_4]^{8+}$  (figure 4.2). In the solid state there are four Zn<sup>2+</sup> metal ions coordinated by four **L<sup>fff</sup>** ligands with all Zn<sup>2+</sup> ions adopting six coordinate distorted octahedral geometry, arising from the coordination of two tridentate tz-py-py domains from two different ligands. The 1,3-pyrene spacers bridge each of the tridentate domains in an 'over and under' conformation (figure 4.2). Analysis by <sup>1</sup>H NMR showed that full conversion to the tetranuclear assembly took 48 hours at 60 °C.

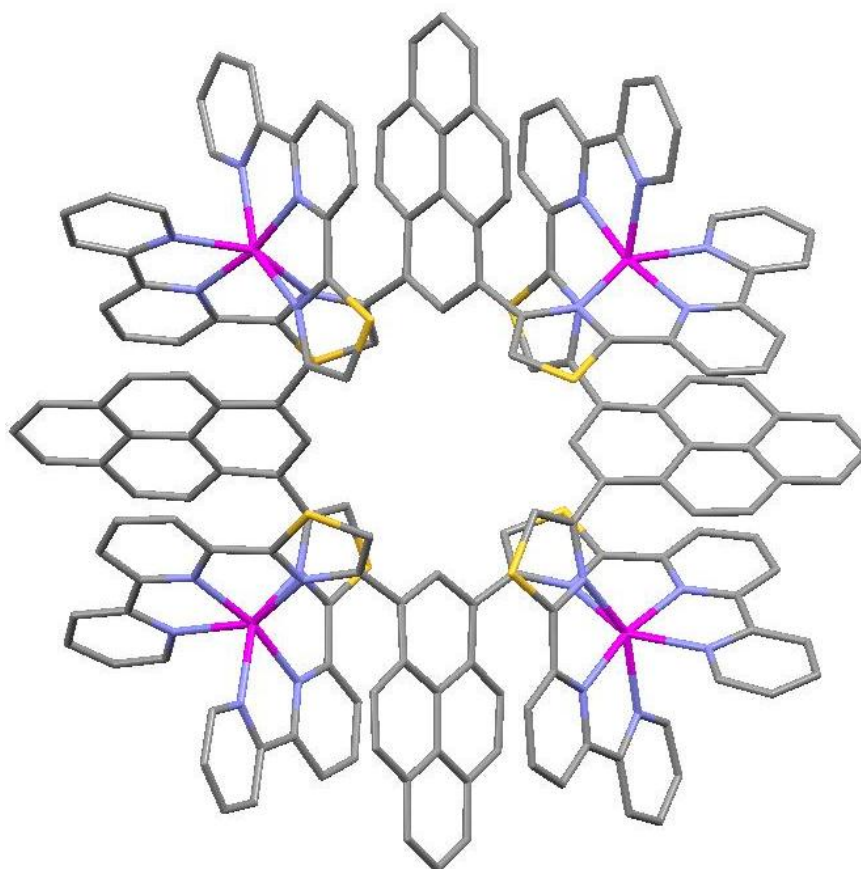


**Figure 4.2** The tetranuclear circular helicate  $[Zn_4(L^{fff})_4]^{8+}$  reported by M. Whitehead in 2010.<sup>135</sup>

This chapter focuses on extending the chemistry of the 1,3 pyrene containing ligand  $L^{fff}$  in order to express higher order complexity, namely the formation of a head-to-tail tetranuclear circular helicate. Described in this chapter is the synthesis and coordination chemistry of a potentially pentadentate N-donor ligand. The unsymmetrical ligand  $L^8$ , contains two different binding domains; which consist of a tridentate thiazole-pyridyl-pyridyl  $N_3$  domain and a bidentate tz-py  $N_2$  domain separated by a 1,3-pyrene unit (figure 4.3).

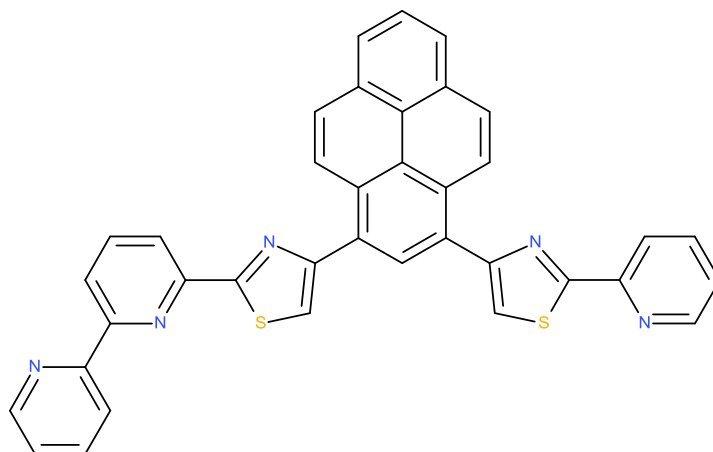
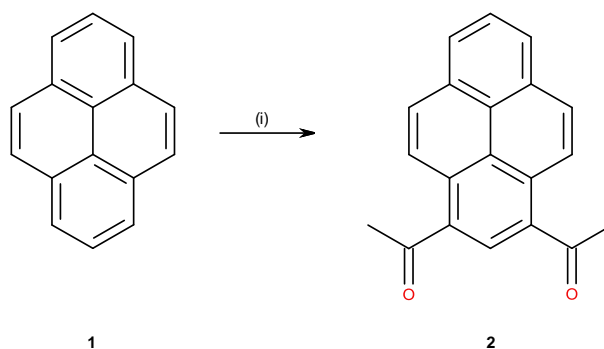


**Figure 4.3** Ligand L<sup>8</sup>

## 4.1 Ligand synthesis

### 4.1.1 Freidel-Craft acylation of pyrene

Synthesis of 1,3-diacetylpyrene (2) was achieved by Freidel-Crafts acylation of pyrene (1) with excess acetyl chloride and aluminium chloride resulting in the desired 1,3- isomer, as well as the unwanted 1,8- and 1,10- isomers (scheme 4.1). Although the 1,3-isomer was the minor product (> 3 %) it can be isolated in usable quantities through a combination of crystallisation and extensive column chromatography.<sup>136, 137</sup>

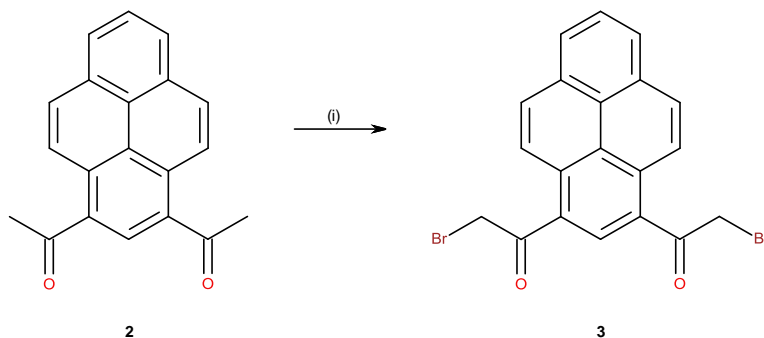


**Scheme 4.1** Synthesis of 1,3-diacetylpyrene. Reagents and conditions: (i) AlCl<sub>3</sub>, CH<sub>3</sub>COCl, CS<sub>2</sub>, 60 °C

### 4.1.2 Synthesis of 1,3-di(α-bromoacetyl)pyrene (3)

The synthesis of 1,3-di(α-bromoacetyl)pyrene (3) is outlined in scheme 4.2 and was carried out in a similar manner to that previously reported.<sup>135</sup> Reaction of 1,3-diacetylpyrene (2) with bromine in acetic acid gave the mono, di, tri and tetra- brominated species, purification of the crude material via column chromatography gave the dibrominated product (3). <sup>1</sup>H NMR confirms the successful formation of 1,3-di(α-bromoacetyl)pyrene (3); with a shift in ppm and change in integration in the spectra from

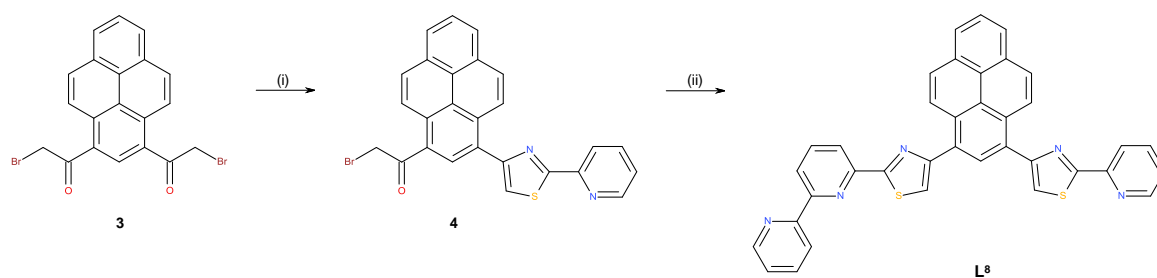
2.94 ppm for  $-\text{COCH}_3$ , that integrates to 6H, to 4.71 ppm for  $-\text{CH}_2\text{Br}$ , that integrates to 4H. Furthermore, in the ESI-MS an ion is observed at  $m/z$  445 corresponding to  $(\text{M} + \text{H}^+)$ .



**Scheme 4.2** Synthesis of 1,3-dibromoacetylpyrene (3). Reagents and conditions: (i)  $\text{Br}_2$ ,  $\text{CH}_3\text{COOH}$ ,  $80^\circ\text{C}$

#### 4.1.3 Synthesis of $\text{L}^8$

The synthesis of  $\text{L}^8$  is outlined in scheme 4.3 and was carried out in a similar manner to Rice and co-workers.<sup>110</sup> To a solution of 1,3-di( $\alpha$ -bromoacetyl)pyrene (3) in DCM was added pyridine-2-thioamide and the reaction was stirred at room temperature for 12 hours. The resulting precipitate was isolated by filtration and neutralised. Purification by column chromatography gave the mono-pyridylthiazole species (4). Confirmation of the successful formation of (4) was obtained from  $^1\text{H}$  NMR spectroscopy, which showed 13 different aromatic protons, including a singlet signal at 7.74 ppm that integrates to 1H, showing that one thiazole unit was present. A singlet peak at 4.79 ppm that integrates to 2H showed a  $-\text{CH}_2\text{Br}$  unit was still present; the presence of this methylene group is indicative that the desired material (4) had successfully formed. ESI-MS also confirmed the successful formation of (4) as an ion at  $m/z$  484 ( $\text{M} + \text{H}^+$ ) was observed. Reaction of (4) with 2,2'-bipyridine-6-thioamide in EtOH at reflux for 8 hours resulted in a yellow precipitate, which was isolated by filtration. Suspension in concentrated  $\text{NH}_3$  followed by filtration and washing gave ligand  $\text{L}^8$  as a yellow solid. Confirmation of the successful formation of  $\text{L}^8$  was obtained from  $^1\text{H}$  NMR spectroscopy, which due to the unsymmetrical nature of the ligand showed a total of 21 signals including two different thiazole proton environments at 8.47 ppm and 8.42 ppm. Furthermore, an ion was observed in the ESI-MS at  $m/z$  600, which corresponds to the protonated ligand ( $\text{L}^8 + \text{H}^+$ ).



**Scheme 4.3** Synthesis of  $L^8$ . Reagents and conditions (i) pyridine-2-thioamide, DCM, room temperature. (ii) 2,2'-bipyridine-6-thioamide, EtOH, reflux

## 4.2 Coordination Chemistry

### 4.2.1 Complexes of $L^8$ and copper (II)

The reaction of  $L^8$  with an equimolar amount of  $Cu^{2+}$  in acetonitrile gave a green solution, heating this solution at 60 °C for 36 hours produced a crystalline solid that was deposited upon slow diffusion of chloroform. Single crystal X-ray crystallographic analysis confirmed the formation of a tetranuclear head-to-tail circular helicate  $HT-[Cu_4(L^8)_4]^{8+}$  (figure 4.4).

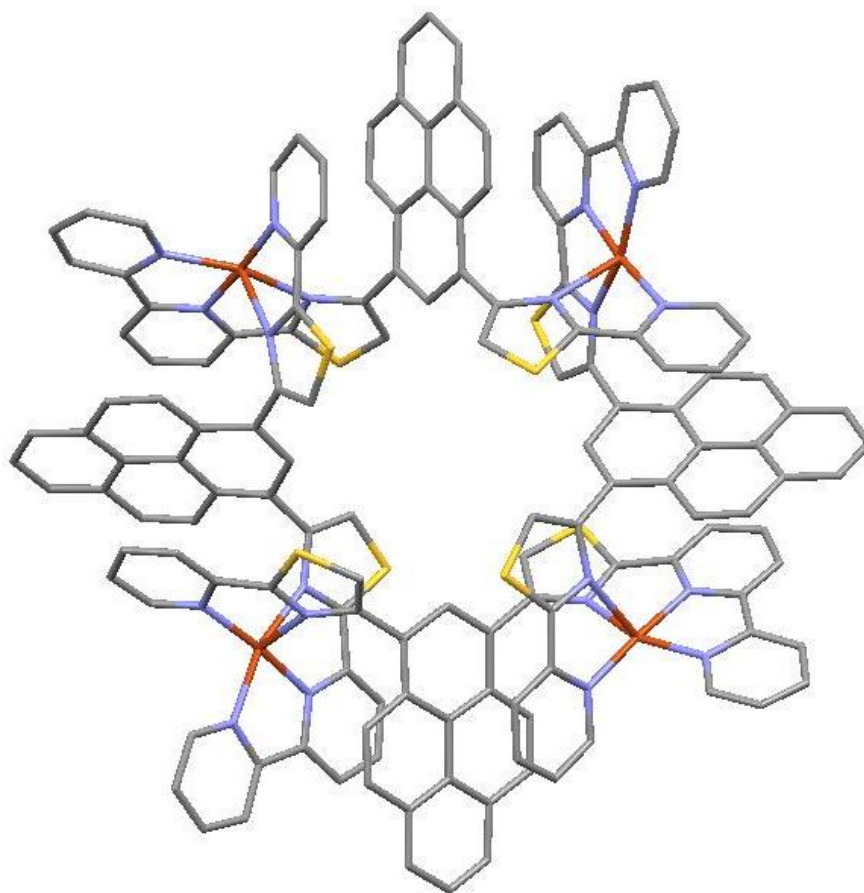


**Figure 4.4** X-ray crystal structure of  $HT-[Cu_4(L^8)_4]^{8+}$

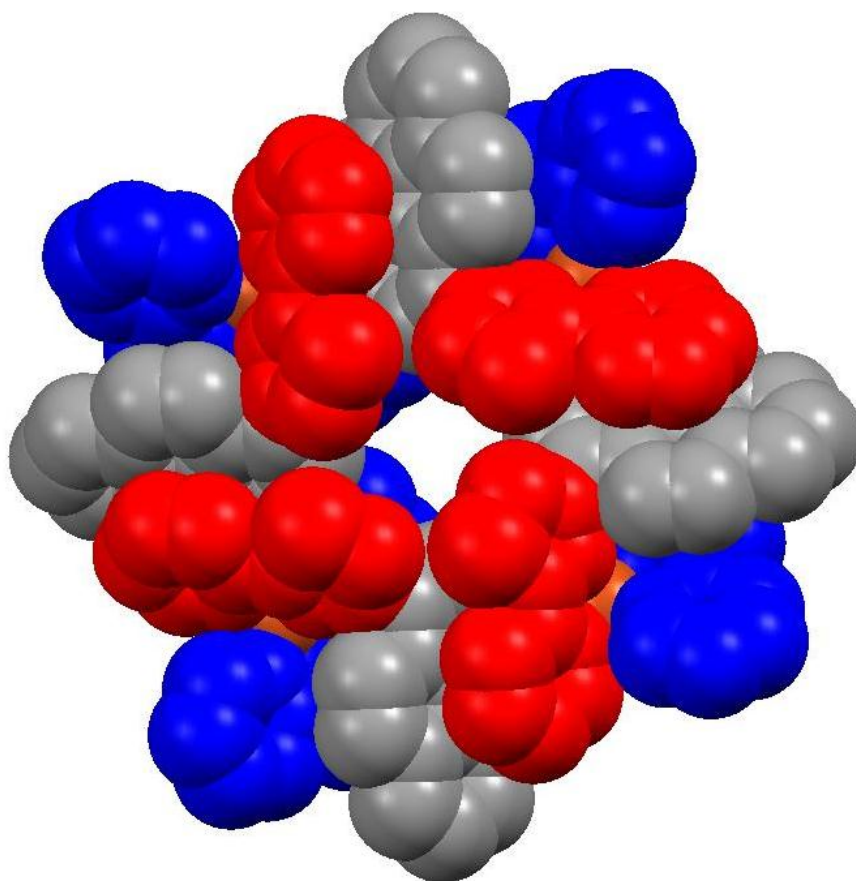


**Figure 4.5** Space filling view of the complex cation  $HT-[Cu_4(L^8)_4]^{8+}$ ; bidentate head = red, tridentate tail = blue and the 1,3-pyrene spacer = grey

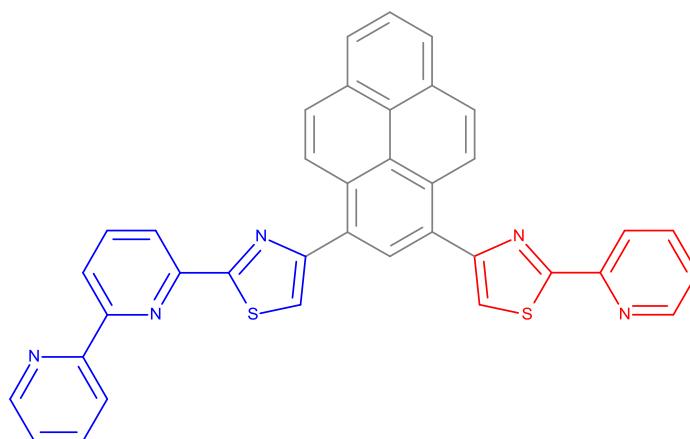


**Figure 4.6** The two different binding domains of  $L^8$ ; red = bidentate head, blue = tridentate tail and the 1,3-pyrene spacer = grey

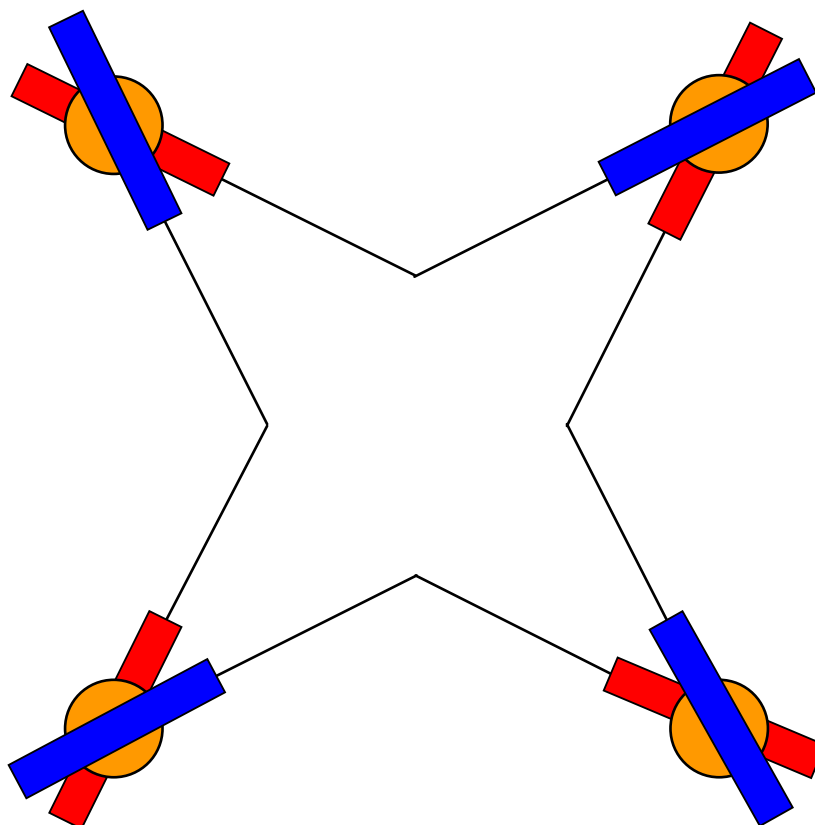


**Figure 4.7** Schematic diagram of  $HT-[Cu_4(L^8)_4]^{8+}$ ; bidentate head = red, tridentate tail = blue, and orange circles =  $Cu^{2+}$

In the crystal structure there are four  $Cu^{2+}$  ions coordinated by four  $L^8$  ligands in a head-to-tail arrangement. All four  $Cu^{2+}$  ions are five-coordinate (a coordination geometry often preferred by  $Cu^{2+}$ ), displaying distorted square-pyramidal geometries (Cu-N: 1.95-2.32 Å), arising as the ligands adopt the anticipated '3+2' binding mode, where the bidentate and tridentate N-donor domains span two different  $Cu^{2+}$  metal centres. Furthermore, the ligands are arranged in such a manner that each metal is coordinated by the bidentate head (red) domain of one ligand and the tridentate tail (blue) domain of a different ligand.

| Bond         | Bond length (Å) | Bond         | Bond length (Å) |
|--------------|-----------------|--------------|-----------------|
| Cu(1)-N(11)  | 2.053(7)        | Cu(2)-N(61)  | 2.321(8)        |
| Cu(1)-N(21)  | 1.945(7)        | Cu(2)-N(71)  | 1.972(7)        |
| Cu(1)-N(31)  | 2.139(6)        | Cu(2)-N(81)  | 2.054(7)        |
| Cu(1)-N(131) | 2.313(7)        | Cu(2)-N(91)  | 1.951(7)        |
| Cu(1)-N(141) | 1.975(7)        | Cu(2)-N(101) | 2.144(7)        |

**Table 4.1** Selected bond lengths (Å) for the complex  $HT-[Cu_4(L^8)_4]^{8+}$

| Bond                    | Bond angle (°) | Bond               | Bond angle (°) |
|-------------------------|----------------|--------------------|----------------|
| N(11)-Cu(1)-N(31)       | 159.9(3)       | N(71)-Cu(2)-N(61)  | 78.4(3)        |
| N(11)-Cu(1)-N(31)       | 104.3(3)       | N(71)-Cu(2)-N(81)  | 97.4(3)        |
| N(21)-Cu(1)-N(11)       | 79.9(3)        | N(71)-Cu(2)-N(101) | 103.2(3)       |
| N(21)-Cu(1)-N(31)       | 80.1(3)        | N(81)-Cu(2)-N(61)  | 105.0(3)       |
| N(21)-Cu(1)-N(131)      | 106.9(3)       | N(81)-Cu(2)-N(101) | 159.3(3)       |
| N(21)-Cu(1)-N(141)      | 174.3(3)       | N(91)-Cu(2)-N(61)  | 105.2(3)       |
| N(31)-Cu(1)-N(131)      | 83.6(2)        | N(91)-Cu(2)-N(71)  | 176.1(3)       |
| N(141)-Cu(1)-N(11)      | 96.4(3)        | N(91)-Cu(2)-N(81)  | 80.3(3)        |
| N(141)-Cu(1)-N(31)      | 103.4(2)       | N(91)-Cu(2)-N(101) | 79.0(3)        |
| N(141)-Cu(1)-<br>N(131) | 78.2(3)        | N(101)-Cu(2)-N(61) | 82.3(3)        |

**Table 4.2** Selected bond angles (°) for the complex  $HT-[Cu_4(L^8)_4]^{8+}$

### 4.3 Solution Studies

#### 4.3.1 Solution state characterisation of $HT-[Cu_4(L^8)_4]^{8+}$

ESI-MS of a solution of  $Cu^{2+}$  and  $L^8$  gave ions at  $m/z$  1412, 2133 and 3696 corresponding to  $\{[Cu_2(L^9)_4](CF_3SO_3)_2\}^{2+}$ ,  $\{[Cu_3(L^9)_2](CF_3SO_3)_5\}^+$  and  $\{[Cu_4(L^9)_4](CF_3SO_3)_7\}^+$  respectively. The isotope pattern of the ion at  $m/z$  1773 indicates that both the doubly charged  $\{[Cu_4(L^9)_4](CF_3SO_3)_6\}^{2+}$  and singly charged  $\{[Cu_2(L^9)_2](CF_3SO_3)_3\}^+$  species are present (figure 4.8 and 4.9). The presence of the lower nuclearity species in the ESI-MS is due to fragmentation of the tetranuclear assembly.

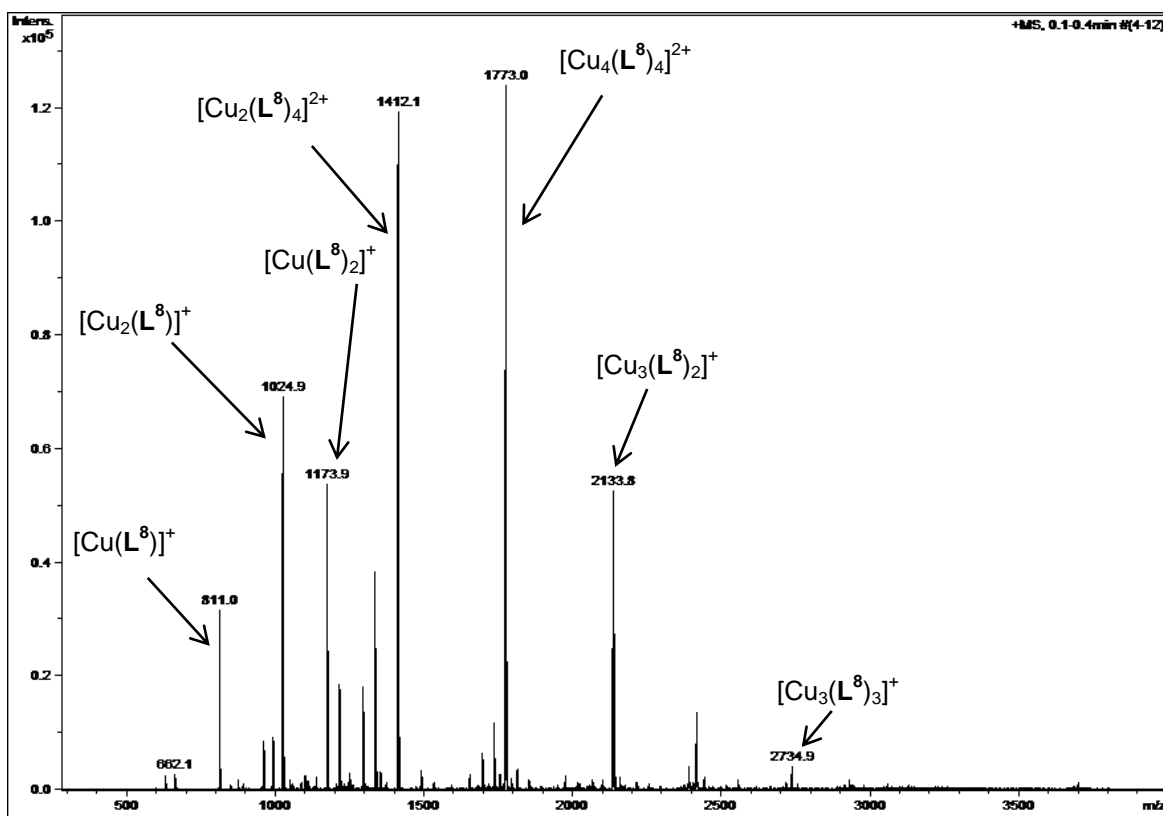
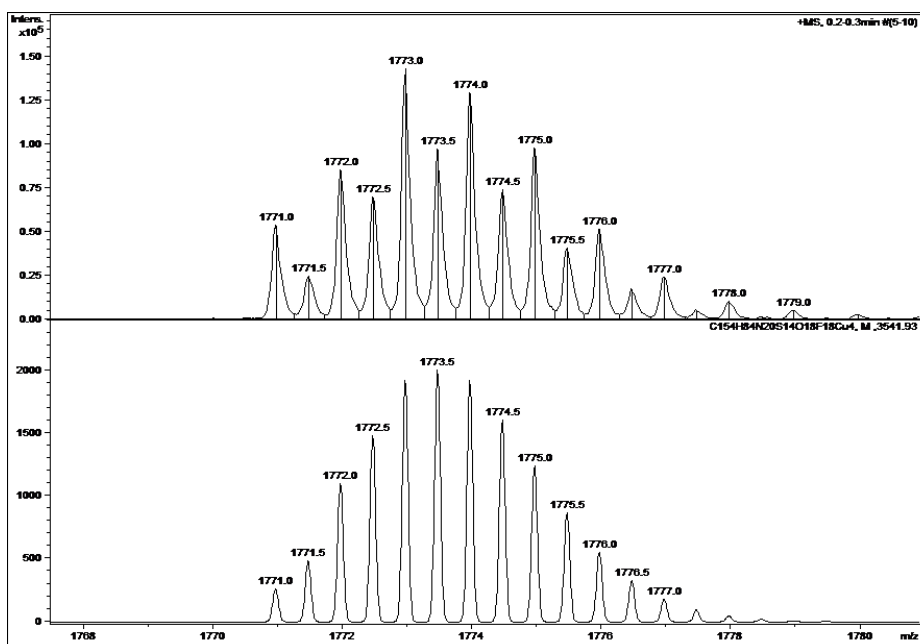


Figure 4.8 Selected assignments in the ESI-MS of the solution containing  $L^8$  and  $Cu^{2+}$



**Figure 4.9** Isotope pattern distribution for the  $[\text{Cu}_4(\text{L}^8)_4(\text{CF}_3\text{SO}_3)_6]^{2+}$  ion; top = observed, calculated = bottom

#### 4.4 Discussion

It is clear that reaction of the 1,3-pyrene containing head-to-tail ligand  $\text{L}^8$  with  $\text{Cu}^{2+}$  forms the head-to-tail tetranuclear circular helicate  $HT\text{-}[\text{Cu}_4(\text{L}^8)_4]^{8+}$ . In an analogous fashion to the circular helicates reported by Rice and co-workers and the circular helicates reported previously on the 1,3-phenol spacer, the formation of these circular species is controlled by the spacer unit.<sup>109, 110</sup> The unit; whether the 1,3-phenyl, 1,3-phenol or 1,3-pyrene, prevents the formation of the ‘simple’ dinuclear double helicates due to intra-ligand steric interactions. Both the pyrene and the phenyl spacer units have the same 1,3- substitution pattern, however the 1,3-phenylene analogues result in the pentanuclear species  $[\text{M}_5(\text{L})_5]^{10+}$  in comparison to the tetranuclear species  $[\text{M}_4(\text{L})_4]^{8+}$  formed by the 1,3-pyrene analogues. The formation of the lower nuclearity species is a consequence of the ability of pyrene to  $\pi$ -stack, which is observed frequently with pyrene.<sup>138-140</sup> Furthermore, the  $\pi$ -stacking also explains why the reaction needed to be heated at 60 °C for 36 hours to go to completion, as prolonged reaction times and heating is required to “disassemble” the kinetic products formed initially to give the final thermodynamic product. The angles between the planes formed by the two tz-py-py domains is 16.66° in the pentanuclear  $[\text{Zn}_5(\text{L}^{\text{jj}})_5]^{10+}$  circular helicate, but in the tetranuclear species this angle is reduced to 9.71°. As a result of the  $\pi$ -stacking interactions between the pyrene unit and the tz-py-py domain and also the reduction in the angle, the two domains are close to parallel, a requirement for the four-sided species (figure 4.10).<sup>109, 110</sup>

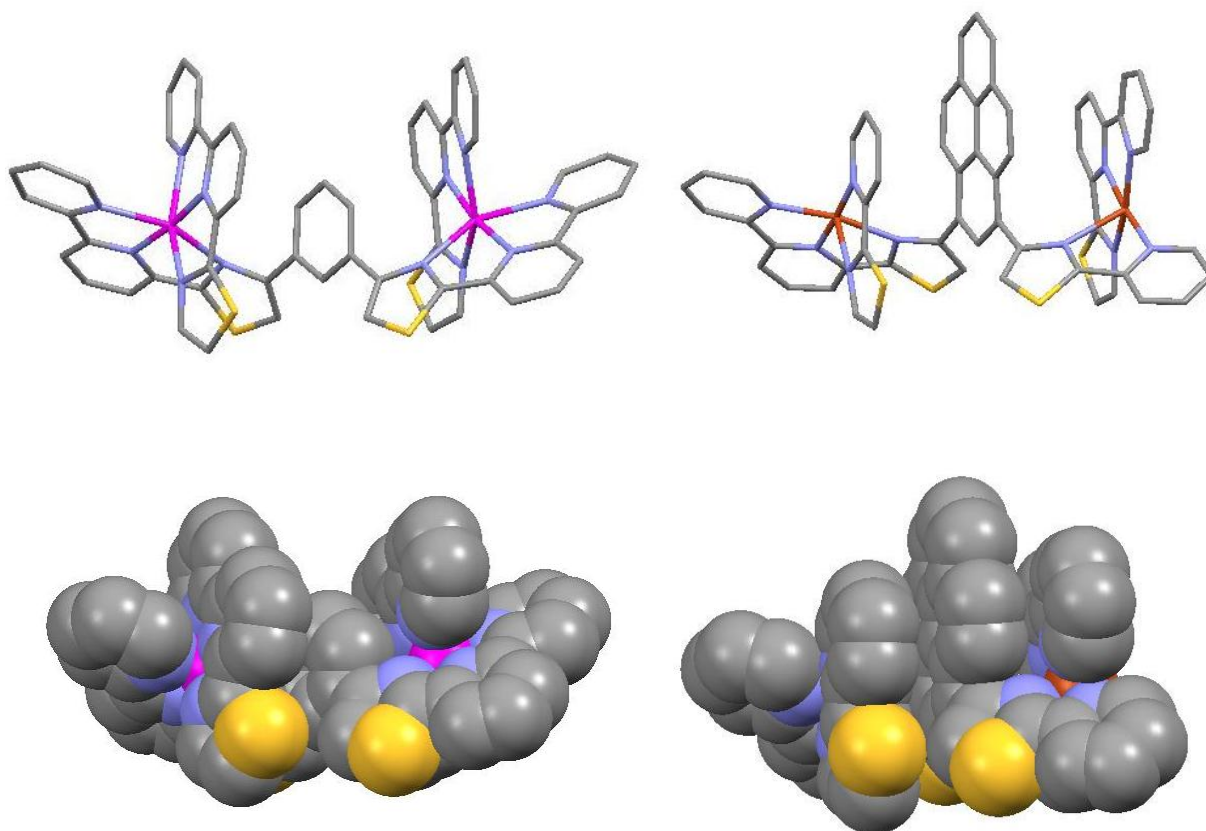


**Figure 4.10** Two views of  $[\text{Zn}_5(\text{L}^{\text{j}})_5]^{10+}$  (left) and  $[\text{Cu}_4(\text{L}^{\text{8}})_4]^{8+}$  (right).<sup>109</sup>

As in other reports,  $\text{Cu}^{2+}$  was chosen as the metal ion as amongst its possible coordination geometries, five-coordinate  $\text{Cu}^{2+}$  ions are frequently observed.<sup>141, 142</sup> Reaction of  $\text{L}^{\text{8}}$  with  $\text{Cu}^{2+}$  results in the head-to-tail tetranuclear circular helicate  $HT\text{-}[\text{Cu}_4(\text{L}^{\text{8}})_4]^{8+}$ , as the metal ion is coordination by the bidentate and tridentate domains from the unsymmetrical ligand. Solution studies of this material showed a number of low-nuclearity fragments, but also a peak at  $m/z$  1773 where the isotope pattern indicates that both  $\{[\text{Cu}_4(\text{L}^{\text{8}})_4](\text{CF}_3\text{SO}_3)_6\}^{2+}$  and  $\{[\text{Cu}_2(\text{L}^{\text{8}})_2](\text{CF}_3\text{SO}_3)_3\}^+$  are present. X-ray structural analysis confirmed the formation of a tetranuclear species, in the complex  $\text{L}^{\text{8}}$  adopts the anticipated '3+2' binding mode, seen previously with the 1,3-phenylene ligand  $\text{L}^{\text{kk}}$  (figure 1.45). The bidentate and tridentate N-donor domains span two different  $\text{Cu}^{2+}$  centres, the ligands are arranged that a given metal is coordinated by the bidentate domain of one ligand and the tridentate domain of the next. The ability for  $\text{L}^{\text{8}}$  to partition into two different binding domains to generate the head-to-tail motif is in agreement with other ligands reported previously.<sup>81</sup>

We have demonstrated the first reported example of a head-to-tail tetranuclear circular helicate. Both solid state and solution studies indicate that the tetranuclear circular helicate  $HT\text{-}[\text{Cu}_4(\text{L}^{\text{8}})_4]^{8+}$  is formed. The structure of  $HT\text{-}[\text{Cu}_4(\text{L}^{\text{8}})_4]^{8+}$  is analogous to its linear counterpart by virtue of the specific design principles involved in the synthesis, ensuring

that the ligand contains the specific structural features. The formation of this head-to-tail circular helicate is a result of two key factors: the 1,3-pyrene spacer preventing the formation of the linear double stranded assemblies and secondly the stereoelectronic preference of  $\text{Cu}^{2+}$ . In summary, we have established that some of the basic algorithms for programming structural complexity in linear helicates can also be applied to related cyclic complexes.

## 5. Solid state studies of the coordination chemistry of diphenylcarbazide and dithizone

### 5.1 Introduction

#### 5.1.1 Diphenylcarbazide

In 1888 the synthesis of diphenylcarbazide (DPC) and its colorimetric reactions with  $\text{Cu}^{2+}$  and  $\text{Hg}^{2+}$  was reported, since then DPC and its dehydrogenated derivative diphenylcarbazone (DPCO) have become a useful reagent for the colorimetric determination of a variety of different metal ions (figure 5.1). DPC is used by the Environmental Protection Agency (US EPA) for the determination of high oxidation states of chromium. However, even though DPC is a useful test for metal ions the coordination chemistry of these species is not fully understood. A vast amount has been reported on the chemistry of the colour reactions of DPC with various metal ions but a definite answer on how DPC coordinates to the metal ions has not been provided.

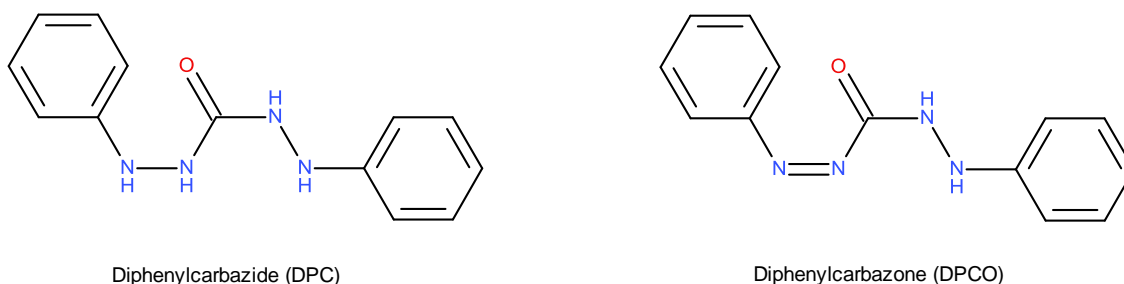


**Figure 5.1** Diphenylcarbazide (DPC) and diphenylcarbazone (DPCO)

The use of DPC in determining the presence of transition metals was first reported in 1888 by Skinner and Ruhemann, they discovered that an intense violet colour formed when DPC is reacted with both  $\text{Cu}^{2+}$  and  $\text{Hg}^{2+}$  and that this colouration was so intense and distinctive that it could be used as a qualitative test. A drop of dilute copper sulphate solution was added to DPC and an intense colouration was produced, adding ammonia to this made it scarlet and the addition of iron (II) chloride produces a red colour, but excess destroys it. When mercuric chloride is added to DPC, it acquires the same intense violet colour produced with copper sulphate. Analysis of the product from the reaction of mercury (II) chloride and DPC revealed a double compound of the composition  $\text{CO}(\text{NH}\cdot\text{NH}\cdot\text{C}_6\text{H}_5)_2\text{HgCl}_2$ , this was obtained by reaction of an alcoholic solution of DPC with an aqueous solution of mercury (II) chloride, which gave a deep violet colour. As the alcohol became more dilute a precipitate formed, which was recrystallised from hot alcohol to give a crystalline substance in which the composition was established. The synthesis

and properties of DPC are also identified in this report. The authors explained that this intense colour formation is due to the oxidising action of the metal and also noting that DPC could be oxidised to DPCO.<sup>143</sup>

In 1900 Cazeneuve was the first to observe that the reaction of  $\text{Cr}^{6+}$  with DPC produces a magenta colour with a  $\lambda_{\text{max}}$  of 540 nm. This compound was isolated in the form of a violet amorphous powder but its composition varied with the conditions of the preparation, nevertheless he suggested that an organometallic compound of a chromium complex with DPCO formed.<sup>144</sup> A report by Stover a few years later agreed with the theory Cazeneuve proposed; in acidic media (sulphuric, acetic or citric) the reaction of DPC with  $\text{Cr}^{6+}$  produced a violet colour, it was proposed that the colour produced by the reagent is probably due to oxidation by the dichromate. Stover also noted that the intensity of the violet colour varied with the amount of dichromate present, therefore making DPC an ideal test for the colorimetric determination of chromium.<sup>145</sup>

Babko and Paulii proposed in 1950 that the coloured compound contains no chromium and is rather an oxidation product of the DPC reagent, without any complex formation. That was based on their findings that when the violet coloured solution is extracted with amyl alcohol from aqueous solution it contains no chromium, the chromium was found to be retained in the colourless aqueous layer. It was also reported that the oxidation is very selective since none of the other common oxidising agents tested (ceric salts, permanganate and persulphate) gave similar results.<sup>146</sup> In 1954 Feigl agreed with this proposal that the coloured material is merely an oxidation product of the reagent.<sup>147</sup>

Bose carried out a series of studies on the reaction of  $\text{Cr}^{6+}$  and DPC and concluded that the coloured substance is a complex of  $\text{Cr}^{2+}$  and DPCO. Bose described that the reaction is a composite one, involving preliminary oxidation/reduction followed by subsequent complex formation. A striking feature of the reaction between  $\text{Cr}^{6+}$  and DPC is that the reaction medium must be sufficiently acidic (pH 2.0), if the solution is alkaline DPC does not react with the chromate and no colour formation occurs, indicating that the reaction is primarily a redox one. However, since other oxidising agents like nitrate, permanganate and iodine fail to produce the characteristic violet colour with DPC, secondary complex formation must occur. The reaction of  $\text{Cr}^{6+}$  at acidic pH leads to the metal being reduced to the trivalent oxidation state; Bose suggests that  $\text{Cr}^{3+}$  is non-reactive towards DPC and DPCO. The study is summarised that DPC is oxidised by  $\text{Cr}^{6+}$  to give DPCO and that the chromium is simultaneously reduced to  $\text{Cr}^{3+}$ , but as this is non-reactive it is chromium in the bivalent state that is the ion responsible for the colour reaction. The findings were achieved by absorption, migration, extraction and magnetic susceptibility studies. The examination of four different systems was carried out by Bose;  $\text{Cr}^{6+}$  and DPC,  $\text{Cr}^{6+}$  and

DPCO,  $\text{Cr}^{2+}$  and DPC and  $\text{Cr}^{2+}$  and DPCO. The reaction of DPC with  $\text{Cr}^{2+}$  failed to produce any colouration, but the reaction of DPCO with  $\text{Cr}^{2+}$  does, therefore it seems probable that the oxidation of DPC by chromate produces DPCO which reacts with the  $\text{Cr}^{2+}$  produced by the reduction of  $\text{Cr}^{6+}$ . All the absorption spectra found to be of similar nature and showed a maximum absorbance at 540 nm, thus indicating that the coloured reaction products in the three systems are identical.<sup>148, 149</sup>

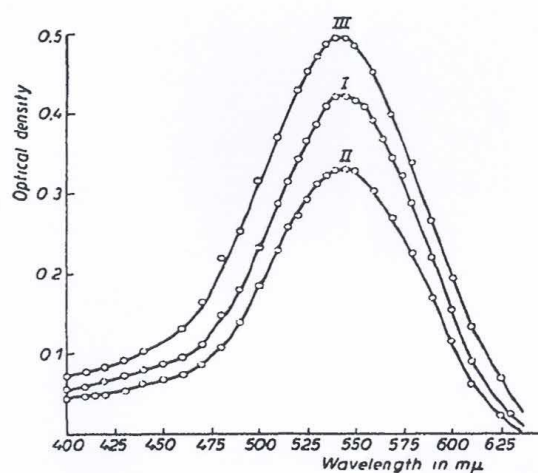
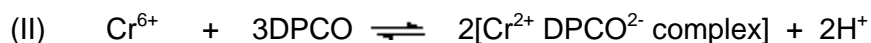
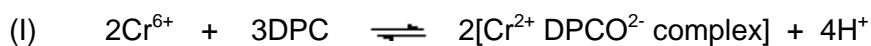


**Figure 5.2** The absorption spectra of three different systems;  $\text{Cr}^{6+}$ -DPC (I),  $\text{Cr}^{6+}$ -DPCO (II) and  $\text{Cr}^{2+}$ -DPCO (III), reported by Bose in 1954.<sup>148, 149</sup>

It was concluded that DPCO is the only organic molecule involved in the colour formation; this is deduced from the fact that it is the only common constituent present in the three different systems. The result of adding excess  $\text{Cr}^{2+}$  or  $\text{Cr}^{6+}$  was also examined in which it was found to cause the discharge of the colour initially produced, this was explained as being due to the reduction of the DPCO complex to DPC thus destroying the colour forming capacity. Bose pointed out that the solubility of a compound in various non-polar solvents usually indicates the inner complex nature therefore DPC was dissolved in different non-polar solvents and was added to an acidified chromic acid solution, this was then shaken and left to settle. The nature of the acid employed to acidify the reaction had a pronounced effect on the partition of the coloured product; using the organic acetic acid with various solvents (benzene and chloroform) greatly favoured the distribution of the coloured product into the organic solvent, whereas the use of mineral acids like sulphuric acid left the organic layer almost completely colourless. It is speculated that chromium metal ion may either be a monovalent cation or an inner complex salt but the initial study completed by Bose does not throw any light onto the exact composition of the complex formed.

Bose extended his previous work later on that year with another study, in which the same three systems were investigated: Cr<sup>6+</sup> and DPC (I), Cr<sup>6+</sup> and DPCO (II) and Cr<sup>2+</sup> and DPCO (III). The formation of the same coloured species was obtained for all the reactions and from studies in equimolecular solutions; the maximum composition values for the reactions were ascertained. The values were 2:3 for Cr<sup>6+</sup>-DPC, 1:3 for Cr<sup>6+</sup>-DPCO and 1:1 for Cr<sup>2+</sup>-DPCO. The formulation of these three systems is given below:



Bose explained that the reason the maximum composition of reaction (I) and (II) does not lead to unequivocal formation of either the composition of the complex or stoichiometry of the corresponding reaction in the case of these reactions as they are both rather complex, involving preliminary oxidation coupled with subsequent complex formation. It was described in this study that the molar susceptibility value of 4.6 Bohr magnetrons calculated on the basis of the 1:1 Cr<sup>2+</sup> and DPCO (III) ratio, indicates ionic bonding in the complex, this also confirms the presence of Cr<sup>2+</sup>.<sup>150</sup>

A detailed study on the nature of the chromium diphenylcarbazide reaction was reported by Pflaum and Howick in 1956. Several factors were investigated; comparison of absorptiometry data, stoichiometry of the various systems, effect of pH, extractability of the coloured reaction into non-aqueous media and the behaviour of the complexes under the influence of an electric field. The reaction of DPC with Cr<sup>6+</sup> in slightly acidic aqueous solution produces the intense magenta colour with an absorption maximum at 540 nm as expected, although the reaction of DPC and Cr<sup>3+</sup> does not cause immediate formation of the famous purple colour, it does however eventually develop, the observations of DPC not reacting with Cr<sup>2+</sup> made in the previous studies by Bose are repeated here. DPCO does not react with Cr<sup>6+</sup> ions, but does react with Cr<sup>3+</sup> and contrary to DPC, also reacts with Cr<sup>2+</sup>. The results of the colorimetric study show that the same absorbing species can be obtained by the reaction of the three oxidation states.<sup>151</sup>

| System                 | $\lambda$ max (nm) | $\epsilon$ ( $M^{-1} \text{ cm}^{-1}$ ) |
|------------------------|--------------------|---|
| DPC (pH 1.5)           | 285                | 2490                                    |
| DPC (pH 12)            | 490                | 4280                                    |
| DPCO (pH 1.5)          | 303                | 11,300                                  |
| DPCO (pH 12)           | 487                | 1,800                                   |
| $\text{Cr}^{6+}$ -DPC  | 540                | 26,000                                  |
| $\text{Cr}^{3+}$ -DPC  | 550                | *                                       |
| $\text{Cr}^{3+}$ -DPCO | 550                | *                                       |
| $\text{Cr}^{2+}$ -DPCO | 540                | 25,000                                  |
| * Time Dependant       |                    |   |

**Table 5.1** Summary of the colorimetric data obtained by Pflaum and Howick in 1956

Pflaum and Howick confirm that the violet coloured species is not due to either DPC or DPC alone, likewise the colour is not due to the higher oxidation product, diphenylcarbadiazone (DPDCO) (figure 5.3), which is known to be colourless and non-reactive towards metal ions.<sup>147</sup>

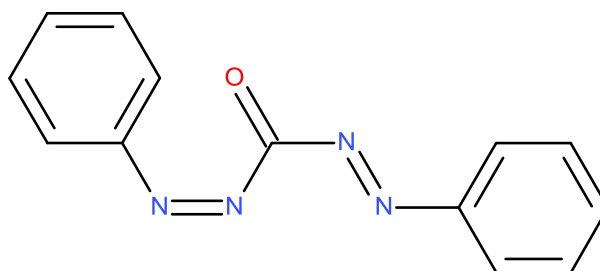


**Figure 5.3** Diphenylcarbadiazone (DPCDO)

The effects of pH show that the maximum colour formation for the DPC  $\text{Cr}^{6+}$  reaction occurs at a pH range of 1.0-1.4. Both reagents also react with numerous metal ions (copper, mercury and nickel) to produce the distinct purple coloured species. The ratio of the reaction is in agreement with the reduction of two moles of  $\text{Cr}^{6+}$  to  $\text{Cr}^{3+}$  and the oxidation of three moles DPC to DPCO, the determination of this formula was established by the method of continuous variation. Continuous variation data was obtained for the  $\text{Cr}^{3+}$ -DPC and  $\text{Cr}^{3+}$ -DPCO reactions and the 3:2 ratio of reagent to metal ions was evident: reaction of  $\text{Cr}^{2+}$  with DPCO also gave a 3:2 reagent to metal ratio. Extraction studies show

that the coloured material formed between all of the reactions, in the various oxidation states and both reagents, is not readily extractable into non-aqueous media. The coloured material was extracted into benzene, chloroform and cyclohexanol in the presence of an acetate ion, which agreed with the studies by Bose. Migration studies were designed to determine the charge on the complexed chromium, the coloured complex migrated to the cathode under the influence of an electric field, indicating that the coloured complex is a charged cation. Pflaum and Howick propose that the reaction of  $\text{Cr}^{6+}$  with DPC involves the oxidation of the reagent to DPCO with simultaneous reduction of the chromium to  $\text{Cr}^{3+}$ , they summarise that a complex species is responsible for the colour reaction; however the composition of this complex is not identified.

In 1958 Lichenstein and Allen completed extraction studies on the  $\text{Cr}^{6+}$  DPC reaction to conclude whether the violet coloured compound that forms in the reaction contains chromium. The product of the reaction was extracted into isoamyl alcohol, analysis of this extract revealed that chromium was present, disagreeing with the work completed by Babko and Paulii. It was suggested by Lichenstein and Allen that the possible forms that the chromium might be present after the reaction with DPC are the  $\text{Cr}^{2+}$  ion,  $\text{Cr}^{3+}$  ion, hydrogen chromate or an organometallic complex. The first three possibilities were eliminated due to the knowledge that in air the  $\text{Cr}^{3+}$  ion is rapidly oxidised to the  $\text{Cr}^{2+}$  ion, which is not extracted by isoamyl alcohol, hydrogen chromate will extract but not as readily as the product from the  $\text{Cr}^{6+}$ -DPC reaction. They conclude that the chromium is present as an organometallic complex.<sup>152</sup>

In 1977 Willems and co-workers completed qualitative and quantitative measurements on the three oxidation states of chromium with the three different reagents (DPC, DPCO and DPCDO). The qualitative data summarised in table 5.2 highlighting that DPCDO is colourless and non-reactive towards metal ions concurs with the previous work published by Pflaum and Howick.<sup>153</sup>

| Metal            | Ligand           | Solvent (99-1)  | Colour formation |
|------------------|------------------|-----------------|------------------|
| Cr <sup>6+</sup> | DPC              | water - acetone | +                |
|                  | DPC              | acetone - water | +                |
|                  | DPCO             | water - acetone | -                |
|                  | DPCO             | acetone - water | +                |
|                  | DPCDO            | water           | -                |
| Cr <sup>3+</sup> | DPC              | water - acetone | -                |
|                  | DPCO             | water - acetone | -                |
|                  | DPCO             | acetone         | +                |
|                  | DPCDO            | acetone         | -                |
|                  | Cr <sup>2+</sup> | DPC             | water - acetone  |
| DPCO             |                  | water - acetone | +                |
| DPCO             |                  | acetone - water | +                |
| DPCDO            |                  | water           | -                |
| DPCDO            |                  | acetone - water | -                |

**Table 5.2** Results of the qualitative tests for the interaction of Cr<sup>6+</sup>, Cr<sup>3+</sup> and Cr<sup>2+</sup> with DPC, DPCO and DPCDO

Willems and co-workers suggest that the colour formation results from a single definite complex, as the absorption spectra for the positive colour reactions are the same. They conclude that the stoichiometry of the reaction between Cr<sup>3+</sup> and DPCO is in a 2:3 ratio respectively, corresponding to the following:



In 1996 the characteristic DPC test for Cr<sup>6+</sup> was discussed in Vogel's qualitative inorganic analysis, suggesting that during the reaction of DPC and Cr<sup>6+</sup> the chromate is reduced to Cr<sup>3+</sup> and forms a complex with DPCO (figure 5.4).<sup>154</sup> Although it is proposed that the

reagent involved in the coordination with the  $\text{Cr}^{3+}$  the reagent in the illustration is that of the fully oxidised DPCDO.

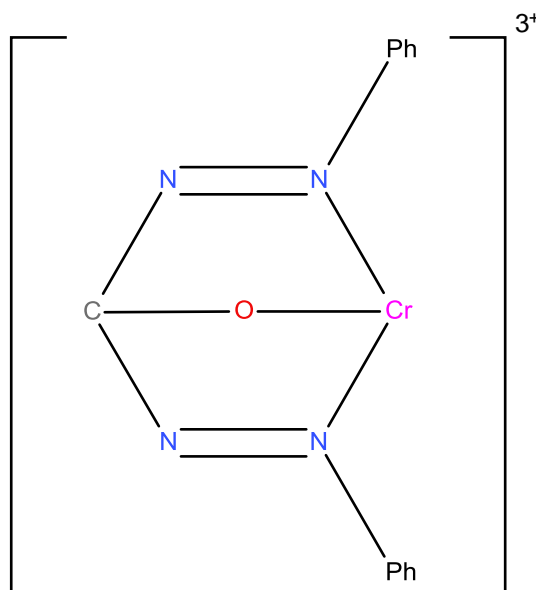


**Figure 5.4** The complex formed in the reaction of DPC with  $\text{Cr}^{6+}$  as demonstrated in Vogel's qualitative inorganic analysis

A more recent study in 2005 suggests that in the reaction of  $\text{Cu}^{2+}$  and DPC, the  $\text{Cu}^{2+}$  acts as a catalyst and catalyses the reagent to the oxygen mediated oxidation derivative DPCO, following the formation of a  $\text{Cu}^+$ -DPCO complex. Therefore the signal observed in the absorption spectra, at 450 nm, corresponds to the oxidation product DPCO. Crespo and co-workers mention that the reaction of DPC with  $\text{Cu}^{2+}$  develops a red colour over time which is influenced by the concentration of  $\text{Cu}^{2+}$ . The reaction between  $\text{Cu}^{2+}$  and DPC involves numerous intermediate species, which are dependent on the concentration of the  $\text{Cu}^{2+}$  and pH medium. A high pH of the medium favours the oxidation of DPC to DPCO, but at very high  $\text{Cu}^{2+}$  concentrations DPC is fully converted to DPCDO and DPCO is not observed.<sup>155</sup>

A great deal of work has been published on substituted derivatives of the DPCO reagents and the complexes formed with several transition metals by Siddalingaiah and co-workers. The phenyl ring on the DPCO reagent was substituted with 2,6-dichloro, 4-ethyl, 4-fluoro and 4-methyl groups. The transition metals that have been used in the complexes include;  $\text{Cd}^{2+}$ ,  $\text{Co}^{2+}$ ,  $\text{Cu}^{2+}$ ,  $\text{Ni}^{2+}$ ,  $\text{Pd}^{2+}$  and  $\text{Zn}^{2+}$ . The work completed by Siddalingaiah and co-workers has never included chromium and the reagents are always substituted, however information can be gathered from their studies. The complexes synthesised by Siddalingaiah and co-workers were characterised using a range of methods including; magnetic moment, IR, NMR, fluorescence and elemental analysis. Using the results

obtained from the elemental analysis and magnetic moment studies it is concluded that the stoichiometry of the complex is 1:2, metal to ligand ratio, and that the complexes have square planar geometry (figure 5.5). The IR spectrum of the substituted ligands show peaks at 3420 and 3440  $\text{cm}^{-1}$  for the -NH vibrations, the band at around 1700  $\text{cm}^{-1}$  is assigned to the C=O stretching. It is the disappearance of the band at around 1700  $\text{cm}^{-1}$  in the spectra of the various complexes that indicates that the oxygen atom of the ligand is involved in the coordination with the metal, the appearance of a band at around 1600  $\text{cm}^{-1}$  due to the C=N stretching further confirms the coordination. The  $^1\text{H}$  NMR spectral studies observed that the singlet due to the amide (NH) proton ( $\sim 8.74$  ppm) in the spectrum of the ligand disappears in the spectra of the diamagnetic complexes; indicating that the absence of the amide group and the formation of a metal to oxygen bond. Siddalingaiah and co-workers report that all the complexes are highly coloured, non-hygroscopic, air stable, soluble in non-polar solvents and insoluble in water. The studies concluded that the reagents behave as a bidentate monoanionic ligand coordinating through the enolised ketonic oxygen and azo nitrogen and the metals are in the bivalent oxidation state. Although a range of approaches were undertaken, attempts to isolate the complexes as crystals suitable for single crystal studies were unsuccessful.<sup>156-159</sup>

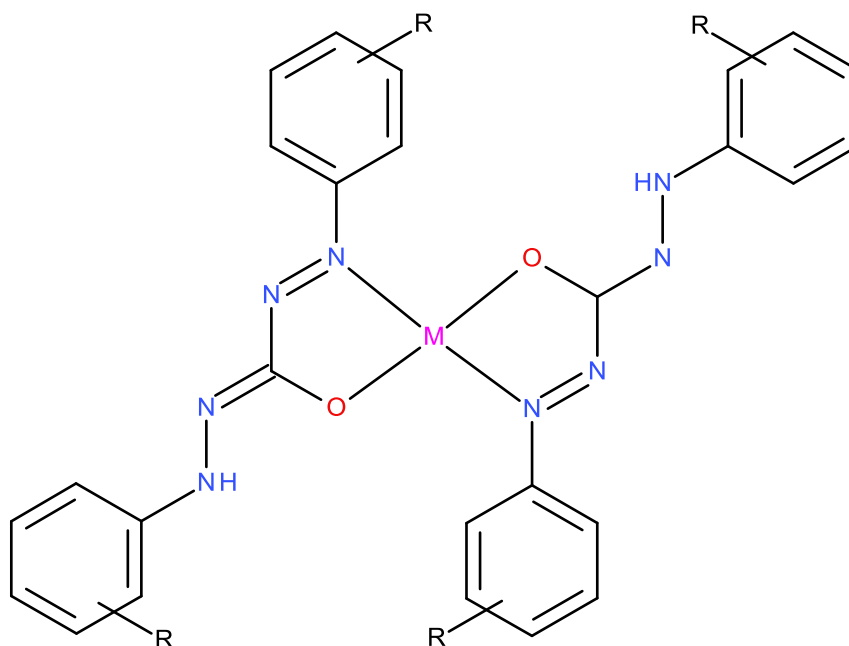


**Figure 5.5** The complex formed between substituted derivatives of DPCO and transition metal ions.  $M = \text{Cd}^{2+}$ ,  $\text{Co}^{2+}$ ,  $\text{Cu}^{2+}$ ,  $\text{Ni}^{2+}$ ,  $\text{Pd}^{2+}$  or  $\text{Zn}^{2+}$ .  $R = 2,6$ -dichloro, 4-ethyl, 4-fluoro and 4-methyl

Alternative reagents for the determination of chromium are available including the use of a stable, colourless cadmium iodide-starch reagent which is oxidised by  $\text{Cr}^{6+}$  which in turn makes the reagent blue is reported.<sup>160</sup> Fang and Miao use 2-(5-bromo-2-pyridylazo)-5-

diethylaminophenol as a photometric reagent for the spectrophotometric determination of a chromium, in which it is reported that it forms a coloured complex with both  $\text{Cr}^{6+}$  and  $\text{Cr}^{3+}$  without prior conversion of the valence state.<sup>161</sup> Stover commented on the use of the ether–hydrogen method to determine chromium, but he mentioned that it is not as sensitive as the standard DPC method.<sup>145</sup> Blundy describes the DPC reaction as the most sensitive method known for the determination of chromium. The advantages of using DPC are the sensitivity, selectivity, reproducibility and low cost when detecting chromium and other metal ions.<sup>162</sup> It is reported that DPC is used to detect chromium in rock minerals, iron and steel, water, soil, air, leather and biological materials.<sup>163</sup> DPC is sensitive to 0.005 ppm in the biological materials; blood, urine and tissue samples.<sup>164, 165</sup> The reagent DPC is also used for the determination of other metal ions and is sensitive to one part mercury in 100,000 parts water.<sup>166</sup> Despite all the studies over many years, the colourimetric reaction of DPC with various metal ions is still not understood.

### 5.1.2 Dithizone

Reaction of dithizone (referred to as DPTC or diphenylthiocarbazone) with a variety of different metal ions gives a wide range of different colorimetric responses and due to this it has become an essential reagent for the determination of first, second and third row metal ions.<sup>167, 168</sup> The enormous potential of DPTC for the qualitative and quantitative analysis of heavy metal ions was first identified in 1878 by Fischer and it is still in use today for the quick, accurate and easy determination of the concentration of metal ions.<sup>169</sup> There has been extensive research over the past 100 years into the coordination chemistry of DPTC, despite this there is still some significant unexplained chemistry associated with this ligand, just like the oxygen derivative DPC.

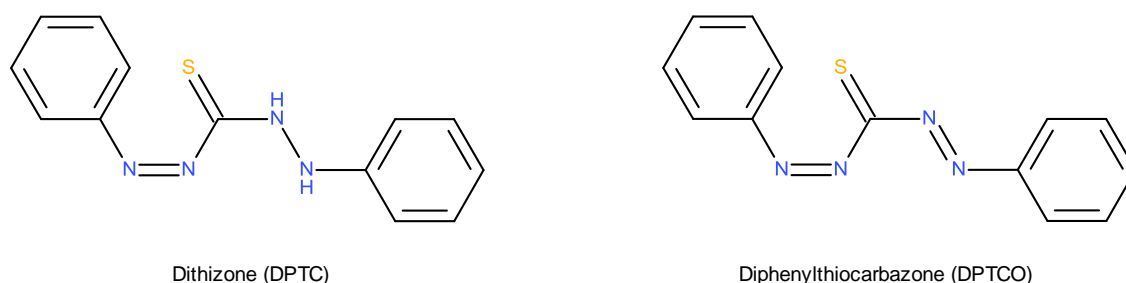


**Figure 5.6** Dithizone (DPTC) and diphenylthiocarbazone (DPTCO)

Even though DPTC is used extensively in analysis, examination of the literature reveals a lot of unexplained observations, with literature sources proposing contradictory statements about species that have not been elucidated. In 1925 Fisher it was speculated that in addition to the normal keto chelate (figure 5.7 left) formed upon reaction of DPTC with metals ions, a second thioenol complex (figure 5.7 right) also formed with some metals,  $\text{Cu}^{2+}$ ,  $\text{Hg}^{2+}$  and  $\text{Ag}^+$  (figure 5.7). The keto chelate was prepared in an acidic solution with an excess of ligand, whereas the thioenol chelate appeared to be favoured by a higher pH and excess metal. According to Fisher the hydrogen of the imide group of the dithizone is replaced by the metal to give the primary complex, and the remaining hydrogen of the thiol form is also replaced to give the secondary complex.<sup>170</sup>

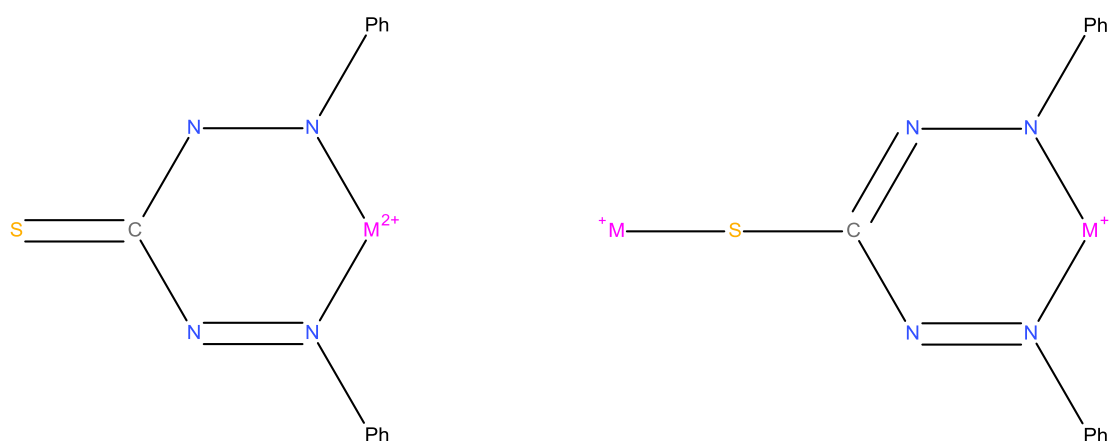


**Figure 5.7** Structures of Fischer's keto (left) and thioenol (right) chelates

The assumptions of Fischer went unchallenged until 1954, when Irving and co-workers showed that dithizone forms metal complexes that appear to be derived from the thiol form of dithizone (figure 5.8).<sup>167, 171</sup> The structure postulated by H. Irving was supported by the theory that losing the remaining proton from the thiol form would require at least pH 14.<sup>172</sup>

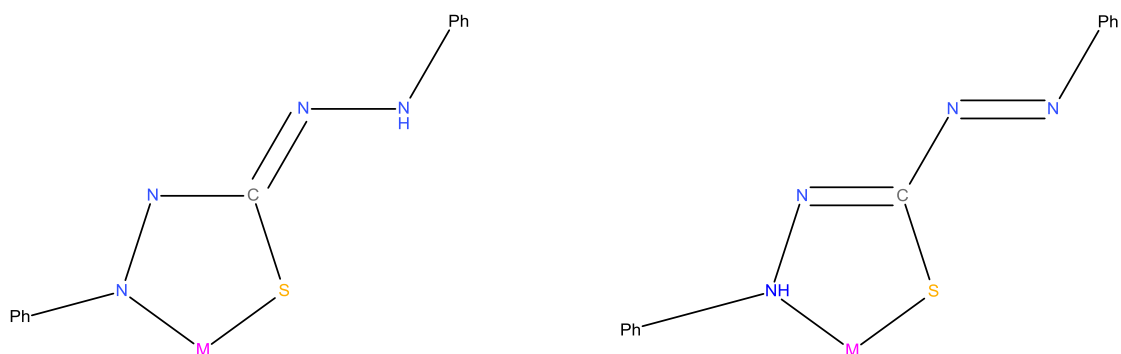


**Figure 5.8** Structures of Irving's postulations

Irving and co-workers furthered their work and reported that a solution of a metal dithizonate complex could be mixed with a second metal solution to create a mixed secondary complex. It was found that if a yellow solution of mercury dithizonate was mixed with a concentrated solution of  $\text{AgNO}_3$ , a magenta colour formed. Irving and co-workers suggested that although isolating a pure specimen was not possible they postulated the conformation of the magenta species. Reaction of DPTC with  $\text{Ag}^+$  and  $\text{Hg}^{2+}$  resulted in a complex containing one  $\text{Hg}^{2+}$ , two  $\text{Ag}^+$  ions and two DPTC ligands (figure 5.9). The two DPTC ligand undergoes deprotonation and coordinate both the  $\text{Hg}^{2+}$  and  $\text{Ag}^+$  ions via the bridging S-donor atom and the bridging N-donor atom from the deprotonated amine.<sup>173</sup>

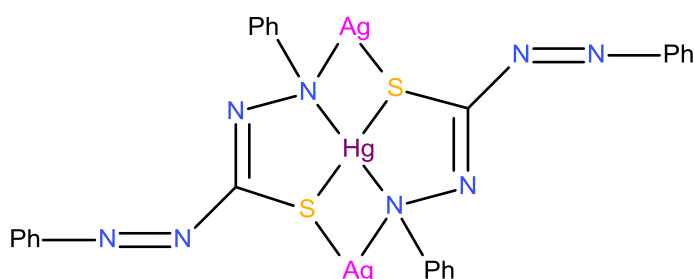


**Figure 5.9** Mix metal structure of DPTC with  $\text{Ag}^+$  and  $\text{Hg}^{2+}$

A considerable amount of work has been carried out on the reaction of lead with DPTC, giving various methods of extraction before quantitative colorimetric analysis.<sup>174</sup> Milkey determined that for lead dithizonate the most expected structure would be the keto form bonding through four nitrogen atoms from two ligands, rather than the thioenol form which would bond via the sulphur atom and two nitrogen atoms from a single ligand (figure 5.10 left). Milkey suggested that the thioenol form would be highly unlikely as the bond angles would create extreme tension in the molecule.<sup>175</sup> However, Laing disputed the keto form of lead dithizonate, by stating that DPTC bonds to metal ions through the sulphur atom and one of the nitrogen atoms was attached to a phenyl ring.<sup>176</sup>

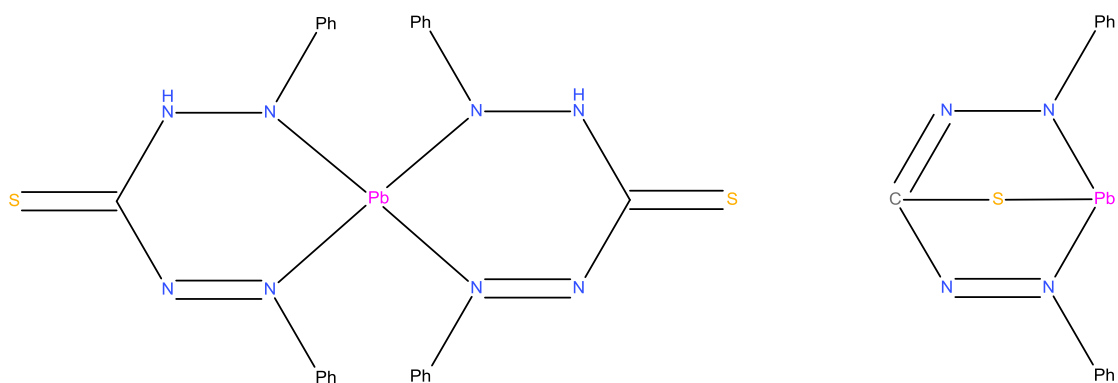


**Figure 5.10** Structures of keto (left) and thioenol (right) forms of lead dithizonate reported by Milkey in 1952

There are very few X-ray structural reports compiled on the complexes formed with DPTC and transition metal ions, it is generally accepted that the hydrazine hydrogen atom adjacent to the thiocarbonyl deprotonates forming the monoanionic ligand (figure 5.11). In most cases the ligand behaves as a bidentate chelating agent coordinating through both the nitrogen and sulphur donor atoms to give a five-membered ring structure of the type shown (figure 5.11). A review into characterising metal dithizonates by IR and UV-Vis spectroscopy highlighted that complexes of the same stereochemistry generally have similar spectra.<sup>177</sup>

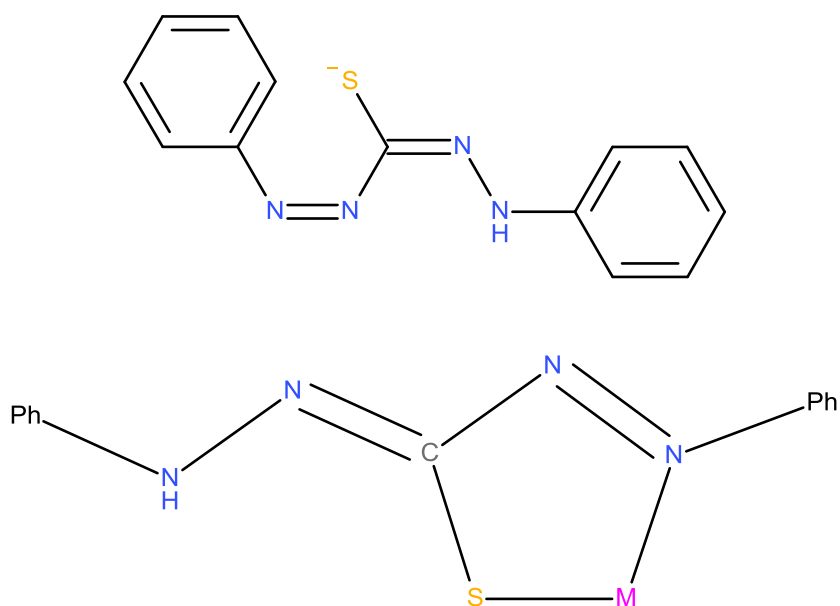


**Figure 5.11** Top = deprotonated ligand, for simplicity the neutral ligand is referred to as DPTC-H and the deprotonated species DPTC. Bottom = Coordination mode of DPTC

A preliminary report published in 1961 by Bryan and Knopf on the crystal structure of DPTC with  $\text{Cu}^{2+}$  indicates that the complex has square-planar configuration about the  $\text{Cu}^{2+}$  metal atom, coordinating via the N-donor and S-donor atoms. Complete refinement was not possible at this stage but they predict that the DPTC is in the monoanionic form.<sup>178</sup>

In 1970 Math and Freiser reported a mixed ligand crystal structure involving  $\text{Ni}^{2+}$ , DPTC and bipyridine, the presence of bipyridine was due to difficulties in obtaining crystals which was overcome by choosing heterocyclic nitrogen solvents with a slight excess of bipyridine. The octahedral  $\text{Ni}^{2+}$  metal centre is coordinated by two DPTC molecules, coordinating via the S-donor and N-donor atoms, and the bipyridine N-donor atoms. An interesting feature of this  $[\text{Ni}(\text{DPTC})_2(\text{bipy})]^{2+}$  structure is the cis-position of the two bonding sulphur atoms, which is different to the trans-position obtained for the  $\text{Cu}^{2+}$  and  $\text{Hg}^{2+}$  complexes. Complete refinement of the crystal structure is not available in this report, however Math and Freiser postulate that the DPTC ligand undergoes deprotonation and forms DPTCO.<sup>179</sup>

A different DPTC  $\text{Ni}^{2+}$  structure was obtained by Laing and Sommerville in the absence of bipyridine. The  $\text{Ni}^{2+}$  metal centre displays square planar coordination geometry arising from the coordination of the N-donor and S-donor atoms from two different DPTC ligands (figure 5.12). The two S-donor atoms in the structure are trans to one another, a result which is not consistent with previous nickel structure.<sup>180</sup>

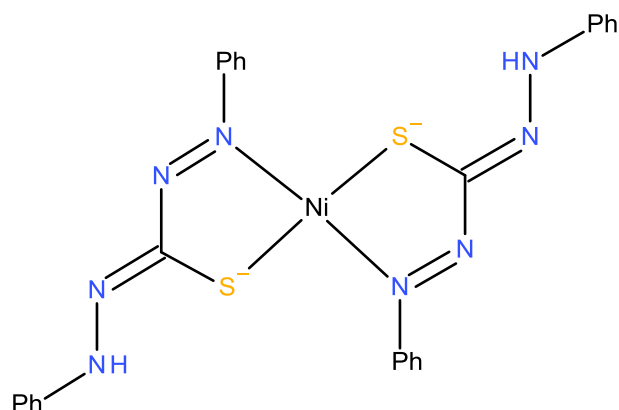


**Figure 5.12**  $[\text{Ni}(\text{DPTC})_2]$  complex reported by Laing and Sommerville

The reaction of  $\text{Zn}^{2+}$  and DPTC has been studied by two different groups, in 1970 by Math and Freiser and again in 1971 by Mawby and Irving. Both groups report that the complex consists of two bidentate dithizone molecules coordinate the tetrahedral  $\text{Zn}^{2+}$  metal ions via the N-donor and S-donor atoms. The shorter bond lengths for the  $\text{N}=\text{N}$  double bond

and the presence of hydrogen atoms on two N-H molecules confirm that DPTC is in the monoanionic form and is coordinating via the azo N-donor and the sulphur atom.<sup>179, 181</sup>

A crystal structure involving  $\text{Hg}^{2+}$  and DPTC was reported by Hutton and co-workers. A mercury dithiozonate complex was reported previously in 1958 by Harding, the complex containing two DPTC ligands is coordinating through the two sulphur atoms, and weak coordination of the terminal azo group is also present. Unfortunately full refinement was not successful due to the presence of pyridine solvent molecules.<sup>182</sup> Reaction of DPTC with either phenylmercury or methylmercury results in a similar structure containing one  $\text{Hg}^{2+}$  ion and one DPTC ligand. The three coordinate  $\text{Hg}^{2+}$ , has approximately T shaped geometry is also coordinated by the organic phenyl or methyl group from the preparation (figure 5.13). They also note that hydrogen bonding is present between the NH group and the sulphur atom.<sup>183-185</sup>

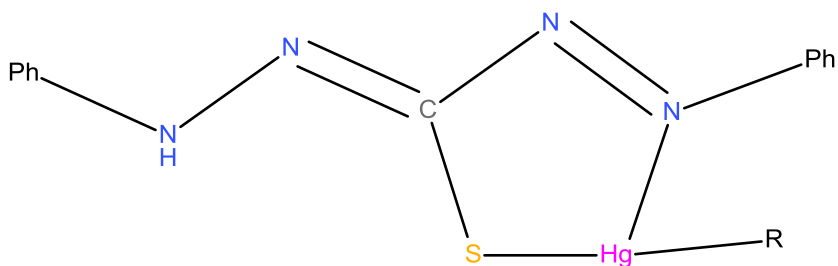


**Figure 5.13** The three coordinate  $\text{Hg}^{2+}$  DPTC complex. R = methyl or phenyl

A report published in 1982 by Niven and co-workers on a complex with  $\text{Bi}^{3+}$  and DPTC gives a triple stranded complex. This was achieved by liquid-liquid extraction from an acidic aqueous phase, where the organic chloroform layer was evaporated to give bronze crystals suitable for X-ray analysis. The coordination about the  $\text{Bi}^{3+}$  metal ion is described as distorted octahedral, arising from the coordination of three DPTC ligands in a facial arrangement. Each DPTC ligand coordinates via the S-donor and N-donor atoms, the shorter N=N double bond lengths confirm that the terminal azo nitrogen group is involved in the coordination with the metal ion (figure 5.14). Niven and co-workers state that intramolecular hydrogen bonding is definitely present in this structure, between the lone pair on the sulphur atom and the hydrogen atom on the amide.<sup>186</sup>

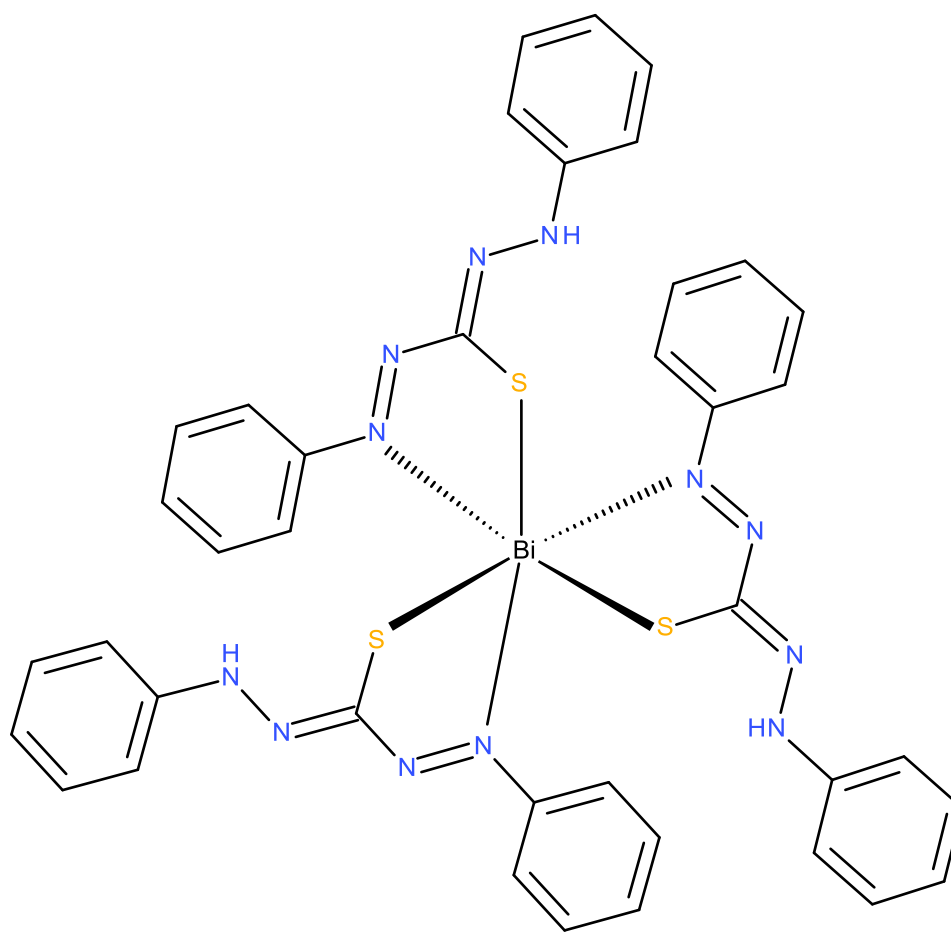


**Figure 5.14** The triple stranded [Bi(DPTC)<sub>3</sub>] complex reported by Niven and co-workers

Another triple stranded structure was published in 1983 involving  $\text{In}^{3+}$  and DPTC, which contrasts to the previous reports published on DPTC complexes. The five coordinate  $\text{In}^{3+}$  metal ion occupies trigonal bipyramidal geometry arising from the coordination of three DPTC ligands, but in two different modes. Two of the ligands are coordinating in the common bidentate chelating way via the S-donor and N-donor atoms, while the third is unidentate and coordinates via the S-donor atom only (figure 5.15). The two bidentate ligands are coordinating in the axial and equatorial positions whereas the unidentate ligand is coordinating equatorially. The presence of a five-coordinate  $\text{In}^{3+}$  ion environment suggests that steric crowding about the metal ion, due to the presence of the bulky phenyl substituents. Although the data is not sufficiently refined to enable location of one of the key hydrogen atoms Harrowfield and co-workers suggest that all three ligands are in the usual monoanionic form.<sup>187</sup>

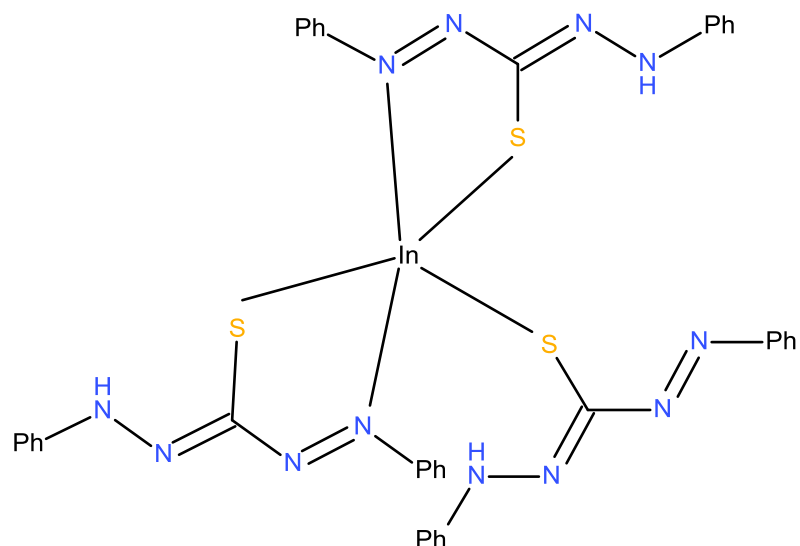


**Figure 5.15** The triple stranded  $\text{In}^{3+}$  DPTC complex. Phenyl units omitted for clarity

In 2003 Seamans and co-workers reported a DPTC ruthenium complex, the  $\text{Ru}^{2+}$  centre shows the typical characteristics of a *cis*- $\text{Ru}(\text{bipy})_2$  complex. In the  $[\text{Ru}(\text{DPTC})_2(\text{bipy})_2]$  complex the DPTC ligands are acting as a monodentate donor, coordinating through the negatively charged sulphur atoms of two different ligands, the coordination geometry is completed by the N-donor atoms from two bipyridine units (figure 5.16).<sup>188</sup>

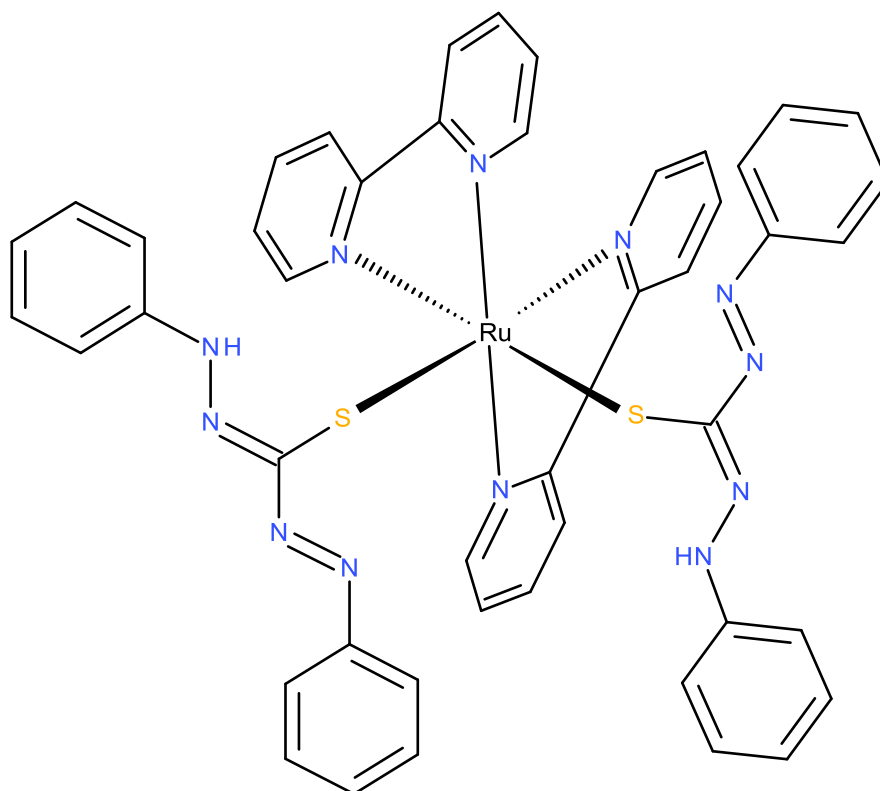


**Figure 5.16**  $[\text{Ru}(\text{DPTC})_2(\text{bipy})_2]$  complex reported by Seamans and co-workers

In 2009 Delgado and co-workers reported the X-ray crystal structure of a tin complex with dithizone which was characterised by single crystal X-ray diffraction, theoretical calculations, UV-Vis and IR spectroscopy. Dark red crystals were formed when DPTC was reacted with dimethyltin(IV) dichloride to form  $[\text{Sn}(\text{DPTC})(\text{CH}_3)_2\text{Cl}]$ . The analysis of these crystals showed a five-coordinated tin complex in distorted trigonal bipyramidal geometry. The coordination geometry is completed by the coordination of two methyl groups and one chloride ion. The equatorial plane is occupied by the S-donor atom and the two methyl groups with a nitrogen and chlorine atom in apical positions (figure 5.17). Theoretical calculations were also completed to establish the most stable structure of the complex, it was concluded that according to the values of total energy obtained for the three isomers that the structure highlighted in figure 5.15 is the most stable. The UV-Vis absorption spectra of the complex and the related dithizone ligand are shown, a shift in the HOMO/LUMO band for the complex is a clear indication of coordination of the DPTC ligand. The IR studies completed on the complex showed several significant changes to the bands corresponding to the ligand. The changes appear to occur on complexation which suggests that coordination is through the azo nitrogen and sulphur of the thiol form of DPTC. Originally bands were seen at  $3437\text{ cm}^{-1}$ ,  $1440\text{ cm}^{-1}$  and  $1064\text{ cm}^{-1}$  corresponding to  $\nu(\text{N-H})$ ,  $\nu(\text{N=N})$  and  $\nu(\text{C=S})$  respectively. After complexation, the  $\nu(\text{C=S})$  band was

absent and new bands at  $1637\text{ cm}^{-1}$ ,  $686\text{ cm}^{-1}$  and  $425\text{ cm}^{-1}$  were seen corresponding to  $\nu(\text{C}=\text{N})$ ,  $\nu(\text{C}-\text{S})$  and  $\nu(\text{Sn}\leftarrow\text{N})$  respectively. This shows how the reaction of DPTC with metal ions can change the bonding of the ligand structure.<sup>189</sup>

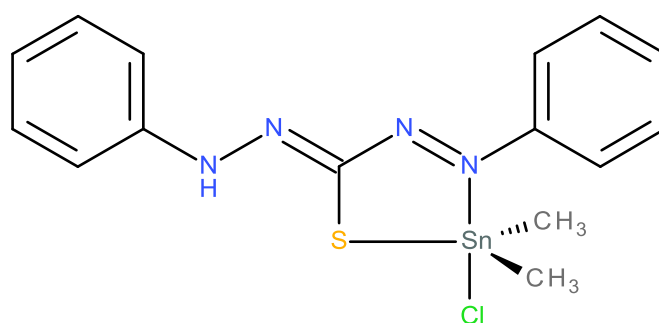


**Figure 5.17** The  $[\text{Sn}(\text{DPTC})(\text{CH}_3)_2\text{Cl}]$  complex formed upon reaction of tin with DPTC

DPTC is known to undergo single and double deprotonation but the most well-known complexes are those formed with the monoanion, normally referred to as a dithizonate ion (figure 5.11). As the dithizonate ion can exist in tautomeric forms, the complexes can take many different forms due to linkage isomerisation (figure 5.18). To resolve the issue of which form complexes take crystallographic studies have been undertaken, studies suggest that the form which is most preferred that shown in figure 5.11.

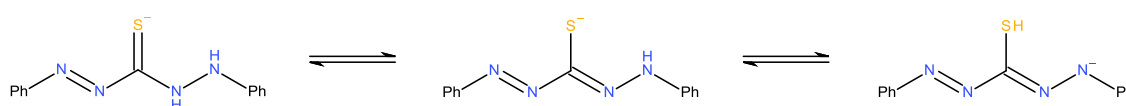


**Figure 5.18** Isomeric forms of DPTC

DPTC is known to undergo full oxidation and intramolecular cyclisation to form the nitrogen containing heterocycle 2,3-diphenyltetrazolium-5-thiolate (DPTZ), and this can also be reduced back to DPTC as described by VonEschwege and Swarts.<sup>190</sup> DPTZ has not been extensively studied as a ligand; in general tetrazoles can coordinate to metal centres through the 1 or 4 nitrogen<sup>191, 192</sup>, through the 2 or 3 nitrogen<sup>193, 194</sup> or through two nitrogens acting as a bridging ligand<sup>195, 196</sup>. DPTZ can also coordinate through the sulphur atom, which will be discussed.

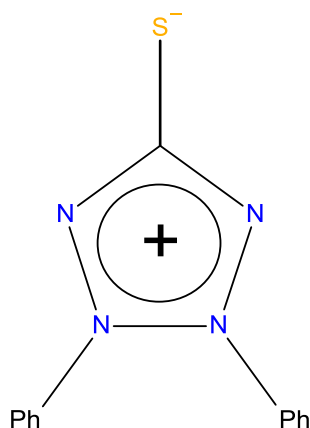


**Figure 5.19** 2,3-diphenyltetrazolium-5-thiolate (DPTZ)

An  $\text{Hg}^{2+}$  complex with DPTZ was reported in 1973 by Kozarek and Fernado, the X-ray crystal data shows a structure which contained two  $\text{Hg}^{2+}$  ions, two DPTZ ligands and four chloride anions. Each  $\text{Hg}^{2+}$  is coordinated by the S-donor atom from the DPTZ and two chloride anions to give a distorted tetrahedral geometry.<sup>197</sup> Oxidation of DPTC with potassium hexacyanoferrate followed by recrystallisation from ethanol resulted in pure DPTZ, synthesised by Fabretti. Reaction with  $\text{Co}^{2+}$  resulted complexes of several stoichiometries.  $[\text{Co}(\text{DPTZ})_2\text{X}_2]$  ( $\text{X} = \text{Cl}^-$  or  $\text{Br}^-$ ),  $[\text{Co}(\text{DPTZ})_3\text{X}_2]$  ( $\text{X} = \text{Br}^-$  or  $\text{I}^-$ ) and  $[\text{Co}(\text{DPTZ})_4\text{X}_2]$  ( $\text{X} = \text{Br}^-$ ,  $\text{I}^-$ ,  $\text{ClO}_4^-$  or  $\text{BF}_4^-$ ) formed depending on the anions and the preparation conditions. The magnetic moments lie in the range expected for tetrahedral  $\text{Co}^{2+}$  (4.3-4.8 B.M). IR studies of the complex and the DPTZ ligand confirm the presence of sulphur coordination to the metal ion.<sup>198</sup> Fabretti furthered the work in 1977 with the addition of  $\text{Ni}^{2+}$  and  $\text{Co}^{2+}$  complexes with DPTZ, metal-ligand clusters similar to the previous  $\text{Co}^{2+}$  example are observed.<sup>199</sup> Coordination of DPTZ to  $\text{Ru}^{2+}$  complex resulted in the formation of  $[\text{Ru}(\text{DPTZ})(\text{terpy})(\text{bipy})]^{2+}$  structure, confirmed by single crystal X-ray diffraction. The six-coordinate  $\text{Ru}^{2+}$  metal centre is coordinated by the S-donor atom from the DPTZ ligand, three N-donor atoms from the terpyridine and two N-donor atoms from a bipyridine unit.<sup>200</sup> The tetrazolium ring is essentially planar with the phenyl substituents lying close to the plane, as in the structure reported by Kushi in 1965.<sup>201</sup>

DPTC reacts with transition metal ions to produce highly coloured solutions, making it the most widely used organic reagent for the quick, accurate and easy determination of the concentration of metal ions.<sup>202-205</sup> First reported in 1878 by Fischer, it is still in use today for the indispensable analysis of trace metal systems. A recent report commented on spectrophotometric detection limits of the DPTC system, the analysis of lead in plant materials was achieved down to 12 parts per billion.<sup>206</sup> DPTC is an essential medical tool, Vallee and Gibson reported a procedure for determining small quantities of zinc in blood

and tissue samples.<sup>207</sup> DPTC is a selective stain for pancreatic islets which facilitates their identification and is also of special interest in human islet isolation assessment.<sup>208</sup> Hansen and co-workers reported on the use of DPTC for the selective staining of Langerhans islets and the diagnostic potential in the *in vivo* identification of viable transplanted pancreatic islets.<sup>209</sup> In 2005 Cheng and Dong reported a technique for determining trace amounts of  $Zn^{2+}$ ,  $Cd^{2+}$  and  $Cu^{2+}$  by forming metal-DPTC complexes and pre-concentrating them into an organic solvent by solvent sublation.  $Zn^{2+}$  was then determined by flame atomic absorption spectrometry; graphite furnace atomic absorption spectroscopy determined both  $Cd^{2+}$  and  $Cu^{2+}$  in real water samples. The detection limits were  $1.0 \mu\text{gL}^{-1}$ ,  $0.006 \mu\text{gL}^{-1}$  and  $0.06 \mu\text{gL}^{-1}$  for  $Zn^{2+}$ ,  $Cd^{2+}$  and  $Cu^{2+}$  respectively.<sup>210</sup> Mahmoud and co-workers reported in 2010 the removal of  $Pb^{2+}$  and other heavy metals ions from water by alumina adsorbents developed by surface-adsorbed dithizone.<sup>211</sup> Even today research into the development of DPTC continues a recent example by Leng in 2013 involving DTPC-modified gold nanoparticles which show a response to 10 different metal cations. Hexadecyltrimethyl ammonium bromide and a DPTC modified gold nanoparticle dispersion is developed for the colourimetric response of metal ions including  $Cr^{6+}$ ,  $Cr^{3+}$ ,  $Mn^{2+}$ ,  $Co^{2+}$ ,  $Ni^{2+}$ ,  $Cu^{2+}$ ,  $Zn^{2+}$ ,  $Cd^{2+}$ ,  $Hg^{2+}$  and  $Pb^{2+}$ . The colour change of the modified gold nanoparticles is instantaneous and distinct for each metal ion, resulting from electronic transitions, cation- $\pi$  interactions, formation of coordination bonds, and metal induced aggregation of gold nanoparticles.<sup>212</sup>

### 5.1.3 Aim

Described in this chapter is the coordination chemistry of DPC and dithizone DPTC; despite the wide use of both reagents the literature sources propose contradictory and non-definite explanations on the coordination chemistry, with a wide range of possible coordination modes (figure 5.20).

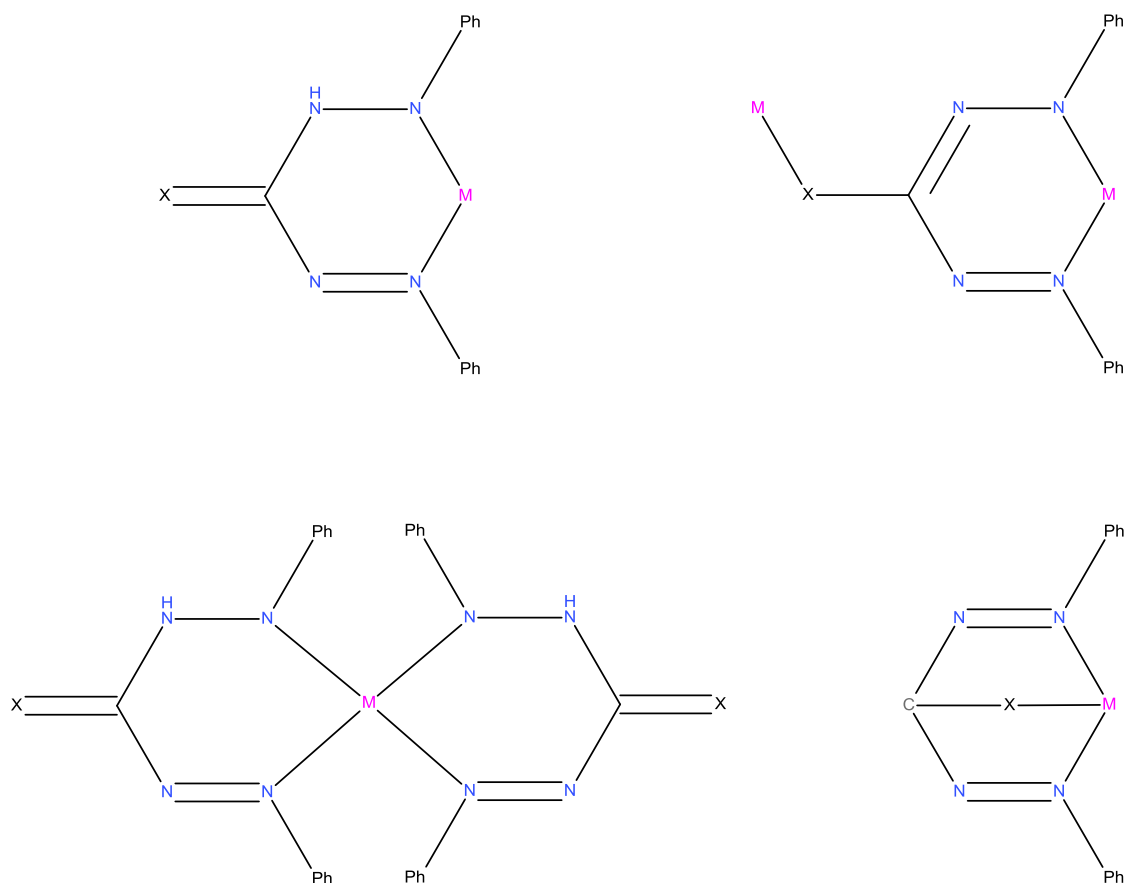


**Figure 5.20** Postulated coordination modes of DPC ( $X = O$ ) and DPTC ( $X = S$ )

Although the DPC reaction is widely used for the determination of chromium in a variety of samples and is a standard EPA method (7196A) surprisingly the nature of the complex is unknown. The literature regarding this reaction is very inconsistent and has many unexplained observations, with different studies having very different theories. Despite the length of time this reaction has been known, there is no definitive explanation of the chemistry of the magenta coloured compound in the literature. The pioneer of this reaction, Cazeneuve, first proposed that the coloured substance is an organometallic compound. Babko and Paulii postulate that it is merely an oxidation product of the reagent and contains no chromium. Bose concluded that the coloured substance is a complex of  $Cr^{2+}$  and DPCO, whereas Pflaum and Howick suggest that it is the  $Cr^{3+}$  ion and DPCO that is

responsible for the coloured reaction. There is a difference in opinion as to whether the coloured compound even contains chromium, if it does the oxidation states differ and whether the compound is with DPC or its oxidation derivatives DPCO or DPCDO.

Despite the uncertainty regarding the composition of DPTC complexes it has been used for decades as a ligand in the colorimetric determination of a variety of metal ions. It often acts as a bidentate ligand, binding through the sulphur and one nitrogen atom to form a five-membered ring with metal ions to give the DPTC excellent analytical and spectroscopic applications. The pioneering work by Fischer suggested a primary keto complex and a secondary thiol complex, with DPTC reducing to DPTCO. Irving and co-workers concluded that dithizone forms metal complexes that appear to be derived from the thiol form of dithizone, forming a five-membered ring involving the metal ions. Two different theories on the structure formed between DPTC and  $Pb^{2+}$  were reported by Milkey and Laing. There are very few X-ray structural reports compiled on the complexes formed with DPTC and transition metal ions, but in most cases the ligand behaves as a bidentate chelating agent to give a five-membered ring structure. However, the structures depicted do not show the full coordination properties of the dithizonate ligand as they only refer to metals with single oxidation states and generally, low coordination numbers. The actual displacement of hydrogen from DPTC by the metal ions involved in complex formation has been experimentally demonstrated in some cases, inferred in others, but rarely has the exact number of hydrogen atoms displaced by the metal been established by precise analysis of pure solid complex. Most studies have only established the number of DPTC molecules that react with each individual metal ion. In order to fully understand the formation of metal complexes with DPTC clarification is needed on the structural properties of DPTC and its metal complexes.

## 5.2 Coordination chemistry of DPC

### 5.2.1 Complexes of DPC and cadmium (II)

The reaction of DPC with  $\text{Cd}^{2+}$  in MeCN results in a pale pink solution initially, after 30 minutes the colour changes to an intense pink solution. ESI-MS of the resulting solution confirmed the formation of a mononuclear complex with an ion observed at  $m/z = 697$  corresponding to the complex  $\{[\text{Cd}(\text{DPC})_2]\text{ClO}_4\}^+$ . Slow diffusion of diethyl ether vapour into the resulting pink solution afforded colourless crystals of X-ray quality. Single crystal X-ray diffraction studies confirmed the formation of the mononuclear species  $[\text{Cd}(\text{DPC})_2]^{2+}$  (figure 5.21).

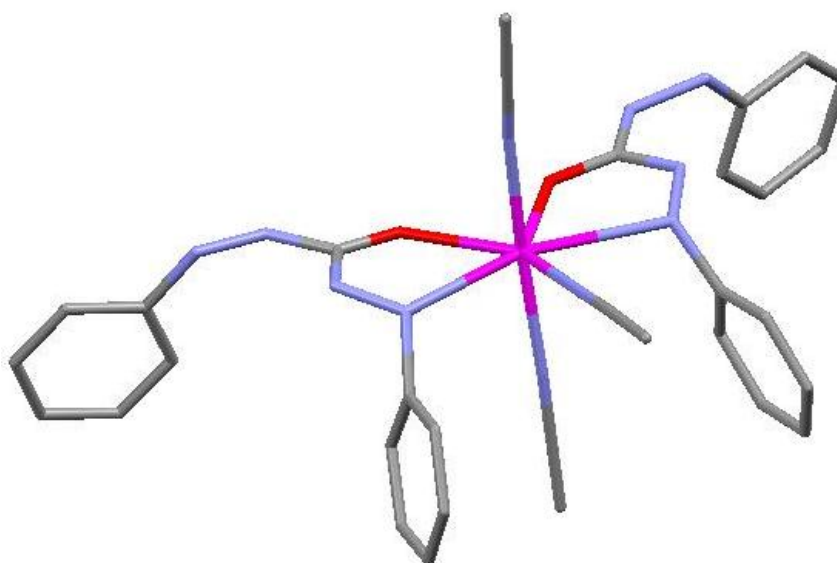


**Figure 5.21** X-ray crystal structure of  $[\text{Cd}(\text{DPC})_2]^{2+}$

The solid state structure (figure 5.21) shows that the  $\text{Cd}^{2+}$  ion is coordinated by two DPC ligands in the equatorial positions via both the phenyl nitrogen atom and the carbonyl oxygen atom. The 7-coordinate cadmium ion is further coordinated by three acetonitrile molecules (Cd-N: 2.29-2.61 Å; Cd-O: 2.30 Å). Each of the oxygen donor atoms are mutually *cis* to each other resulting in the two uncoordinated phenyl-hydrazine (Ph-NH-NH-) units adopting a *sym* geometry to each other.

| Bond       | Bond length (Å) |
|------------|-----------------|
| Cd(1)-N(1) | 2.6098 (15)     |
| Cd(1)-N(5) | 2.286(2)        |
| Cd(1)-N(6) | 2.417(2)        |
| Cd(1)-N(7) | 2.303(2)        |
| Cd(1)-O(5) | 2.3024(12)      |

**Table 5.3** Selected bond lengths (Å) for the complex [Cd(DPC)<sub>2</sub>]<sup>2+</sup>

| Bond            | Bond angle (°) | Bond            | Bond angle (°) |
|-----------------|----------------|-----------------|----------------|
| N(1)-Cd(1)-N(1) | 149.83(6)      | N(6)-Cd(1)-N(5) | 92.11(7)       |
| N(1)Cd(1)-O(5)  | 67.15(4)       | N(6)-Cd(1)-O(5) | 141.24(3)      |
| N(1)Cd(1)-O(5)  | 142.96(4)      | N(7)-Cd(1)-N(1) | 88.95(4)       |
| N(5)-Cd(1)-N(1) | 89.14(3)       | N(7)-Cd(1)-N(5) | 172.68(8)      |
| N(5)-Cd(1)-O(5) | 95.23(5)       | N(7)-Cd(1)-N(6) | 80.57(8)       |
| N(5)-Cd(1)-O(1) | 95.24(6)       | N(7)-Cd(1)-O(5) | 90.54(6)       |
| N(6)-Cd(1)-N(1) | 74.98(3)       | O(5)-Cd(1)-O(5) | 75.82(6)       |

**Table 5.4** Selected bond angles (°) for the complex [Cd(DPC)<sub>2</sub>]<sup>2+</sup>

### 5.2.2 Complexes of DPC and copper (II)

The reaction of DPC with an equimolar amount of  $\text{Cu}^{2+}$  in acetone results in a colourless solution, which after two hours changes to an intense violet colour. ESI-MS analysis of the crystalline material does not give a molecular ion for the trinuclear species, however it does show ions present at  $m/z$  876, 1614 and 1835 corresponding to  $\{[\text{Cu}(\text{DPTO})_3(\text{ClO}_4)]\}^+$ ,  $\{[\text{Cu}_2(\text{DPTO})_5(\text{ClO}_4)_3]\}^+$  and  $\{[\text{Cu}_3(\text{DPTO})_6(\text{ClO}_4)_3]\}^+$ . Furthermore, all these species show the correct isotope pattern for the fully oxidised and cyclised ligand DPTO ( $\text{C}_{13}\text{H}_{10}\text{N}_4\text{O}$ ). Slow diffusion of diethyl ether into the resulting solution afforded colourless crystals of X-ray quality. Single crystal X-ray crystallographic analysis showed a cluster of three copper ions  $[\text{Cu}_3\text{OH}(\text{OH}_2)_3(\text{DPTO})_6]^{5+}$  (figure 5.22).

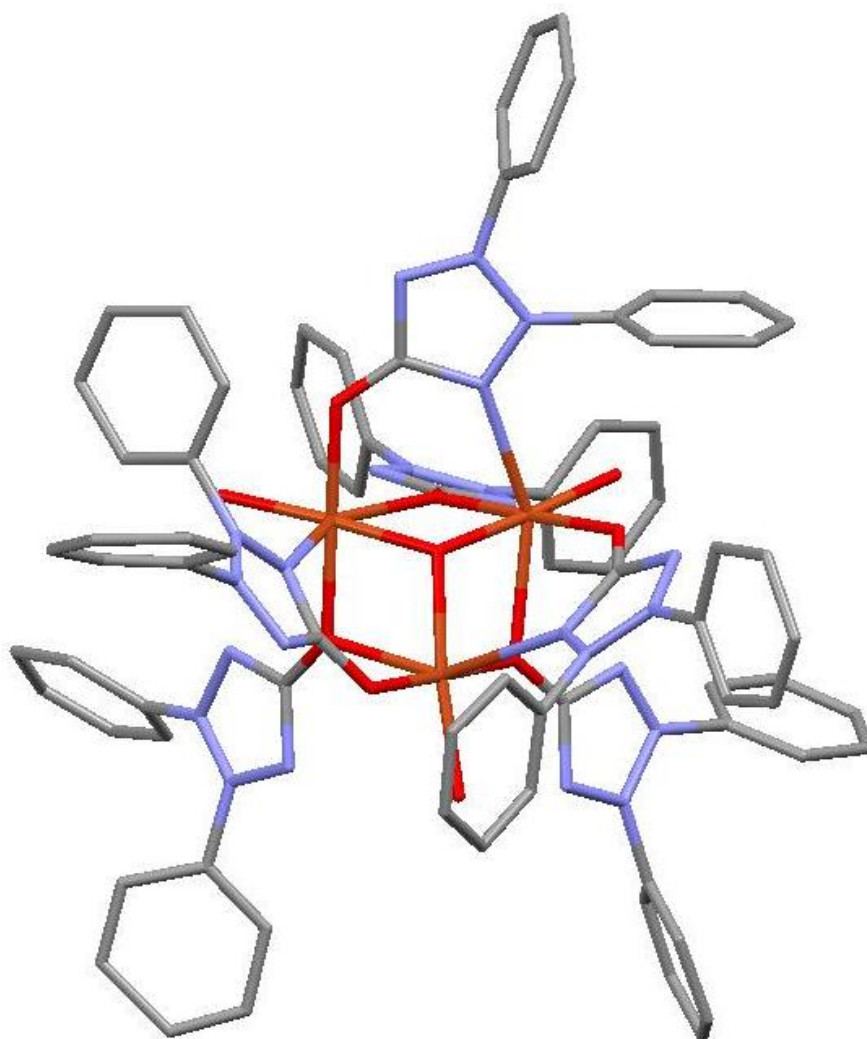


**Figure 5.22** X-ray crystal structure of  $[\text{Cu}_3\text{OH}(\text{OH}_2)_3(\text{DPTO})_6]^{5+}$

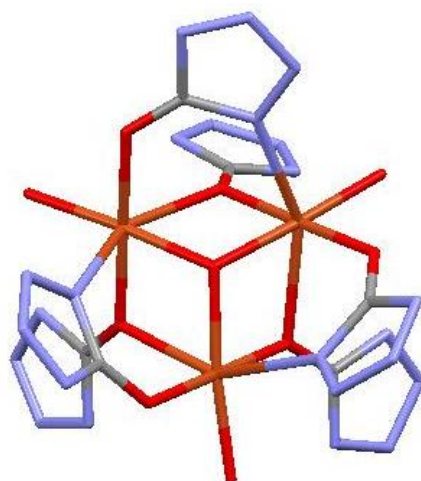


**Figure 5.23** The cluster formed in the  $[\text{Cu}_3\text{OH}(\text{OH}_2)_3(\text{DPTO})_6]^{5+}$  complex, phenyl groups omitted for clarity

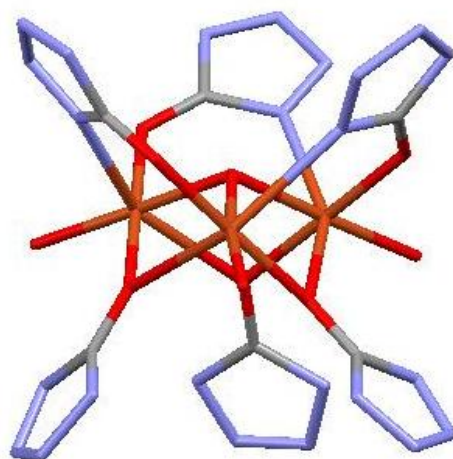


**Figure 5.24** The different binding modes present in the  $[\text{Cu}_3\text{OH}(\text{OH}_2)_3(\text{DPTO})_6]^{5+}$  complex

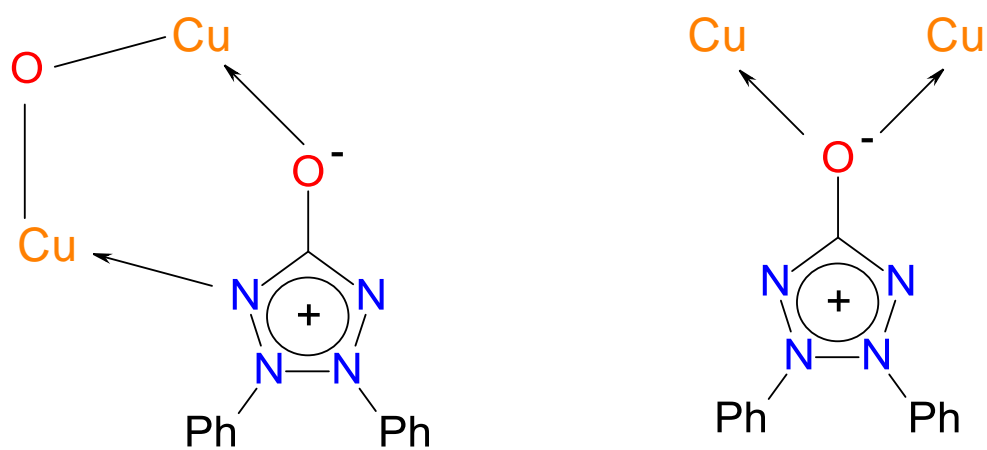


**Figure 5.25** Schematic diagram of the different binding modes present in the  $[\text{Cu}_3\text{OH}(\text{OH}_2)_3(\text{DPTO})_6]^{5+}$  complex

In the crystal structure there is a cluster of three copper ions, each of the  $\text{Cu}^{2+}$  ions is 6-coordinate formed from coordination to a central hydroxide ion (Cu-O: 1.97-1.98 Å) as well as a molecule of water (Cu-O: 1.95 Å) (figure 5.23). The remaining four donor atoms arise from the DPC ligand which has undergone oxidative intramolecular cyclisation to form the nitrogen containing heterocycle 2,3-diphenyltetrazolium-5-olate (DPTO). This heterocycle binds the  $\text{Cu}^+$  ions in two modes. On the upper rim of the cluster the DPTO coordinates via only the oxygen carbonyl which bridges two  $\text{Cu}^{2+}$  centres (Cu-O: 1.96-2.38 Å). In the lower rim DPTO coordinates one copper ion via the carbonyl donor and an adjacent metal ion via the amide nitrogen atom (Cu-N: 2.39-2.48 Å; Cu-O: 1.93-1.95 Å) (figure 5.25).

| Bond        | Bond length (Å) | Bond        | Bond length (Å) |
|-------------|-----------------|-------------|-----------------|
| Cu(1)-O(1)  | 1.970(4)        | Cu(2)-O(10) | 1.945(5)        |
| Cu(1)-O(3)  | 1.964(5)        | Cu(2)-O(11) | 1.945(5)        |
| Cu(1)-O(4)  | 2.380(5)        | Cu(2)-N(13) | 2.388(7)        |
| Cu(1)-O(5)  | 1.947(5)        | Cu(3)-O(1)  | 1.985(5)        |
| Cu(1)-O(6)  | 1.948(5)        | Cu(3)-O(2)  | 1.953(5)        |
| Cu(1)-N(21) | 2.479(6)        | Cu(3)-O(3)  | 2.319(5)        |
| Cu(2)-O(1)  | 1.980(5)        | Cu(3)-O(8)  | 1.931(5)        |
| Cu(2)-O(2)  | 2.323(5)        | Cu(3)-O(9)  | 1.946(5)        |
| Cu(2)-O(4)  | 1.993(4)        | Cu(3)-N(1)  | 2.389(7)        |

**Table 5.5** Selected bond lengths (Å) for the complex  $[\text{Cu}_3\text{OH}(\text{OH}_2)_3(\text{DPTO})_6]^{5+}$

| Bond             | Bond angle (°) | Bond              | Bond angle (°) |
|------------------|----------------|-------------------|----------------|
| O(1)-Cu(1)-O(4)  | 74.67(17)      | O(10)-Cu(2)-O(2)  | 91.8(2)        |
| O(1)-Cu(1)-N(21) | 77.40(19)      | O(10)-Cu(2)-O(4)  | 178.6(2)       |
| O(3)-Cu(1)-O(1)  | 82.59(19)      | O(10)-Cu(2)-O(11) | 84.4(2)        |
| O(3)-Cu(1)-O(4)  | 91.11(18)      | O(10)-Cu(2)-N(13) | 95.0(2)        |
| O(3)-Cu(1)-N(21) | 82.7(2)        | O(11)-Cu(2)-O(1)  | 177.3(2)       |
| O(4)-Cu(1)-N(21) | 151.95(18)     | O(11)-Cu(2)-O(2)  | 109.1(2)       |
| O(5)-Cu(1)-O(1)  | 95.3(2)        | O(11)-Cu(2)-O(4)  | 95.49(19)      |
| O(5)-Cu(1)-O(3)  | 176.8(2)       | O(11)-Cu(2)-N(13) | 98.6(2)        |
| O(5)-Cu(1)-O(4)  | 90.61(19)      | O(1)-Cu(3)-O(3)   | 73.73(17)      |
| O(5)-Cu(1)-O(6)  | 87.3(2)        | O(1)-Cu(3)-N(1)   | 76.26(2)       |
| O(5)-Cu(1)-N(21) | 94.5(2)        | O(2)-Cu(3)-O(1)   | 82.36(19)      |
| O(6)-Cu(1)-O(1)  | 175.3(2)       | O(2)-Cu(3)-O(3)   | 89.68(19)      |
| O(6)-Cu(1)-O(3)  | 94.7(2)        | O(2)-Cu(3)-N(1)   | 99.25(18)      |
| O(6)-Cu(1)-O(4)  | 109.4(2)       | O(8)-Cu(3)-O(1)   | 96.0(2)        |
| O(1)-Cu(2)-O(2)  | 73.61(18)      | O(8)-Cu(3)-O(2)   | 177.6(2)       |
| O(1)-Cu(2)-O(4)  | 83.97(18)      | O(8)-Cu(3)-O(3)   | 91.54(19)      |
| O(1)-Cu(2)-N(13) | 78.7(2)        | O(8)-Cu(3)-O(9)   | 89.1(2)        |
| O(2)-Cu(2)-N(13) | 152.0(2)       | O(8)-Cu(3)-N(1)   | 90.80(13)      |
| O(4)-Cu(2)-O(2)  | 89.55(18)      | O(9)-Cu(3)-O(1)   | 173.3(2)       |
| O(4)-Cu(2)-N(13) | 83.6(2)        | O(9)-Cu(3)-O(2)   | 92.5(2)        |
| O(10)-Cu(2)-O(1) | 96.04(19)      | O(9)-Cu(3)-O(3)   | 110.7(2)       |

**Table 5.6** Selected bond angles (°) for the complex  $[\text{Cu}_3\text{OH}(\text{OH}_2)_3(\text{DPTO})_6]^{5+}$

### 5.2.3 Complexes of DPC with chromium (III) and vanadium (III)

Reaction of DPC with either  $\text{Cr}^{3+}$  or  $\text{V}^{3+}$  results in an intense violet or magenta coloured solution, respectively. From which colourless crystalline material was produced upon slow diffusion of diethyl ether. Although with both of these metal ions no crystals of their complexes was obtained. However, crystalline material corresponding to the 2,3-diphenyltetrazolium-5-olate (DPTO) species was confirmed by single crystal X-ray diffraction (figure 5.26). The solid-state analysis shows that DPC has undergone oxidative intramolecular cyclisation to form the nitrogen containing heterocycle 2,3-diphenyltetrazolium-5-olate (DPTO).

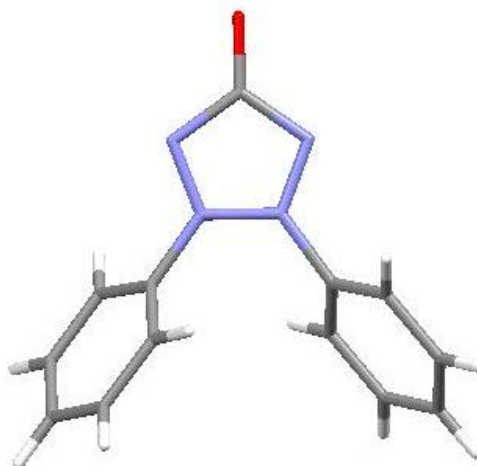


**Figure 5.26** X-ray crystal structure of 2,3-diphenyltetrazolium-5-olate (DPTO)

| Bond       | Bond length (Å) | Bond        | Bond length (Å) |
|------------|-----------------|-------------|-----------------|
| C(1)-C(2)  | 1.385(3)        | C(10)-C(11) | 1.389(3)        |
| C(1)-C(6)  | 1.379(3)        | C(11)-C(12) | 1.393(2)        |
| C(2)-C(3)  | 1.392(2)        | N(1)-N(2)   | 1.3136(19)      |
| C(3)-C(4)  | 1.381(3)        | N(1)-C(13)  | 1.392(2)        |
| C(4)-C(5)  | 1.387(3)        | N(2)-C(1)   | 1.444(2)        |
| C(5)-C(6)  | 1.397(2)        | N(2)-N(3)   | 1.3333(17)      |
| C(7)-C(8)  | 1.385(3)        | N(3)-C(7)   | 1.438(2)        |
| C(7)-C(12) | 1.386(3)        | N(3)-N(4)   | 1.3186(18)      |
| C(8)-C(9)  | 1.395(2)        | N(4)-C(13)  | 1.388(2)        |
| C(9)-C(10) | 1.385(3)        | O(1)-C(13)  | 1.244(2)        |

**Table 5.7** Selected bond lengths (Å) for 2,3-diphenyltetrazolium-5-olate (DPTO)

| Bond            | Bond angle (°) | Bond              | Bond angle (°) |
|-----------------|----------------|-------------------|----------------|
| N(4)-Cd(1)-N(4) | 149.70(6)      | N(7)-Cd(1)-N(6)   | 80.57(8)       |
| C(1)-C(2)-C(3)  | 117.73(18)     | C(10)-C(11)-C(12) | 120.18(18)     |
| C(1)-C(6)-C(5)  | 117.94(17)     | C(12)-C(7)-N(3)   | 117.56(16)     |
| C(2)-C(1)-N(2)  | 117.26(15)     | N(1)-N(2)-C(1)    | 123.20(13)     |
| C(3)-C(4)-C(5)  | 120.40(17)     | N(1)-N(2)-N(3)    | 110.94(13)     |
| C(4)-C(3)-C(2)  | 120.62(18)     | N(2)-N(1)-C(13)   | 104.33(13)     |
| C(4)-C(5)-C(6)  | 120.14(17)     | N(2)-N(3)-C(7)    | 125.85(13)     |
| C(6)-C(1)-C(2)  | 123.15(16)     | N(3)-N(2)-C(1)    | 125.75(13)     |
| C(6)-C(1)-N(2)  | 119.55(16)     | N(3)-N(4)-C(13)   | 104.27(13)     |

|                  |            |                 |            |
|------------------|------------|-----------------|------------|
| C(7)-C(8)-C(9)   | 117.69(17) | N(4)-C(13)-N(1) | 109.60(14) |
| C(7)-C(12)-C(11) | 117.93(18) | N(4)-N(3)-C(7)  | 123.29(12) |
| C(8)-C(7)-C(12)  | 123.17(16) | N(4)-N(3)-N(2)  | 110.85(13) |
| C(8)-C(7)-N(3)   | 119.11(16) | O(1)-C(13)-N(1) | 124.74(15) |
| C(10)-C(9)-C(8)  | 120.48(18) | O(1)-C(13)-N(4) | 125.65(15) |
| C(9)-C(10)-C(11) | 120.53(17) |                 |            |

**Table 5.8** Selected bond angles (°) for 2,3-diphenyltetrazolium-5-olate (DPTO)

## 5.3 Coordination chemistry of DPTC

### 5.3.1 Complexes of DPTC and mercury (II)

Reaction of DPTC with half an equivalent of  $\text{Hg}^{2+}$  yielded a dark red solution, from which colourless crystalline material was produced after slow concentration of the acetonitrile solvent. ESI-MS indicated that a mononuclear complex had formed with a peak at  $m/z = 713$  corresponding to  $\{[\text{Hg}(\text{DPTC})(\text{DPTC-H})]\}^+$ . The single crystal X-ray structure confirmed the presence of the mononuclear species  $[\text{Hg}(\text{DPTC})_2]$  (figure 5.27).

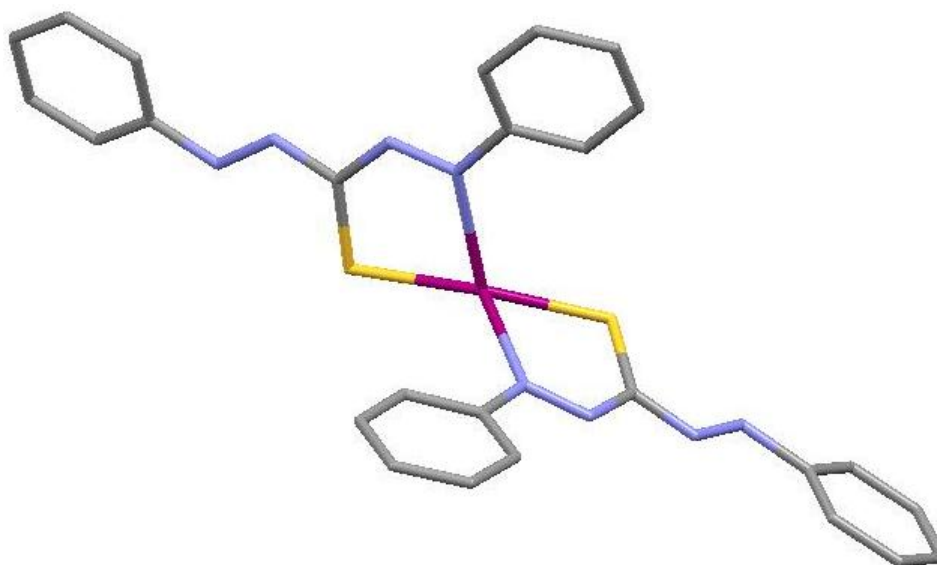


**Figure 5.27** X-ray crystal structure of  $[\text{Hg}(\text{DPTC})_2]$

Solid state analysis shows that the mercury ion is coordinated by two DPTC ligands, with the  $\text{Hg}^{2+}$  adopting a four-coordination distorted tetrahedral geometry. Each ligand acts as a bis-bidentate donor coordinating via the N-donor and the S-donor atoms (Hg-N: 2.53 Å; Hg-S: 2.37 Å). Each of the ligands has deprotonated and acts as an anionic species.

| Bond       | Bond length (Å) |
|------------|-----------------|
| Hg(1)-N(4) | 2.526(4)        |
| Hg(1)-N(4) | 2.526(4)        |
| Hg(1)-S(1) | 2.3685(11)      |
| Hg(1)-S(1) | 2.3685(11)      |

**Table 5.9** Selected bond lengths (Å) for  $[\text{Hg}(\text{DPTC})_2]$

| Bond            | Bond angle (°) | Bond            | Bond angle (°) |
|-----------------|----------------|-----------------|----------------|
| C(2)-N(4)-Hg(1) | 129.5(3)       | S(1)-Hg(1)-N(4) | 118.75(9)      |
| N(3)-N(4)-Hg(1) | 116.5(3)       | S(1)-Hg(1)-N(4) | 118.75(9)      |
| N(4)-Hg(1)-N(4) | 101.05(18)     | S(1)-Hg(1)-S(1) | 156.78(6)      |
| S(1)-Hg(1)-N(4) | 76.99(9)       | C(1)-Hg(1)-S(1) | 100.84(15)     |
| S(1)-Hg(1)-N(4) | 76.99(9)       |                 |                |

**Table 5.10** Selected bond angles (°) for [Hg(DPTC)<sub>2</sub>]

### 5.3.2 Complexes of DPTC with mercury (II) and silver (I)

Reaction of the [Hg(DPTC)<sub>2</sub>] complex with Ag<sup>+</sup> produces a red coloured solution. Analysis by ESI-MS shows ions at  $m/z = 1737$  and  $1531$  corresponding to  $\{[(DPTC)_2Hg_2]Ag_2(CIO_4)\}^+$  and  $\{[(DPTC)_2Hg_2]Ag\}^+$  respectively. Slow diffusion of diethyl ether into the resulting solution produced red crystals. Analysis by single crystal X-ray diffraction confirmed the formation of [Hg<sub>2</sub>Ag<sub>2</sub>(DPTC)<sub>4</sub>(acetone)<sub>2</sub>(ClO<sub>4</sub>)<sub>2</sub>] (figure 5.28).

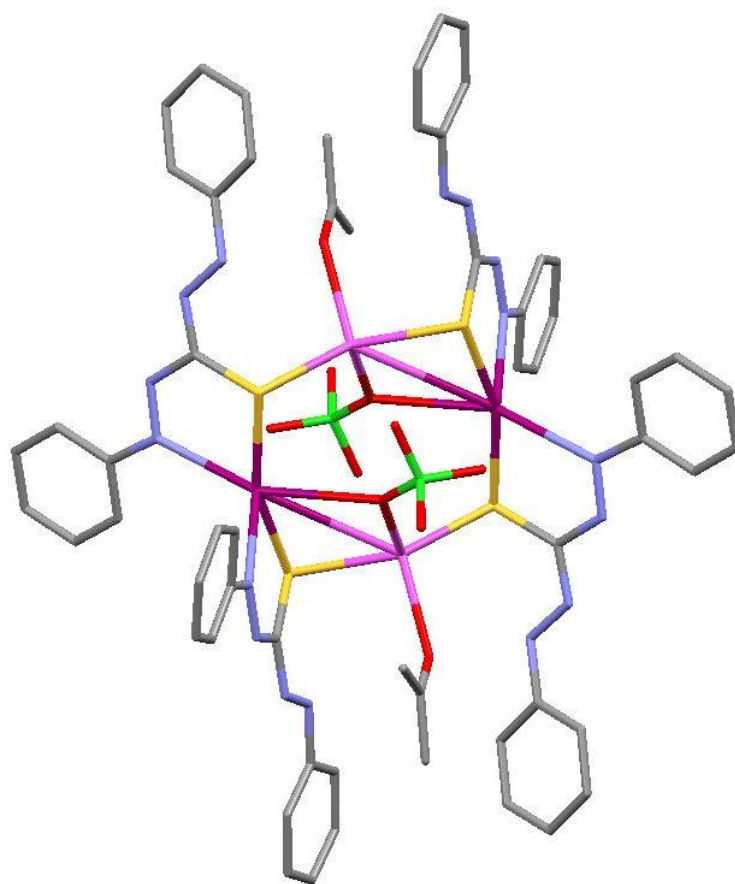


**Figure 5.28** X-ray crystal structure of [Hg<sub>2</sub>Ag<sub>2</sub>(DPTC)<sub>4</sub>(acetone)<sub>2</sub>(ClO<sub>4</sub>)<sub>2</sub>]

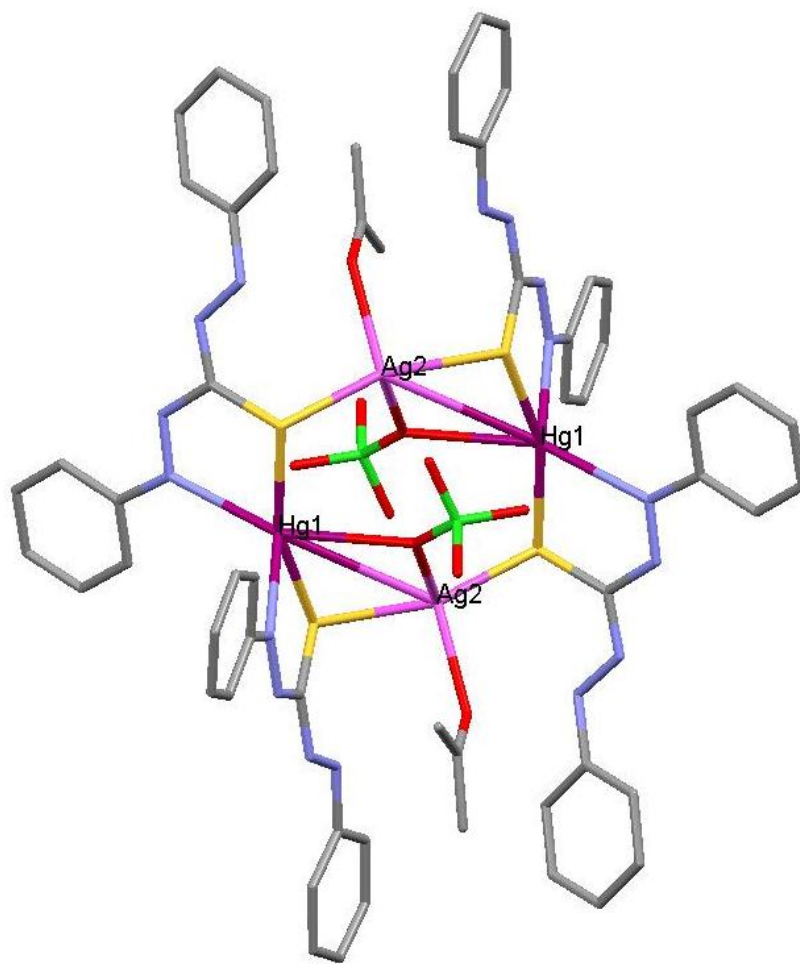


**Figure 5.29** Labelled metal ions in the X-ray crystal structure of  $[\text{Hg}_2\text{Ag}_2(\text{DPTC})_4(\text{acetone})_2(\text{ClO}_4)_2]$

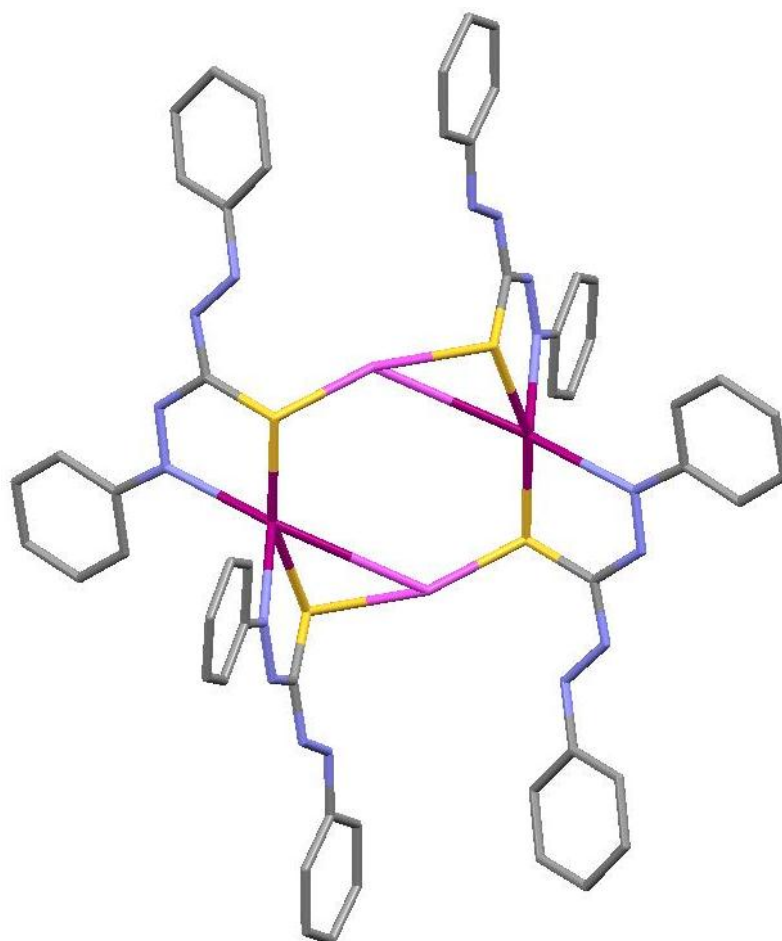


**Figure 5.30** X-ray crystal structure of  $[\text{Hg}_2\text{Ag}_2(\text{DPTC})_4(\text{acetone})_2(\text{ClO}_4)_2]$ , solvent and anions molecules omitted for clarity

In the solid state the reaction of DPTC with  $\text{Hg}^{2+}$  and  $\text{Ag}^+$  results in a complex that comprises of four ligands, two  $\text{Hg}^{2+}$  ions and two  $\text{Ag}^+$ . Each 6-coordinate  $\text{Hg}^{2+}$  ion is coordinated by the nitrogen and sulphur atoms of two different DPTC ligands (Hg:N: 2.50-2.52 Å; Hg-S: 2.42 Å), a perchlorate anion bridges both mercury (II) (Hg-O: 2.94 Å) and a silver (I) ion (Hg-Ag: 3.60 Å). Both five-coordinate  $\text{Ag}^+$  metal ions are coordinated by a bridging sulphur atom of a DPTC ligand (Ag:S: 2.48-2.51 Å), a bridging perchlorate molecule (Ag-O: 2.52 Å) and an acetone solvent molecule (Ag-O: 2.43 Å).

| Bond        | Bond length (Å) |
|-------------|-----------------|
| Ag(2)-O(1)  | 2.4272(18)      |
| Ag(2)-O(2)  | 2.518(4)        |
| Ag(2)-S(1)  | 2.4787(6)       |
| Ag(2)-S(2)  | 2.5086(6)       |
| Hg(1)-Ag(2) | 3.603(6)        |
| Hg(1)-N(1)  | 2.5156(19)      |
| Hg(1)-N(6)  | 2.4968(18)      |
| Hg(1)-O(2)  | 2.944(4)        |
| Hg(1)-S(1)  | 2.4185(5)       |
| Hg(1)-S(2)  | 2.4202(6)       |

**Table 5.11** Selected bond lengths (Å) for [Hg<sub>2</sub>Ag<sub>2</sub>(DPTC)<sub>4</sub>(acetone)<sub>2</sub>(ClO<sub>4</sub>)]

| Bond             | Bond angle (°) | Bond            | Bond angle (°) |
|------------------|----------------|-----------------|----------------|
| C(2)-N(4)-Hg(1)  | 129.5(3)       | S(1)-Hg(1)-N(4) | 118.75(9)      |
| C(7)-S(1)-Ag(2)  | 104.84(7)      | N(6)-Hg(1)-N(1) | 117.14(6)      |
| C(7)-S(1)-Hg(1)  | 101.07(7)      | O(1)-Ag(2)-O(2) | 101.2(5)       |
| C(8)-S(2)-Ag(2)  | 101.53(8)      | O(1)-Ag(2)-S(1) | 108.73(5)      |
| C(8)-S(2)-Hg(1)  | 101.15(8)      | O(1)-Ag(2)-S(2) | 97.44(5)       |
| C(9)-N(6)-Hg(1)  | 126.04(14)     | S(1)-Ag(2)-O(2) | 108.1(5)       |
| C(22)-N(1)-Hg(1) | 127.76(14)     | S(1)-Ag(2)-S(2) | 142.300(19)    |
| C(28)-O(1)-Ag(2) | 140.58(19)     | S(1)-Hg(1)-N(1) | 75.67(4)       |
| Cl(1)-O(2)-Ag(2) | 134.9(4)       | S(1)-Hg(1)-N(6) | 115.84(4)      |

|                  |            |                 |             |
|------------------|------------|-----------------|-------------|
| Hg(1)-S(1)-Ag(2) | 100.40(2)  | S(1)-Hg(1)-S(2) | 159.313(19) |
| Hg(1)-S(2)-Ag(2) | 93.92(4)   | S(2)-Hg(1)-N(1) | 115.29(5)   |
| N(2)-N(1)-Hg(1)  | 117.84(14) | S(2)-Hg(1)-N(6) | 76.04(4)    |
| N(5)-N(6)-Hg(1)  | 118.91(14) | S(2)-Ag(2)-O(2) | 92.3(3)     |

**Table 5.12** Selected bond angles (°) for [Hg<sub>2</sub>Ag<sub>2</sub>(DPTC)<sub>4</sub>(acetone)<sub>2</sub>(ClO<sub>4</sub>)<sub>2</sub>]

### 5.3.3 Complexes of DPTC with copper (II) perchlorate

The reaction of DPTC with Cu(ClO<sub>4</sub>)<sub>2</sub>·6H<sub>2</sub>O in acetone results in a dark brown coloured solution which gradually turns red over a period of 24 hours. Analysis by ESI-MS shows clusters of high nuclearity with ions {[Cu<sub>n-1</sub>(DPTC)<sub>n</sub>], [Cu<sub>n</sub>(DPTC)<sub>n</sub>] and [Cu<sub>n+1</sub>(DPTC)<sub>n</sub>] where n = 3-9 observed, including an ion at *m/z* = 2549 corresponding to [Cu<sub>8</sub>(DPTC)<sub>8</sub>]. Slow diffusion of dichloromethane into the resulting solution afforded colourless crystals of X-ray quality. Single crystal X-ray diffraction studies confirmed the formation of an octanuclear species K<sub>2</sub>[Cu<sub>8</sub>(DPTC)<sub>8</sub>(ClO<sub>4</sub>)<sub>2</sub>]<sup>2+</sup> (figure 5.31).

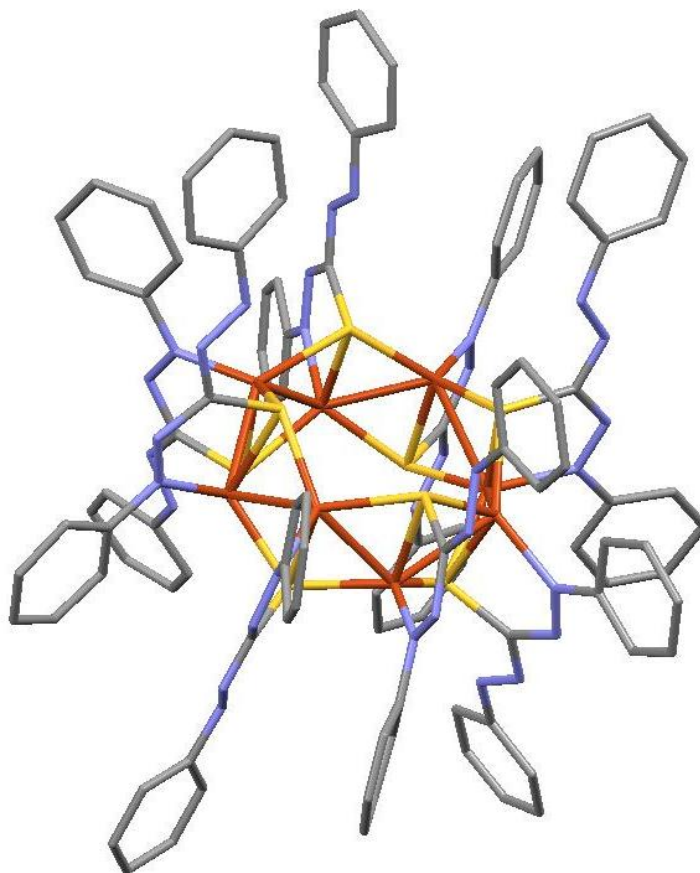


**Figure 5.31** X-ray crystal structure of K<sub>2</sub>[Cu<sub>8</sub>(DPTC)<sub>8</sub>(ClO<sub>4</sub>)<sub>2</sub>]<sup>2+</sup>

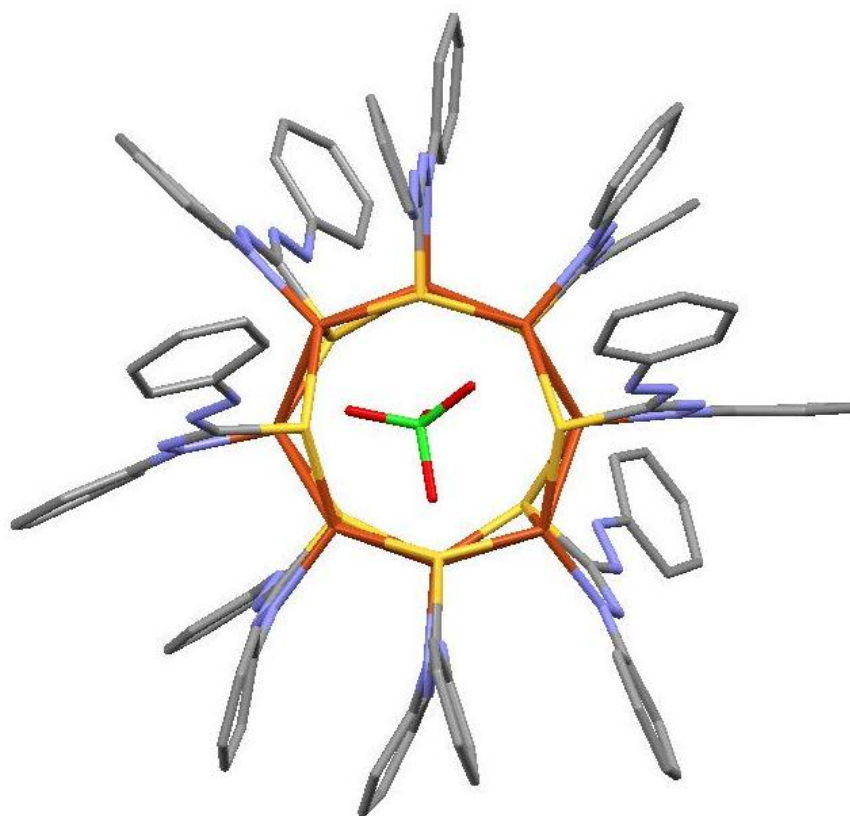


**Figure 5.32** X-ray crystal structure showing the top view of  $\text{K}_2[\text{Cu}_8(\text{DPTC})_8(\text{ClO}_4)_2]^{2+}$ , perchlorate anion in the central cavity

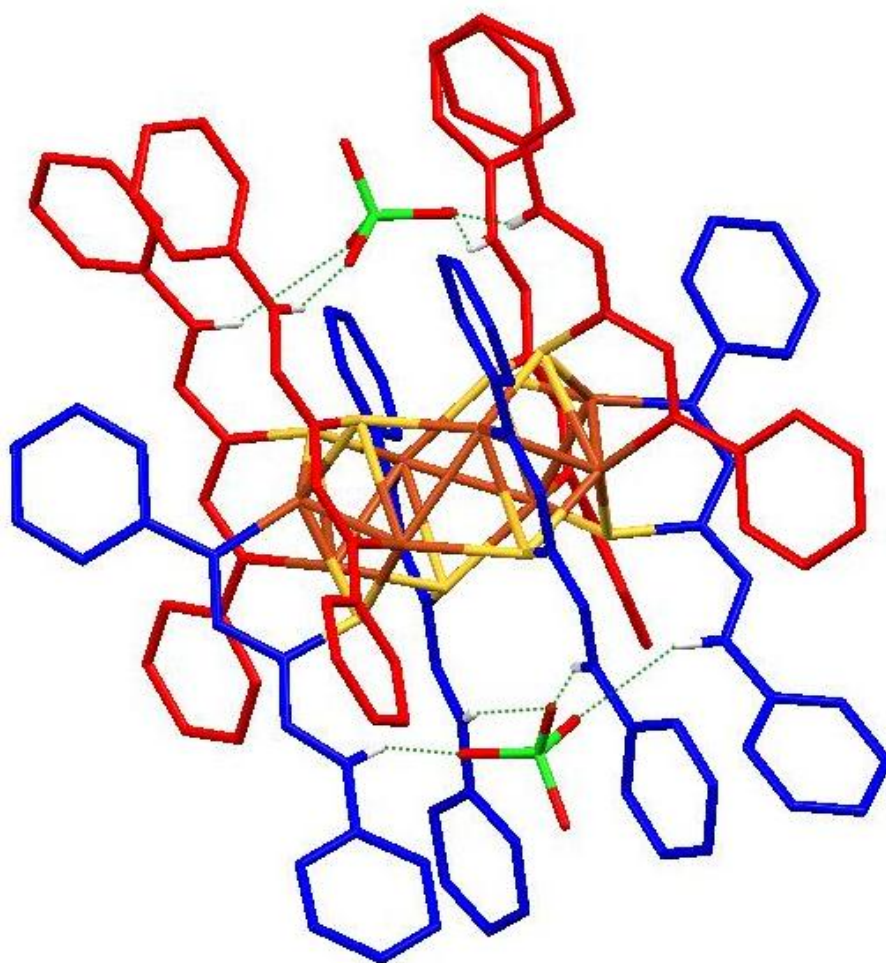


**Figure 5.33** X-ray crystal structure of  $K_2[Cu_8(DPTC)_8(ClO_4)_2]^{2+}$ , showing the perchlorate anion hydrogen bonding to the DPTC ligands

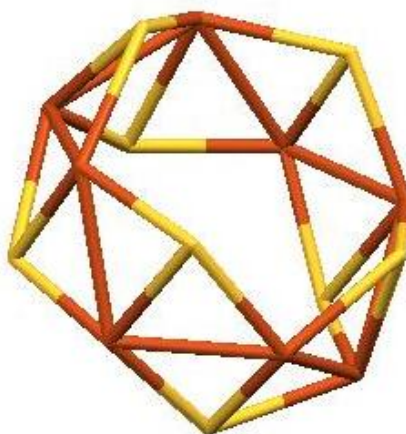


**Figure 5.34** X-ray crystal structure of the  $K_2[Cu_8(DPTC)_8(ClO_4)_2]^{2+}$  core

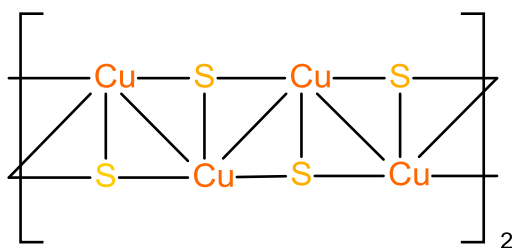


**Figure 5.35** Schematic diagram of the  $K_2[Cu_8(DPTC)_8(ClO_4)_2]^{2+}$  core

In the solid state an octanuclear species is formed by the coordination of eight copper ions with eight ligands,  $[Cu_8(DPTC)_8]$ . In this species each of the  $Cu^{2+}$  is coordinated by the sulphur and nitrogen atoms of an anionic ligand, the sulphur atom of this unit coordination two further  $[CuDPTC]$  units either side of itself, which continues in a cyclic manner giving the octanuclear  $[Cu_8(DPTC)_8]$  with a band of eight sulphur and eight copper atoms (figure 5.34) (Cu-Cu: 2.55-2.59 Å; Cu-N: 1.98-2.02 Å; Cu-S: 2.25-2.45 Å).

The uncoordinated azo-end of the ligand alternates around the ' $Cu_8$ ' core such that four -NH groups point up and the remaining four point in the opposite direction. This gives rise to a cavity containing four C=N-NHPh units, which act as a hydrogen bond donor to a perchlorate anion, which sits in both cavities (figure 5.33).

| Bond        | Bond length (Å) | Bond       | Bond length (Å) |
|-------------|-----------------|------------|-----------------|
| Cu(1)-Cu(1) | 2.5516(13)      | Cu(3)-S(1) | 2.2979(15)      |
| Cu(1)-Cu(3) | 2.5923(10)      | Cu(3)-S(2) | 2.2986(16)      |
| Cu(1)-N(10) | 1.993(5)        | Cu(3)-S(4) | 2.5054(15)      |
| Cu(1)-S(1)  | 2.445(14)       | Cu(4)-N(4) | 1.984(5)        |
| Cu(1)-S(4)  | 2.2532(15)      | Cu(4)-S(2) | 2.4170(15)      |
| Cu(2)-Cu(2) | 2.5787(14)      | Cu(4)-S(3) | 2.2843(16)      |
| Cu(2)-Cu(4) | 2.5667(10)      | Cu(4)-S(4) | 2.2626(16)      |
| Cu(2)-N(16) | 2.016(5)        | S(1)-Cu(1) | 2.4445(14)      |
| Cu(2)-S(2)  | 2.2848(16)      | S(1)-Cu(3) | 2.2980(15)      |
| Cu(2)-S(3)  | 2.424 (15)      | S(3)-Cu(2) | 2.4240(15)      |

|             |            |            |            |
|-------------|------------|------------|------------|
| Cu(3)-Cu(4) | 2.5455(10) | S(3)-Cu(4) | 2.2844(16) |
| Cu(3)-N(15) | 2.006(5)   |            |            |

**Table 5.12** Selected bond lengths (Å) for of  $K_2[Cu_8(DPTC)_8(ClO_4)_2]^{2+}$

| Bond              | Bond angle (°) | Bond                | Bond angle (°) |
|-------------------|----------------|---------------------|----------------|
| C(19)-N(16)-Cu(2) | 122.4(4)       | N(15)-Cu(3)-S(2)    | 136.53(15)     |
| C(37)-S(3)-Cu(2)  | 90.64(2)       | N(15)-Cu(3)-S(4)    | 82.73(15)      |
| C(37)-S(3)-Cu(4)  | 106.2(2)       | N(16)-Cu(2)-Cu(2)   | 99.75(15)      |
| C(38)-S(1)-Cu(1)  | 104.74(19)     | N(16)-Cu(2)-Cu(4)   | 102.42(14)     |
| C(38)-S(1)-Cu(3)  | 106.27(19)     | N(16)-Cu(2)-S(2)    | 121.51(15)     |
| C(39)-S(4)-Cu(1)  | 108.5(2)       | N(16)-Cu(2)-S(3)    | 84.43(15)      |
| C(39)-S(4)-Cu(3)  | 89.37(19)      | N(16')-Cu(2')-S(3') | 114.94(15)     |
| C(39)-S(4)-Cu(4)  | 104.3(2)       | S(1)-Cu(1)-Cu(1)    | 54.67(4)       |
| C(40)-N(15)-Cu(3) | 122.6(4)       | S(1)-Cu(1)-Cu(1)    | 60.29(4)       |
| C(52)-S(2)-Cu(2)  | 99.5(2)        | S(1)-Cu(1)-Cu(3)    | 141.87(5)      |
| C(52)-S(2)-Cu(3)  | 114.5(2)       | S(1)-Cu(1)-Cu(3)    | 54.19(4)       |
| C(52)-S(2)-Cu(4)  | 90.26(19)      | S(1)-Cu(3)-Cu(1)    | 59.63(4)       |
| Cu(1)-Cu(1)-Cu(3) | 102.34(3)      | S(1)-Cu(3)-Cu(4)    | 130.38(5)      |
| Cu(1)-S(1)-Cu(1)  | 65.04(4)       | S(1)-Cu(1)-S(1)     | 114.36(4)      |
| Cu(1)-S(1)-Cu(3)  | 121.45(6)      | S(1)-Cu(3)-S(2)     | 96.71(5)       |
| Cu(1)-S(4)-Cu(3)  | 65.77(4)       | S(1)-Cu(3)-S(4)     | 109.89(5)      |
| Cu(1)-S(4)-Cu(4)  | 118.61(6)      | S(2)-Cu(2)-Cu(2)    | 136.37(4)      |
| Cu(2)-S(2)-Cu(3)  | 119.46(6)      | S(2)-Cu(2)-Cu(4)    | 59.42(4)       |

|                   |            |                  |           |
|-------------------|------------|------------------|-----------|
| Cu(2)-S(2)-Cu(4)  | 66.10(4)   | S(2)-Cu(2)-S(3)  | 112.66(5) |
| Cu(2)-S(3)-Cu(2)  | 66.48(5)   | S(2)-Cu(3)-Cu(1) | 126.73(5) |
| Cu(2)-S(3)-Cu(4)  | 121.05(6)  | S(2)-Cu(3)-Cu(4) | 59.60(4)  |
| Cu(3)-Cu(4)-Cu(2) | 101.49(3)  | S(2)-Cu(3)-S(4)  | 109.39(5) |
| Cu(3)-S(1)-Cu(1)  | 66.18(4)   | S(2)-Cu(4)-Cu(2) | 54.47(4)  |
| Cu(3)-S(2)-Cu(4)  | 65.28(4)   | S(2)-Cu(4)-Cu(3) | 55.11(4)  |
| Cu(4)-Cu(2)-Cu(2) | 100.95(3)  | S(3)-Cu(2)-Cu(2) | 53.98(4)  |
| Cu(4)-Cu(3)-Cu(1) | 98.19(3)   | S(3)-Cu(2)-Cu(2) | 59.53(4)  |
| Cu(4)-S(3)-Cu(2)  | 65.99(4)   | S(3)-Cu(2)-Cu(4) | 54.39(4)  |
| Cu(4)-S(4)-Cu(3)  | 64.30(4)   | S(3)-Cu(2)-S(2)  | 108.45(6) |
| N(3)-N(16)-Cu(2)  | 122.4(4)   | S(3)-Cu(2)-S(3)  | 112.98(5) |
| N(4)-Cu(4)-Cu(2)  | 101.60(14) | S(3)-Cu(4)-Cu(2) | 59.62(4)  |
| N(4)-Cu(4)-Cu(3)  | 102.70(15) | S(3)-Cu(4)-Cu(3) | 135.46(5) |
| N(4)-Cu(4)-S(2)   | 85.08(14)  | S(3)-Cu(4)-S(2)  | 112.94(5) |
| N(4)-Cu(4)-S(3)   | 119.82(15) | S(4)-Cu(1)-Cu(1) | 134.43(4) |
| N(4)-Cu(4)-S(4)   | 129.84(15) | S(4)-Cu(1)-Cu(3) | 61.80(4)  |
| N(10)-Cu(1)-Cu(1) | 97.20(13)  | S(4)-Cu(1)-S(1)  | 104.42(5) |
| N(10)-Cu(1)-Cu(3) | 102.38(14) | S(4)-Cu(1)-S(1)  | 113.65(6) |
| N(10)-Cu(1)-S(1)  | 83.86(14)  | S(4)-Cu(3)-Cu(1) | 52.43(4)  |
| N(10)-Cu(1)-S(4)  | 127.02(14) | S(4)-Cu(3)-Cu(4) | 53.22(4)  |
| N(14)-N(15)-Cu(3) | 123.4(4)   | S(4)-Cu(4)-Cu(2) | 127.61(5) |
| N(15)-Cu(3)-Cu(1) | 94.27(15)  | S(4)-Cu(4)-Cu(3) | 62.48(4)  |

|                   |            |                 |           |
|-------------------|------------|-----------------|-----------|
| N(15)-Cu(3)-Cu(4) | 105.67(15) | S(4)-Cu(4)-S(2) | 113.85(6) |
| N(15)-Cu(3)-S(1)  | 118.80(16) | S(4)-Cu(4)-S(3) | 95.85(6)  |

**Table 5.13** Selected bond angles (°) for  $K_2[Cu_8(DPTC)_8(ClO_4)_2]^{2+}$

#### 5.3.4 Complexes of DPTC with copper (II) tetrafluoroborate

The reaction of DPTC with  $Cu(BF_4)_2 \cdot 6H_2O$  in acetone results in a dark brown coloured solution. Analysis by ESI-MS gave ions at  $m/z = 2549$  which correspond to  $\{[Cu_8(DPTC)_8]\}$ . Slow diffusion of dichloromethane into the resulting solution afforded colourless crystals of X-ray quality. Single crystal X-ray diffraction studies confirmed the formation of an octanuclear species  $[Cu_8(DPTC)_8(BF_4)_2]^{8+}$  (figure 5.36).

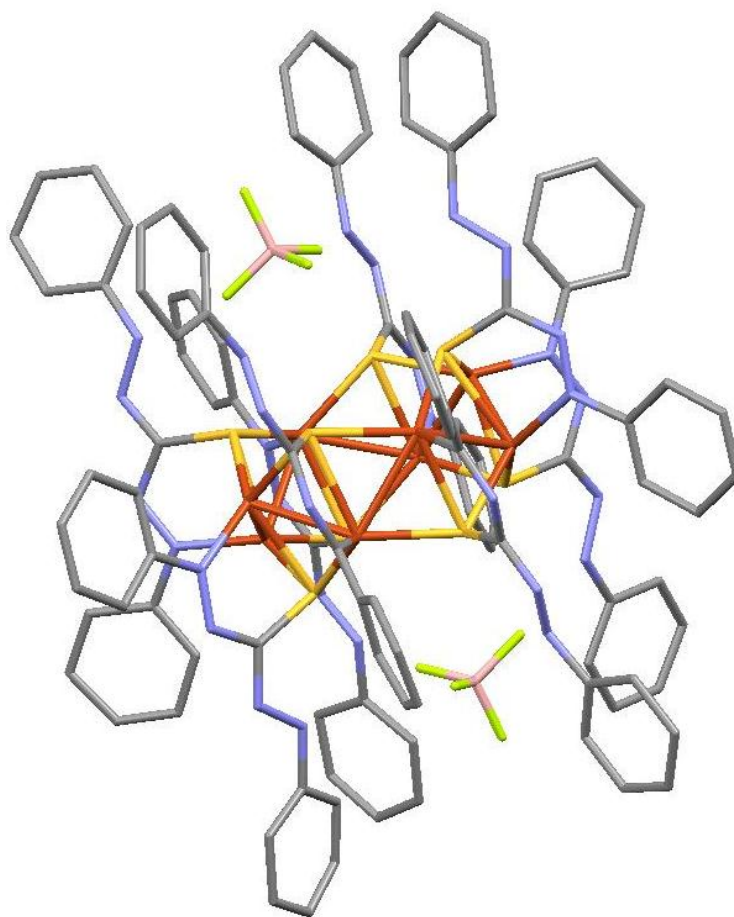


**Figure 5.36** X-ray crystal structure of  $[K_2[Cu_8(DPTC)_8(BF_4)_2]^{2+}$

In a similar manner to the perchlorate structure, the reaction of DPTC with copper tetrafluoroborate results in a octanuclear species, which is formed by the coordination of eight copper ions with eight ligands,  $[\text{Cu}_8(\text{DPTC})_8]$ . The DPTC ligand coordinate via the sulphur and nitrogen atoms, with the sulphur atom coordinating two further  $[\text{CuDPTC}]$  units either side of itself, which continues in a cyclic manner giving the octanuclear  $[\text{Cu}_8(\text{DPTC})_8]$  with a band of eight sulphur and eight copper atoms (figure 5.34) (Cu-Cu: 2.55-2.59 Å; Cu-N: 1.98-2.02 Å; Cu-S: 2.26-2.51 Å).

As with the previous example, the uncoordinated azo-end of the ligand alternates around the 'Cu<sub>8</sub>' core such that four point up and the remaining four point in the opposite direction (figure 5.33). This gives rise to a cavity containing four C=N-NHPh units, which act as a hydrogen bond donor to a tetrafluoroborate anion, which sits in both cavities (figure 5.36).

| Bond        | Bond length (Å) | Bond        | Bond length (Å) |
|-------------|-----------------|-------------|-----------------|
| Cu(1)-Cu(3) | 2.5451(14)      | Cu(3)-N(4)  | 1.991(6)        |
| Cu(1)-Cu(4) | 2.5727(13)      | Cu(3)-S(6)  | 2.299(2)        |
| Cu(1)-N(12) | 1.982(6)        | Cu(3)-S(7)  | 2.310(2)        |
| Cu(1)-S(5)  | 2.286(2)        | Cu(3)-S(8)  | 2.507(2)        |
| Cu(1)-S(6)  | 2.426(2)        | Cu(4)-Cu(4) | 2.5591(19)      |
| Cu(1)-S(8)  | 2.259(2)        | Cu(4)-N(8)  | 2.017(7)        |
| Cu(2)-Cu(2) | 2.5551(18)      | Cu(4)-S(5)  | 2.278(2)        |
| Cu(2)-Cu(3) | 2.5925(14)      | Cu(4)-S(5)  | 2.431(2)        |
| Cu(2)-N(13) | 1.996(7)        | Cu(4)-S(6)  | 2.286(2)        |
| Cu(2)-S(7)  | 2.4442(19)      | S(5)-Cu(4)  | 2.279(2)        |
| Cu(2)-S(7)  | 2.291(2)        | S(7)-Cu(2)  | 2.4442(19)      |
| Cu(2)-S(8)  | 2.256(2)        | S(7)-Cu(3)  | 2.310(2)        |

**Table 5.14** Selected bond lengths (Å) for of  $[\text{K}_2[\text{Cu}_8(\text{DPTC})_8(\text{BF}_4)_2]^{2+}$

| Bond              | Bond angle (°) | Bond              | Bond angle (°) |
|-------------------|----------------|-------------------|----------------|
| C(34)-S(5)-Cu(1)  | 105.2(3)       | N(12)-Cu(1)-S(6)  | 84.88(18)      |
| C(34)-S(5)-Cu(4)  | 90.5(3)        | N(12)-Cu(1)-S(8)  | 130.0(2)       |
| C(35)-S(6)-Cu(1)  | 89.8(2)        | N(13)-Cu(2)-Cu(2) | 96.77(17)      |
| C(35)-S(6)-Cu(3)  | 114.8(3)       | N(13)-Cu(2)-Cu(3) | 102.11(18)     |
| C(35)-S(6)-Cu(4)  | 99.0(3)        | N(13)-Cu(2)-S(7)  | 83.94(18)      |
| C(36)-S(8)-Cu(1)  | 105.1(3)       | N(13)-Cu(2)-S(8)  | 126.44(18)     |
| C(36)-S(8)-Cu(2)  | 109.0(3)       | S(5)-Cu(1)-Cu(3)  | 135.02(7)      |
| C(36)-S(8)-Cu(3)  | 89.4(3)        | S(5)-Cu(1)-Cu(4)  | 59.70(6)       |
| C(55)-S(7)-Cu(2)  | 90.4(2)        | S(5)-Cu(1)-S(6)   | 112.87(7)      |
| C(55)-S(7)-Cu(2)  | 104.7(3)       | S(5)-Cu(4)-Cu(1)  | 54.29(6)       |
| C(55)-S(7)-Cu(3)  | 105.0(3)       | S(5)-Cu(4)-Cu(4)  | 54.26(6)       |
| Cu(1)-Cu(3)-Cu(2) | 97.61(4)       | S(5)-Cu(4)-Cu(4)  | 60.01(6)       |
| Cu(1)-S(5)-Cu(4)  | 66.01(6)       | S(5)-Cu(4)-S(5)   | 113.64(6)      |
| Cu(1)-S(8)-Cu(3)  | 64.31(6)       | S(5)-Cu(4)-S(6)   | 108.01(8)      |
| Cu(2)-Cu(2)-Cu(3) | 102.87(5)      | S(6)-Cu(1)-Cu(3)  | 55.05(6)       |
| Cu(2)-S(7)-Cu(2)  | 65.21(6)       | S(6)-Cu(1)-Cu(4)  | 54.33(5)       |
| Cu(2)-S(7)-Cu(3)  | 122.03(8)      | S(6)-Cu(3)-Cu(1)  | 59.83(6)       |
| Cu(2)-S(8)-Cu(1)  | 117.78(8)      | S(6)-Cu(3)-Cu(2)  | 125.93(7)      |
| Cu(2)-S(8)-Cu(3)  | 65.71(6)       | S(6)-Cu(3)-S(7)   | 95.71(7)       |
| Cu(3)-Cu(1)-Cu(4) | 101.19(4)      | S(6)-Cu(3)-S(8)   | 109.62(8)      |
| Cu(3)-S(6)-Cu(1)  | 65.12(6)       | S(6)-Cu(4)-Cu(1)  | 59.55(5)       |

|                   |            |                  |           |
|-------------------|------------|------------------|-----------|
| Cu(3)-S(7)-Cu(2)  | 66.02(6)   | S(6)-Cu(4)-Cu(4) | 136.93(6) |
| Cu(4)-Cu(4)-Cu(1) | 101.45(5)  | S(6)-Cu(4)-S(5)  | 112.66(8) |
| Cu(4)-S(5)-Cu(1)  | 120.97(9)  | S(7)-Cu(2)-Cu(2) | 54.51(5)  |
| Cu(4)-S(5)-Cu(4)  | 65.73(6)   | S(7)-Cu(2)-Cu(2) | 60.28(6)  |
| Cu(4)-S(6)-Cu(1)  | 66.12(6)   | S(7)-Cu(2)-Cu(3) | 54.49(5)  |
| Cu(4)-S(6)-Cu(3)  | 119.17(9)  | S(7)-Cu(2)-S(7)  | 114.11(6) |
| N(4)-Cu(3)-Cu(1)  | 106.3(2)   | S(7)-Cu(3)-Cu(1) | 129.29(7) |
| N(4)-Cu(3)-Cu(2)  | 94.98(19)  | S(7)-Cu(3)-Cu(2) | 59.48(5)  |
| N(4)-Cu(3)-S(6)   | 136.8(2)   | S(7)-Cu(3)-S(8)  | 109.82(7) |
| N(4)-Cu(3)-S(7)   | 119.3(2)   | S(8)-Cu(1)-Cu(3) | 62.56(6)  |
| N(4)-Cu(3)-S(8)   | 82.98(18)  | S(8)-Cu(1)-Cu(4) | 127.69(7) |
| N(8)-Cu(4)-Cu(1)  | 101.89(19) | S(8)-Cu(1)-S(5)  | 95.70(8)  |
| N(8)-Cu(4)-Cu(4)  | 99.2(2)    | S(8)-Cu(1)-S(6)  | 113.97(8) |
| N(8)-Cu(4)-S(5)   | 84.09(19)  | S(8)-Cu(2)-Cu(2) | 135.46(6) |
| N(8)-Cu(4)-S(5)   | 115.3(2)   | S(8)-Cu(2)-Cu(3) | 61.80(6)  |
| N(8)-Cu(4)-S(6)   | 121.5(2)   | S(8)-Cu(2)-S(7)  | 104.79(8) |
| N(12)-Cu(1)-Cu(3) | 102.92(19) | S(8)-Cu(2)-S(7)  | 113.96(8) |
| N(12)-Cu(1)-Cu(4) | 101.31(19) | S(8)-Cu(3)-Cu(1) | 53.13(5)  |
| N(12)-Cu(1)-S(5)  | 119.9(2)   | S(8)-Cu(3)-Cu(2) | 52.49(5)  |

**Table 5.15** Selected bond angles (°) for  $[K_2[Cu_8(DPTC)_8(BF_4)_2]^{2+}$

### 5.3.5 Complexes of DPTC with copper (II) acetate

The reaction of DPTC with  $\text{Cu}(\text{CH}_3\text{CO}_2)_2 \cdot \text{H}_2\text{O}$  in acetone initially gives a brown coloured solution which turns red after several hours. Analysis by ESI-MS gave ions at  $m/z = 892$  which corresponds to  $[\text{Cu}_2(\text{DPTC})_2(\text{DPTCO})]$ . Small needle shaped crystals were formed overnight, analysis by single crystal X-ray diffraction studies confirmed the formation of a dinuclear species  $[\text{Cu}_2(\text{DPTC})_2(\text{DPTCO})]$  (figure 5.37).

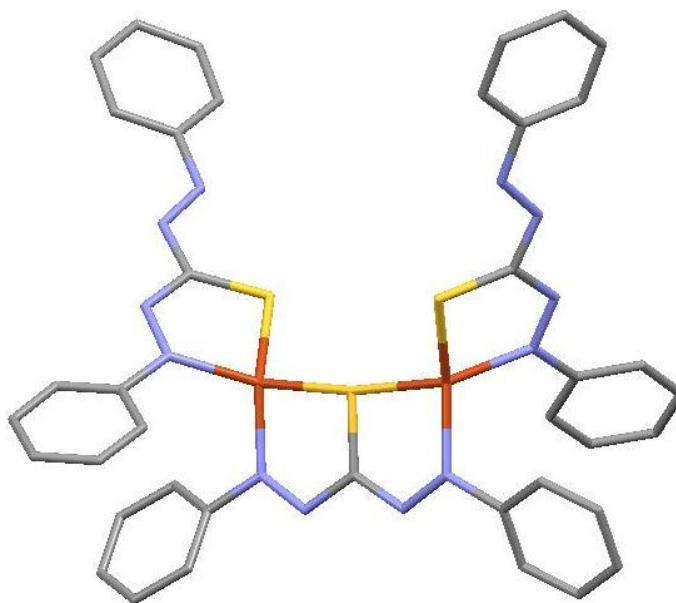


Figure 5.37 X-ray crystal structure of  $[\text{Cu}_2(\text{DPTC})_2(\text{DPTCO})]$

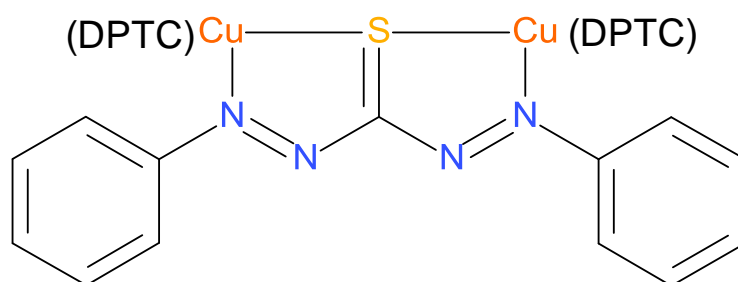


Figure 5.38 Schematic diagram of  $[\text{Cu}_2(\text{DPTC})_2(\text{DPTCO})]$

The solid state structure  $[\text{Cu}_2(\text{DPTC})_2(\text{DPTCO})]$  shows a complex that contains three ligands and two copper ions. Each  $\text{Cu}^+$  ions adopt a distorted tetrahedral geometry and is coordinated by the sulphur and terminal azo nitrogen atoms of two DPTC ligands. The coordination geometry is completed by a DPTCO ligand, which coordinates via the sulphur atom, which bridges two metal ions and by both of the terminal nitrogen atoms (Cu-N (DPTC): 1.98-2.00 Å; Cu-S (DPTC): 2.21-2.24 Å; Cu-N (DPTCO): 1.93-1.94 Å; Cu-S (DPTCO): 2.25 Å).

| Bond       | Bond length (Å) |
|------------|-----------------|
| Cu(1)-N(4) | 1.937(3)        |
| Cu(1)-N(5) | 2.003(3)        |
| Cu(1)-S(3) | 2.2473(12)      |
| Cu(1)-S(5) | 2.2090(13)      |
| Cu(2)-N(1) | 1.931(3)        |
| Cu(2)-N(9) | 1.981(3)        |
| Cu(2)-S(3) | 2.2143(13)      |
| Cu(2)-S(4) | 2.2403(12)      |

**Table 5.16** Selected bond lengths (Å) for [Cu<sub>2</sub>(DPTC)<sub>2</sub>(DPTO)]

| Bond             | Bond angle (°) | Bond             | Bond angle (°) |
|------------------|----------------|------------------|----------------|
| C(38)-S(3)-Cu(1) | 94.14(15)      | S(5)-Cu(1)-S(3)  | 106.82(5)      |
| C(46)-S(5)-Cu(1) | 93.38(16)      | N(1)-Cu(2)-N(9)  | 108.50(14)     |
| C(7)-S(4)-Cu(2)  | 93.35(15)      | N(1)-Cu(2)-S(3)  | 85.07(10)      |
| C(38)-S(3)-Cu(2) | 94.70(14)      | N(1)-Cu(2)-S(4)  | 141.99(12)     |
| N(4)-Cu(1)-N(5)  | 110.38(14)     | N(9)-Cu(2)-S(3)  | 140.21(11)     |
| N(4)-Cu(1)-S(3)  | 85.19(11)      | N(9)-Cu(2)-S(4)  | 87.39(11)      |
| N(4)-Cu(1)-S(5)  | 141.93(12)     | S(4)-Cu(2)-S(3)  | 104.81(5)      |
| N(5)-Cu(1)-S(3)  | 134.12(11)     | Cu(2)-S(3)-Cu(1) | 170.96(6)      |
| N(5)-Cu(1)-S(5)  | 87.29(11)      |                  |                |

**Table 5.17** Selected bond angles (°) for [Cu<sub>2</sub>(DPTC)<sub>2</sub>(DPTO)]

## 5.4 Discussion

It is clear that the reaction of  $\text{Cd}^{2+}$  and DPC results in the mononuclear complex  $[\text{Cd}(\text{DPC})_2]^{2+}$  as the sole product. The simple mononuclear complex involves two DPC ligands coordinating the  $\text{Cd}^{2+}$  ion as a bidentate donor via the N-donor and O-donor atoms, with three solvent acetonitrile molecules completing the seven-coordinate geometry. In the case of DPC one of the most pressing issues is whether the ligand involved in the coordination with metal ions is DPC or its oxidative derivatives. The ESI-MS studies confirm that both ligands involved in the coordination with the  $\text{Cd}^{2+}$  metal centre are DPC with a molecular ion at  $m/z$  697 corresponding to  $\{[\text{Cd}(\text{DPC})_2](\text{ClO}_4)\}^+$  confirming that both ligands have four -NH groups. Interestingly Siddalingaiah suggested that upon reaction of DPC with  $\text{Cd}^{2+}$  the DPC ligands behave as a bidentate monoanionic ligand coordinating through the enolised ketonic oxygen and the azo nitrogen.<sup>156-159</sup> This study has shown this to be incorrect, the DPC ligand is simply coordinating through both the N-donor and O-donor domains. The presence of two perchlorate ions in the structure demonstrates that the ligand remains unprotonated. As a result it is clear from this structure that the ligand is neither oxidised or deprotonated.

Reaction of DPC and  $\text{Cu}^{2+}$  is more complex than the previous  $\text{Cd}^{2+}$  reaction, the resulting structure comprises of six ligands and three metal ions. Each of the copper ions is the bivalent  $\text{Cu}^{2+}$  ion (as there are five perchlorate anions present and it is assumed that the central oxygen atom is  $\text{OH}^-$ ) and has distorted octahedral coordination, arising from the coordination of two ligands, a water ligand and a central hydroxide ion coordinates all three metal centres. The four coordination sites donated by the ligands are in two different modes; 3 ligands coordinate via the O-donor atom only which bridges two metal ions, whereas the other 3 ligands coordinate via both the N-donor and O-donor atoms. The DPC ligand undergoes oxidative intramolecular cyclisation to form the nitrogen containing heterocycle 2,3-diphenyltetrazolium-5-olate (DPTO) giving the trinuclear cluster  $[\text{Cu}_3\text{OH}(\text{OH}_2)_3(\text{DPTO})_6]^{5+}$ . Although the ESI-MS studies did not give a molecular ion for the trinuclear species, as it is likely that the molecular ion fragments during the mass spectrometry process, the peaks present corresponding to the smaller species all show the correct isotope pattern for the fully oxidised DPTO ligand. This result disapproves the study produced by Iñón and co-workers, in which they suggested that in the reaction of  $\text{Cu}^{2+}$  and DPC the metal ion oxidises the ligand to DPCO.<sup>155</sup> It is clear that the colorimetric reaction with  $\text{Cu}^{2+}$  is a direct result of the coordination of DPC to the  $\text{Cu}^{2+}$  ions, from ESI-MS and X-ray crystallography studies the coordination with DPC results in clusters of ligands and metal ions. The initial complex is not stable, as previous literature suggests, however it is clear that this instability is due to oxidation of the ligand to the cyclic DPTO

species which results in the formation of the colourless trinuclear species  $[\text{Cu}_3\text{OH}(\text{OH}_2)_3(\text{DPTO})_3]^{5+}$ . Reaction of DPCO with  $\text{Cu}^{2+}$  results in the same trinuclear species, the ligand undergoes oxidative intramolecular cyclisation to form the nitrogen containing heterocycle 2,3-diphenyltetrazolium-5-olate (DPTO) to give the trinuclear cluster  $[\text{Cu}_3\text{OH}(\text{OH}_2)_3(\text{DPTO})_6]^{5+}$ .

Despite exhaustive attempts, crystals of a chromium or vanadium complex with DPC were not achieved; however the cyclised ligand was isolated. Reaction of  $\text{Cr}^{3+}$  with DPC results in a highly coloured species which produces colourless crystals of the cyclised ligand 2,3-diphenyltetrazolium-5-olate (DPTO). The molecular weight of the crystals produced is 238.25, corresponding to  $\text{C}_{13}\text{H}_{10}\text{N}_4\text{O}$ , indicating that the crystal structure is that of 2,3-diphenyltetrazolium-5-olate (DPTO), which is a product of the oxidative intramolecular cyclisation of DPC to form the nitrogen containing heterocycle. A comprehensive study on 2,3-diphenyltetrazolium-5-olate (DPTO) was reported by King and co-workers, the comparison of the bond angles in the  $\text{N}_4\text{CO}$  ring correspond with only slight discrepancies (figure 5.39). King and co-workers suggested that the phenyl substituents are nearly equally inclined to the heterocyclic ring with a slight twist in the angles at  $65.4^\circ$ , this is confirmed in the crystal structure obtained in this study. The crystal data obtained for both studies is also complementary, summarised in table 5.18.<sup>213</sup>

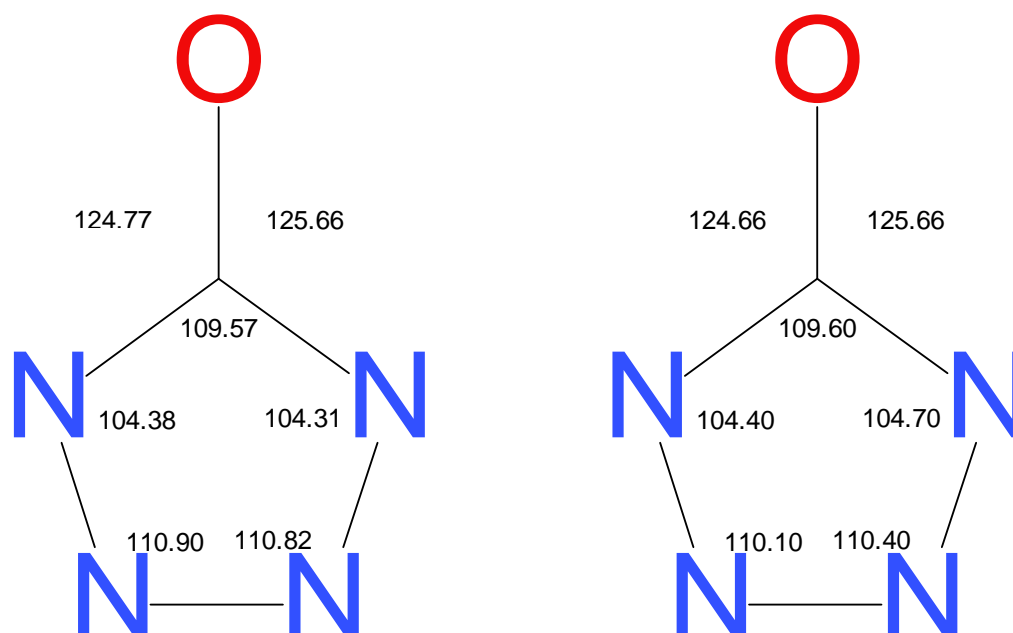


**Figure 5.39** Comparison of the bond angles from this study (left) and the results reported by King and co-workers (right)

|               |              | King and co-workers |
|---------------|--------------|---------------------|
| M             | 238.25       | 238.2               |
| Space group   | Orthorhombic | Orthorhombic        |
| Cell length a | 6.237        | 6.454               |
| Cell length b | 11.523       | 11.406              |
| Cell length c | 16.078       | 16.132              |

**Table 5.18** Comparison of the results from this study (left) and the results reported by King and co-workers (right)

In both cases ( $[\text{Cd}(\text{DPC})_2]^{2+}$  and  $[\text{Cu}_3\text{OH}(\text{OH}_2)_3(\text{DPTO})_6]^{5+}$ ) the crystals of the isolated and characterised material are colourless. This is interesting and has implications in the chromogenesis of DPC, the source of much argument and contradiction in the literature. Reaction of  $\text{Cd}^{2+}$  with DPC gives a dark-pink coloured solution yet that cadmium complex is colourless. It therefore may be possible that colour does not originate from the complex itself but oxidation products of the ligand. However, analysis by EPR shows no organic radicals produced so the generation of colour by radical cations can be ruled out. However, it is possible (and perhaps most likely) that the colour is generated from the neutral cadmium complex e.g. DPC is deprotonated and acts as a bidentate anionic ligand. Unfortunately, production of crystals of this material suitable for X-ray analysis has been unsuccessful.

Reaction of DPC with  $\text{Cu}^{2+}$  initially gives an intense violet colour which dissipates to give colourless crystals of  $[\text{Cu}_3\text{OH}(\text{OH}_2)_3(\text{DPTO})_6]^{5+}$ . It is therefore unlikely that the oxidised and cyclised ligand DPTO generates the intense colours and it is highly likely that the colour is due to the anionic ligand coordinating the copper ions. However, this does answer why the solutions of DPC are unstable and the colour fades over times and this is obviously due to cyclisation and oxidation as isolated samples of this material are colourless.

Reaction of DPTC with various metal ions resulted in the deprotonation of the ligand to form the monoanionic species, which coordinates the metal ions via the S-donor and N-donor atoms. This behaviour is supported by the bond lengths observed (table 5.19); the nitrogen-nitrogen double bond distance for the azo-group ( $\text{N}^3\text{-N}^4$ ) is shorter than the nitrogen-nitrogen single bond ( $\text{N}^1\text{-N}^2$ ). Also the distances between the nitrogen atoms and the thiocarbonyl carbon atom are also consistent with deprotonation, as the  $\text{N}^3\text{-CS}$  is longer than the  $\text{N}^1\text{-CS}$  bond length (figure 5.40).

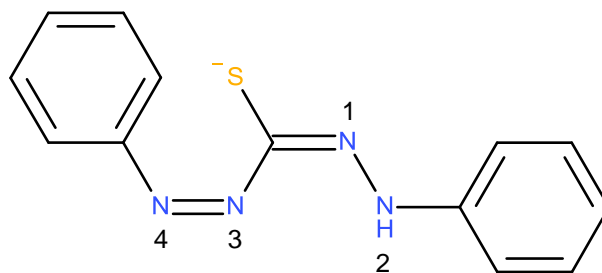


**Figure 5.40** Monoanionic form of DPTC that is involved in the coordination

|                                | [Hg(DPTC) <sub>2</sub> ] <sup>a</sup> | [Hg <sub>2</sub> Ag <sub>2</sub> (DPTC) <sub>4</sub> ] <sup>a</sup> | [Cu <sub>8</sub> (DPTC) <sub>8</sub> ] <sup>a</sup> | [Cu <sub>2</sub> (DPTC) <sub>2</sub> (DPTCO)] |                    |
|--------------------------------|---------------------------------------|---|---|---|--------------------|
| N <sup>1</sup> -N <sup>2</sup> | 1.340                                 | 1.321   | 1.316   | 1.335 <sup>a</sup>                            | 1.304 <sup>b</sup> |
| N <sup>3</sup> -N <sup>4</sup> | 1.272                                 | 1.268   | 1.285   | 1.287 <sup>a</sup>                            | 1.308 <sup>b</sup> |
| N <sup>1</sup> -C=S            | 1.319                                 | 1.313   | 1.366   | 1.321 <sup>a</sup>                            | 1.363 <sup>b</sup> |
| N <sup>3</sup> -C=S            | 1.391                                 | 1.387   | 1.341   | 1.378 <sup>a</sup>                            | 1.330 <sup>b</sup> |

**Table 5.19** Bond lengths of the donor framework in DPTC and DPTCO complexes. <sup>a</sup> = DPTC ligand, <sup>b</sup> = DPTCO ligand

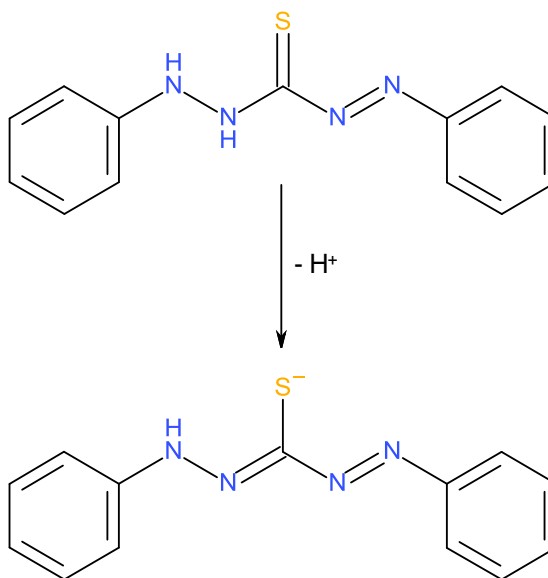


**Figure 5.41** Deprotonation of DPTC

It is clear that the reaction of Hg<sup>2+</sup> and DPTC results in the mononuclear complex [Hg(DPTC)<sub>2</sub>] as the sole product. The simple mononuclear complex involves two DPTC ligands coordinating the four-coordinate Hg<sup>2+</sup> ion as a bidentate donor via the N-donor and S-donor atoms. The absence of anions confirms that the complex is neutral, resulting from

the monoanionic form of the ligand. This is unlike DPC but expected due to the increased acidity of the thioamide (c.f. the amide of DPC). The ESI-MS studies confirm molecular ion at  $m/z$  713 corresponding to  $\{[\text{Hg}(\text{DPTC})(\text{DPTC-H})]\}^+$ , however this does not contradict the solid state studies but it is an artefact of the ESI-MS ionisation process. Irving and co-workers report that upon reaction of DPTC with  $\text{Hg}^{2+}$  the same mononuclear structure exist, although they suggest that the ligand coordinates through the thiol sulphur and the amide group.<sup>167</sup> The bond lengths for the  $[\text{Hg}(\text{DPTC})_2]$  complex confirm that the shorter double bond terminal azo N-donor (1.27 Å) is involved in the coordination and not the amine N-donor (1.34 Å).

The reaction of DPTC with both  $\text{Hg}^{2+}$  and  $\text{Ag}^+$  results in an interesting structure containing two  $\text{Ag}^+$ , two  $\text{Hg}^{2+}$  and four DPTC ligands. The DPTC appears to first react with  $\text{Hg}^{2+}$  to form the previous  $[\text{Hg}(\text{DPTC})_2]$  complex, this then acts as a bidentate ligand, coordinating *via* the S-donor atom and the  $\text{Hg}^{2+}$  itself to form the  $[\text{Hg}_2\text{Ag}_2(\text{DPTC})_4(\text{acetone})_2(\text{ClO}_4)_2]$  complex, two acetone solvent molecules and two perchlorate anions complete the coordination geometry. The four DPTC ligands are coordinating the metal ions in a similar manner to the previous  $[\text{Hg}(\text{DPTC})_2]$  complex, binding through the S-donor and the shorter double bond terminal azo N-donor (1.267-1.269 Å) rather than the amine N-donor (1.324-1.329 Å). ESI-MS confirms that the ligands in the complex are DPTC, each containing one -NH group and have deprotonated to form the monoanionic species. In 1971 Irving and co-workers extended their research and suggested that the reaction of DPTC with  $\text{Ag}^+$  and  $\text{Hg}^{2+}$  resulted in a complex containing one  $\text{Hg}^{2+}$ , two  $\text{Ag}^+$  ions and two DPTC ligands (figure 5.9). They postulated that the two DPTC ligands had undergone deprotonation and coordinated both the  $\text{Hg}^{2+}$  and  $\text{Ag}^+$  ions via the bridging S-donor atom and the bridging N-donor atom from the deprotonated amine.<sup>173</sup> Examination by ESI-MS coupled with the solution-state UV-Vis work of Irving shows the tetranuclear assembly persists in solution.

The reaction of DPTC with  $\text{Cu}^{2+}$ , whether the anion is perchlorate or tetrafluoroborate, results in a very interesting structure, which comprises of eight DPTC ligands and eight  $\text{Cu}^+$  metal ions. Single-crystal X-ray analysis of this material shows that the copper is reduced to  $\text{Cu}^+$  and eight of these ions are coordinated by eight DPTC ligands forming the octanuclear cluster  $[\text{Cu}_8(\text{DPTC})_8]$ . In the solid state there are close  $\text{Cu}^+-\text{Cu}^+$  metal interactions which possibly precludes the formation of this type of cluster with divalent and trivalent ions on electrostatic grounds. In an analogous manner to the previous DPTC structures the eight DPTC ligands coordinate through the S-donor atom and the terminal azo N-donor atom. Each S-donor atom bridges three copper ions and each copper ion also bridges two other copper ions, creating a core belt of sulphur and copper ions. The reaction of  $\text{Cu}^{2+}$  with DPTC results in the  $\text{Cu}^{2+}$  reducing to  $\text{Cu}^+$  and simultaneously the

DPTC deprotonates to form the monoanionic form (figure 5.41). The cavity containing four C=N-NHPh units, acts as a hydrogen bond donor to an anion ( $\text{ClO}_4^-$  or  $\text{BF}_4^-$ ), which sits in both cavities (figure 5.42). It is possible that the anion acts as a template and the formation of the “Cu<sub>8</sub>” is a result of the presence of the anion, which is accompanied by a potassium ion giving a species of the overall formula  $\text{K}_2[(\text{DPTC})_8\text{Cu}_8(\text{X})_2]$  ( $\text{X} = \text{ClO}_4^-$  or  $\text{BF}_4^-$ ). It is likely that the s-block cation is present as a result of impurities present in the DPTC. Examination by ESI-MS confirms that multiple coordination of “[CuDPTC]” can occur and shows clusters of three ions corresponding to  $n = 3-7$  and  $n = 9$ . This strongly indicates that the formation of the octanuclear species  $[\text{Cu}_8(\text{DPTC})_8]$  in the solid state is due to templation by the anion as in the gas-phase many species, including larger homologues, are present. This result contradicts the numerous studies on the reaction of  $\text{Cu}^{2+}$  and DPTC. Fabretti and co-workers suggested a dimeric structure involving two mesoionic DPTC ligands, coordinating via a bridging S-donor domain and the terminal N-donors.<sup>214</sup> Koksharova and co-workers agreed with Fabretti, apart from the addition of two water ligand to the  $\text{Cu}^{2+}$  metal centres.<sup>215</sup> Larin and co-workers stated that DPTC forms a bis-chelate compound with  $\text{Cu}^{2+}$ , acting as a bidentate ligand coordinating through the S-donor and N-donor atoms creating a five-membered metallocycle.

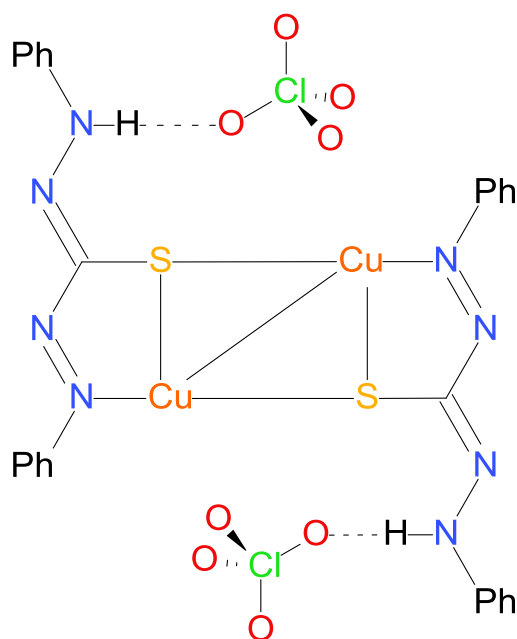


**Figure 5.42** Anion templation in the  $\text{K}_2[\text{Cu}_8(\text{DPTC})_8(\text{ClO}_4)_2]^{2+}$  complex, also occurs with  $\text{BF}_4^-$

It was of interest to investigate the reaction of  $\text{Cu}^{2+}$  and DPTC without the presence of an anion to template the assembly, so the acetate metal salt was used. The resulting  $[\text{Cu}_2(\text{DPTC})_2(\text{DPTCO})]$  structure contains three ligands and two reduced distorted tetrahedral  $\text{Cu}^+$  ions. Each  $\text{Cu}^+$  ion has four-coordinate geometry arising from the coordination of two different forms of the DPTC ligands. Two of the ligands present are the monoanionic DPTC, coordinating via the S-donor and terminal N-donor azo atoms. Whereas the third ligand has completely oxidised to form DPTCO, coordinating via both the terminal N-donor azo N-donor atoms, the sulphur atom bridges both of the metal ions. In the DPTCO ligand both nitrogen-nitrogen and nitrogen-thiocarbonyl bond lengths are very similar and this suggests that this species is the oxidised ligand which contains two azo nitrogen-nitrogen double bonds giving diphenylthiocarbadiazone (DPTCO).  $[\text{Cu}_2(\text{DPTC})_2(\text{DPTCO})]$  is a transient species which will eventually form  $[(\text{DPTC})_n\text{Cu}_n]$ , it is only isolated due to its lack of solubility in the reaction medium. This is supported by the ESI-MS which is a complex spectrum, and shows fragments of  $[(\text{DPTC})\text{Cu}]_n$  ( $n = 3-9$ ) in an analogous fashion to that observed for  $[(\text{DPTC})_8\text{Cu}_8]$ . This may be expected as the complex contains units of "LCu" from the higher nuclearity species which are observed due to aggregation in the ESI-MS process. However, an ion at  $m/z$  892 corresponding to  $[\text{Cu}_2(\text{DPTC})_2(\text{DPTCO})]$  is of much greater relative intensity in the ESI-MS than the mass spectrum of  $[\text{Cu}_8(\text{DPTC})_8]$ . The formation of  $[\text{Cu}_2(\text{DPTC})_2(\text{DPTCO})]$  occurs as using copper (II) acetate results in deprotonation of the ligand and generation of acetic acid. Without an anion to template the formation of  $[\text{Cu}_8(\text{DPTC})_8]$  the  $[\text{Cu}_2(\text{DPTC})_2(\text{DPTCO})]$  complex forms.

In conclusion, this work answers some of the questions regarding the chemistry of DPC and DPTC, demonstrating that the coordination behaviour is much more complex than previously thought. Additionally it is quite remarkably that two reagents, discovered over a century ago, which have numerous uses across the scientific disciplines can lead to such fascinating self-assembled species.

The literature surrounding DPC is inconsistent, over the past 100 years there have been a vast amount of inconsistent reports on the chemistry of DPC, but a definitive answer on how DPC coordinates metal ions has not been provided. In this work we have demonstrated that DPC can coordinate as a bidentate donor coordinating via the phenyl nitrogen atom and the carbonyl unit to give the self-assembled species  $[\text{Cd}(\text{DPC})_2]^{2+}$ . Contrary to the speculation that reaction of DPC with  $\text{Cu}^{2+}$  results in oxidation of the reagent to DPCO and subsequent reduction of the metal ion to  $\text{Cu}^+$ , DPC undergoes intramolecular cyclisation to form the nitrogen containing heterocycle. The resulting cyclic species can either coordinate via both the oxygen and amide nitrogen atoms or the

carbonyl unit can act as a bridging ligand. Despite exhaustive attempts crystals of a DPC complex with either chromium or vanadium were not achieved, however the cyclised ligand was isolated, highlighting that the oxidation and cyclisation of DPC is important in the coordination chemistry of these ions.

These results contradict the speculation surrounding the use of DPTC for the colorimetric determination of metal ions. Over the past century it was believed that DPTC can only coordinate via the terminal hydrazine nitrogen and the sulphur thiocarbonyl atom. However, the sulphur atom can be involved in further coordination, acting as a bridging ligand, to give different self-assembled species such as  $[\text{Hg}_2\text{Ag}_2(\text{DPTC})_4]$  and  $[\text{Cu}_8(\text{DPTC})_8]$ . Furthermore, only when the ligand is oxidised to the dia-azo diphenylthiocarbadiazone (DPTCO) species can the other nitrogen atoms in the ligand framework act as donor atoms.

## 6. Conclusion

In conclusion eight novel polydentate ligands,  $\mathbf{L}^1$ - $\mathbf{L}^8$ , have been successfully synthesised and the coordination chemistry of all these ligands investigated. Furthermore the coordination chemistry of diphenylcarbazide and dithizone has been investigated to reveal some interesting results.

The polydentate ligands  $\mathbf{L}^1$ - $\mathbf{L}^4$  contain both N-donor and N-oxide donor atoms. Reaction of  $\mathbf{L}^1$  with  $\text{Cu}^{2+}$  results in the formation of a mononuclear complex  $[\text{Cu}(\mathbf{L}^1)(\text{ClO}_4)_2(\text{sol})]$ . The ligand  $\mathbf{L}^1$  acts as a tridentate donor, coordinating the  $\text{Cu}^{2+}$  metal centre via the thiazole-pyridyl-pyridyl-N-oxide donor unit, two counter ions and a solvent molecule (acetonitrile or water) complete the geometry. The potentially hexadentate ligand  $\mathbf{L}^2$  contains two identical thiazole-pyridyl-pyridyl domains. Reaction of  $\mathbf{L}^2$  with  $\text{Ni}^{2+}$  results in the dinuclear double helicate  $[\text{Ni}_2(\mathbf{L}^2)_2]^{4+}$ , where each ligand strand partitions into two tridentate domains, twisting through the thiazole-thiazole bond. Ligand  $\mathbf{L}^3$  is a potentially pentadentate ligand containing a bidentate and tridentate N-donor domain separated by a 1,3-phenylene spacer. Reaction of  $\mathbf{L}^3$  with  $\text{Cu}^{2+}$  results in the dinuclear double helicate  $[\text{Cu}_2(\mathbf{L}^3)_2]^{4+}$ . Each  $\text{Cu}^{2+}$  metal centre adopts a 5-coordinate geometry formed by the coordination of the bidentate domain of one ligand strand and the tridentate domain of a different ligand strand, resulting in a head-to-tail dinuclear double helicate. The N-oxide units imparts flexibility in the ligand strand and where the unoxidised ligand strand forms a circular helicate, the incorporation of an N-oxide unit allows the formation of the dinuclear double helicate. Reaction of  $\mathbf{L}^4$  with  $\text{Co}^{2+}$  results in the formation of a tetranuclear circular helicate  $[\text{Co}_4(\mathbf{L}^4)_4]^{8+}$ . All four of the  $\text{Co}^{2+}$  metal ions are six-coordinate, arising from the coordination of a tridentate tz-py-py N-donor domain from two different ligands. In each ligand the two tridentate domains are partitioned by a 1,3-phenol spacer, which bridge the domains in an 'over and under' conformation. Analogous complexes that contain ligands with a 1,3-phenyl spacer unit give pentanuclear circular helicates, the difference in the nuclearity of the circular helicates is due to the steric bulk of the methyl group on the central phenol spacer. In the dinuclear double complex  $[\text{Cu}_2(\mathbf{L}^3)_2]^{4+}$  the N-oxide unit allows the ligand to flex, whereas the steric bulk of the  $-\text{OH}$  unit in  $\mathbf{L}^4$  is sufficiently large that even with the added flexibility that the N-oxide units imparts a double helicate cannot be formed.

Ligands  $\mathbf{L}^5$ - $\mathbf{L}^7$  are polydentate N-donor ligands, partitioned into different binding domains due to separation by a 1,3-phenol spacer unit. Reaction of the potentially hexadentate ligand  $\mathbf{L}^5$  with  $\text{Zn}^{2+}$  results in the formation of a tetranuclear circular helicate  $[\text{Zn}_4(\mathbf{L}^5)_4]^{8+}$ . Each  $\text{Zn}^{2+}$  is coordinated by the tridentate domain of two different ligands, the ligands are partitioned by the spacer unit which bridge the domains in an 'over and under' conformation. Reaction of  $\mathbf{L}^6$  with  $\text{Ag}^+$  results in a dinuclear double *meso*-helicate

$[\text{Ag}_2(\text{L}^6)_2]^{2+}$ . Reaction of  $\text{L}^6$  with  $\text{Cd}^{2+}$  produces a crystalline material that consists of both colourless and orange species. The colourless crystals correspond to the mononuclear complex  $[\text{Cd}(\text{L}^6)_2(\text{MeCN})_2]^{2+}$ , whereas the orange crystals produce the dinuclear double *meso*-helicite  $[\text{Cd}_2(\text{L}^6)_2]^{2+}$ . This difference in self-assembly is a direct result of the -OH unit on the 1,3-phenol spacer; if protonated the mononuclear complex forms, however deprotonation results in the dinuclear complex. Reaction of the unsymmetrical ligand  $\text{L}^7$  with  $\text{Co}^{2+}$  results in a dinuclear double helicite  $[\text{Co}_2(\text{L}^7)_2]^{3+}$ . Upon close inspection of the X-ray crystal structural data the cobalt metal centres in the complex occupy different oxidation states;  $\text{Co}^{2+}$  and  $\text{Co}^{3+}$ , to give a mixed valence helicite. The ligand  $\text{L}^7$ , which contains the same basic ligand chain as  $\text{L}^6$  but contains an extra pyridyl unit, results in a crystalline material that contains both the mononuclear  $[\text{Zn}(\text{L}^7)_2]^{2+}$  and dinuclear  $[\text{Zn}_2(\text{L}^6)_2]^{3+}$  species. Although the difference in the  $\text{L}^7$ - $\text{Zn}^{2+}$  structures is attributed to stoichiometry; the reaction is in equilibrium as both structures are proposed when equimolar amounts of  $\text{L}^7$  and  $\text{Zn}^{2+}$  are used. The self-assembled architectures resulting from the polydentate ligands  $\text{L}^6$  and  $\text{L}^7$  can be controlled by the stoichiometry of the reaction and the -OH unit from the 1,3-phenol spacer.

The ability of a ligand strand that contains a 1,3-pyrene spacer unit to form circular helicates with 1<sup>st</sup> row transition metal ions allows the formation of tetranuclear circular helicite of further complexity. The ligand  $\text{L}^8$  contains both a bidentate and tridentate domain separated by a 1,3-pyrene unit. Reaction of  $\text{L}^8$  with  $\text{Cu}^{2+}$  results in the formation of a tetranuclear circular helicite  $[\text{Cu}_4(\text{L}^8)_4]^{8+}$ . Each of the  $\text{Cu}^{2+}$  ions adopts a 5-coordinate geometry formed by the coordination of the bidentate domain of one ligand strand and the tridentate domain of a different ligand strand, resulting in a head-to-tail tetranuclear circular helicite.

The use of DPC and DPTC as reagents for the colorimetric determination of a variety of metal ions has been well documented over the years; however examination of the scientific literature over the past 100 years shows that the coordination chemistry of DPC and DPTC is inconsistent, with literature sources proposing contradictory and non-definitive explanations. Reaction of DPC with  $\text{Cd}^{2+}$  results in the mononuclear species  $[\text{Cd}(\text{DPC})_2]^{2+}$ , the two ligands are coordinating through both the N-donor and O-donor domains. The ligands in the complex have not deprotonated and exist as DPC, contradicting the previous reports surrounding this reagent. Reaction of DPC with  $\text{Cu}^{2+}$  results in the formation of the  $[\text{Cu}_3\text{OH}(\text{OH}_2)_3(\text{DPTO})_6]^{5+}$  complex. This complicated structure contains six ligands and three metal ions; it is also generated when reacting DPCO with  $\text{Cu}^{2+}$ . The DPC ligands undergo oxidative intramolecular cyclisation to form the nitrogen containing heterocycle 2,3-diphenyltetrazolium-5-olate (DPTO) and coordinates

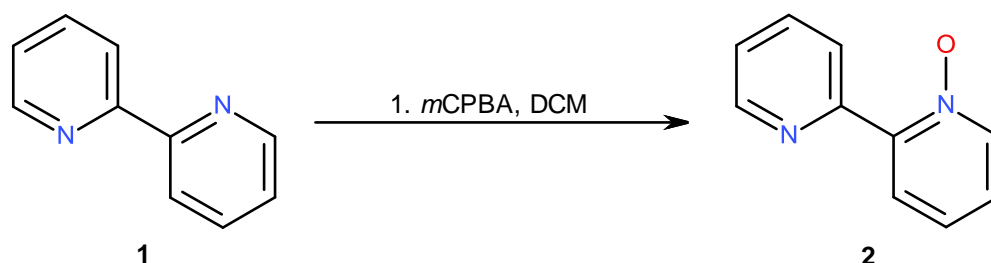
the  $\text{Cu}^{2+}$  metal centres in two different modes: via both the oxygen and amide nitrogen atoms or by the bridging carbonyl unit. The  $[\text{Cu}_3\text{OH}(\text{OH}_2)_3(\text{DPTO})_6]^{5+}$  complex contradicts the literature which suggests a  $\text{Cu}^+$  complex with DPCO. Despite exhaustive attempts a crystal of a chromium or vanadium complex with DPC was not achieved; however the cyclised ligand was isolated, highlighting that the oxidation and cyclisation of DPC is important in the coordination chemistry of these ions. Reaction of the sulphur derivative DPTC with various metal ions results in the deprotonation of the ligand to form the monoanionic species, which coordinates the metal ions via the S-donor and azo N-donor atoms. DPTC reacts with  $\text{Hg}^{2+}$  to form the mononuclear complex  $[\text{Hg}(\text{DPTC})_2]$ , coordinating via the N-donor and S-donor atoms. Literature suggests that mixed metal complexes can occur with DPTC, reaction of DPTC with both  $\text{Hg}^{2+}$  and  $\text{Ag}^+$  results in the formation of  $[\text{Hg}_2\text{Ag}_2(\text{DPTC})_4(\text{acetone})_2(\text{ClO}_4)_2]$ . This complex contains two  $\text{Ag}^+$ , two  $\text{Hg}^{2+}$  and four DPTC ligands, it appears that the previous  $[\text{Hg}(\text{DPTC})_2]$  complex is formed first, this then acts as a bidentate ligand, coordinating via the S-donor atom and the  $\text{Hg}^{2+}$  itself to form the final structure. This result contradicts the previous reports by Irving in 1971. Reaction of DPTC with  $\text{Cu}^{2+}$  results in the formation of  $[\text{Cu}_8(\text{DPTC})_8]$ , the  $\text{Cu}^{2+}$  reducing to  $\text{Cu}^+$  and simultaneously the DPTC deprotonates to form the monoanionic form. The self-assembly is templated by the counter-anion, whether it be perchlorate or tetrafluoroborate, the counter-anions sits in the pocket created and templates the  $[\text{Cu}_8(\text{DPTC})_8]$  structure. Without the presence of a counter-anion the resulting structure is  $[\text{Cu}_2(\text{DPTC})_2(\text{DPTCO})]$ , generated from the reaction of DPTC with copper (II) acetate. The structure contains three ligands and two  $\text{Cu}^+$  ions. Two of the ligands present are the monoanionic DPTC, coordinating via the S-donor and terminal N-donor azo atoms. Whereas the third ligand has completely oxidised to form DPTCO, coordinating via both the terminal N-donor azo N-donor atoms, the sulphur atom bridges both of the metal ions.

It has been shown in this thesis that the careful pre-programming of ligands so that they contain all the specific requirements needed for metal ions provides control over the self-assembly process. For example addition of an N-oxide unit into a ligand strand imparts flexibility in the ligand strand so the entropically favoured dimer is produced. The nuclearity of circular helicates is governed by the spacer unit. Two different crystalline materials are formed under the same reaction; the outcome of the self-assembly is a result of the stoichiometry of the reaction and the deprotonation of the  $-\text{OH}$  unit. Circular helicates can be extended to express higher order of complexity by elaborating the basic algorithms for programming structural complexity in linear helicates, to form a head-to-tail tetranuclear circular helicate. Finally the solid state studies of diphenylcarbazide and dithizone has been extended to allow further understanding of these fascinating reagents.

## 7. Experimental

### 7.1 Preparation of L<sup>1</sup>, L<sup>2</sup>, L<sup>3</sup> and L<sup>4</sup>

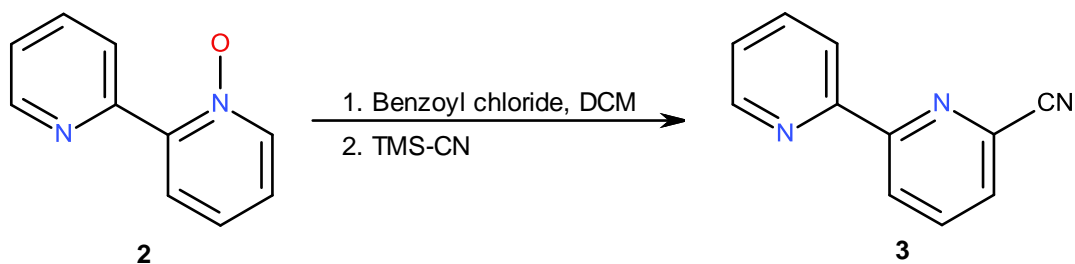
#### 7.1.1 Synthesis of bipyridine 1-N-oxide (2)



The synthesis of bipyridine 1-N-oxide, (**2**) was carried out in a similar manner to the procedure described previously by Rice and co-workers.<sup>127</sup> To a solution of 2,2'-bipyridine (**1**) (1.00 g, 6.4 mmol) in DCM (50 ml), *m*CPBA (77%, 1.44 g, 8.32 mmol) was added slowly over 8 hours whilst spinning at room temperature. The reaction was continually followed by TLC until it was judged that the maximum quantity of the product (**2**) had formed. Upon completion the solvent was removed by rotary evaporation, resulting in a viscous oil containing a mixture of both mono and bis N-oxidised derivatives and also unreacted bipyridine. Purification of the crude product *via* column chromatography (Al<sub>2</sub>O<sub>3</sub>, 1% MeOH in DCM) gave (**2**) as a pale yellow viscous oil (0.89 g, 5.17 mmol, 81%).

<sup>1</sup>H NMR (400 MHz, CDCl<sub>3</sub>) δ (ppm) 8.88 (d, *J* = 8.1, 1H), 8.71 (d, *J* = 4.1, 1H), 8.30 (d, *J* = 6.5, 1H), 8.16 (dd, *J* = 8.0, 1.7, 1H), 7.81 (dt, *J* = 7.8, 1.4 Hz, 1H), 7.34 (m, 2H), 7.26 (m, 1H).

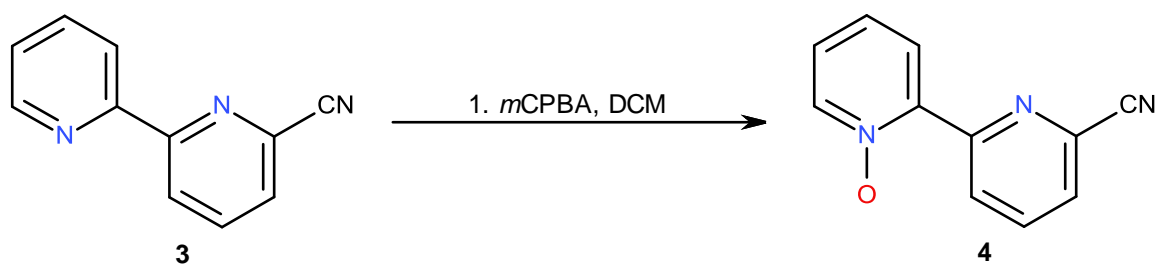
### 7.1.2 Synthesis of 6-cyanitrile-2,2'-bipyridine (**3**)



The synthesis of 6-cyanitrile-2,2'-bipyridine, (**3**) was carried out in a similar manner to the procedure described previously by Rice and co-workers.<sup>127</sup> To a solution of bipyridine 1-N-oxide (**2**) (0.89, 5.17 mmol) in DCM (50 ml) was added benzoyl chloride (1.09 g, 7.75 mmol, 0.90 ml) and trimethylsilyl cyanide (0.77 g, 7.75 mmol, 0.97 ml) and the reaction was refluxed for 12 hours. After cooling the reaction was suspended in  $\text{NaHCO}_3(\text{aq})$  and extracted into DCM, dried with  $\text{MgSO}_4$  and evaporated by rotary-evaporation. The crude product was purified by column chromatography ( $\text{Al}_2\text{O}_3$ , DCM) to give (**3**) as a white solid (0.86 g, 4.75 mmol, 92%).

$^1\text{H}$  NMR (400 MHz,  $\text{CDCl}_3$ )  $\delta$  (ppm) 8.68 (d,  $J = 4.7$ , 1H), 8.66 (d,  $J = 8.2$ , 1H), 8.45 (d,  $J = 8.0$ , 1H), 7.94 (t,  $J = 7.9$ , 1H), 7.85 (dt,  $J = 7.8, 1.7$ , 1H), 7.69 (d,  $J = 7.8$ , 1H), 7.36 (ddd,  $J = 4.8, 1.2$  Hz, 1H).

### 7.1.3 Synthesis of 6'-cyano-2,2'-bipyridine-1-oxide (**4**)

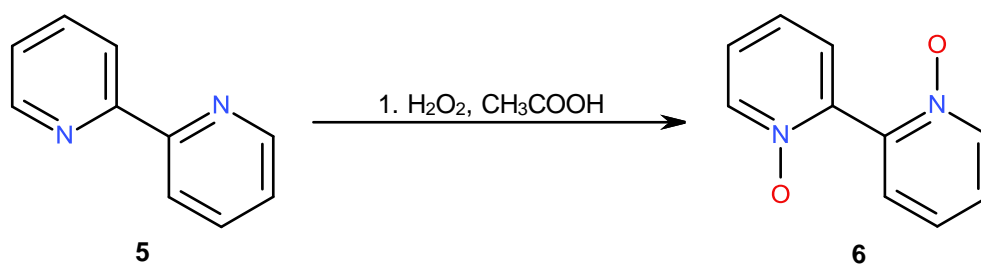


To a solution of 6'-cyano-2,2'-bipyridine (**3**) (0.62g, 3.42 mmol) was added DCM (50 ml) and a slight excess of *m*CPBA (77%, 1.15 g, 5.13 mmol) was added slowly over a period of 2 hours. After complete addition the reaction was allowed to stir at room temperature for 8 hours. After which the solvent was evaporated and the resulting solid was purified by column chromatography ( $\text{Al}_2\text{O}_3$ , 2% MeOH in DCM) to give 6'-cyano-2,2'-bipyridine-1-oxide (**4**) as a white solid (0.66 g, 3.35 mmol, 98%).

$^1\text{H}$  NMR (500 MHz,  $\text{CDCl}_3$ )  $\delta$  (ppm) 9.19 (dd,  $J = 8.3, 1.0$ , 1H), 8.25 (dd,  $J = 6.2, 1.0$ , 1H), 8.20 (dd,  $J = 8.1, 2.3$ , 1H), 7.91 (t,  $J = 7.7$ , 1H), 7.68 (dd,  $J = 7.7, 1.0$ , 1H), 7.35 (dt,  $J = 7.7, 1.0$ , 1H), 7.28 (ddd,  $J = 7.7, 2.3, 1.0$  Hz, 1H).

ESI-MS  $m/z$  220 ( $\text{M} + \text{Na}^+$ ). HR ESI-MS found 220.0480  $\text{C}_{11}\text{H}_7\text{N}_3\text{NaO}$  requires 220.0481 (error = 0.46 ppm).

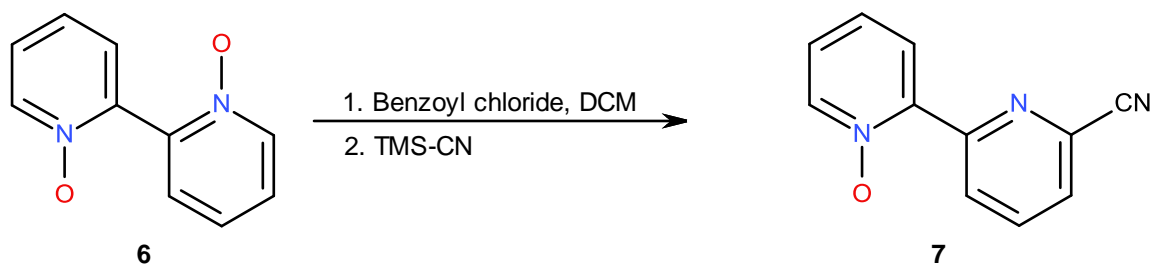
#### 7.1.4 Synthesis of 2,2'-bipyridine-bis-1,1'-oxide (6)



2,2'-bipyridine (**5**) (5.0 g, 32.01 mmol), hydrogen peroxide (5.0 ml, 30%) and glacial acetic acid (50 ml) was heated at 80°C for 3 hours. Hydrogen peroxide (5.0 ml, 30%) was added and the heating continued for another 4 hours. The yellow solution was cooled to room temperature and slowly added to acetone (300 ml). Upon cooling, a white solid of 2,2'-bipyridine-N,N'-dioxide (**6**) precipitated and was collected by filtration, washed with acetone (2 × 10 ml) and air-dried. (5.6 g, 29.76 mmol, 93%).

<sup>1</sup>H NMR (400 MHz, DMSO) δ (ppm) 8.35 (d, *J* = 6.7, 2H), 7.63 (dd, *J* = 7.8, 2.1, 2H), 7.52 (m, 2H), 7.42 (dt, *J* = 7.7, 1.1 Hz, 2H).

### 7.1.5 Synthesis of 6'-cyano-2,2'-bipyridine-1-oxide (4)

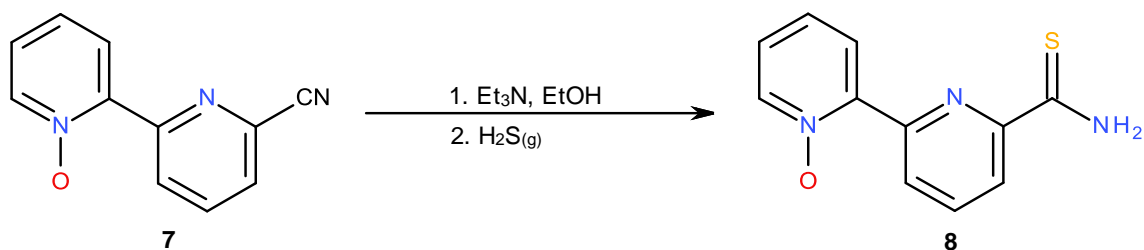


A solution of 2,2'-bipyridine-N,N'-dioxide (**6**) (0.20 g, 1.06 mmol), benzoyl chloride (0.15 g, 1.06 mmol, 0.12 ml) and trimethylsilyl cyanide (0.10 g, 1.06 mmol, 0.13 ml) in DCM (50 ml) was heated under reflux. The reaction was continually monitored by TLC ( $\text{Al}_2\text{O}_3$ , 2% MeOH in DCM) until it was assumed the maximum amount of mono-cyano compound had formed, (between four and six hours). The reaction was then cooled to room temperature, filtered and the solvent was reduced by rotary evaporation. Resulting in a viscose oil containing a mixture of both mono and bis cyanide derivatives and also any unreacted 2,2'-bipyridine-N,N'-dioxide. Purification of the crude product *via* column chromatography ( $\text{Al}_2\text{O}_3$ , 1% MeOH in DCM until first fraction eluted, then 2% MeOH in DCM) gave (**7**) as a sandy solid (0.12 g, 0.61 mmol, 57%).

$^1\text{H}$  NMR (500 MHz,  $\text{CDCl}_3$ )  $\delta$  (ppm) 9.19 (dd,  $J = 8.3, 1.0$ , 1H), 8.25 (dd,  $J = 6.2, 1.0$ , 1H), 8.20 (dd,  $J = 8.1, 2.3$ , 1H), 7.91 (t,  $J = 7.7$ , 1H), 7.68 (dd,  $J = 7.7, 1.0$ , 1H), 7.35 (dt,  $J = 7.7, 1.3$ , 1H), 7.28 (ddd,  $J = 7.7, 2.3, 1.0$  Hz, 1H).

ESI-MS  $m/z$  220 ( $\text{M} + \text{Na}^+$ ). HR ESI-MS found 220.0480  $\text{C}_{11}\text{H}_7\text{N}_3\text{NaO}$  requires 220.0481 (error = 0.46 ppm).

### 7.1.6 Synthesis of 1-N-oxide-2,2'-bipyridine-6'-thioamide (**8**)

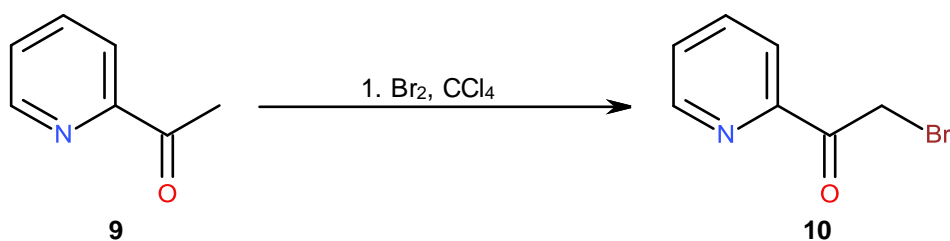


To a solution of the cyano compound (**7**) (0.70 g, 3.55 mmol) in ethanol (20 ml), triethylamine (1.0 g, 9.9 mmol, 1.38 ml) was added and H<sub>2</sub>S was slowly bubbled through the solution for 15 minutes, during which time the solution turned yellow. The yellow solution was allowed to stand for 48 hours during which time a yellow solid slowly precipitated. Collection via filtration gave pure (**8**) as a yellow solid (0.70 g, 3.03 mmol, 85% yield).

<sup>1</sup>H NMR (400 MHz, CDCl<sub>3</sub>) δ (ppm) 9.37 (broad s, 1H, NH), 8.95 (dd, *J* = 7.9, 0.7, 1H), 8.75 (dd, *J* = 7.8, 0.7, 1H), 8.33 (dd, *J* = 7.9, 2.1, 1H), 8.01 (dd, *J* = 8.0, 2.1, 1H), 7.98 (t, *J* = 7.9, 1H), 7.74 (broad s, 1H, NH), 7.38 (dt, *J* = 7.6, 1.2, 1H), 7.32 (dt, *J* = 7.5, 2.2 Hz, 1H).

ESI-MS *m/z* 254 (M + Na<sup>+</sup>). HR ESI-MS found 254.0371 C<sub>11</sub>H<sub>9</sub>N<sub>3</sub>NaOS requires 254.0359 (error = -4.79 ppm).

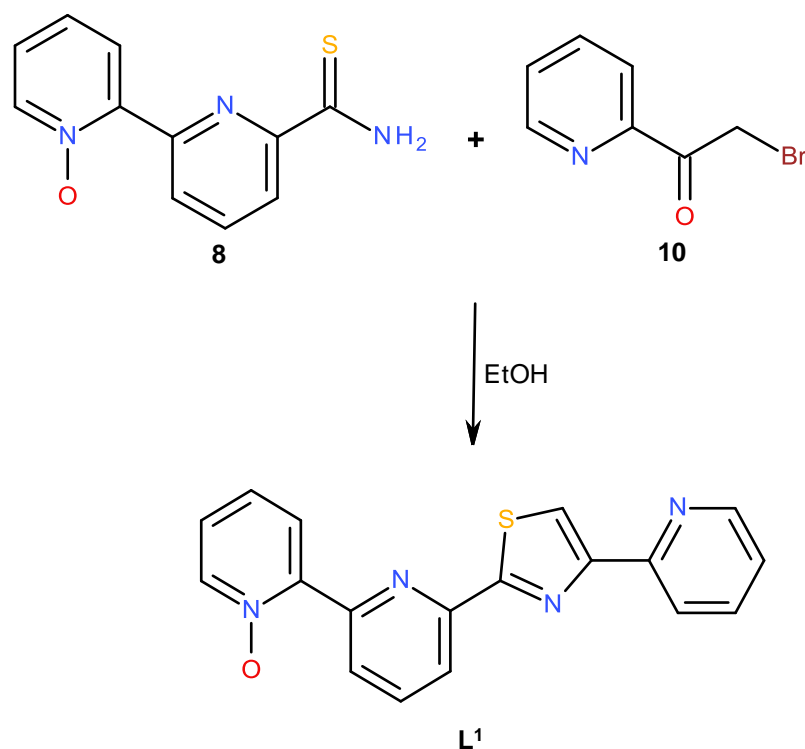
### 7.1.7 Synthesis of 2-( $\alpha$ -bromoacetyl)pyridine (**10**)



The synthesis of 2-( $\alpha$ -bromoacetyl)pyridine (**10**) was carried out in a similar manner to the procedure described previously by Rice and co-workers.<sup>128</sup> A solution of 2-acetylpyridine (**9**) (5.4 g, 44.58 mmol, 5 ml) in  $\text{CCl}_4$  (40 ml) was heated at 80 °C. To this was added a solution of  $\text{Br}_2$  (7.1 g, 44.58 mmol, 2.5 ml) in 20 ml  $\text{CCl}_4$ , using a pressure equalising dropping funnel, over 5 hours. After complete addition the reaction was allowed to heat for a further 30 minutes, during which time a precipitate formed, this was filtered via vacuum and washed with  $\text{Et}_2\text{O}$  (2  $\times$  5 ml). The resulting hydrobromide salt was partitioned between  $\text{NaHCO}_{3(\text{aq})}$  and DCM, separation of the organic layer, drying and evaporation gave the crude product. Purified by column chromatography ( $\text{SiO}_2$ , DCM) gave 2-( $\alpha$ -bromoacetyl)pyridine (**10**) as a light brown oil (8.0 g, 39.99 mmol, 89%).

$^1\text{H}$  NMR (400 MHz,  $\text{CDCl}_3$ )  $\delta$  (ppm) 8.69 (d,  $J = 4.7$ , 1H), 8.09 (d,  $J = 7.8$ , 1H), 7.89 (dt,  $J = 7.7$ , 1.9, 1H), 7.54 (d,  $J = 4.9$ , 2.0 Hz, 1H), 4.88 (s, 2H,  $-\text{CH}_2\text{Br}$ ).

### 7.1.8 Synthesis of L<sup>1</sup>

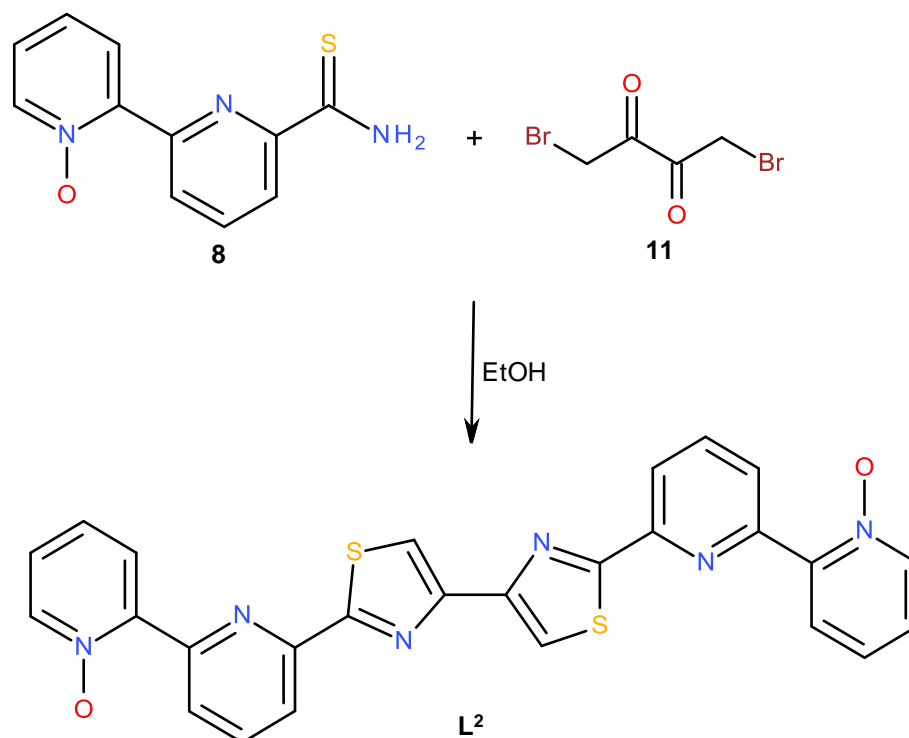


To a suspension of 1-*N*-oxide-2,2'-bipyridine-6'-thioamide (**8**) (0.1 g, 0.43 mmol) in EtOH (20 ml) was added 2-(α-bromoacetyl)pyridine (**10**) (0.11 g, 0.52 mmol) and the reaction was refluxed for 8 hours, during which time all the reactants dissolved. The reaction was allowed to stand at room temperature for 12 hours and the resulting precipitate was filtered and washed with EtOH (2 × 2 ml) and Et<sub>2</sub>O (2 × 2 ml) to give L<sup>1</sup>·HBr. The hydrobromide salt was then suspended in concentrated ammonia (10 ml) for 12 hours, filtered and washed with H<sub>2</sub>O (2 × 2 ml), EtOH (2 × 2 ml) and Et<sub>2</sub>O (2 × 2 ml) giving L<sup>1</sup> as a pale yellow solid (0.081 g, 0.24 mmol, 57%).

<sup>1</sup>H NMR (400 MHz, DMSO) δ (ppm) 8.86 (d, *J* = 7.8, 1H, py), 8.68 (d, *J* = 4.3, 1H, py), 8.47 (s, 1H, tz), 8.44 (d, *J* = 5.6, 1H, py), 8.36 (d, *J* = 7.8, 1H, py), 8.26-8.16 (m, overlapping, 3H, py), 7.98 (t, *J* = 7.7 Hz, 1H, py), 7.57-7.56 (m, overlapping, 2H, py), 7.42 (m, overlapping, 1H, py).

ESI-MS *m/z* 333 (M + H<sup>+</sup>). Found C, 64.7; H, 3.8; N, 16.5%; C<sub>18</sub>H<sub>12</sub>N<sub>4</sub>OS requires C, 65.0; H, 3.6; N, 16.9%.

### 7.1.9 Synthesis of $L^2$

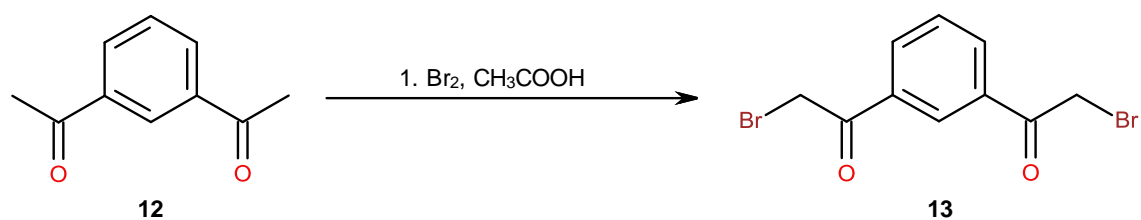


To a round bottomed flask charged with 1-*N*-oxide-2,2'-bipyridine-6'-thioamide (**8**) (0.1 g, 0.43 mmol) and 1,4-dibromo-2,3-dione (**11**)<sup>114</sup> (0.053 g, 0.22 mmol) was added EtOH (25 ml) and the reaction was refluxed for 12 hours, after which time a precipitate formed. Filtration under vacuum followed by washing with EtOH (2 × 2 ml) and Et<sub>2</sub>O (2 × 2 ml) gave  $L^2 \cdot HBr$ . Suspension in concentrated ammonia for 12 hours, followed by filtration and washing with H<sub>2</sub>O (2 × 2 ml), EtOH (2 × 2 ml) and Et<sub>2</sub>O (2 × 2 ml) gave  $L^2$  as pale yellow solid (0.087 g, 0.17 mmol, 78%).

<sup>1</sup>H NMR was inconclusive as the solubility of the ligand was very poor, even in d<sup>6</sup>-DMSO at 80 °C.

ESI-MS *m/z* 509 (M + H<sup>+</sup>). Found C, 61.6; H, 3.5; N, 16.0%; C<sub>26</sub>H<sub>16</sub>N<sub>6</sub>O<sub>2</sub>S<sub>2</sub> requires C, 61.4; H, 3.2; N, 16.5%.

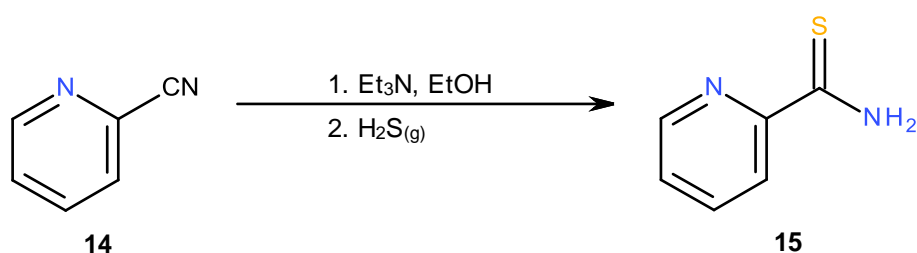
### 7.1.10 Synthesis of 1,3-di( $\alpha$ -bromoacetyl)benzene (**13**)



The synthesis of 1,3-di( $\alpha$ -bromoacetyl)benzene (**13**) was carried out in a similar manner to the procedure described previously by Rice and co-workers.<sup>109</sup> To a solution of 1,3-diacetylbenzene (**12**) (0.25 g, 1.54 mmol) in CHCl<sub>3</sub> (20 ml) at 80 °C, Br<sub>2</sub> (0.49 g, 3.08 mmol, 0.16 ml) in 1 ml CHCl<sub>3</sub> was added dropwise, continuously and consistently. The reaction was continually monitored by TLC (SiO<sub>2</sub>, 1% MeOH in DCM) until it was assumed the maximum amount of di-bromo compound had formed, cooled to room temperature and the solvent removed by rotary evaporation. The crude product containing mono, di, tri and tetra brominated species was purified by column chromatography (SiO<sub>2</sub>, DCM) to give 1,3-diacetylbenzene (**13**) as a yellow solid (0.20 g, 0.63 mmol, 41%).

<sup>1</sup>H NMR (400 MHz, CDCl<sub>3</sub>)  $\delta$  (ppm) 8.61 (s, 1H, phy), 8.26 (dd,  $J$  = 7.8, 1.8, 2H, phy), 7.69 (t,  $J$  = 7.7, 1H, phy), 4.51 (s, 4H, -CH<sub>2</sub>Br).

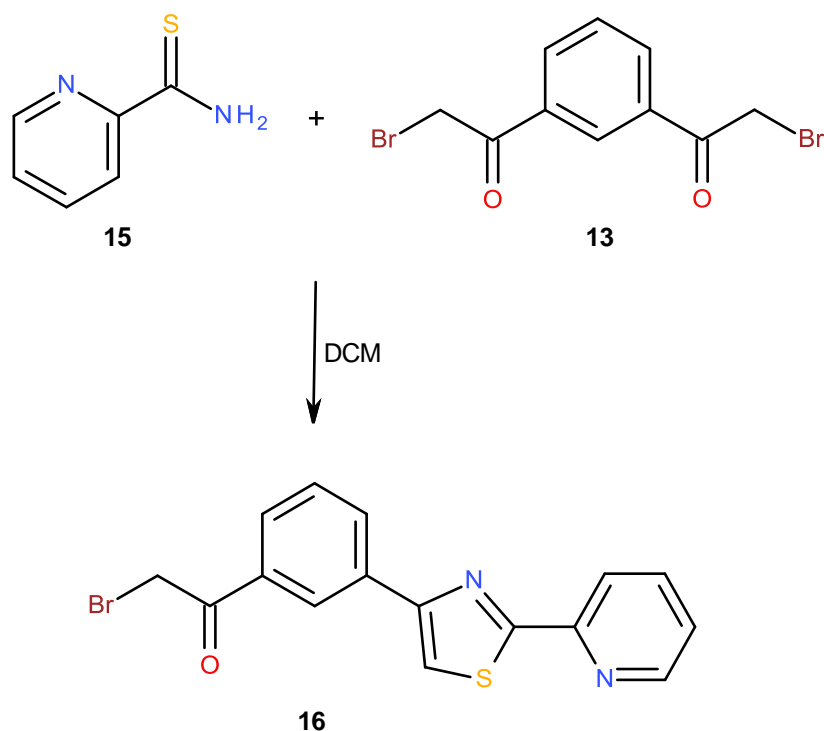
### 7.1.11 Synthesis of 2-pyridine thioamide (15)



The synthesis of 2'-pyridine thioamide (**15**) was carried out in a similar manner to the previous procedure described by Rice and co-workers.<sup>127</sup> To a solution of 2'-pyridinecarbonitrile (**14**) (1.00 g, 9.61 mmol) in ethanol (20 ml), triethylamine (1.0 g, 12.18 mmol, 1.7 ml) was added and H<sub>2</sub>S was slowly bubbled through the solution for 15 minutes, during which time the solution turned yellow. The yellow solution was allowed to stand for 24 hours during which time a yellow solid slowly precipitated. Collection via filtration gave pure 2'-pyridine thioamide (**15**) as a yellow solid (1.2 g, 8.68 mmol, 92 %).

<sup>1</sup>H NMR (400 MHz, CDCl<sub>3</sub>) δ (ppm) 9.52 (broad s, 1H, -NH), 8.69 (d, *J* = 8.0, 1H), 8.51 (d, *J* = 4.3, 1H), 7.83 (dt, *J* = 7.7, 1.7, 1H), 7.79 (broad s, 1H, NH), 7.44 (ddd, *J* = 7.4, 4.8, 1.1 Hz, 1H).

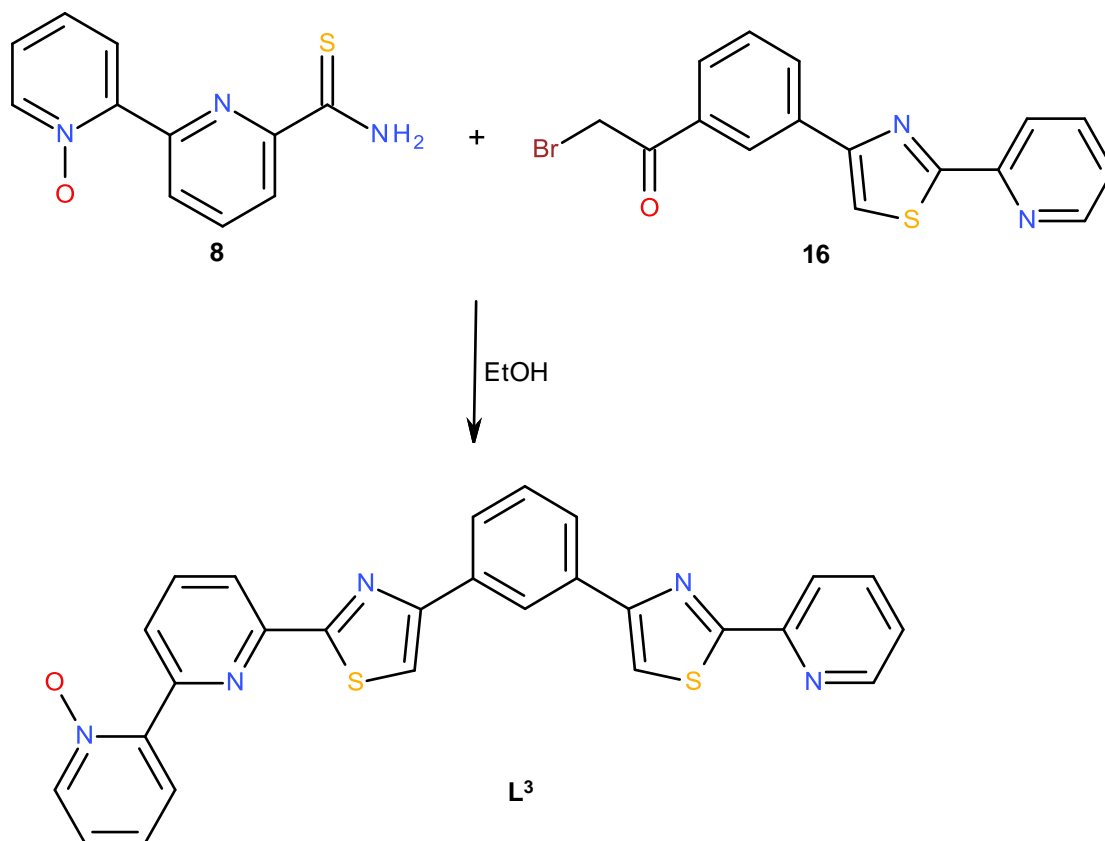
### 7.1.12 Synthesis of py-tz-phy bidentate bromoacetyl (**16**)



The synthesis of (**16**) was carried out in a similar manner to the procedure described previously by Rice and co-workers.<sup>110</sup> To a solution of 1,3-di( $\alpha$ -bromoacetyl)benzene (**13**) (0.15 g, 0.47 mmol) in DCM (15 ml), was added drop wise a solution of pyridine-2-thioamide (**15**) (0.065 g, 0.47 mmol) in DCM (5 ml) and the reaction was stirred at room temperature for 24 hours. The resulting precipitate was isolated by filtration, suspended in NaHCO<sub>3(aq)</sub> and extracted into DCM. Purification by column chromatography (SiO<sub>2</sub>, 1 % MeOH in DCM) giving the mono-pyridyl-thiazole (**16**) as a yellow solid (0.11 g, 0.31 mmol, 66%).

<sup>1</sup>H NMR (500 MHz, CDCl<sub>3</sub>)  $\delta$  (ppm) 8.66 (d,  $J$  = 4.8, 1H, py), 8.64 (s, 1H, phy), 8.37 (d,  $J$  = 7.9, 1H, py), 8.26 (d,  $J$  = 7.9, 1H, phy), 7.99 (d,  $J$  = 7.8, 1H, phy), 7.87 (dt,  $J$  = 7.7, 1.7, 1H, py), 7.73 (s, 1H, tz), 7.61 (t,  $J$  = 7.8, 1H, phy), 7.38 (ddd,  $J$  = 4.8, 1.1 Hz, 1H, py), 4.57 (s, 2H, -CH<sub>2</sub>Br).

### 7.1.13 Synthesis of $L^3$

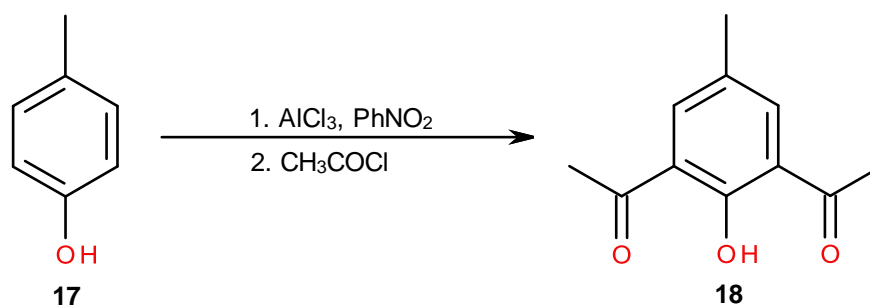


Reaction of (**16**) (0.10 g, 0.28 mmol) with 1-N-oxide-2,2'-bipyridine-6'-thioamide (**8**) (0.077 g, 0.33 mmol) in EtOH (25 ml) at reflux for 8 hours results in a yellow precipitate which was isolated by filtration, washed with EtOH (2 × 2 ml) and Et<sub>2</sub>O (2 × 2 ml). Suspension in concentrated NH<sub>3</sub> (10 ml) followed by filtration and washing with H<sub>2</sub>O (2 × 2 ml), EtOH (2 × 2 ml) and Et<sub>2</sub>O (2 × 2 ml) gave the ligand  $L^3$  as a yellow solid (0.056 g, 0.11 mmol, 41%).

<sup>1</sup>H NMR (500 MHz, DMSO) δ (ppm) 8.86 (d, *J* = 7.9, 1H, py), 8.75 (s, 1H, phy), 8.68 (d, *J* = 4.8, 1H, py), 8.49 (s, 1H, tz), 8.46-8.42 (m, overlapping, 3H), 8.35 (d, *J* = 7.8, 1H, py), 8.23 (dd, *J* = 9.1, 2.4, 1H, py), 8.20 (t, *J* = 7.8, 1H, py), 8.13-8.09 (m, overlapping, 3H), 8.04 (dt, *J* = 7.7, 1.6, 1H, py), 7.63 (t, *J* = 7.8 Hz, 1H, phy), 7.60-7.55 (m, overlapping, 2H).

ESI-MS *m/z* 492 (M + H<sup>+</sup>). Found C, 66.4; H, 3.6; N, 13.9%; C<sub>27</sub>H<sub>17</sub>N<sub>5</sub>OS<sub>2</sub> requires C, 66.0; H, 3.5; N, 14.2%.

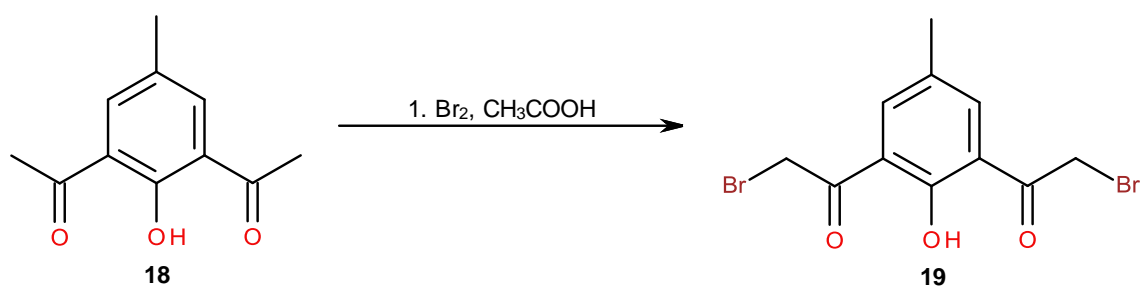
### 7.1.14 Synthesis of 1,3-diacetyl cresol (**18**)



The synthesis of 1,3-diacetyl cresol (**18**) was carried out in a similar manner to the procedure described previously by Mandal & Nag in 1983.<sup>129</sup> To a solution of *p*-cresol (4.0 g, 36.99 mmol) in nitrobenzene (60 ml) at 0 °C, AlCl<sub>3</sub> (28.0 g, 0.21 mmol) was added to the mixture whilst stirring, after addition the solution was allowed to stir for a further 10 minutes. To this acetyl chloride (7.71 g, 98.17 mmol, 6.98 ml) was added dropwise whilst maintaining the temperature at 0 °C, after this time the solution was heated to 80 °C for 3 hours. After cooling to room temperature the reaction was poured onto ice and HCl (12 M, 10 ml) and the solution was left to warm up to room temperature for 30 minutes. The reaction was separated from the aqueous layer by extraction; DCM (2 × 20 ml) was added to the reaction to enhance the separation. The organic layer was removed by steam distillation on the rotary evaporator; H<sub>2</sub>O (3 × 50 ml) was added to aid this process. The product was re-crystallised from hexane giving 1,3-diacetyl cresol (**18**) as a pale brown solid which was isolated by filtration (2.8 g, 14.57 mmol, 40%).

<sup>1</sup>H NMR (400 MHz, CDCl<sub>3</sub>) δ (ppm) 13.12 (s, 1H, OH), 7.77 (s, 2H, pho), 2.67 (s, 6H, -OCH<sub>3</sub>) 2.32 (s, 3H, -CH<sub>3</sub>).

### 7.1.15 Synthesis of 1,3-( $\alpha$ -bromoacetyl)cresol (**19**)

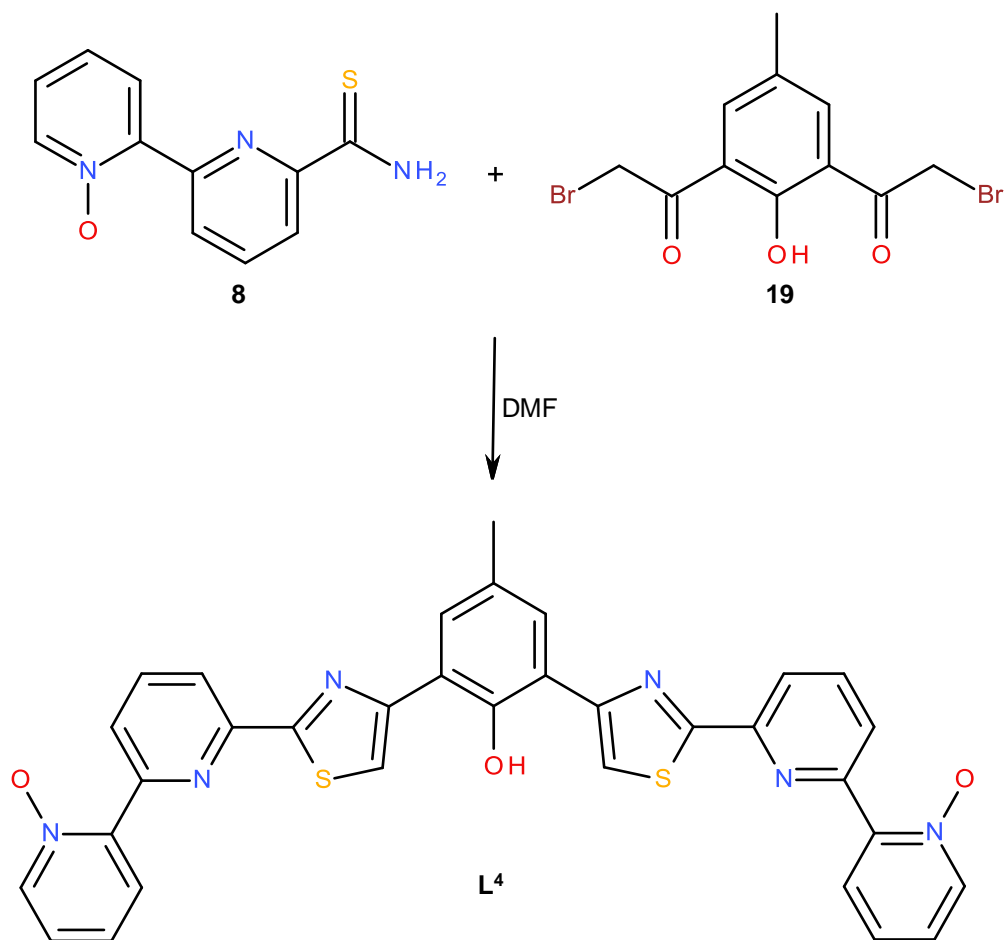


1,3-diacetyl cresol (**18**) (0.50 g, 2.60 mmol) was suspended in concentrated acetic acid (20 ml) and heated to 80 °C. Once the solution had reached the appropriate temperature  $\text{Br}_2$  (0.83 g, 5.20 mmol, 0.27 ml) in 1 ml acetic acid was added dropwise, continuously and consistently. The reaction was continually monitored by TLC ( $\text{SiO}_2$ , 1% hexane in DCM) until it was assumed the maximum amount of di-bromo compound had formed, cooled to room temperature and solvent removed by rotary evaporation. The crude product containing mono, di, tri and tetra brominated species was purified by column chromatography ( $\text{SiO}_2$ , 1% hexane in DCM) to give 1,3-( $\alpha$ -bromoacetyl)cresol (**19**) as a yellow solid (0.47 g, 1.34 mmol, 52%).

$^1\text{H}$  NMR (400 MHz,  $\text{CDCl}_3$ )  $\delta$  (ppm) 12.75 (s, 1H, OH), 7.86 (s, 2H, pho), 4.57 (s, 4H, - $\text{CH}_2\text{Br}$ ), 2.38 (s, 3H, - $\text{CH}_3$ ).

ESI-MS  $m/z$  372 ( $\text{M} + \text{Na}^+$ ). HR ESI-MS found 370.8889  $\text{C}_{11}\text{H}_{10}\text{Br}_2\text{NaO}_3$  requires 370.8889 (error = -0.07 ppm).

### 7.1.16 Synthesis of L<sup>4</sup>



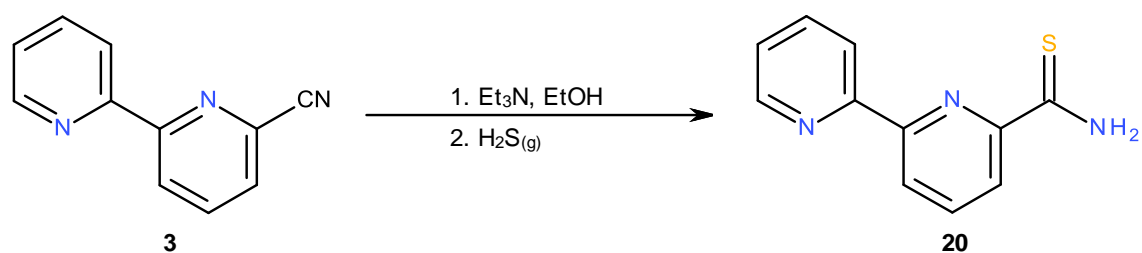
To a suspension of 1-*N*-oxide-2,2'-bipyridine-6'-thioamide (**8**) (0.1 g, 0.43 mmol) in DMF (10 ml) was added 1,3-( $\alpha$ -bromoacetyl)cresol (**19**) (0.076 g, 0.22 mmol) and the reaction heated at 80 °C for 12 hours. The reaction was allowed to cool to room temperature, the resulting precipitate was filtered and washed with EtOH (2  $\times$  2 ml) and Et<sub>2</sub>O (2  $\times$  2 ml) to give L<sup>4</sup>·HBr. The hydrobromide salt was suspended in concentrated ammonia (10 ml) for 12 hours, followed by filtration and washing with H<sub>2</sub>O (2  $\times$  2 ml), EtOH (2  $\times$  2 ml) and Et<sub>2</sub>O (2  $\times$  2 ml) gave L<sup>4</sup> as pale yellow solid (0.065 g, 0.11 mmol, 49%).

<sup>1</sup>H NMR was inconclusive as the solubility of the ligand was very poor, even in d<sup>6</sup>-DMSO at 80 °C.

ESI-MS *m/z* 616 (M + H<sup>+</sup>). Found C, 64.8; H, 3.9; N, 13.2%; C<sub>33</sub>H<sub>22</sub>N<sub>6</sub>O<sub>3</sub>S<sub>2</sub> requires C, 64.5; H, 3.6; N, 13.7%.

## 7.2 Preparation of L<sup>5</sup>, L<sup>6</sup> and L<sup>7</sup>

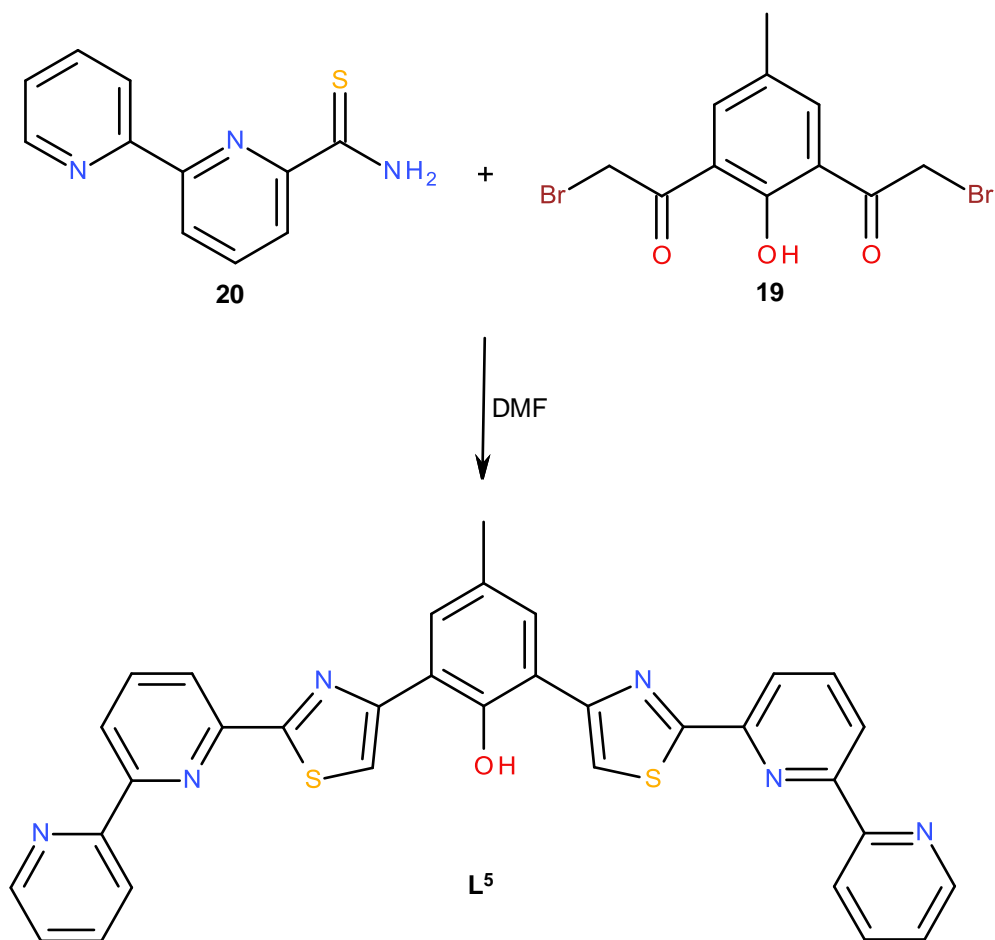
### 7.2.1 Synthesis of 2,2'-bipyridine thioamide (**20**)



The synthesis of 2,2'-bipyridine thioamide (**20**) was carried out in a similar manner to the previous procedure described by Rice and co-workers.<sup>127</sup> To a solution of 2,2'-bipyridine-6-carbonitrile (**3**) (0.70 g, 3.86 mmol) in ethanol (20 ml), triethylamine (1.2 g, 9.90 mmol, 1.7 ml) was added and H<sub>2</sub>S was slowly bubbled through the solution for 15 minutes, during which time the solution turned yellow. The yellow solution was allowed to stand for 24 hours during which time a yellow solid slowly precipitated. Collection via filtration gave pure 2,2'-bipyridine thioamide (**20**) as a yellow solid (0.7 g, 3.26 mmol, 84 %).

<sup>1</sup>H NMR (400 MHz, CDCl<sub>3</sub>) δ (ppm) 9.59 (broad s, 1H, NH), 8.73 (d, *J* = 7.8, 1H), 8.70 (d, *J* = 4.7, 1H), 8.58 (d, *J* = 7.9, 1H), 8.33 (d, *J* = 7.9, 1H), 7.98 (t, *J* = 7.9, 1H), 7.90 (broad s, 1H, NH), 7.83 (dt, *J* = 7.7, 1.8, 1H), 7.35 (ddd, *J* = 7.5, 4.8, 0.9 Hz, 1H).

### 7.2.2 Synthesis of $L^5$

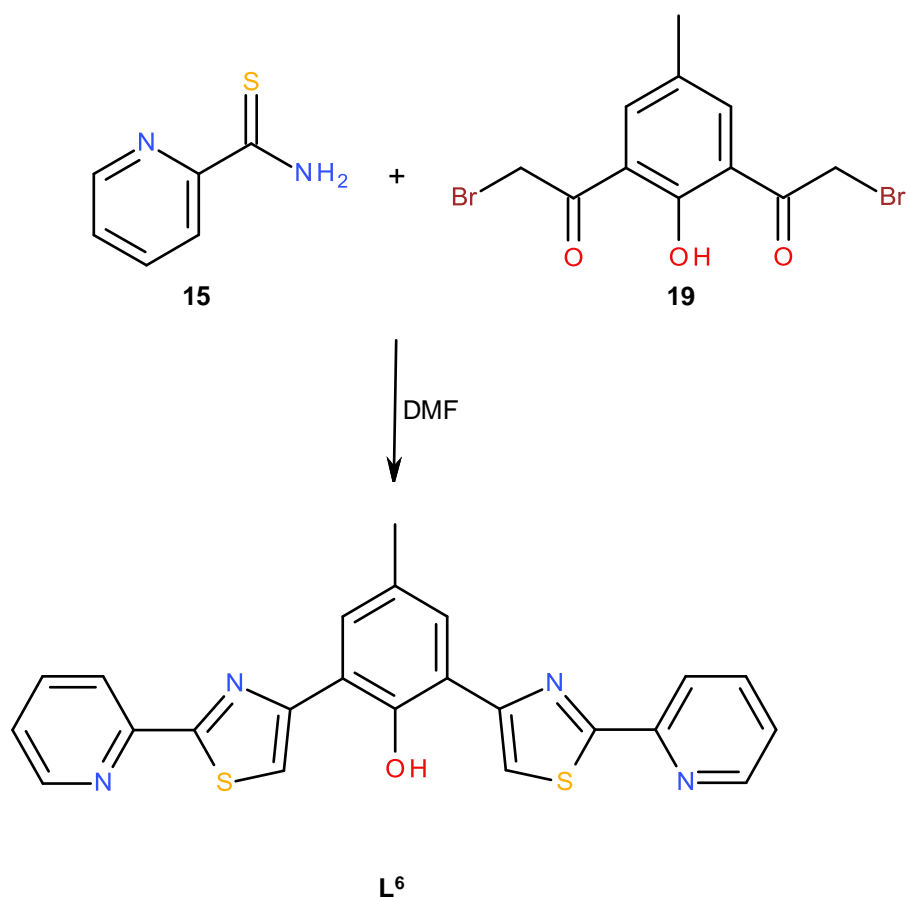


The synthesis of ligand  $L^5$  was carried out in a similar manner to the previous procedure described by Rice and co-workers.<sup>130</sup> To a suspension of 2,2'-bipyridine thioamide (**20**) (0.20 g, 0.94 mmol) in DMF (10 ml) was added 1,3-( $\alpha$ -bromoacetyl)cresol (**19**) (0.15 g, 0.43 mmol) and the reaction heated at 80 °C for 24 hours. The reaction was allowed to cool to room temperature, the resulting precipitate was filtered and washed with EtOH (2  $\times$  2 ml) and Et<sub>2</sub>O (2  $\times$  2 ml) to give  $L^5 \cdot HBr$ . The hydrobromide salt was then suspended in concentrated ammonia (10 ml) for 12 hours, followed by filtration and washing with H<sub>2</sub>O (2  $\times$  2 ml), EtOH (2  $\times$  2 ml) and Et<sub>2</sub>O (2  $\times$  2 ml) gave  $L^5$  as pale yellow solid (0.21 g, 0.36 mmol, 84 %).

<sup>1</sup>H NMR (500 MHz, DMSO)  $\delta$  (ppm) <sup>1</sup>H NMR (500 MHz, CDCl<sub>3</sub>)  $\delta$  12.33 (s, 1H, OH), 8.77 (m, 2H), 8.53 (m, 4H), 8.51 (s, 2H, tz), 8.34 (dd,  $J = 7.7$ , 2H), 8.21 (t,  $J = 7.7$ , 2H), 8.07 (dt,  $J = 7.7$ , 1.8, 2H), 8.02 (s, 2H, pho), 7.54 (ddd,  $J = 7.5$ , 4.8, 1.2 Hz, 2H), 2.41 (s, 3H, CH<sub>3</sub>).

ESI-MS  $m/z$  583 (M + H<sup>+</sup>).

### 7.2.3 Synthesis of **L**<sup>6</sup>

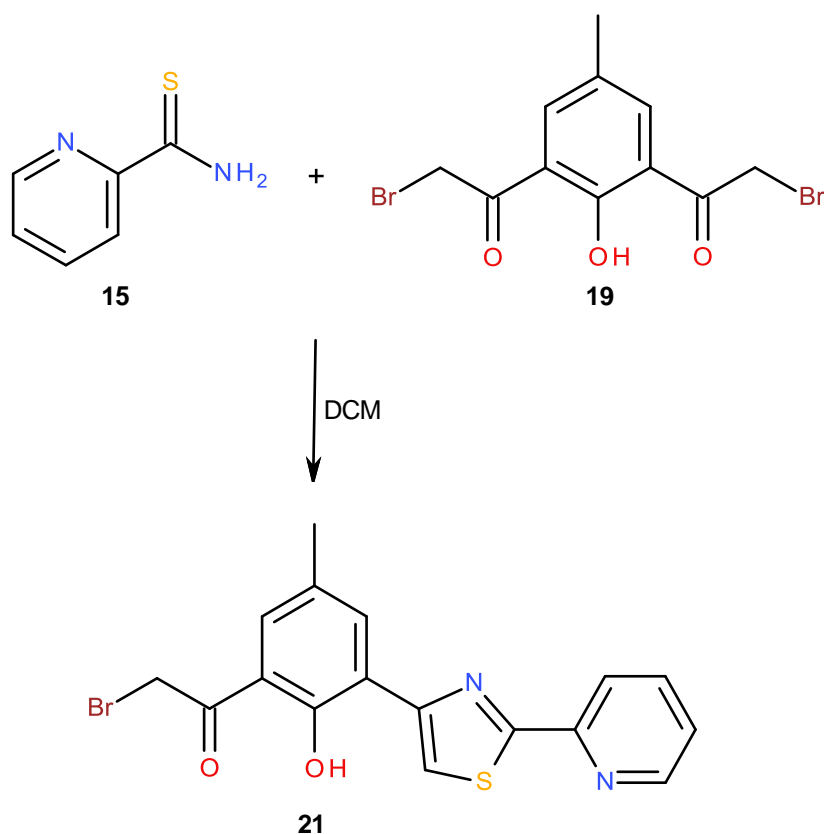


The synthesis of ligand **L**<sup>6</sup> was carried out in a similar manner to the previous procedure described by Rice and co-workers.<sup>109</sup> To a round bottom flask charged with pyridine-2-thioamide (**15**) (0.16 g, 1.16 mmol) and 1,3-di(α-bromoacetyl)phenol (**19**) (0.18 g, 0.51 mmol) was added EtOH (25 ml) and the reaction was heated in an oil bath at 80 °C (8 hrs), during which time a precipitate formed. This was filtered and washed with EtOH (2 x 2 ml) and Et<sub>2</sub>O (2 x 2 ml) and suspended in concentrated NH<sub>3</sub> (24 hrs). Filtration followed by washing with H<sub>2</sub>O (2 x 2 ml), EtOH (2 x 2 ml) and Et<sub>2</sub>O (2 x 2 ml) gave **L**<sup>6</sup> as a cream solid (0.16 g, 0.37 mmol, 72 %).

<sup>1</sup>H NMR (400 MHz, DMSO) δ (ppm) 12.46 (s, 1H, OH), 8.69 (d, *J* = 4.7, 2H), 8.47 (s, 2H, tz), 8.27 (d, *J* = 7.9, 2H), 8.05 (dt, *J* = 7.7, 1.6 Hz, 2H), 7.98 (s, 2H, pho), 7.56 (m, 2H), 2.41 (s, 3H, CH<sub>3</sub>).

ESI-MS *m/z* 429 (M + H<sup>+</sup>).

#### 7.2.4 Preparation of **L**<sup>7</sup>

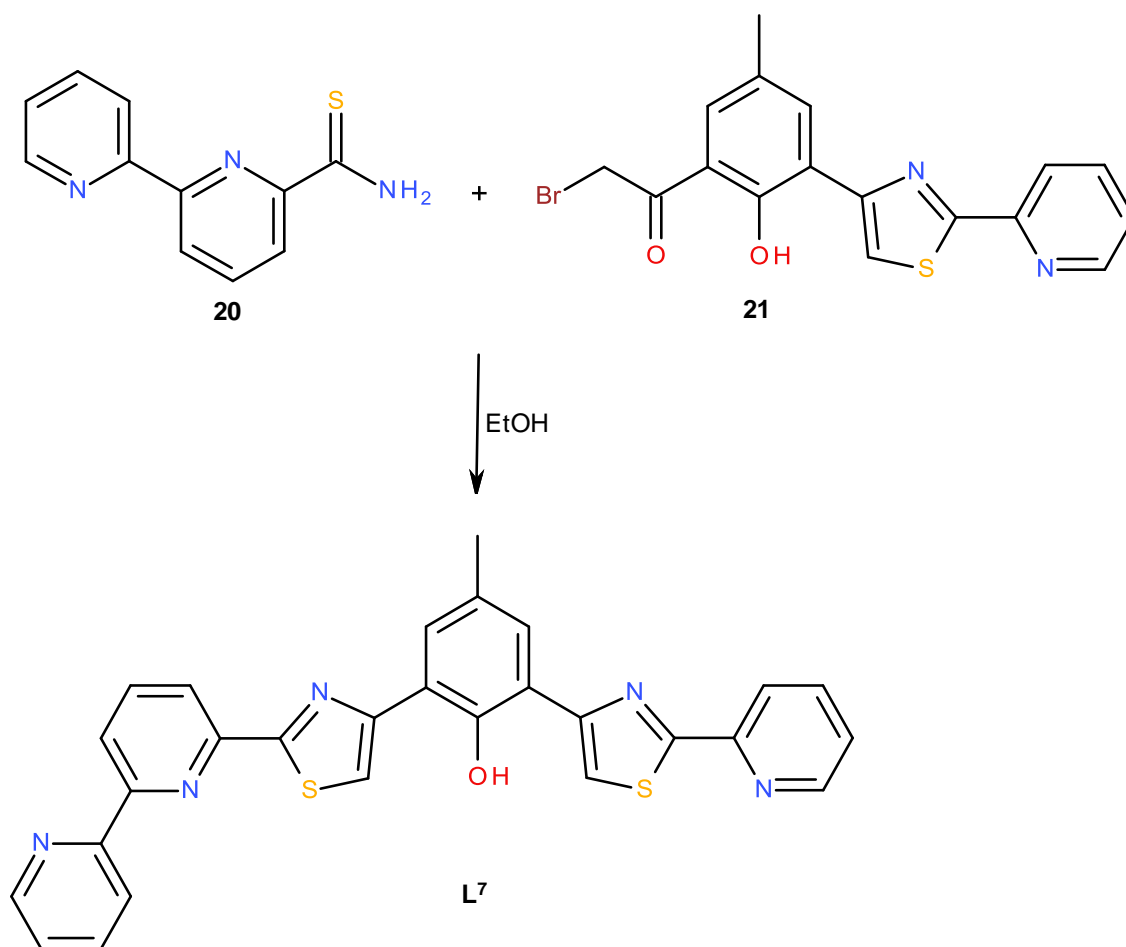


The preparation of ligand **L**<sup>7</sup> was carried out in a similar manner to the previous procedure described by Rice and co-workers.<sup>110</sup> To a solution of 1,3-di(α-bromoacetyl)phenol (**19**) (0.25 g, 0.71 mmol) in DCM (15 ml), was added drop wise a solution of pyridine-2-thioamide (**15**) (0.99 g, 0.71 mmol) in DCM (5 ml) and the reaction was stirred at room temperature for 24 hours. The resulting precipitate was isolated by filtration, suspended in NaHCO<sub>3(aq)</sub> and extracted into DCM. Purification by column chromatography (SiO<sub>2</sub>, 1 % MeOH in DCM) giving the mono-pyridyl-thiazole (**21**) as a yellow solid (0.22 g, 0.57 mmol, 79 %).

<sup>1</sup>H NMR (400 MHz, CDCl<sub>3</sub>) δ (ppm) 12.73 (s, 1H, OH), 8.64 (d, *J* = 4.5, 1H), 8.31 (s, 1H, tz), 8.28 (d, *J* = 7.8, py, 1H), 8.15 (s, 1H, pho), 7.84 (dt, *J* = 7.8, 1.5, 1H), 7.56 (d, *J* = 1.5 Hz, 1H, pho), 7.35 (m, 1H), 4.59 (s, 2H, CH<sub>2</sub>Br), 2.41 (s, 3H, CH<sub>3</sub>).

ESI-MS *m/z* 390 (M + H<sup>+</sup>).

### 7.2.5 Synthesis of $L^7$



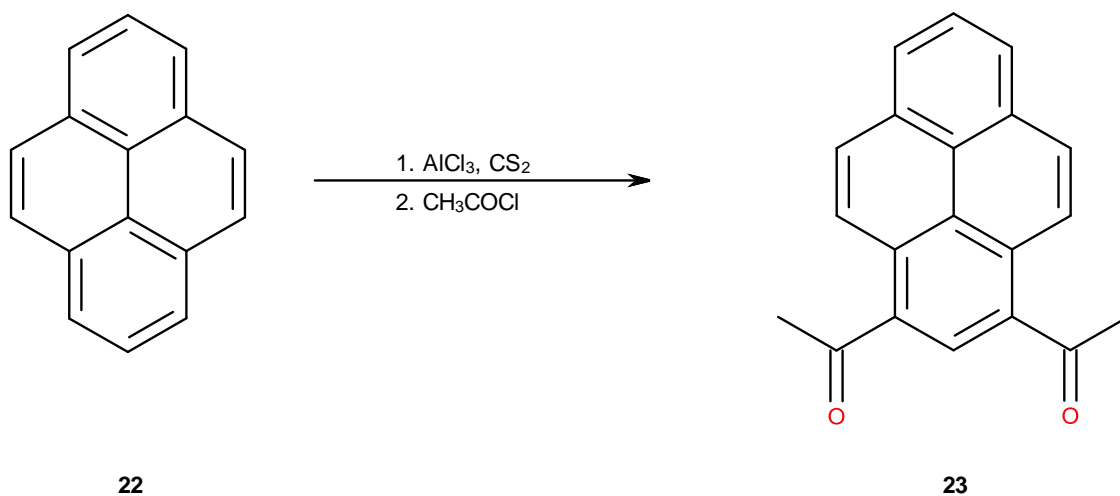
Reaction of (**21**) (0.22 g, 0.57 mmol) with 2,2'-bipyridine thioamide (**20**) (0.12 g, 0.57 mmol) in EtOH (25 ml) heated at 80°C for 48 hours results in a yellow precipitate which was isolated by filtration, washed with EtOH (2 × 2 ml) and Et<sub>2</sub>O (2 × 2 ml). Suspension for 24 hours of the hydrobromide salt in concentrated NH<sub>3</sub> (10 ml) followed by filtration and washing with H<sub>2</sub>O (2 × 2 ml), EtOH (2 × 2 ml) and Et<sub>2</sub>O (2 × 2 ml) gave the ligand  $L^7$  as a yellow solid (0.20 g, 0.40 mmol, 71 %).

<sup>1</sup>H NMR (500 MHz, DMSO) δ (ppm) 12.49 (s, 1H, OH), 8.75 (d, *J* = 4.7, py, 1H), 8.69 (d, *J* = 4.7, py, 1H), 8.52 (s, 1H, tz), 8.50 (m, py, 2H), 8.47 (s, 1H, tz), 8.31 (dd, *J* = 7.8, 0.9, py, 1H), 8.26 (dd, *J* = 7.8, 0.9, py, 1H), 8.19 (t, *J* = 7.3, py, 1H), 8.06 (dt, *J* = 7.7, 3.9, py, 1H), 8.04 (dt, *J* = 7.7, 3.8, py, 1H), 8.01 (d, *J* = 1.7, pho, 1H), 7.96 (d, *J* = 1.7, pho, 1H), 7.55 (ddd, *J* = 7.6, 3.8, 1.1, py, 1H), 7.53 (ddd, *J* = 7.7, 3.9, 1.1 Hz, py, 1H), 2.42 (s, 1H, CH<sub>3</sub>).

ESI-MS *m/z* 506 (M + H<sup>+</sup>).

## 7.3 Preparation of L<sup>8</sup>

### 7.3.1 Synthesis of 1,3-diacetyl pyrene (23)

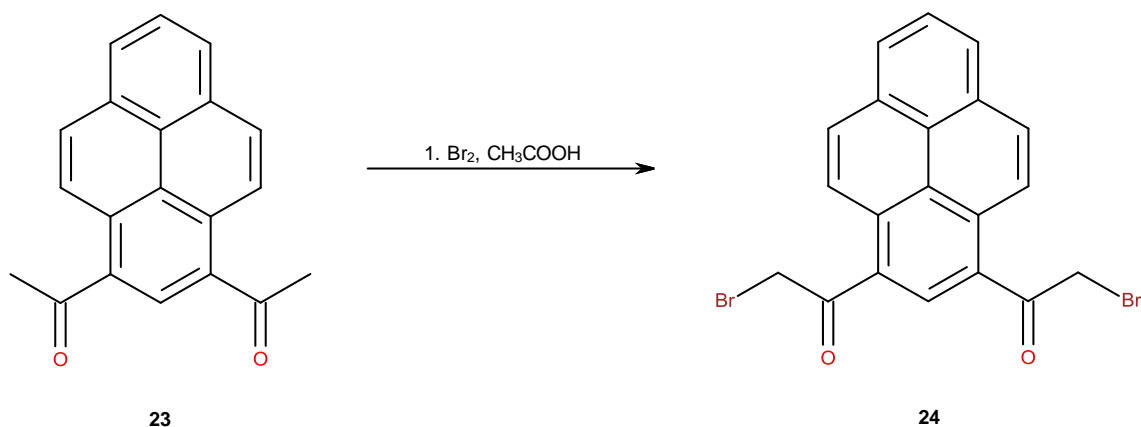


The synthesis of 1,3-diacetyl pyrene (**23**) was carried out in a similar manner to the procedure described by Harvey and co-workers.<sup>136, 137</sup>

To a solution of pyrene (**22**) (2.5 g, 12.36 mmol) in carbon disulfide (75 ml) at 0°C was added AlCl<sub>3</sub> (10.01 g, 75.07 mmol) whilst stirring, after addition the solution was allowed to stir for a further 15 minutes. To this CH<sub>3</sub>COCl (4.28 g, 53.84 mmol) was added drop wise at 0°C, after which time the solution was heated to 60°C for 2 hours. After cooling to room temperature, ice (10 g) and HCl (12 M, 20 ml) was added, the resulting yellow precipitate was then removed by filtration, washed with CS<sub>2</sub> (30 ml) and H<sub>2</sub>O (2 × 30 ml). After drying for 48 hours in the desiccator the solid was purified by column chromatography (SiO<sub>2</sub>, DCM) giving 1,3-diacetyl pyrene (**23**) as a yellow solid (0.12 g, 0.42 mmol, 3.4 %).

<sup>1</sup>H NMR (400 MHz, CDCl<sub>3</sub>) δ (ppm) 8.98 (d, *J* = 9.4, 2H), 8.69 (s, 1H), 8.32 (d, *J* = 7.6, 2H), 8.30 (d, *J* = 9.4, 2H), 8.11 (t, *J* = 7.6 Hz, 1H), 2.94 (s, 6H, CH<sub>3</sub>).

### 7.3.2 Synthesis of 1,3-dibromo-diacetyl pyrene (24)

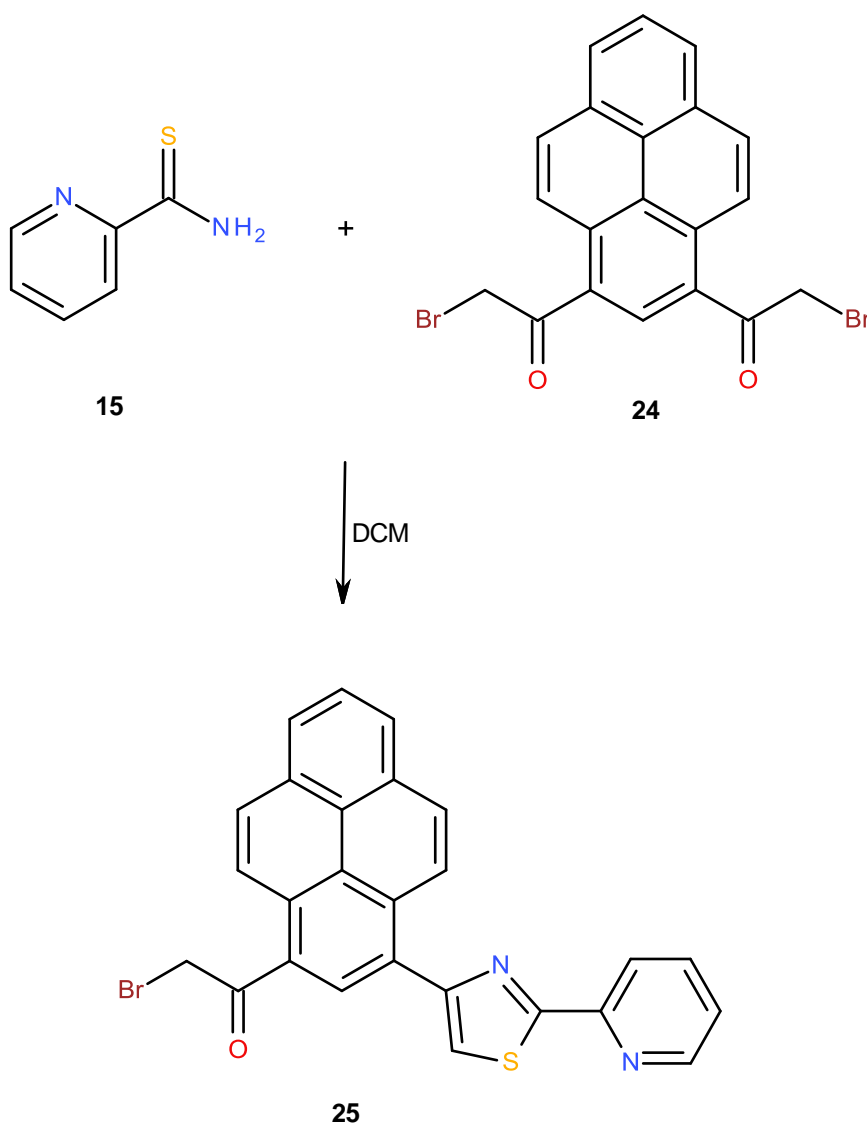


The synthesis of 1,3-dibromo-diacetyl pyrene (**24**) was carried out in a similar manner to the procedure outlined by Whitehead and co-workers in 2010.<sup>135</sup> To a solution of 1,3-diacetylpyrene (**23**) (0.10 g, 0.35 mmol) in acetic acid (20 ml) at 80°C Br<sub>2</sub> (0.11 g, 0.035 ml, 0.70 mmol) in 1 ml acetic acid was added drop wise, continuously and consistently. Once all the Br<sub>2</sub> solution was added the reaction was heated further for 30 minutes and then cooled to room temperature. Water was then added drop wise (10 ml) until a yellow precipitate formed. The solid was then filtered and re-dissolved in DCM, dried with MgSO<sub>4</sub> and evaporated to dryness. Purification by column chromatography (SiO<sub>2</sub>, DCM) gave the dibrominated species (**24**) as a light brown solid (0.09 g, 0.20 mmol, 58 %).

<sup>1</sup>H NMR (400 MHz, CDCl<sub>3</sub>) δ 8.96 (d, *J* = 9.4, 2H), 8.77 (s, 1H), 8.38 (d, *J* = 9.0, 4H), 8.16 (t, *J* = 7.4, 1H), 4.71 (s, 4H, CH<sub>2</sub>Br).

ESI-MS *m/z* 445 (M + H<sup>+</sup>).

### 7.3.3 Preparation of **L**<sup>8</sup>



To a solution of 1,3-dibromo-diacetyl pyrene (**24**) (0.077 g, 0.17 mmol) in DCM (25 ml), stirring at room temperature, was added drop wise a solution of pyridine-2-thioamide (**15**) (0.023 g, 0.17 mmol) in DCM (5 ml) and the reaction was stirred at room temperature for 18 hours. The resulting precipitate was isolated by filtration, suspended in H<sub>2</sub>O and exhaustively extracted with 2% MeOH in DCM. Purification by column chromatography (SiO<sub>2</sub>, 1 % MeOH in DCM) giving the mono-pyridyl-thiazole (**25**) as a yellow oil (0.045 g, 0.093 mmol, 55 %).

<sup>1</sup>H NMR (400 MHz, CDCl<sub>3</sub>) δ 8.95 (d, *J* = 9.4, 1H, pe), 8.69 (d, *J* = 4.1, 1H, py), 8.65 (s, 1H, pe), 8.64 (d, *J* = 9.2, 1H, pe), 8.36 (d, *J* = 4.6, 1H, py), 8.31 (d, *J* = 7.7, 1H, pe), 8.28

(d,  $J = 8.0$ , 2H, pe), 8.23 (d,  $J = 7.7$ , 1H, pe), 8.09 (t,  $J = 7.6$ , 1H, pe), 7.74 (s, 1H, tz), 7.85 (dt,  $J = 7.7$ , 1.7, 1H, py), 7.38 (ddd,  $J = 4.7$ , 1.1 Hz, 1H, py) 4.79 (s, 2H, CH<sub>2</sub>Br).

ESI-MS  $m/z$  484 (M + H<sup>+</sup>).



1H, py), 8.35 (d,  $J = 4.9$ , 2H, pe), 8.32 (d,  $J = 7.0$ , 2H, py), 8.36 (d,  $J = 6.8$ , 1H, py), 8.19 (t,  $J = 7.0$ , 1H, py), 8.17 (t,  $J = 7.7$ , 1H, pe), 8.10 (dt,  $J = 7.8$ , 1.6, 1H, py), 8.03 (dt,  $J = 7.9$ , 1.6, 1H, py), 7.57 (ddd  $J = 4.1$ , 1.1 Hz, 2H, py).

ESI-MS  $m/z$  600 ( $M + H^+$ ).

## 7.4 Synthesis of complexes

### 7.4.1 Synthesis of complex $[Cu(L^1)(ClO_4)_2(sol)]$

Reaction of  $L^1$  (5 mg, 0.015 mmol) with  $Cu(ClO_4)_2 \cdot 6H_2O$  (5.6 mg, 0.015 mmol) in MeCN (2 ml) gave a green solution. Filtration followed by the slow diffusion of ethyl acetate into the MeCN solution resulted in the formation of pale green crystals of  $[Cu(L^1)(ClO_4)_2(sol)]$ . ESI-MS  $m/z$  494 corresponding to  $\{[Cu(L^1)]ClO_4\}^+$ .

### 7.4.2 Synthesis of complex $[Ni_2(L^2)_2]^{4+}$

Reaction of  $L^2$  (5 mg,  $9.8 \times 10^{-3}$  mmol) with  $Ni(ClO_4)_2 \cdot 6H_2O$  (3.6 mg,  $9.8 \times 10^{-3}$  mmol) in  $MeNO_2$  (2 ml) gave a green solution. Filtration followed by the slow diffusion of THF into the  $MeNO_2$  solution resulted in the formation of light green crystals of  $[Ni_2(L^2)_2]^{4+}$ . ESI-MS  $m/z$  1433, 922 and 665 corresponding to  $\{[Ni_2(L^2)_2](ClO_4)_3\}^+$ ,  $\{[Ni_2(L^2)](ClO_4)_3\}^+$  and  $\{[Ni_2(L^2)_2](ClO_4)_2\}^{2+}$  respectively.

### 7.4.3 Synthesis of complex $[Cu_2(L^3)_2]^{4+}$

Reaction of  $L^3$  (5 mg, 0.010 mmol) with  $Cu(ClO_4)_2 \cdot 6H_2O$  (3.8 mg, 0.010 mmol) in  $MeNO_2$  (2 ml) gives a green solution from which green crystals were produced upon slow diffusion of DCM. Resulting in the formation of light green crystals of  $[Cu_2(L^3)_2]^{4+}$ . ESI-MS  $m/z$  1407 and 915 corresponding to  $\{[Cu_2(L^3)_2](ClO_4)_3\}^+$  and  $\{[Cu_2(L^3)](ClO_4)_3\}^+$  respectively.

### 7.4.4 Synthesis of complex $[Co_4(L^4)_4]^{8+}$

Reaction of  $L^4$  (5 mg,  $8.1 \times 10^{-3}$  mmol) with  $Co(BF_4)_2 \cdot 6H_2O$  (2.8 mg,  $8.1 \times 10^{-3}$  mmol) in  $MeNO_2$  (2 ml) produced an orange solution from which crystalline material was produced upon slow diffusion of DCM into the solution. Resulting in the formation of light orange crystals of  $[Co_4(L^4)_4]^{8+}$ . ESI-MS  $m/z$  1607 corresponding to  $\{[Co_4(L^4)_4](ClO_4)_6\}^{2+}$ .

### 7.4.5 Synthesis of complex $[Zn_4(L^5)_4]^{8+}$

Reaction of  $L^5$  (5 mg,  $8.9 \times 10^{-3}$  mmol) with  $Zn(CF_3SO_3)_2$  (3.1 mg,  $8.9 \times 10^{-3}$  mmol) in MeCN (2 ml) produced an orange solution from which crystalline material was produced upon slow diffusion of diisopropyl ether into the solution. Resulting in the formation of light orange crystals of  $[Zn_4(L^5)_4]^{8+}$ . ESI-MS  $m/z$  1742 corresponding to  $\{[Zn_4(L^5)_4](CF_3SO_3)_6\}^{2+}$ .

### 7.4.6 Synthesis of complex $[Ag_2(L^6)_2]^{2+}$

Reaction of  $L^6$  (5 mg,  $11.6 \times 10^{-3}$  mmol) with  $Ag(ClO_4)_2 \cdot 4H_2O$  (3.8 mg,  $11.6 \times 10^{-3}$  mmol) in  $MeNO_2$  (2 ml) produced a yellow solution from which crystalline material was produced

upon slow diffusion of  $\text{CHCl}_3$  into the solution. Resulting in the formation of pale yellow crystals of  $[\text{Ag}_2(\mathbf{L}^6)_2]^{2+}$ . ESI-MS  $m/z$  1171 corresponding to  $\{[\text{Ag}_2(\mathbf{L}^6)_2](\text{ClO}_4)\}^+$ .

#### 7.4.7 Synthesis of complex $[\text{Cd}(\mathbf{L}^6)_2(\text{MeCN})_2]^{2+}$ and $[\text{Cd}_2(\mathbf{L}^6)_2]^{3+}$

Reaction of  $\mathbf{L}^6$  (5 mg,  $11.6 \times 10^{-3}$  mmol) with  $\text{Cd}(\text{ClO}_4)_2 \cdot 6\text{H}_2\text{O}$  (4.9 mg,  $11.6 \times 10^{-3}$  mmol) in MeCN (2 ml) produced a yellow solution from which crystalline material was produced upon slow diffusion of  $\text{Et}_2\text{O}$  into the solution. Resulting in the formation of colourless crystals of  $[\text{Cd}(\mathbf{L}^6)_2(\text{MeCN})_2]^{2+}$  and orange crystals of  $[\text{Cd}_2(\mathbf{L}^6)_2]^{3+}$ . ESI-MS  $m/z$  1069 corresponding to  $\{[\text{Cd}(\mathbf{L}^6)_2](\text{ClO}_4)\}^+$  and 1179 corresponding to  $\{[\text{Cd}_2(\mathbf{L}^6)_2](\text{ClO}_4)\}^+$ .

#### 7.4.8 Synthesis of complex $[\text{Co}_2(\mathbf{L}^7)_2]^{3+}$

Reaction of  $\mathbf{L}^7$  (5 mg,  $9.9 \times 10^{-3}$  mmol) with  $\text{Co}(\text{BF}_4)_2 \cdot 6\text{H}_2\text{O}$  (3.4 mg,  $9.9 \times 10^{-3}$  mmol) in  $\text{MeNO}_2$  (2 ml) produced a yellow solution from which crystalline material was produced upon slow diffusion of DCM into the solution. Resulting in the formation of pale yellow crystals of  $[\text{Co}_2(\mathbf{L}^7)_2]^{3+}$ . ESI-MS  $m/z$  1213 corresponding to  $\{[\text{Co}_2(\mathbf{L}^7)_2](\text{BF}_4)\}^+$ .

#### 7.4.9 Synthesis of complex $[\text{Zn}(\mathbf{L}^7)_2]^{2+}$ and $[\text{Zn}_2(\mathbf{L}^7)_2]^{3+}$

Reaction of  $\mathbf{L}^7$  (5 mg,  $9.9 \times 10^{-3}$  mmol) with  $\text{Zn}(\text{ClO}_4)_2 \cdot 6\text{H}_2\text{O}$  (3.7 mg,  $9.9 \times 10^{-3}$  mmol) in  $\text{MeNO}_2$  (2 ml) produced a yellow solution from which crystalline material was produced upon slow diffusion of  $\text{Et}_2\text{O}$  into the solution. Resulting in the formation of colourless crystals of  $[\text{Zn}(\mathbf{L}^7)_2]^{2+}$  and orange crystals of  $[\text{Zn}_2(\mathbf{L}^7)_2]^{3+}$ . ESI-MS  $m/z$  1175 corresponding to  $\{[\text{Zn}(\mathbf{L}^7)_2](\text{ClO}_4)\}^+$  and 1239 corresponding to  $\{[\text{Zn}_2(\mathbf{L}^7)_2](\text{ClO}_4)\}^+$ .

#### 7.4.10 Synthesis of complex $[\text{Cu}_4(\mathbf{L}^8)_4]^{8+}$

Reaction of  $\mathbf{L}^8$  (5 mg,  $7.4 \times 10^{-3}$  mmol) with  $\text{Cu}(\text{CF}_3\text{SO}_3)$  (2.7 mg,  $7.4 \times 10^{-3}$  mmol) in MeCN (2 ml) afforded a green solution. Heating this solution at  $60^\circ\text{C}$  for 36 hours produced a crystalline solid that was deposited upon slow diffusion of chloroform, to produce green crystals of  $[\text{Cu}_4(\mathbf{L}^8)_4]^{8+}$ . ESI-MS  $m/z$  1773 corresponding to  $\{[\text{Cu}_4(\mathbf{L}^8)_4](\text{CF}_3\text{SO}_3)_6\}^{2+}$ .

#### 7.4.11 Synthesis of complex $[\text{Cd}(\mathbf{DPC})_2]^{2+}$

Reaction of **DPC** (5 mg, 0.021 mmol) with  $\text{Cd}(\text{ClO}_4)_2 \cdot 6\text{H}_2\text{O}$  (4.3 mg, 0.010 mmol) in MeCN (2 ml) gave a pale pink solution. Filtration followed by the slow diffusion of diethyl ether into the MeCN solution resulted in the formation of colourless crystals of  $[\text{Cd}(\mathbf{DPC})_2]^{2+}$ . ESI-MS  $m/z$  697 corresponding to the complex  $\{[\text{Cd}(\mathbf{DPC})_2]\text{ClO}_4\}^+$ .

#### 7.4.12 Synthesis of complex $[Cu_3OH(OH_2)_3(DPTO)_3]^{5+}$

Reaction of **DPC** (5 mg, 0.021 mmol) with  $Cu(ClO_4)_2 \cdot 6H_2O$  (3.8 mg, 0.010 mmol) in acetone (2 ml) result in an intense violet coloured solution. Filtration followed by the slow diffusion of diethyl ether into the acetone solution resulted in the formation of colourless crystals of  $[Cu_3OH(OH_2)_3(DPTO)_3]^{5+}$ . ESI-MS analysis of the crystalline material does not give a molecular ion for the trinuclear species, however it does show ions present at  $m/z$  876, 1614 and 1835 corresponding to  $\{[Cu(DPTO)_3(ClO_4)]\}^+$ ,  $\{[Cu_2(DPTO)_5(ClO_4)_3]\}^+$  and  $\{[Cu_2(DPTO)_6(ClO_4)_3]\}^+$ .

#### 7.4.13 Synthesis of 2,3-diphenyltetrazolium-5-olate

Reaction of **DPC** (5 mg, 0.021 mmol) with  $Cr(ClO_4)_3 \cdot 6H_2O$  (9.5 mg, 0.021 mmol) in MeOH (2 ml) resulted in an intense violet coloured solution. Filtration followed by the slow diffusion of diethyl ether into the acetone solution resulted in the formation of colourless crystals of 2,3-diphenyltetrazolium-5-olate.

Reaction of **DPC** (5 mg, 0.021 mmol) with  $V(C_5H_7O_2)_3$  (7.2 mg, 0.021 mmol) in MeOH (2 ml) resulted in a deep green coloured solution. Filtration followed by the slow diffusion of diethyl ether into the acetone solution resulted in the formation of colourless crystals of 2,3-diphenyltetrazolium-5-olate.

#### 7.4.14 Synthesis of complex $[Hg(DPTC)_2]^+$

Reaction of **DPTC** (5 mg, 0.020 mmol) with  $Hg(ClO_4)_2 \cdot 6H_2O$  (5.0 mg, 0.010 mmol) in MeCN (2 ml) result in an intense red coloured solution. Filtration followed by the slow evaporation of the MeCN solution resulted in the formation of red crystals of  $[Hg(DPTC)_2]^+$ . ESI-MS  $m/z$  713 corresponding to  $\{[Hg(DPTC)(DPTC-H)]\}^+$ .

#### 7.4.15 Synthesis of complex $[Hg_2Ag_2(DPTC)_4(acetone)_2(ClO_4)_2]$

Reaction of **DPTC** (5 mg, 0.020 mmol) with  $Hg(ClO_4)_2 \cdot 6H_2O$  (5.0 mg, 0.010 mmol) and  $AgNO_3$  (1.7 mg, 0.010 mmol) in acetone (2 ml) result in a red coloured solution. Filtration followed by the slow diffusion of diethyl ether vapour into the acetone solution resulted in the formation of red crystals of  $[Hg_2Ag_2(DPTC)_4(acetone)_2(ClO_4)_2]$ . ESI-MS  $m/z$  1737 corresponding to  $\{[((DPTC)_2Hg)_2Ag_2(ClO_4)]\}^+$ .

#### 7.4.16 Synthesis of complex $K_2[Cu_8(DPTC)_8(ClO_4)_2]^{2+}$

Reaction of **DPTC** (5 mg, 0.020 mmol) with  $Cu(ClO_4)_2 \cdot 6H_2O$  (7.2 mg, 0.020 mmol) in acetone (2 ml) initially gave a brown coloured solution, which gradually turned red over a

period of 24 hours. Filtration followed by the slow diffusion of dichloromethane into the acetone solution resulted in the formation of a red crystalline material of  $[\text{Cu}_8(\text{DPTC})_8(\text{ClO}_4)_2]^{8+}$ . ESI-MS  $m/z$  2549 corresponding to  $\{[\text{Cu}_8(\text{DPTC})_8]\}$ .

#### 7.4.17 Synthesis of complex $K_2[\text{Cu}_8(\text{DPTC})_8(\text{BF}_4)_2]^{2-}$

Reaction of **DPTC** (5 mg, 0.020 mmol) with  $\text{Cu}(\text{BF}_4)_2 \cdot 6\text{H}_2\text{O}$  (6.9 mg, 0.020 mmol) in acetone (2 ml) initially gave a brown coloured solution, which gradually turned red over a period of 24 hours. Filtration followed by the slow diffusion of dichloromethane into the acetone solution resulted in the formation of a red crystalline material of  $[\text{Cu}_8(\text{DPTC})_8(\text{BF}_4)_2]^{8+}$ . ESI-MS  $m/z$  2549 corresponding to  $\{[\text{Cu}_8(\text{DPTC})_8]\}$ .

#### 7.4.18 Synthesis of complex $[\text{Cu}_2(\text{DPTC})_2(\text{DPTO})]$

Reaction of **DPTC** (5 mg, 0.020 mmol) with  $\text{Cu}(\text{CH}_3\text{CO}_2)_2 \cdot \text{H}_2\text{O}$  (3.9 mg, 0.020 mmol) in acetone (2 ml) initially gave a brown coloured solution, which gradually turned red after hours, small needle shaped crystals are formed overnight. Examination of this crystalline material showed the complex  $[\text{Cu}_2(\text{DPTC})_2(\text{DPTO})]$ . ESI-MS  $m/z$  892 corresponding to  $\{[\text{Cu}_2(\text{DPTC})_2(\text{DPTO})]\}$ .

## 8. References

1. J. M. Lehn, '*Supramolecular Chemistry: Concepts and Perspectives*', VCH, 1995.
2. P. D. Beer, P. A. Gale and D. K. Smith, *Supramolecular chemistry*, Oxford University Press, 1999.
3. N. F. Curtis, *Journal of the Chemical Society (Resumed)*, 1964, 2644-2650.
4. J. D. Curry and D. H. Busch, *Journal of the American Chemical Society*, 1964, **86**, 592-594.
5. E. G. Jäger and E. Uhlig, *Zeitschrift für Chemie*, 1964, **4**, 437-437.
6. C. J. Pedersen, *Journal of the American Chemical Society*, 1967, **89**, 2495-2496.
7. C. J. Pedersen, *Journal of the American Chemical Society*, 1967, **89**, 7017-7036.
8. D. J. Cram, *Angewandte Chemie International Edition in English*, 1986, **25**, 1039-1057.
9. B. Dietrich, J. M. Lehn and J. P. Sauvage, *Tetrahedron Letters*, 1969, **10**, 2885-2888.
10. J. Steed and J. Atwood, *Supramolecular Chemistry*, VCH, New York, 1999.
11. E. C. Constable and A. M. W. C. Thompson, *Journal of the Chemical Society, Dalton Transactions*, 1994, 1409-1418.
12. E. Fischer, *Berichte der deutschen chemischen Gesellschaft*, 1894, **27**, 2985-2993.
13. J. M. Timko, R. C. Helgeson and D. J. Cram, *Journal of the American Chemical Society*, 1978, **100**, 2828-2834.
14. C. J. Pedersen, *Angewandte Chemie International Edition in English*, 1988, **27**, 1021-1027.
15. S. A. McFarland and N. S. Finney, *Chemical Communications*, 2003, **0**, 388-389.
16. T. Gunnlaugsson, B. Bichell and C. Nolan, *Tetrahedron*, 2004, **60**, 5799-5806.
17. T. Gunnlaugsson, M. Nieuwenhuyzen, L. Richard and V. Thoss, *Tetrahedron Letters*, 2001, **42**, 4725-4728.
18. T. Kaneda, K. Sugihara, H. Kamiya and S. Misumi, *Tetrahedron Letters*, 1981, **22**, 4407-4408.
19. B. Dietrich, J. M. Lehn and J. P. Sauvage, *Tetrahedron Letters*, 1969, **10**, 2889-2892.
20. M. D. Pluth and K. N. Raymond, *Chemical Society Reviews*, 2007, **36**, 161-171.
21. D. Philp and J. F. Stoddart, *Angewandte Chemie International Edition in English*, 1996, **35**, 1154-1196.
22. J. Stoddart and D. Philp, *Angew. Chem., Int. Ed. Engl.*, 1996, **35**, 1154-1196.
23. J.-M. Lehn, *Chemical Society Reviews*, 2007, **36**, 151-160.
24. S. Leininger, B. Olenyuk and P. J. Stang, *Chemical Reviews*, 2000, **100**, 853-908.
25. G. S. Hanan, C. R. Arana, J.-M. Lehn and D. Fenske, *Angewandte Chemie International Edition in English*, 1995, **34**, 1122-1124.
26. G. S. Hanan, C. R. Arana, J.-M. Lehn, G. Baum and D. Fenske, *Chemistry – A European Journal*, 1996, **2**, 1292-1302.
27. H. Sleiman, P. Baxter, J.-M. Lehn and K. Rissanen, *Journal of the Chemical Society, Chemical Communications*, 1995, **0**, 715-716.
28. H. Sleiman, P. N. W. Baxter, J.-M. Lehn, K. Airola and K. Rissanen, *Inorganic Chemistry*, 1997, **36**, 4734-4742.
29. P. N. W. Baxter, G. S. Hanan and J.-M. Lehn, *Chemical Communications*, 1996, **0**, 2019-2020.
30. K. Nicole Power, T. L. Hennigar and M. J. Zaworotko, *New Journal of Chemistry*, 1998, **22**, 177-181.
31. H. W. Roesky and M. Andruh, *Coordination Chemistry Reviews*, 2003, **236**, 91-119.
32. J. R. Price, N. G. White, A. Perez-Velasco, G. B. Jameson, C. A. Hunter and S. Brooker, *Inorganic Chemistry*, 2008, **47**, 10729-10738.
33. J. I. van der Vlugt, S. Demeshko, S. Dechert and F. Meyer, *Inorganic Chemistry*, 2008, **47**, 1576-1585.

34. L. N. Dawe and L. K. Thompson, *Dalton Transactions*, 2008, 3610-3618.
35. A. R. Stefankiewicz, G. Rogez, J. Harrowfield, M. Drillon and J.-M. Lehn, *Dalton Transactions*, 2009, 5787-5802.
36. M. Ruben, J. Rojo, F. J. Romero-Salguero, L. H. Uppadine and J.-M. Lehn, *Angewandte Chemie International Edition*, 2004, **43**, 3644-3662.
37. P. N. Baxter, J. M. Lehn, J. Fischer and M. T. Youinou, *Angewandte Chemie International Edition in English*, 1994, **33**, 2284-2287.
38. G. S. Hanan, D. Volkmer, U. S. Schubert, J.-M. Lehn, G. Baum and D. Fenske, *Angewandte Chemie International Edition in English*, 1997, **36**, 1842-1844.
39. D. W. Johnson and K. N. Raymond, *Supramolecular Chemistry*, 2001, **13**, 639-659.
40. T. Kusukawa and M. Fujita, *Journal of the American Chemical Society*, 2002, **124**, 13576-13582.
41. M. Kawano, Y. Kobayashi, T. Ozeki and M. Fujita, *Journal of the American Chemical Society*, 2006, **128**, 6558-6559.
42. F. Ibukuro, T. Kusukawa and M. Fujita, *Journal of the American Chemical Society*, 1998, **120**, 8561-8562.
43. M. Fujita, S. Nagao and K. Ogura, *Journal of the American Chemical Society*, 1995, **117**, 1649-1650.
44. K. Nakabayashi, M. Kawano, M. Yoshizawa, S.-i. Ohkoshi and M. Fujita, *Journal of the American Chemical Society*, 2004, **126**, 16694-16695.
45. M. Yoshizawa, K. Kumazawa and M. Fujita, *Journal of the American Chemical Society*, 2005, **127**, 13456-13457.
46. M. Yoshizawa, T. Kusukawa, M. Kawano, T. Ohhara, I. Tanaka, K. Kurihara, N. Niimura and M. Fujita, *Journal of the American Chemical Society*, 2005, **127**, 2798-2799.
47. M. Fujita, D. Oguro, M. Miyazawa, H. Oka, K. Yamaguchi and K. Ogura, *Nature*, 1995, **378**, 469-471.
48. M. Fujita, S.-Y. Yu, T. Kusukawa, H. Funaki, K. Ogura and K. Yamaguchi, *Angewandte Chemie International Edition*, 1998, **37**, 2082-2085.
49. R. L. Paul, Z. R. Bell, J. S. Fleming, J. C. Jeffery, J. A. McCleverty and M. D. Ward, *Heteroatom Chemistry*, 2002, **13**, 567-573.
50. R. L. Paul, S. M. Couchman, J. C. Jeffery, J. A. McCleverty, Z. R. Reeves and M. D. Ward, *Journal of the Chemical Society, Dalton Transactions*, 2000, **0**, 845-851.
51. S. P. Argent, T. Riis-Johannessen, J. C. Jeffery, L. P. Harding and M. D. Ward, *Chemical Communications*, 2005, **0**, 4647-4649.
52. Z. R. Bell, J. C. Jeffery, J. A. McCleverty and M. D. Ward, *Angewandte Chemie International Edition*, 2002, **41**, 2515-2518.
53. S. P. Argent, H. Adams, T. Riis-Johannessen, J. C. Jeffery, L. P. Harding and M. D. Ward, *Journal of the American Chemical Society*, 2005, **128**, 72-73.
54. J. S. Fleming, K. L. V. Mann, C.-A. Carraz, E. Psillakis, J. C. Jeffery, J. A. McCleverty and M. D. Ward, *Angewandte Chemie International Edition*, 1998, **37**, 1279-1281.
55. M. D. Ward, *Chemical Communications*, 2009, 4487-4499.
56. M. D. Ward, J. A. McCleverty and J. C. Jeffery, *Coordination Chemistry Reviews*, 2001, **222**, 251-272.
57. S. P. Argent, H. Adams, T. Riis-Johannessen, J. C. Jeffery, L. P. Harding, O. Mamula and M. D. Ward, *Inorganic Chemistry*, 2006, **45**, 3905-3919.
58. S. Turega, M. Whitehead, B. R. Hall, A. J. H. M. Meijer, C. A. Hunter and M. D. Ward, *Inorganic Chemistry*, 2013, **52**, 1122-1132.
59. I. S. Tidmarsh, T. B. Faust, H. Adams, L. P. Harding, L. Russo, W. Clegg and M. D. Ward, *Journal of the American Chemical Society*, 2008, **130**, 15167-15175.
60. S. Turega, M. Whitehead, B. R. Hall, M. F. Haddow, C. A. Hunter and M. D. Ward, *Chemical Communications*, 2012, **48**, 2752-2754.
61. M. Whitehead, S. Turega, A. Stephenson, C. A. Hunter and M. D. Ward, *Chemical Science*, 2013, **4**, 2744-2751.
62. J. D. Watson and F. H. C. Crick, *Nature*, 1953, **171**, 737-738.

63. J. M. Lehn, A. Rigault, J. Siegel, J. Harrowfield, B. Chevrier and D. Moras, *Proceedings of the National Academy of Sciences*, 1987, **84**, 2565-2569.
64. C. Piguet, G. Bernardinelli and G. Hopfgartner, *Chemical Reviews*, 1997, **97**, 2005-2062.
65. M. Albrecht, *Chemical Reviews*, 2001, **101**, 3457-3498.
66. C. Piguet, G. Bernardinelli, B. Bocquet, A. Quattropiani and A. F. Williams, *Journal of the American Chemical Society*, 1992, **114**, 7440-7451.
67. E. C. Constable, *Tetrahedron*, 1992, **48**, 10013-10059.
68. E. C. Constable, M. D. Ward and D. A. Tocher, *Journal of the American Chemical Society*, 1990, **112**, 1256-1258.
69. E. C. Constable, M. D. Ward and D. A. Tocher, *Journal of the Chemical Society, Dalton Transactions*, 1991, **0**, 1675-1683.
70. K. T. Potts, K. A. G. Raiford and M. Keshavarz-K, *Journal of the American Chemical Society*, 1993, **115**, 2793-2807.
71. M. Shaul and Y. Cohen, *The Journal of Organic Chemistry*, 1999, **64**, 9358-9364.
72. M. Greenwald, D. Wessely, E. Katz, I. Willner and Y. Cohen, *The Journal of Organic Chemistry*, 2000, **65**, 1050-1058.
73. B. Hasenknopf, J. M. Lehn, G. Baum and D. Fenske, *Proceedings of the National Academy of Sciences*, 1996, **93**, 1397-1400.
74. V. C. M. Smith and J.-M. Lehn, *Chemical Communications*, 1996, **0**, 2733-2734.
75. K. T. Potts, M. Keshavarz-K, F. S. Tham, H. D. Abruna and C. Arana, *Inorganic Chemistry*, 1993, **32**, 4450-4456.
76. D. M. L. Goodgame, S. P. W. Hill and D. J. Williams, *Journal of the Chemical Society, Chemical Communications*, 1993, **0**, 1019-1021.
77. E. C. Constable, S. M. Elder, J. Healy and D. A. Tocher, *Journal of the Chemical Society, Dalton Transactions*, 1990, **0**, 1669-1674.
78. C. Piguet, G. Hopfgartner, A. F. Williams and J.-C. G. Bunzli, *Journal of the Chemical Society, Chemical Communications*, 1995, **0**, 491-493.
79. C. Piguet, E. Rivara-Minten, G. Hopfgartner and J.-C. G. Bünzli, *Helvetica Chimica Acta*, 1995, **78**, 1541-1566.
80. E. C. Constable, F. R. Heitzler, M. Neuburger and M. Zehnder, *Chemical Communications*, 1996, **0**, 933-934.
81. C. R. Rice, C. J. Baylies, H. J. Clayton, J. C. Jeffery, R. L. Paul and M. D. Ward, *Inorganica Chimica Acta*, 2003, **351**, 207-216.
82. E. C. Constable and J. V. Walker, *Journal of the Chemical Society, Chemical Communications*, 1992, 884-886.
83. E. C. Constable, A. J. Edwards, P. R. Raithby, D. R. Smith, J. V. Walker and L. Whall, *Chemical Communications*, 1996, 2551-2552.
84. E. C. Constable, A. J. Edwards, P. R. Raithby and J. V. Walker, *Angewandte Chemie International Edition in English*, 1993, **32**, 1465-1467.
85. S. Bullock, L. J. Gillie, L. P. Harding, C. R. Rice, T. Riis-Johannessen and M. Whitehead, *Chemical Communications*, 2009, **0**, 4856-4858.
86. J. W. Steed, D. R. Turner and K. Wallace, *Core concepts in supramolecular chemistry and nanochemistry*, John Wiley & Sons, 2007.
87. E. C. Constable, T. Kulke, M. Neuburger and M. Zehnder, *Chemical Communications*, 1997, 489-490.
88. E. C. Constable, C. E. Housecroft, T. Kulke, G. Baum and D. Fenske, *Chemical Communications*, 1999, **0**, 195-196.
89. H. Mürner, A. von Zelewsky and G. Hopfgartner, *Inorganica Chimica Acta*, 1998, **271**, 36-39.
90. G. Baum, E. C. Constable, D. Fenske, C. E. Housecroft and T. Kulke, *Chemistry – A European Journal*, 1999, **5**, 1862-1873.
91. A. M. García-Deibe, J. Sanmartín Matalobos, M. Fondo, M. Vázquez and M. R. Bermejo, *Inorganica Chimica Acta*, 2004, **357**, 2561-2569.
92. J. Fielden, D.-L. Long, C. Evans and L. Cronin, *European Journal of Inorganic Chemistry*, 2006, **2006**, 3930-3935.

93. M. Albrecht, *Chemistry – A European Journal*, 2000, **6**, 3485-3489.
94. I. Janser, M. Albrecht, K. Hunger, S. Burk and K. Rissanen, *European Journal of Inorganic Chemistry*, 2006, **2006**, 244-251.
95. J. Xu, T. N. Parac and K. N. Raymond, *Angewandte Chemie International Edition*, 1999, **38**, 2878-2882.
96. D. J. Cooke, J. M. Cross, R. V. Fennessy, L. P. Harding, C. R. Rice and C. Slater, *Chemical Communications*, 2013, **49**, 7785-7787.
97. B. Hasenknopf, J.-M. Lehn, B. O. Kneisel, G. Baum and D. Fenske, *Angewandte Chemie International Edition in English*, 1996, **35**, 1838-1840.
98. B. Hasenknopf, J.-M. Lehn, N. Boumediene, E. Leize and A. Van Dorsselaer, *Angewandte Chemie International Edition*, 1998, **37**, 3265-3268.
99. B. Hasenknopf, J.-M. Lehn, N. Boumediene, A. Dupont-Gervais, A. Van Dorsselaer, B. Kneisel and D. Fenske, *Journal of the American Chemical Society*, 1997, **119**, 10956-10962.
100. H. B. Tanh Jeazet, K. Gloe, T. Doert, O. N. Kataeva, A. Jager, G. Geipel, G. Bernhard, B. Buchner and K. Gloe, *Chemical Communications*, 2010, **46**, 2373-2375.
101. C. Provent, S. Hewage, G. Brand, L. J. Charbonnière, A. F. Williams and G. Bernardinelli, *Angewandte Chemie International Edition in English*, 1997, **36**, 1287-1289.
102. L. J. Childs, N. W. Alcock and M. J. Hannon, *Angewandte Chemie International Edition*, 2002, **41**, 4244-4247.
103. L. J. Childs, M. Pascu, A. J. Clarke, N. W. Alcock and M. J. Hannon, *Chemistry – A European Journal*, 2004, **10**, 4291-4300.
104. E. C. Constable, C. E. Housecroft, T. Kulke, G. Baum and D. Fenske, *Chemical Communications*, 1999, 195-196.
105. O. Mamula, A. von Zelewsky and G. Bernardinelli, *Angewandte Chemie International Edition*, 1998, **37**, 289-293.
106. O. Mamula, F. J. Monlien, A. Porquet, G. Hopfgartner, A. E. Merbach and A. von Zelewsky, *Chemistry – A European Journal*, 2001, **7**, 533-539.
107. Y. Pang, S. Cui, B. Li, J. Zhang, Y. Wang and H. Zhang, *Inorganic Chemistry*, 2008, **47**, 10317-10324.
108. J. Hamblin, F. Tuna, S. Bunce, L. J. Childs, A. Jackson, W. Errington, N. W. Alcock, H. Nierengarten, A. Van Dorsselaer, E. Leize-Wagner and M. J. Hannon, *Chemistry – A European Journal*, 2007, **13**, 9286-9296.
109. L. Bain, S. Bullock, L. Harding, T. Riis-Johannessen, G. Midgley, C. R. Rice and M. Whitehead, *Chemical Communications*, 2010, **46**, 3496-3498.
110. K. E. Allen, R. A. Faulkner, L. P. Harding, C. R. Rice, T. Riis-Johannessen, M. L. Voss and M. Whitehead, *Angewandte Chemie International Edition*, 2010, **49**, 6655-6658.
111. R. Kramer, J. M. Lehn and A. Marquis-Rigault, *Proceedings of the National Academy of Sciences*, 1993, **90**, 5394-5398.
112. E. C. Constable, R. Chotalia and D. A. Tocher, *Journal of the Chemical Society, Chemical Communications*, 1992, 771-773.
113. R. Chotalia, E. C. Constable, M. Neuburger, D. R. Smith and M. Zehnder, *Journal of the Chemical Society, Dalton Transactions*, 1996, **0**, 4207-4216.
114. C. R. Rice, S. Worl, J. C. Jeffery, R. L. Paul and M. D. Ward, *Chemical Communications*, 2000, **0**, 1529-1530.
115. C. R. Rice, C. J. Baylies, L. P. Harding, J. C. Jeffery, R. L. Paul and M. D. Ward, *Journal of the Chemical Society, Dalton Transactions*, 2001, **0**, 3039-3044.
116. C. R. Rice, S. Worl, J. C. Jeffery, R. L. Paul and M. D. Ward, *Journal of the Chemical Society, Dalton Transactions*, 2001, **0**, 550-559.
117. J. Rebek, J. E. Trend, R. V. Wattlely and S. Chakravorti, *Journal of the American Chemical Society*, 1979, **101**, 4333-4337.
118. J. Rebek and R. V. Wattlely, *Journal of the American Chemical Society*, 1980, **102**, 4853-4854.

119. N. G. Berry, T. W. Shimell and P. D. Beer, *Journal of Supramolecular Chemistry*, 2002, **2**, 89-92.
120. C. J. Baylies, T. Riis-Johannessen, L. P. Harding, J. C. Jeffery, R. Moon, C. R. Rice and M. Whitehead, *Angewandte Chemie International Edition*, 2005, **44**, 6909-6912.
121. E. C. Constable, G. Zhang, C. E. Housecroft and J. A. Zampese, *CrystEngComm*, 2010, **12**, 3724-3732.
122. C. R. Rice, A. Guerrero, Z. R. Bell, R. L. Paul, G. R. Motson, J. C. Jeffery and M. D. Ward, *New Journal of Chemistry*, 2001, **25**, 185-187.
123. C. J. Baylies, L. P. Harding, J. C. Jeffery, T. Riis-Johannessen and C. R. Rice, *Angewandte Chemie International Edition*, 2004, **43**, 4515-4518.
124. A. J. Amoroso, M. W. Burrows, A. A. Dickinson, C. Jones, D. J. Willock and W.-T. Wong, *Journal of the Chemical Society, Dalton Transactions*, 2001, **0**, 225-227.
125. A. J. Amoroso, M. W. Burrows, T. Gelbrich, R. Haigh and M. B. Hursthouse, *Journal of the Chemical Society, Dalton Transactions*, 2002, **0**, 2415-2416.
126. G. Bokolinis, T. Riis-Johannessen, J. C. Jeffery and C. R. Rice, *New Journal of Chemistry*, 2008, **32**, 115-119.
127. T. Riis-Johannessen, L. P. Harding, J. C. Jeffery, R. Moon and C. R. Rice, *Dalton Transactions*, 2007, **0**, 1577-1587.
128. C. J. Baylies, L. P. Harding, J. C. Jeffery, R. Moon, C. R. Rice and T. Riis-Johannessen, *New Journal of Chemistry*, 2007, **31**, 1525-1529.
129. S. K. Mandal and K. Nag, *Journal of the Chemical Society, Dalton Transactions*, 1983, **0**, 2429-2434.
130. S. J. Bullock, L. P. Harding, M. P. Moore, A. Mills, S. A. F. Piela, C. R. Rice, L. Towns-Andrews and M. Whitehead, *Dalton Transactions*, 2013, **42**, 5805-5811.
131. L. Zhang, Z.-L. You and Q.-Z. Jiao, *Transition Met Chem*, 2008, **33**, 573-577.
132. C. Piguet, G. Bernardinelli, B. Bocquet, O. Schaad and A. F. Williams, *Inorganic Chemistry*, 1994, **33**, 4112-4121.
133. F. Tuna, G. Clarkson, N. W. Alcock and M. J. Hannon, *Dalton Transactions*, 2003, **0**, 2149-2155.
134. C.-F. Wang, E.-Q. Gao, Z. He and C.-H. Yan, *Chemical Communications*, 2004, 720-721.
135. M. Whitehead, University of Huddersfield, 2010.
136. R. G. Harvey, J. Pataki and H. Lee, *Organic Preparations and Procedures International*, 1984, **16**, 144-148.
137. L. T. Scott and A. Necula, *The Journal of Organic Chemistry*, 1996, **61**, 386-388.
138. M. Munakata, J. Dai, M. Maekawa, K.-S. Takayoshi and J.-t. Fukui, *Journal of the Chemical Society, Chemical Communications*, 1994, 2331-2332.
139. C. Bonnefous, N. Bellec and R. P. Thummel, *Chemical Communications*, 1999, **0**, 1243-1244.
140. Y. Sagara and T. Kato, *Nat Chem*, 2009, **1**, 605-610.
141. M. Barley, E. C. Constable, S. A. Corr, R. C. S. McQueen, J. C. Nutkins, M. D. Ward and M. G. B. Drew, *Journal of the Chemical Society, Dalton Transactions*, 1988, **0**, 2655-2662.
142. E. C. Constable, C. E. Housecroft, J. R. Price and J. A. Zampese, *CrystEngComm*, 2010, **12**, 3163-3171.
143. S. Skinner and S. Ruhemann, *Journal of the Chemical Society, Transactions*, 1888, **53**, 550-558.
144. P. Cazeneuve, *Bull. Soc. Chim. Paris*, 1900, **23**, 701-706.
145. N. M. Stover, *Journal of the American Chemical Society*, 1928, **50**, 2363-2366.
146. A. Babko, *Zhur. Anal. Khim*, 1950, **5**, 272.
147. F. Feigl, Elsevier Publishing Co., Amsterdam, The Netherlands, Editon edn., 1954.
148. M. Bose, *Nature*, 1952, **170**, 213-213.
149. M. Bose, *Analytica Chimica Acta*, 1954, **10**, 201-208.
150. M. Bose, *Analytica Chimica Acta*, 1954, **10**, 209-221.

151. R. T. Pflaum and L. C. Howick, *Journal of the American Chemical Society*, 1956, **78**, 4862-4866.
152. I. E. Lichtenstein and T. L. Allen, *Journal of the American Chemical Society*, 1959, **81**, 1040-1042.
153. G. J. Willems, N. M. Blaton, O. M. Peeters and C. J. De Ranter, *Analytica Chimica Acta*, 1977, **88**, 345-352.
154. G. Svehla, Longman group limited, Editon edn.
155. G. A. Crespo, F. J. Andrade, F. A. Iñón and M. B. Tudino, *Analytica Chimica Acta*, 2005, **539**, 317-325.
156. A. H. M. Siddalingaiah and S. G. Naik, *Journal of Molecular Structure: THEOCHEM*, 2002, **581**, 149-156.
157. A. H. M. Siddalingaiah and S. G. Naik, *Journal of Molecular Structure: THEOCHEM*, 2002, **582**, 129-136.
158. A. H. M. Siddalingaiah, S. G. Naik, B. S. Sherigara and B. E. Kumara Swamy, *Journal of Molecular Structure: THEOCHEM*, 2002, **582**, 69-75.
159. A. H. M. Siddalingaiah and G. N. Sunil, *Journal of Molecular Structure: THEOCHEM*, 2001, **571**, 183-189.
160. G. Halliwell, *Analytical Chemistry*, 1960, **32**, 1041-1042.
161. G.-z. Fang and C.-y. Miao, *Analyst*, 1985, **110**, 65-70.
162. P. D. Blundy, *Analyst*, 1958, **83**, 555-558.
163. B. E. Saltzman, *Analytical Chemistry*, 1952, **24**, 1016-1020.
164. P. F. Urone and H. K. Anders, *Analytical Chemistry*, 1950, **22**, 1317-1321.
165. H. J. Cahnmann and R. Bisen, *Analytical Chemistry*, 1952, **24**, 1341-1345.
166. F. W. Laird and S. A. Smith, *Industrial & Engineering Chemistry Analytical Edition*, 1938, **10**, 576-578.
167. H. Irving, S. J. H. Cooke, S. C. Woodger and R. J. P. Williams, *Journal of the Chemical Society (Resumed)*, 1949, 1847-1855.
168. H. M. Irving and E. J. Butler, *Analyst*, 1953, **78**, 571-580.
169. E. Fischer, *Justus Liebigs Annalen der Chemie*, 1878, **190**, 67-183.
170. H. Fischer, in *Wissenschaftliche Veröffentlichungen aus dem Siemens-Konzern*, Springer, Editon edn., 1925, pp. 158-170.
171. H. Irving and C. F. Bell, *Journal of the Chemical Society (Resumed)*, 1954, 4253-4256.
172. R. W. Geiger and E. B. Sandell, *Analytica Chimica Acta*, 1953, **8**, 197-208.
173. H. M. N. H. Irving and T. Nowicka-Jankowska, *Analytica Chimica Acta*, 1971, **54**, 55-64.
174. L. J. Synder, *Analytical Chemistry*, 1947, **19**, 684-687.
175. R. G. Milkey, *Analytical Chemistry*, 1952, **24**, 1675-1676.
176. M. Laing, *Journal of the Chemical Society, Perkin Transactions 2*, 1977, 1248-1252.
177. L. S. Meriwether, E. C. Breitner and C. L. Sloan, *Journal of the American Chemical Society*, 1965, **87**, 4441-4448.
178. R. F. K. Bryan, P. M. , *Proceedings of the Chemical Society*, 1961, 185-228.
179. K. S. Math and H. Freiser, *Journal of the Chemical Society D: Chemical Communications*, 1970, 110-111.
180. M. Laing, P. Sommerville and P. A. Alsop, *Journal of the Chemical Society A: Inorganic, Physical, Theoretical*, 1971, 1247-1251.
181. A. Mawby and H. M. N. H. Irving, *Analytica Chimica Acta*, 1971, **55**, 269-272.
182. M. M. Harding, *Journal of the Chemical Society (Resumed)*, 1958, 4136-4143.
183. A. T. Hutton and H. M. N. H. Irving, *Journal of the Chemical Society, Chemical Communications*, 1979, 1113-1114.
184. A. T. Hutton and H. M. N. H. Irving, *Journal of the Chemical Society, Perkin Transactions 2*, 1980, 139-145.
185. A. T. Hutton, H. M. N. H. Irving, L. R. Nassimbeni and G. Gafner, *Acta Crystallographica Section B*, 1980, **36**, 2064-2070.

186. M. L. Niven, H. M. N. H. Irving, L. R. Nassimbeni and A. T. Hutton, *Acta Crystallographica Section B*, 1982, **38**, 2140-2145.
187. J. M. Harrowfield, C. Pakawatchai and A. H. White, *Journal of the Chemical Society, Dalton Transactions*, 1983, 1109-1113.
188. G. L. Seamans, J. L. Walsh, M. Krawiec and W. T. Pennington, *Acta Crystallographica Section C: Crystal Structure Communications*, 2003, **59**, m268-m270.
189. J. A. Delgado, C. K. Y. A. Okio and R. Welter, *Inorganic Chemistry Communications*, 2009, **12**, 1074-1076.
190. K. G. von Eschwege and J. C. Swarts, *Polyhedron*, 2010, **29**, 1727-1733.
191. L. Tomcsányi, *Analytica Chimica Acta*, 1977, **88**, 371-376.
192. S. J. Blunden, M. F. Mahon, K. C. Molloy and P. C. Waterfield, *Journal of the Chemical Society, Dalton Transactions*, 1994, 2135-2143.
193. R. Guillard, S. S. Gerges, A. Tabard, P. Richard, M. A. El Borai and C. Lecomte, *Journal of the American Chemical Society*, 1987, **109**, 7228-7230.
194. R. Das, P. Paul, K. Nag and K. Venkatsubramanian, *Inorganica Chimica Acta*, 1991, **185**, 221-227.
195. E. O. John, R. D. Willett, B. Scott, R. L. Kirchmeier and J. n. M. Shreeve, *Inorganic Chemistry*, 1989, **28**, 893-897.
196. L. A. Oro, M. T. Pinillos, C. Tejel, M. C. Apreda, C. Foces-Foces and F. H. Cano, *Journal of the Chemical Society, Dalton Transactions*, 1988, 1927-1933.
197. W. J. Kozarek and Q. Fernando, *Inorganic Chemistry*, 1973, **12**, 2129-2131.
198. A. C. Fabretti, G. Peyronel and G. C. Franchini, *Journal of Coordination Chemistry*, 1976, **6**, 47-51.
199. G. Peyronel and A. C. Fabretti, *Journal of Coordination Chemistry*, 1977, **7**, 119-124.
200. J. L. Walsh, R. McCracken and A. T. McPhail, *Polyhedron*, 1998, **17**, 3221-3226.
201. Y. Kushi and Q. Fernando, *Journal of the American Chemical Society*, 1970, **92**, 1965-1968.
202. H. J. Wichmann, *Industrial & Engineering Chemistry Analytical Edition*, 1939, **11**, 66-72.
203. B. E. Saltzman, *Analytical Chemistry*, 1953, **25**, 493-496.
204. H. Barnes, *Analyst*, 1947, **72**, 469-472.
205. H. Barnes, *Analyst*, 1951, **76**, 220-223.
206. A. L. D. Comitre and B. F. Reis, *Talanta*, 2005, **65**, 846-852.
207. B. L. Vallee and J. G. Gibson, *Journal of Biological Chemistry*, 1948, **176**, 435-443.
208. S. Bonner-Weir, M. Taneja, G. C. Weir, K. Tatarkiewicz, K.-H. Song, A. Sharma and J. J. O'Neil, *Proceedings of the National Academy of Sciences*, 2000, **97**, 7999-8004.
209. W. Hansen, M. Christie, R. Kahn, A. Norgaard, I. Abel, A. Petersen, D. Jorgensen, S. Bækkeskov, J. Nielsen and A. Lernmark, *Diabetes research (Edinburgh, Scotland)*, 1989, **10**, 53-57.
210. Q. Cheng and H. Dong, *Microchim Acta*, 2005, **150**, 59-65.
211. M. E. Mahmoud, M. M. Osman, O. F. Hafez, A. H. Hegazi and E. Elmelegy, *Desalination*, 2010, **251**, 123-130.
212. Y. Leng, Y. Li, A. Gong, Z. Shen, L. Chen and A. Wu, *Langmuir*, 2013, **29**, 7591-7599.
213. T. J. King, P. N. Preston, J. S. Suffolk and K. Turnbull, *Journal of the Chemical Society, Perkin Transactions 2*, 1979, 1751-1757.
214. A. C. Fabretti and G. Peyronel, *Journal of Inorganic and Nuclear Chemistry*, 1975, **37**, 603-606.
215. T. V. Koksharova and S. V. Fel'dman, *Russian Journal of Coordination Chemistry*, 2001, **27**, 738-740.

## Appendix 1: Crystal Data Tables

In general single crystal X-ray diffraction data was collected at 150(2) K on a Bruker Apex Duo diffractometer equipped with a graphite monochromated Mo(K $\alpha$ ) radiation source and a cold stream of N<sub>2</sub> gas. Solutions were generated by conventional heavy atom Patterson or direct methods and refined by full-matrix least squares on all  $F^2$  data, using SHELXS-97 and SHELXL software respectively.<sup>1</sup> Absorption corrections were applied based on multiple and symmetry-equivalent measurements using SADABS.<sup>2</sup> A number of crystal structures contained anion and or/solvent disorder this was modelled depending on the requirements of the data.

The structure [Co<sub>2</sub>(L<sup>7</sup>)<sub>2</sub>]<sup>3+</sup> contained diffuse areas of electron density, despite exhaustive attempts to collect data and growing the crystals under different conditions (changing solvents, counter ions and temperature) the data contained severe disorder of solvent molecules. To obtain data of reasonable quality the diffuse electron density was removed using the solvent mask facility in Olex2, resulting in very large voids in the crystal structure.<sup>3</sup> The solvent mask removed an area of 586.3 Å<sup>3</sup>, corresponding to a total of 160 electrons which accounts for two molecules of ethyl acetate and nitromethane.

---

<sup>1</sup>SHELXTL Program System, Vers. 5.1, Bruker Analytical X-ray Instruments Inc., Madison, WI, 1998.

<sup>2</sup>G. M. Sheldrick, SADABS: A program for Absorption Correction with the Siemens SMART System, University of Göttingen (Germany), 1996

<sup>3</sup>O. V. Dolomanov, L. J. Bourhis, R. J. Gildea, J. A. K. Howard and H. Puschmann, OLEX2: a complete structure solution, refinements and analysis program. *J. Appl. Cryst.* (2009). **42**, 339-341.

Table A1. Crystallographic data of  $L^1$  complex  $[Cu(L^1)(ClO_4)_2(sol)]$

|  |   |
|--|---|
| Compound                               | $[Cu(L^1)(ClO_4)_2(sol)]$                                   |
| Formula                                | $C_{38}H_{29}C_{16}Cu_2N_9O_{27}S_2$                        |
| M                                      | 1447.60   |
| System                                 | triclinic   |
| Space group                            | P-1   |
| a/ Å                                   | 9.4086(8)   |
| b/ Å                                   | 16.9828(14)   |
| c/ Å                                   | 18.2559(16)   |
| $\alpha/^\circ$                        | 67.070(2)   |
| $\beta/^\circ$                         | 82.993(2)   |
| $\gamma/^\circ$                        | 74.439(2)   |
| V/ Å <sup>3</sup>                      | 2587.5(4)   |
| Z                                      | 2   |
| $\rho_{calc}/Mg\ m^{-3}$               | 1.858   |
| F(000)                                 | 1456  |
| Dimensions/mm <sup>3</sup>             | 0.35 × 0.3 × 0.1  |
| $\mu/mm^{-1}$                          | 0.71073   |
| T/K                                    | 100(2)  |
| Reflections collected                  | 15306   |
| Range                                  | $1.21 \leq \theta \leq 26.02^\circ$                         |
| hkl range indices                      | $-11 \leq h \leq 7, -20 \leq k \leq 20, -21 \leq l \leq 22$ |
| Unique reflections                     | 10037   |
| $R_{int}$                              | 0.0645  |
| $R_w$                                  | 0.1030  |
| R                                      | 0.0581  |
| Reflections with $I > 2\sigma(I)$      | 5604  |
| GOF                                    | 0.986   |
| Refined parameters                     | 777   |
| Restraints                             | 25  |
| Largest peak and hole/eÅ <sup>-3</sup> | 0.592 and -0.687  |

Table A2. Crystallographic data of  $L^2$  complex  $[Ni_2(L^2)_2]^{4+}$

|  |  |
|--|--|
| Compound                               | $[Ni_2(L^2)_2]^{4+}$   |
| Formula                                | $C_{109}H_{78}C_{18}N_{29}Ni_4O_{51}S_8$                     |
| M                                      | 3384.92  |
| System                                 | Triclinic  |
| Space group                            | P-1  |
| a/ Å                                   | 10.7357(5)   |
| b/ Å                                   | 13.4575(6)   |
| c/ Å                                   | 23.2619(11)  |
| $\alpha/^\circ$                        | 82.9930(10)  |
| $\beta/^\circ$                         | 78.8390(10)  |
| $\gamma/^\circ$                        | 82.3710(10)  |
| V/ Å <sup>3</sup>                      | 3252.0(3)  |
| Z                                      | 1  |
| $\rho_{calc}/Mg\ m^{-3}$               | 1.728  |
| F(000)                                 | 1719   |
| Dimensions/mm <sup>3</sup>             | 0.20 × 0.20 × 0.05   |
| $\mu/mm^{-1}$                          | 0.71073  |
| T/K                                    | 150(2)   |
| Reflections collected                  | 57654  |
| Range                                  | $1.70 \leq \theta \leq 30.53$                                |
| hkl range indices                      | $-15 \leq h \leq 15, -19 \leq k \leq 18, -33 \leq l \leq 33$ |
| Unique reflections                     | 19730  |
| $R_{int}$                              | 0.0610   |
| $R_w$                                  | 0.1483   |
| R                                      | 1.036  |
| Reflections with $I > 2\sigma(I)$      | 11017  |
| GOF                                    | 1.036  |
| Refined parameters                     | 983  |
| Restraints                             | 32   |
| Largest peak and hole/eÅ <sup>-3</sup> | 1.180 and -0.903   |

Table A3. Crystallographic data of  $L^3$  complex  $[Cu_2(L^3)_2]^{4+}$

|  |  |
|--|--|
| Compound                               | $[Cu_2(L^3)_2]^{4+}$   |
| Formula                                | $C_{55.38}H_{37.83}C_{14.60}Cu_2N_{11.08}O_{20.16}S_4$       |
| M                                      | 1599.26  |
| System                                 | triclinic  |
| Space group                            | P-1  |
| a/ Å                                   | 12.0799(12)  |
| b/ Å                                   | 14.7340(15)  |
| c/ Å                                   | 17.2067(17)  |
| $\alpha/^\circ$                        | 95.609(2)  |
| $\beta/^\circ$                         | 94.864(2)  |
| $\gamma/^\circ$                        | 90.453(2)  |
| V/ Å <sup>3</sup>                      | 3036.5(5)  |
| Z                                      | 2  |
| $\rho_{calc}/Mg\ m^{-3}$               | 1.749  |
| F(000)                                 | 1618.7   |
| Dimensions/mm <sup>3</sup>             | 0.90 × 0.50 × 0.10   |
| $\mu/mm^{-1}$                          | 0.71073  |
| T/K                                    | 100(2)   |
| Reflections collected                  | 52841  |
| Range                                  | $1.92 \leq \theta \leq 27.88$                                |
| hkl range indices                      | $-10 \leq h \leq 15, -19 \leq k \leq 19, -22 \leq l \leq 22$ |
| Unique reflections                     | 14250  |
| $R_{int}$                              | 0.0400   |
| $R_w$                                  | 0.1073   |
| R                                      | 0.0453   |
| Reflections with $I > 2\sigma(I)$      | 11126  |
| GOF                                    | 1.018  |
| Refined parameters                     | 978  |
| Restraints                             | 135  |
| Largest peak and hole/eÅ <sup>-3</sup> | 1.630 and -1.276   |

Table A4. Crystallographic data of  $L^4$  complex  $[Co_4(L^4)_4]^{8+}$

|  |  |
|--|--|
| Compound                               | $[Co_4(L^4)_4]^{8+}$   |
| Formula                                | $C_{142.65}H_{116.31}B_8Cl_{19.31}Co_4F_{32}N_{25}O_{17}S_8$ |
| M                                      | 4324.00  |
| System                                 | triclinic  |
| Space group                            | P-1  |
| a/ Å                                   | 17.9775(15)  |
| b/ Å                                   | 21.8535(18)  |
| c/ Å                                   | 24.415(2)  |
| $\alpha/^\circ$                        | 105.483(2)   |
| $\beta/^\circ$                         | 95.760(2)  |
| $\gamma/^\circ$                        | 103.275(2)   |
| V/ Å <sup>3</sup>                      | 8862.2(13)   |
| Z                                      | 2  |
| $\rho_{calc}/Mg\ m^{-3}$               | 1.620  |
| F(000)                                 | 4351   |
| Dimensions/mm <sup>3</sup>             | 0.3 × 0.1 × 0.1  |
| $\mu/mm^{-1}$                          | 0.71073  |
| T/K                                    | 150(2)   |
| Reflections collected                  | 164320   |
| Range                                  | $1.52 \leq \theta \leq 27.50$                                |
| hkl range indices                      | $-23 \leq h \leq 23, -26 \leq k \leq 28, -29 \leq l \leq 31$ |
| Unique reflections                     | 39488  |
| $R_{int}$                              | 0.0802   |
| $R_w$                                  | 0.2724   |
| R                                      | 0.0925   |
| Reflections with $I > 2\sigma(I)$      | 21115  |
| GOF                                    | 1.071  |
| Refined parameters                     | 2357   |
| Restraints                             | 401  |
| Largest peak and hole/eÅ <sup>-3</sup> | 2.617 and -1.162   |

Table A5. Crystallographic data of  $L^5$  complex  $[Zn_4(L^5)_4]^{8+}$

|  |  |
|--|--|
| Compound                               | $[Zn_4(L^5)_4]^{8+}$   |
| Formula                                | $C_{156}H_{112}F_{24}N_{32}O_{28}S_{16}Zn_4$                 |
| M                                      | 4113.22  |
| System                                 | monoclinic   |
| Space group                            | C 1 2/c 1  |
| a/ Å                                   | 32.2354(15)  |
| b/ Å                                   | 21.4761(10)  |
| c/ Å                                   | 24.9500(11)  |
| $\alpha/^\circ$                        | 90   |
| $\beta/^\circ$                         | 98.9450(10)  |
| $\gamma/^\circ$                        | 90   |
| V/ Å <sup>3</sup>                      | 17062.6(14)  |
| Z                                      | 4  |
| $\rho_{calc}/Mg\ m^{-3}$               | 1.601  |
| F(000)                                 | 8352   |
| Dimensions/mm                          | 0.25 × 0.1 × 0.1   |
| $\mu/mm^{-1}$                          | 0.71073  |
| T/K                                    | 150.(2)  |
| Reflections collected                  | 81406  |
| Range                                  | $1.65 \leq \theta \leq 28.47$                                |
| hkl range indices                      | $-41 \leq h \leq 43, -19 \leq k \leq 28, -33 \leq l \leq 32$ |
| Unique reflections                     | 21309  |
| $R_{int}$                              | 0.0764   |
| $R_w$                                  | 0.1658   |
| R                                      | 0.0705   |
| Reflections with $I > 2\sigma(I)$      | 11617  |
| GOF                                    | 1.031  |
| Refined parameters                     | 1290   |
| Restraints                             | 159  |
| Largest peak and hole/eÅ <sup>-3</sup> | 1.530 and -1.883   |

Table A6. Crystallographic data of  $L^6$  complex  $[Ag_2(L^6)_2]^+$

|  |  |
|--|--|
| Compound                               | $[Ag_2(L^6)_2]^+$                        |
| Formula                                | $C_{48}H_{34}Ag_2C_{18}N_8O_{10}S_4$     |
| M                                      | 1510.41                                  |
| System                                 | Triclinic                                |
| Space group                            | P-1                                      |
| a/ Å                                   | 7.5797(2)                                |
| b/ Å                                   | 10.6965(3)                               |
| c/ Å                                   | 17.3538(5)                               |
| $\alpha/^\circ$                        | 103.5510(10)                             |
| $\beta/^\circ$                         | 101.6760(10)                             |
| $\gamma/^\circ$                        | 90.4820(10)                              |
| V/ Å <sup>3</sup>                      | 1337.20(6)                               |
| Z                                      | 1  |
| $\rho_{calc}/Mg\ m^{-3}$               | 1.876                                    |
| F(000)                                 | 752                                      |
| Dimensions/mm                          | 0.20 × 0.20 × 0.01                       |
| $\mu/mm^{-1}$                          | 0.71073                                  |
| T/K                                    | 150(2)                                   |
| Reflections collected                  | 31041                                    |
| Range                                  | 1.23 ≤ 30.51                             |
| hkl range indices                      | -10 ≤ h ≤ 10, -15 ≤ k ≤ 15, -24 ≤ l ≤ 24 |
| Unique reflections                     | 8127                                     |
| $R_{int}$                              | 0.0438                                   |
| $R_w$                                  | 0.1308                                   |
| R                                      | 0.0493                                   |
| Reflections with $I > 2\sigma(I)$      | 6240                                     |
| GOF                                    | 1.087                                    |
| Refined parameters                     | 363                                      |
| Restraints                             | 0  |
| Largest peak and hole/eÅ <sup>-3</sup> | 1.736 and -2.228                         |

Table A7. Crystallographic data of  $L^6$  complex  $[Cd(L^6)_2(MeCN)_2]^{2+}$

|  |  |
|--|--|
| Compound                               | $[Cd(L^6)_2(MeCN)_2]^{2+}$                                   |
| Formula                                | $C_{52}H_{41}N_{11}O_{10}S_4Cl_2Cd$                          |
| M                                      | 1291.50  |
| System                                 | triclinic  |
| Space group                            | P-1  |
| a/ Å                                   | 13.697(2)  |
| b/ Å                                   | 14.408(2)  |
| c/ Å                                   | 14.749(2)  |
| $\alpha/^\circ$                        | 102.629(4)   |
| $\beta/^\circ$                         | 96.896(4)  |
| $\gamma/^\circ$                        | 103.104(4)   |
| V/ Å <sup>3</sup>                      | 2721.8(7)  |
| Z                                      | 2  |
| $\rho_{calc}/Mg\ m^{-3}$               | 1.576  |
| F(000)                                 | 1312   |
| Dimensions/mm                          | 0.2 × 0.2 × 0.1  |
| $\mu/mm^{-1}$                          | 0.71073  |
| T/K                                    | 150(2)   |
| Reflections collected                  | 22024  |
| Range                                  | $1.44 \leq \theta \leq 26.65$                                |
| hkl range indices                      | $-16 \leq h \leq 17, -17 \leq k \leq 17, -18 \leq l \leq 18$ |
| Unique reflections                     | 11146  |
| $R_{int}$                              | 0.1203   |
| $R_w$                                  | 0.1203   |
| R                                      | 0.0654   |
| Reflections with $I > 2\sigma(I)$      | 5362   |
| GOF                                    | 0.925  |
| Refined parameters                     | 728  |
| Restraints                             | 15   |
| Largest peak and hole/eÅ <sup>-3</sup> | 0.123 and -1.115   |

Table A8. Crystallographic data of  $L^6$  complex  $[Cd_2(L^6)_2]^{3+}$

|  |  |
|--|--|
| Compound                               | $[Cd_2(L^6)_2]^{3+}$   |
| Formula                                | $C_{47}H_{30}N_9O_{11}S_4Cl_2Cd_2$                           |
| M                                      | 1320.74  |
| System                                 | Monoclinic   |
| Space group                            | C 1 2 /c 1   |
| a/ Å                                   | 13.8805(6)   |
| b/ Å                                   | 24.1373(11)  |
| c/ Å                                   | 15.5574(6)   |
| $\alpha/^\circ$                        | 90.00  |
| $\beta/^\circ$                         | 109.5200(10)   |
| $\gamma/^\circ$                        | 90.00  |
| V/ Å <sup>3</sup>                      | 4912.7(4)  |
| Z                                      | 4  |
| $\rho_{calc}/Mg\ m^{-3}$               | 1.786  |
| F(000)                                 | 2628   |
| Dimensions/mm                          | 0.2 × 0.02 × 0.02  |
| $\mu/mm^{-1}$                          | 0.71073  |
| T/K                                    | 150(2)   |
| Reflections collected                  | 24805  |
| Range                                  | $1.69 \leq \theta \leq 28.92$                                |
| hkl range indices                      | $-18 \leq h \leq 18, -32 \leq k \leq 31, -13 \leq l \leq 20$ |
| Unique reflections                     | 6246   |
| $R_{int}$                              | 0.0561   |
| $R_w$                                  | 0.1119   |
| R                                      | 0.0447   |
| Reflections with $I > 2\sigma(I)$      | 4568   |
| GOF                                    | 1.018  |
| Refined parameters                     | 357  |
| Restraints                             | 36   |
| Largest peak and hole/eÅ <sup>-3</sup> | 1.540 and -1.475   |

Table A9. Crystallographic data of  $L^7$  complex  $[Co_2(L^7)_2]^{3+}$

|  |  |
|--|--|
| Compound                               | $[Co_2(L^7)_2]^{3+}$                                       |
| Formula                                | $C_{28.5}H_{19.5}N_{5.5}O_2S_2CoB_{1.5}F_6$                |
| M                                      | 724.30   |
| System                                 | triclinic  |
| Space group                            | P -1   |
| a/ Å                                   | 15.0469(5)   |
| b/ Å                                   | 15.8504(6)   |
| c/ Å                                   | 16.5883(6)   |
| $\alpha/^\circ$                        | 112.960(1)   |
| $\beta/^\circ$                         | 90.243(1)  |
| $\gamma/^\circ$                        | 112.264(1)   |
| V/ Å <sup>3</sup>                      | 3317.2(2)  |
| Z                                      | 4  |
| $\rho_{calc}/Mg\ m^{-3}$               | 1.4501   |
| F(000)                                 | 1465.2114  |
| Dimensions/mm                          | 0.3 × 0.15 × 0.05  |
| $\mu/mm^{-1}$                          | 0.71073  |
| T/K                                    | 150(2)   |
| Reflections collected                  | 73386  |
| Range                                  | $30.51 \leq \theta \leq 1.35$                              |
| hkl range indices                      | $-21 \leq h \leq 20, -22 \leq k \leq 20, 0 \leq l \leq 23$ |
| Unique reflections                     | 20189  |
| $R_{int}$                              | 0.0606   |
| $R_w$                                  | 0.1177   |
| R                                      | 0.0522   |
| Reflections with $I > 2\sigma(I)$      | 11947  |
| GOF                                    | 0.9897   |
| Refined parameters                     | 914  |
| Restraints                             | 45   |
| Largest peak and hole/eÅ <sup>-3</sup> | 1.0460 and -0.8786   |

Table A10. Crystallographic data of  $L^7$  complex  $[Zn(L^7)_2]^{2+}$

|  |  |
|--|--|
| Compound                               | $[Zn(L^7)_2]^{2+}$   |
| Formula                                | $C_{62.50}H_{51.50}Cl_2N_{14.10}O_{15.30}S_4Zn$              |
| M                                      | 1509.39  |
| System                                 | triclinic  |
| Space group                            | P -1   |
| a/ Å                                   | 14.2989(9)   |
| b/ Å                                   | 14.4169(9)   |
| c/ Å                                   | 18.0643(12)  |
| $\alpha/^\circ$                        | 68.100(2)  |
| $\beta/^\circ$                         | 75.2520(10)  |
| $\gamma/^\circ$                        | 77.0520(10)  |
| V/ Å <sup>3</sup>                      | 3306.5(4)  |
| Z                                      | 2  |
| $\rho_{calc}/Mg\ m^{-3}$               | 1.516  |
| F(000)                                 | 1551   |
| Dimensions/mm                          | 0.600 × 0.180 × 0.130  |
| $\mu/mm^{-1}$                          | 0.71073  |
| T/K                                    | 150.(2)  |
| Reflections collected                  | 62303  |
| Range                                  | $1.49 \leq \theta \leq 28.72$                                |
| hkl range indices                      | $-19 \leq h \leq 19, -19 \leq k \leq 19, -24 \leq l \leq 24$ |
| Unique reflections                     | 16615  |
| $R_{int}$                              | 0.0320   |
| $R_w$                                  | 0.1320   |
| R                                      | 0.0487   |
| Reflections with $I > 2\sigma(I)$      | 12717  |
| GOF                                    | 1.030  |
| Refined parameters                     | 976  |
| Restraints                             | 198  |
| Largest peak and hole/eÅ <sup>-3</sup> | 1.234 and -0.865   |

Table A11. Crystallographic data of  $L^7$  complex  $[Zn_2(L^7)_2]^{3+}$

|  |  |
|--|--|
| Compound                               | $[Zn_2(L^7)_2]^{3+}$   |
| Formula                                | $C_{59}H_{36}Cl_0N_{10}F_9O_{12}S_7Zn_2$                     |
| M                                      | 1603.14  |
| System                                 | orthorhombic   |
| Space group                            | P n a 21   |
| a/ Å                                   | 17.0388(10)  |
| b/ Å                                   | 15.6519(17)  |
| c/ Å                                   | 23.3145(10)  |
| $\alpha/^\circ$                        | 90   |
| $\beta/^\circ$                         | 90   |
| $\gamma/^\circ$                        | 90   |
| V/ Å <sup>3</sup>                      | 6217.7(8)  |
| Z                                      | 4  |
| $\rho_{calc}/Mg\ m^{-3}$               | 1.713  |
| F(000)                                 | 3236   |
| Dimensions/mm                          | 0.2 × 0.1 × 0.1  |
| $\mu/mm^{-1}$                          | 0.71073  |
| T/K                                    | 150(2)   |
| Reflections collected                  | 33610  |
| Range                                  | $2.391 \leq \theta \leq 30.584$                              |
| hkl range indices                      | $-24 \leq h \leq 15, -19 \leq k \leq 22, -29 \leq l \leq 32$ |
| Unique reflections                     | 16749  |
| $R_{int}$                              | 0.0808   |
| $R_w$                                  | 0.1413   |
| R                                      | 0.0759   |
| Reflections with $I > 2\sigma(I)$      | 8703   |
| GOF                                    | 0.995  |
| Refined parameters                     | 894  |
| Restraints                             | 1  |
| Largest peak and hole/eÅ <sup>-3</sup> | 0.896 and -0.736   |

Table A12. Crystallographic data of  $L^8$  complex  $[Cu_4(L^9)_4]^{8+}$

|  |  |
|--|--|
| Compound                               | $[Cu_4(L^9)_4]^{8+}$   |
| Formula                                | $C_{41}H_{24}CuF_6N_6O_6S_4$                                 |
| M                                      | 1002.44  |
| System                                 | monoclinic   |
| Space group                            | C2/c   |
| a/ Å                                   | 25.659(2)  |
| b/ Å                                   | 16.9533(13)  |
| c/ Å                                   | 38.477(3)  |
| $\alpha/^\circ$                        | 90.00  |
| $\beta/^\circ$                         | 92.3880(10)  |
| $\gamma/^\circ$                        | 90.00  |
| V/ Å <sup>3</sup>                      | 16723(2)   |
| Z                                      | 16   |
| $\rho_{calc}/Mg\ m^{-3}$               | 1.593  |
| F(000)                                 | 8112   |
| Dimensions/mm                          | 0.30 × 0.20 × 0.10   |
| $\mu/mm^{-1}$                          | 0.71073  |
| T/K                                    | 150(2)   |
| Reflections collected                  | 34330  |
| Range                                  | $1.52 \leq \theta \leq 20.88$                                |
| hkl range indices                      | $-25 \leq h \leq 25, -16 \leq k \leq 16, -38 \leq l \leq 21$ |
| Unique reflections                     | 8759   |
| $R_{int}$                              | 0.0376   |
| $R_w$                                  | 0.2742   |
| R                                      | 0.0851   |
| Reflections with $I > 2\sigma(I)$      | 6943   |
| GOF                                    | 1.236  |
| Refined parameters                     | 1177   |
| Restraints                             | 1272   |
| Largest peak and hole/eÅ <sup>-3</sup> | 0.771 and -0.884   |

Table A13. Crystallographic data of **DPC** complex  $[\text{Cd}(\text{DPC})_2]^{2+}$

|  |   |
|--|---|
| Compound                               | $[\text{Cd}(\text{DPC})_2]^{2+}$                                    |
| Formula                                | $\text{C}_{36}\text{H}_{43}\text{CdCl}_2\text{N}_{13}\text{O}_{10}$ |
| M                                      | 1001.14   |
| System                                 | orthorhombic  |
| Space group                            | $P n m a$   |
| a/ Å                                   | 17.7433(5)  |
| b/ Å                                   | 29.5869(8)  |
| c/ Å                                   | 8.3209(2)   |
| $\alpha/^\circ$                        | 90  |
| $\beta/^\circ$                         | 90  |
| $\gamma/^\circ$                        | 90  |
| V/ Å <sup>3</sup>                      | 4368.2(2)   |
| Z                                      | 4   |
| $\rho_{\text{calc}}/\text{Mg m}^{-3}$  | 1.5222  |
| F(000)                                 | 2046.8544   |
| Dimensions/mm                          | 0.7 × 0.4 × 0.03  |
| $\mu/\text{mm}^{-1}$                   | 0.71073   |
| T/K                                    | 100.(2)   |
| Reflections collected                  | 25580   |
| Range                                  | $2.30 \leq \theta \leq 29.57^\circ$                                 |
| hkl range indices                      | $-24 \leq h \leq 0, -40 \leq k \leq 0, -11 \leq l \leq 0$           |
| Unique reflections                     | 6230  |
| $R_{\text{int}}$                       | 0.0319  |
| $R_{\text{w}}$                         | 0.0624  |
| R                                      | 0.0287  |
| Reflections with $I > 2\sigma(I)$      | 5165  |
| GOF                                    | 1.026   |
| Refined parameters                     | 299   |
| Restraints                             | 0   |
| Largest peak and hole/eÅ <sup>-3</sup> | 1.005 and -0.787  |

Table A14. Crystallographic data of **DPC** complex  $[\text{Cu}_3\text{OH}(\text{OH}_2)_3(\text{DPTO})_6]^{5+}$

|  |   |
|--|---|
| Compound                               | $[\text{Cu}_3\text{OH}(\text{OH}_2)_3(\text{DPTO})_6]^{5+}$                     |
| Formula                                | $\text{C}_{91.44}\text{H}_{71}\text{Cl}_5\text{Cu}_3\text{N}_{24}\text{O}_{34}$ |
| M                                      | 2417.81   |
| System                                 | Triclinic   |
| Space group                            | P-1   |
| a/ Å                                   | 16.8265(7)  |
| b/ Å                                   | 17.3403(7)  |
| c/ Å                                   | 19.4848(9)  |
| $\alpha/^\circ$                        | 97.6790(10)   |
| $\beta/^\circ$                         | 90.9990(10)   |
| $\gamma/^\circ$                        | 94.8500(10)   |
| V/ Å <sup>3</sup>                      | 5611.7(4)   |
| Z                                      | 2   |
| $\rho_{\text{calc}}/\text{Mg m}^{-3}$  | 1.431   |
| F(000)                                 | 2463  |
| Dimensions/mm                          | 0.40 × 0.15 × 0.05  |
| $\mu/\text{mm}^{-1}$                   | 0.71073   |
| T/K                                    | 100(2)  |
| Reflections collected                  | 57124   |
| Range                                  | $1.69 \leq \theta \leq 22.72$   |
| hkl range indices                      | $-18 \leq h \leq 18, -18 \leq k \leq 18, -21 \leq l \leq 21$                    |
| Unique reflections                     | 15014   |
| $R_{\text{int}}$                       | 0.0625  |
| $R_{\text{w}}$                         | 0.2028  |
| R                                      | 0.0739  |
| Reflections with $I > 2\sigma(I)$      | 10801   |
| GOF                                    | 1.046   |
| Refined parameters                     | 1642  |
| Restraints                             | 6   |
| Largest peak and hole/eÅ <sup>-3</sup> | 1.055 and -0.571  |

Table A15. Crystallographic data of 2,3-diphenyltetrazolium-5-olate (DPTO)

|  |  |
|--|--|
| Compound                               | 2,3-diphenyltetrazolium-5-olate (DPTO)           |
| Formula                                | C <sub>13</sub> H <sub>10</sub> N <sub>4</sub> O |
| M                                      | 238.25   |
| System                                 | Orthorhombic                                     |
| Space group                            | P 21 21 21                                       |
| a/ Å                                   | 6.2372(7)  |
| b/ Å                                   | 11.5227(15)                                      |
| c/ Å                                   | 16.0783(19)                                      |
| α/°                                    | 90   |
| β/°                                    | 90   |
| γ/°                                    | 90   |
| V/ Å <sup>3</sup>                      | 1155.5(2)  |
| Z                                      | 4  |
| ρ <sub>calc</sub> /Mg m <sup>-3</sup>  | 1.369  |
| F(000)                                 | 496  |
| Dimensions/mm                          | 0.330 × 0.200 × 0.200                            |
| μ/mm <sup>-1</sup>                     | 0.71073  |
| T/K                                    | 102.(2)  |
| Reflections collected                  | 8136   |
| Range                                  | 2.17 ≤ θ ≤ 30.03                                 |
| hkl range indices                      | -6 ≤ h ≤ 8, -9 ≤ k ≤ 16, -22 ≤ l ≤ 22            |
| Unique reflections                     | 1958   |
| R <sub>int</sub>                       | 0.0398   |
| R <sub>w</sub>                         | 0.0852   |
| R                                      | 0.0359   |
| Reflections with I > 2σ(I)             | 1698   |
| GOF                                    | 1.013  |
| Refined parameters                     | 163  |
| Restraints                             | 0  |
| Largest peak and hole/eÅ <sup>-3</sup> | 0.239 and -0.206                                 |

Table A16. Crystallographic data of **DPTC** complex [Hg(**DPTC**)<sub>2</sub>]

|  |  |
|--|--|
| Compound                               | [Hg( <b>DPTC</b> ) <sub>2</sub> ]                                |
| Formula                                | C <sub>30</sub> H <sub>30</sub> HgN <sub>10</sub> S <sub>2</sub> |
| M                                      | 795.35   |
| System                                 | monoclinic   |
| Space group                            | C 1 2 1  |
| a/ Å                                   | 21.7448(19)  |
| b/ Å                                   | 5.3260(4)  |
| c/ Å                                   | 13.8216(11)  |
| α/°                                    | 90   |
| β/°                                    | 106.577(2)   |
| γ/°                                    | 90   |
| V/ Å <sup>3</sup>                      | 1534.2(2)  |
| Z                                      | 2  |
| ρ <sub>calc</sub> /Mg m <sup>-3</sup>  | 1.722  |
| F(000)                                 | 784  |
| Dimensions/mm                          | 0.100 × 0.010 × 0.010  |
| μ/mm <sup>-1</sup>                     | 0.71073  |
| T/K                                    | 296.(2)  |
| Reflections collected                  | 7784   |
| Range                                  | 1.54 ≤ θ ≤ 28.42   |
| hkl range indices                      | -13 ≤ h ≤ 28, -6 ≤ k ≤ 7, -18 ≤ l ≤ 18                           |
| Unique reflections                     | 3329   |
| R <sub>int</sub>                       | 0.0440   |
| R <sub>w</sub>                         | 0.0549   |
| R                                      | 0.0323   |
| Reflections with I > 2σ(I)             | 3240   |
| GOF                                    | 0.826  |
| Refined parameters                     | 196  |
| Restraints                             | 1  |
| Largest peak and hole/eÅ <sup>-3</sup> | 0.681 and -0.800   |

Table A17. Crystallographic data of **DPTC** complex  $[\text{Hg}_2\text{Ag}_2(\text{DPTC})_4(\text{acetone})_2(\text{ClO}_4)_2]$

|  |   |
|--|---|
| Compound                               | $[\text{Hg}_2\text{Ag}_2(\text{DPTC})_4(\text{acetone})_2(\text{ClO}_4)_2]$                       |
| Formula                                | $\text{C}_{64}\text{H}_{64}\text{Ag}_2\text{Cl}_2\text{Hg}_2\text{N}_{16}\text{O}_{12}\text{S}_4$ |
| M                                      | 2065.37   |
| System                                 | Triclinic   |
| Space group                            | P -1  |
| a/ Å                                   | 11.7453(4)  |
| b/ Å                                   | 12.3139(4)  |
| c/ Å                                   | 14.0203(4)  |
| $\alpha/^\circ$                        | 100.8190(10)  |
| $\beta/^\circ$                         | 98.4200(10)   |
| $\gamma/^\circ$                        | 107.7650(10)  |
| V/ Å <sup>3</sup>                      | 1851.22(10)   |
| Z                                      | 1   |
| $\rho_{\text{calc}}/\text{Mg m}^{-3}$  | 1.853   |
| F(000)                                 | 1008  |
| Dimensions/mm                          | 0.400 × 0.150 × 0.050   |
| $\mu/\text{mm}^{-1}$                   | 0.71073   |
| T/K                                    | 100.(2)   |
| Reflections collected                  | 39414   |
| Range                                  | $1.79 \leq \theta \leq 29.57$   |
| hkl range indices                      | $-16 \leq h \leq 16, -12 \leq k \leq 17, -19 \leq l \leq 19$                                      |
| Unique reflections                     | 10303   |
| $R_{\text{int}}$                       | 0.0296  |
| $R_{\text{w}}$                         | 0.0437  |
| R                                      | 0.0221  |
| Reflections with $I > 2\sigma(I)$      | 9110  |
| GOF                                    | 1.021   |
| Refined parameters                     | 474   |
| Restraints                             | 1   |
| Largest peak and hole/eÅ <sup>-3</sup> | 0.996 and -0.853  |

Table A18. Crystallographic data of **DPTC** complex  $[\text{Cu}_8(\text{DPTC})_8(\text{ClO}_4)_2]^{8+}$

|  |  |
|--|--|
| Compound                               | $[\text{Cu}_8(\text{DPTC})_8(\text{ClO}_4)_2]^{8+}$  |
| Formula                                | $\text{C}_{106}\text{H}_{88}\text{Cl}_6\text{Cu}_8\text{K}_2\text{N}_{32}\text{O}_8\text{S}_8$ |
| M                                      | 2993.78  |
| System                                 | Monoclinic   |
| Space group                            | C 1 2/c 1  |
| a/ Å                                   | 31.5889(19)  |
| b/ Å                                   | 15.6131(9)   |
| c/ Å                                   | 28.325(3)  |
| $\alpha/^\circ$                        | 90.00  |
| $\beta/^\circ$                         | 115.4120(10)   |
| $\gamma/^\circ$                        | 90.00  |
| V/ Å <sup>3</sup>                      | 12618.2(16)  |
| Z                                      | 4  |
| $\rho_{\text{calc}}/\text{Mg m}^{-3}$  | 1.576  |
| F(000)                                 | 6048   |
| Dimensions/mm                          | 0.80 × 0.50 × 0.10   |
| $\mu/\text{mm}^{-1}$                   | 0.71073  |
| T/K                                    | 150(2)   |
| Reflections collected                  | 54847  |
| Range                                  | $1.49 \leq \theta \leq 28.38$  |
| <i>hkl</i> range indices               | $-42 \leq h \leq 42, -18 \leq k \leq 20, -37 \leq l \leq 35$                                   |
| Unique reflections                     | 15729  |
| $R_{\text{int}}$                       | 0.1027   |
| $R_{\text{w}}$                         | 0.1605   |
| <i>R</i>                               | 0.0639   |
| Reflections with $I > 2\sigma(I)$      | 8905   |
| GOF                                    | 1.012  |
| Refined parameters                     | 803  |
| Restraints                             | 108  |
| Largest peak and hole/eÅ <sup>-3</sup> | 2.106 and -1.447   |

Table A19. Crystallographic data of **DPTC** complex  $[\text{Cu}_8(\text{DPTC})_8(\text{BF}_4)_2]^{8+}$

|  |   |
|--|---|
| Compound                               | $[\text{Cu}_8(\text{DPTC})_8(\text{BF}_4)_2]^{8+}$  |
| Formula                                | $\text{C}_{106}\text{H}_{88}\text{B}_2\text{Cl}_4\text{Cu}_8\text{F}_8\text{K}_{0.75}\text{N}_{32}\text{Na}_{1.25}\text{O}_2\text{S}_8$ |
| M                                      | 2980.29   |
| System                                 | Monoclinic  |
| Space group                            | C 1 2/c 1   |
| a/ Å                                   | 31.5024(16)   |
| b/ Å                                   | 15.5709(8)  |
| c/ Å                                   | 28.1201(16)   |
| $\alpha/^\circ$                        | 90.00   |
| $\beta/^\circ$                         | 114.798(2)  |
| $\gamma/^\circ$                        | 90.00   |
| V/ Å <sup>3</sup>                      | 12521.6(12)   |
| Z                                      | 4   |
| $\rho_{\text{calc}}/\text{Mg m}^{-3}$  | 1.581   |
| F(000)                                 | 150(2)  |
| Dimensions/mm                          | 0.3 × 0.2 × 0.2   |
| $\mu/\text{mm}^{-1}$                   | 0.71073   |
| T/K                                    | 150(2)  |
| Reflections collected                  | 26457   |
| Range                                  | $1.49 \leq \theta \leq 26.38$   |
| hkl range indices                      | $-26 \leq h \leq 39, -18 \leq k \leq 19, -34 \leq l \leq 35$  |
| Unique reflections                     | 12719   |
| $R_{\text{int}}$                       | 0.1094  |
| $R_{\text{w}}$                         | 0.1524  |
| R                                      | 0.0698  |
| Reflections with $I > 2\sigma(I)$      | 6190  |
| GOF                                    | 0.990   |
| Refined parameters                     | 843   |
| Restraints                             | 120   |
| Largest peak and hole/eÅ <sup>-3</sup> | 1.171 and -0.849  |

Table A20. Crystallographic data of **DPTC** complex [ $\text{Cu}_2(\text{DPTC})_2(\text{DPTCO})$ ]

|  |  |
|--|--|
| Compound                               | [ $\text{Cu}_2(\text{DPTC})_2(\text{DPTCO})$ ]                           |
| Formula                                | $\text{C}_{81}\text{H}_{67}\text{Cu}_4\text{N}_{24}\text{O}_6\text{S}_6$ |
| M                                      | 1839.11  |
| System                                 | triclinic  |
| Space group                            | P-1  |
| a/ Å                                   | 12.4147(8)   |
| b/ Å                                   | 12.5005(8)   |
| c/ Å                                   | 15.0246(10)  |
| $\alpha/^\circ$                        | 79.780(2)  |
| $\beta/^\circ$                         | 67.380(2)  |
| $\gamma/^\circ$                        | 88.288(2)  |
| V/ Å <sup>3</sup>                      | 2116.3(2)  |
| Z                                      | 1  |
| $\rho_{\text{calc}}/\text{Mg m}^{-3}$  | 1.443  |
| F(000)                                 | 941  |
| Dimensions/mm                          | 0.15 × 0.10 × 0.05   |
| $\mu/\text{mm}^{-1}$                   | 0.71073  |
| T/K                                    | 150(2)   |
| Reflections collected                  | 13034  |
| Range                                  | $1.49 \leq \theta \leq 23.32$  |
| <i>hkl</i> range indices               | $-13 \leq h \leq 13$ $-13 \leq k \leq 13$ , $-16 \leq l \leq 16$         |
| Unique reflections                     | 6092   |
| $R_{\text{int}}$                       | 0.0532   |
| $R_{\text{w}}$                         | 0.0825   |
| <i>R</i>                               | 0.0433   |
| Reflections with $I > 2\sigma(I)$      | 4197   |
| GOF                                    | 0.994  |
| Refined parameters                     | 533  |
| Restraints                             | 0  |
| Largest peak and hole/eÅ <sup>-3</sup> | 0.395 and -0.318   |

## Appendix 2: Publications